AD-A131 255 SUPPLEMENTAL GROUNDING OF EXTENDED EMP COLLECTORS(U) 1/2
GEORGIA INST OF TECH ATLANTA ENERGY AND MATERIAL
SCIENCES LAB H W DENNY ET AL. 31 JAN 82 DNA-5940F
UNCLASSIFIED DNA001-80-C-0294 F/G 20/14 NL

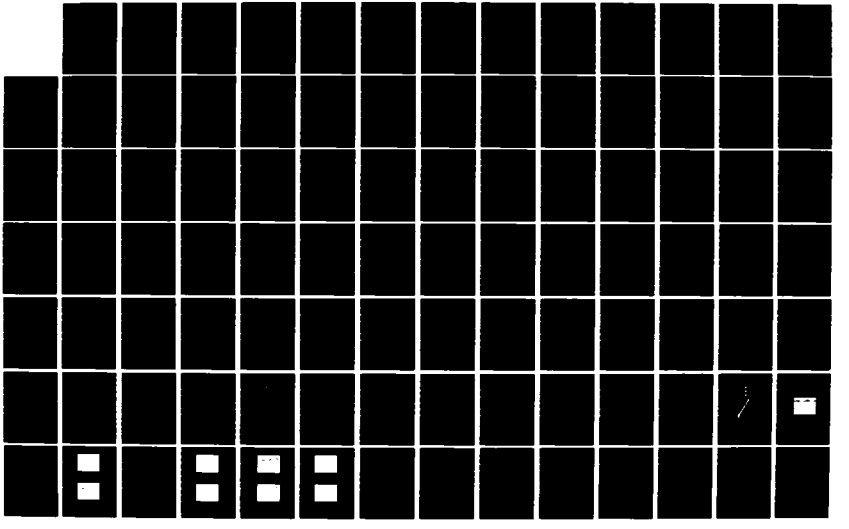

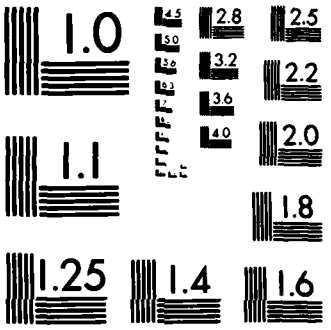

(13)

DNA 5940F

SUPPLEMENTAL GROUNDING OF EXTENDED EMP COLLECTORS

Georgia Institute of Technology
Engineering Experiment Station
Energy and Material Sciences Laboratory
Atlanta, Georgia 30332

31 January 1982

Final Report for Period 1 May 1980—31 January 1982

CONTRACT No. DNA 001-80-C-0294

APPROVED FOR PUBLIC RELEASE;
DISTRIBUTION UNLIMITED.

THIS WORK WAS SPONSORED BY THE DEFENSE NUCLEAR AGENCY
UNDER RDT&E RMSS CODE B363080462 G52AAXEX40602 H2590D.

Prepared for
Director
DEFENSE NUCLEAR AGENCY
Washington, DC 20305

Destroy this report when it is no longer needed. Do not return to sender.

PLEASE NOTIFY THE DEFENSE NUCLEAR AGENCY, ATTN: STTI, WASHINGTON, D.C. 20305, IF YOUR ADDRESS IS INCORRECT, IF YOU WISH TO BE DELETED FROM THE DISTRIBUTION LIST, OR IF THE ADDRESSEE IS NO LONGER EMPLOYED BY YOUR ORGANIZATION.

UNCLASSIFIED

SECURITY CLASSIFICATION OF THIS PAGE *(When Data Entered)*

REPORT DOCUMENTATION PAGE		READ INSTRUCTIONS BEFORE COMPLETING FORM
1. REPORT NUMBER DNA 5940F	2. GOVT ACCESSION NO. A131901	3. RECIPIENT'S CATALOG NUMBER
4. TITLE *(and Subtitle)* SUPPLEMENTAL GROUNDING OF EXTENDED EMP COLLECTORS		5. TYPE OF REPORT & PERIOD COVERED Final Report for Period 1 May 80 to 31 Jan 82
		6. PERFORMING ORG. REPORT NUMBER
7. AUTHOR(s) H. W. Denny, D. W. Acree, G. B. Melson, D. P. Millard		8. CONTRACT OR GRANT NUMBER(s) DNA 001-80-C-0294
9. PERFORMING ORGANIZATION NAME AND ADDRESS Georgia Institute of Technology Engineering Experiment Station Energy and Material Sciences Lab. Atlanta, Georgia 30332		10. PROGRAM ELEMENT, PROJECT, TASK AREA & WORK UNIT NUMBERS Subtask G52AAXEX406-02
11. CONTROLLING OFFICE NAME AND ADDRESS Director Defense Nuclear Agency Washington, DC 20305		12. REPORT DATE 31 January 1982
		13. NUMBER OF PAGES 182
14. MONITORING AGENCY NAME & ADDRESS*(if different from Controlling Office)*		15. SECURITY CLASS. *(of this report)* UNCLASSIFIED
		15a. DECLASSIFICATION/DOWNGRADING SCHEDULE N/A since unclassified

16. DISTRIBUTION STATEMENT *(of this Report)*

Approved for public release; distribution unlimited.

17. DISTRIBUTION STATEMENT *(of the abstract entered in Block 20, if different from Report)*

18. SUPPLEMENTARY NOTES

This work was sponsored by the Defense Nuclear Agency under RDT&E RMSS Code B363080462 G52AAXEX40602 H2590D.

19. KEY WORDS *(Continue on reverse side if necessary and identify by block number)*

EMP	Grounding
Transmission Lines	Earth Electrodes
Shielding	Computer Modeling

20. ABSTRACT *(Continue on reverse side if necessary and identify by block number)*

The external conductors of a facility, particularly long, above ground types, pose a severe EMP threat. A primary purpose of this program was to investigate the premise that supplemental ground connections in these types of conductors could serve to reduce this threat. To support this investigation an External Collector Analysis Model (ECAM) was developed. ECAM was applied to analyzing the EMP-induced current levels appearing at a facility under various conditions of line length, line height, and number of grounds. From the

DD FORM 1 JAN 73 1473 EDITION OF 1 NOV 65 IS OBSOLETE

UNCLASSIFIED

SECURITY CLASSIFICATION OF THIS PAGE *(When Data Entered)*

20. ABSTRACT (Continued)

results, approaches to the treatment of external collector penetrations are suggested.

In addition to the external collector assessments, preliminary studies of internal collector responses are reported. Supplemental studies of techniques for measuring the responses of earth electrode systems over the EMP power spectrum are described. A successful technique utilizing currently available instrumentation was used to validate a test probe and to evaluate scaled models of various commonly used earth electrode geometries. From the measurements, observations relating to the behavior of various geometries up to 500 MHz are made.

SUMMARY

The purpose of this program was to investigate the premise that supplemental grounds on external EMP collectors could serve to reduce the threat levels appearing at equipment terminals inside a facility. The investigation consisted of:

The development of an External Collector Assessment Model (ECAM) which permitted the EMP response of long overhead collectors to be evaluated under varying conditions of line height, line length, and number of grounds;

A limited evaluation of the response of collectors internal to an unshielded facility to suggest the severity of pickup by these collectors relative to that arising from external collectors; and

The development of techniques for characterizing the response of an earth electrode (ground) to an EMP-type waveform.

ECAM was used to evaluate the amplitudes of EMP-induced currents at the termination (facility penetration) of variously configured overhead lines. The results indicate that supplemental grounds exert a primary influence on the induced current only when they are located within some 30-50 m of the penetration point. This effect suggests that the interface between the facility and its external collectors be remotely located with intervening conductors routed underground in noninsulated, metal conduit. A suggested layout is provided for both power lines and signal lines.

The results from the preliminary investigation of internal collector coupling using an available method of moments code strongly suggest that considerably more developmental work is going to be required if an analytical approach is to be used. The limited results that were achieved suggest that internal collector pickup should more thoroughly be evaluated relative to potential effects from external collector pickup. A more promising approach for quantifying the levels of internal collector pickup is that of experimental determination of the nominal shielding effectiveness of a typical, "unshielded" facility. Preliminary results suggest that indeed the inherent protective properties of typical construction may be usable and may be quantifiable. Data on two buildings of standard commercial construction indicate that over the range of frequencies containing most of the energy of an EMP, a general level of protection of from 20 to 40 dB may be realizable without extraordinary effort.

An earth electrode system was verified to behave like a second order, parallel, RLC network. It's low frequency (DC and power frequencies) impedance is predominantly determined by the resistivity of the soil and the length of the conductors. The high frequency (up to 500 MHz) impedance of the electrode is governed primarily by the soil's dielectric properties. The presence of rods appears to be unimportant in so far as the behavior of an electrode system at these higher frequencies is concerned. The contact of the electrode with the soil appears to be the primary factor in determining effectiveness.

For determining the best location for an earth electrode, a resonant antenna method is the most promising candidate for performing rapid ground conductivity and dielectric surveys. This method is portable, does not disurb the site, and accurately indicates performance over the frequency range occupied by the EMP power spectrum. This method can be supplemented with the standard Fall-of-Potential method to determine the low frequency (or DC) resistance of an electrode. High frequency measurements can be made with an RF network analyzer.

PREFACE

This report presents the results of a study to assess the EMP protection benefits of providing supplemental grounds on the extended external collectors associated with electronics facilities. This study was performed for the Defense Nuclear Agency under RDT&E RMSS CODE B363080462 G52AAXEX40602 H2590D as Contract DNA 001-80-C-0294. The program was monitored by Major Blair Williams, RAEE.

The work described in this report was performed by the Electromagnetic Compatibility (EMC) Division, Electronics and Computer Systems Laboratory (ECSL), Georgia Tech Engineering Experiment Station. The described work was directed by Mr. H. W. Denny, Chief of the EMC Division under the general supervision of Mr. F. L. Cain, Director of ECSL. The report was authored by Mr. Denny and by Mr. D. W. Acree, Mr. G. B. Melson, and Mr. D. P. Millard.

TABLE OF CONTENTS

TABLE OF CONTENTS (Concluded)

Appendix

LIST OF ILLUSTRATIONS

LIST OF ILLUSTRATIONS (Continued)

LIST OF ILLUSTRATIONS (Continued)

LIST OF ILLUSTRATIONS (continued)

LIST OF ILLUSTRATIONS (concluded)

LIST OF TABLES

I. INTRODUCTION

1.1 BACKGROUND

Many facilities associated with important elements of the nation's defense system are potentially susceptible to damage and disruption from electromagnetic pulse (EMP) events arising from nuclear weapons detonations. The large and rapidly changing electromagnetic fields associated with an EMP are capable of inducing large currents in conducting objects. Such currents present a serious threat to electrical and electronic components and equipments. For example, consider the typical facility containing sensitive electronic apparatus such as a communications center, message switching center, computer center, etc. When supplied with utilities such as water, fuel, and sewage lines, and with electric power; when provided with external communications links, such as phone and data lines; and when protected against lightning with an appropriate lightning protection system (to include its earth electrode system), a complex array of potential EMP collectors exists. The EMP threat due to the longer collectors external to the facility, e.g., power lines, signal lines, and utility pipes, is well recognized. Other external collectors, such as the lightning downconductor network, have not been as adequately addressed. However, topologically these other conductor networks would also appear to be important contributors to the total EMP current environment against which protection must be provided. For example, Figure 1 shows a code-compatible [1] lightning air-terminal-downconductor network appropriate for a moderate to large size structure. Even simplified earth electrode systems like those shown in Figure 2 (whether outside or inside structural boundaries) appear to offer attractive pickup mechanisms for EMP energy. Either of these facility-related networks (and certainly the total combination) acts as an antenna to intercept the EMP pulse and, as a result, potentially damaging voltages and currents are produced on and between the network elements.

As shown by Figure 3, many occasions also arise where there are internal collections of equipment interconnected with power conductors, signal and control lines, ducts and raceways, and grounding cables. For example, the combined lightning protection, electrical safety/fault protection, and equipment EMI control networks frequently appear like the one shown in Figure 4. Each of these internal conductors is a possible EMP collector which may cause damaging potentials to be produced at critical points within individual pieces of equipment.

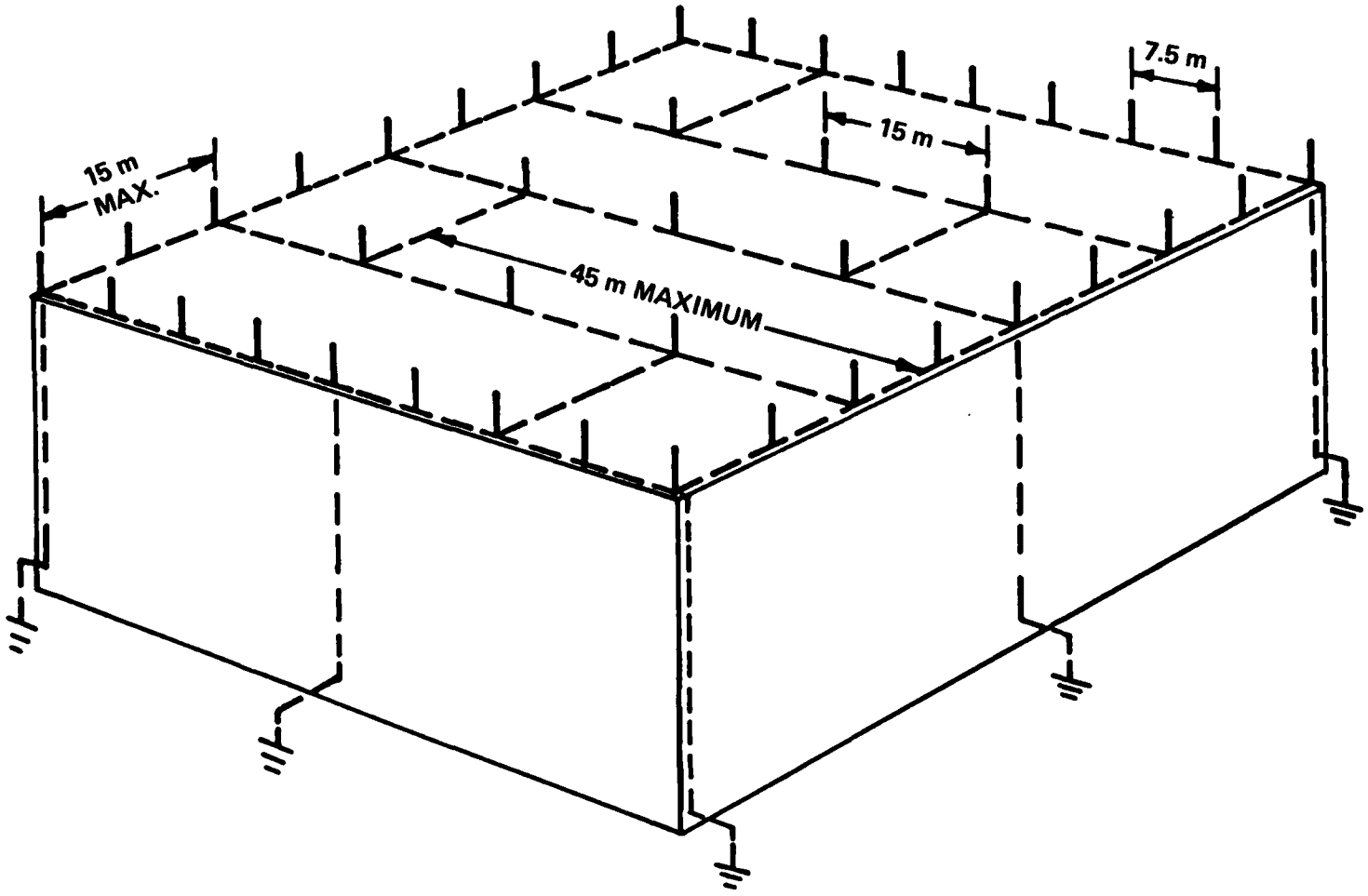

Figure 1. External lightning protection network conforming to the Lightning Protection Code.

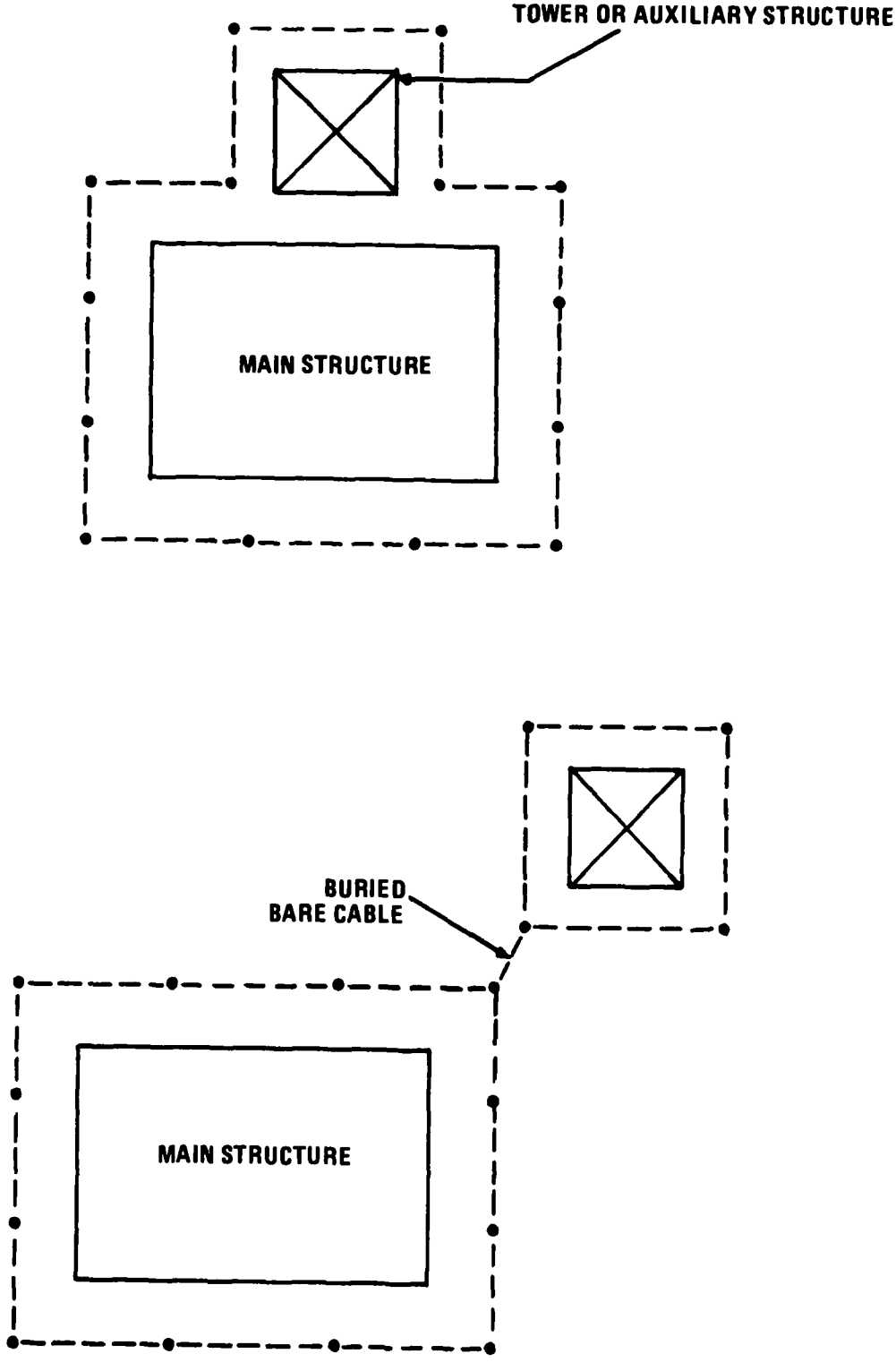

Figure 2. Common earth electrode configurations.

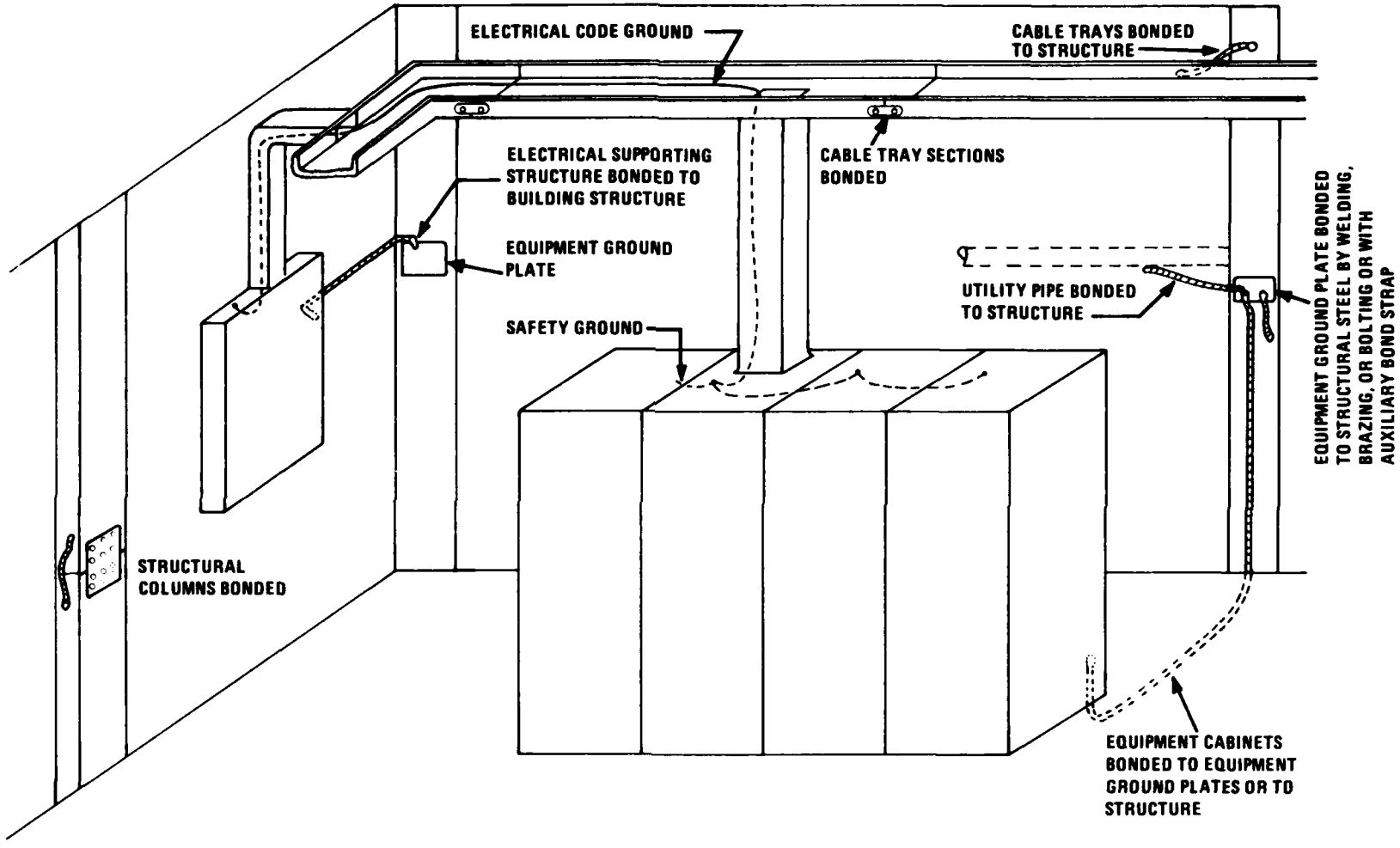

Figure 3. Typical internal EMP collectors.

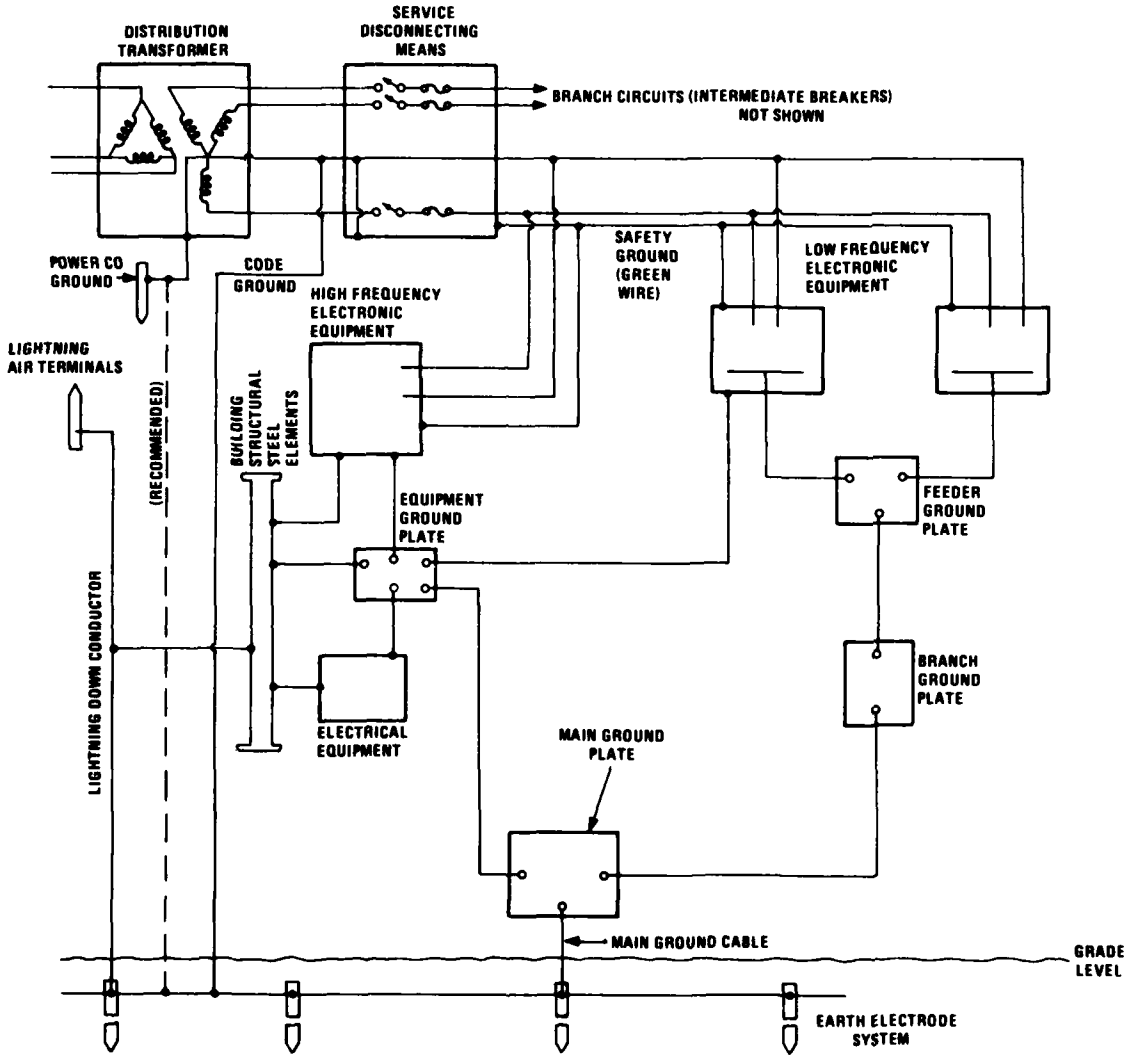

Figure 4. Facility grounding networks.

Many of the internal collectors are short to moderate in length, extending only from equipment rack to equipment rack, from room to room, or from floor to floor and are totally contained within a given volume (cabinet, room, or structure). A commonly suggested approach for protecting these conductors and associated terminating equipment from external electromagnetic fields is to enclose the entire volume in a metal shield, preferably one constructed of heavy gauge steel. Applied to an individual circuit or equipment, total enclosure in a metal shield is compatible with usual practices and, though requiring care in design and construction, does not extravagantly inflate the per unit costs of the protected circuit or equipment. However, where the volume to be protected is large, as, for example, a room or an entire structure, the cost of an adequate EMP shield markedly increases the normal cost of construction [2]. For maximum effectiveness from the shield, particular efforts must be taken to treat the apertures where signals, power, and other conductors enter the shielded region to prevent the EMP energy on these collectors from entering the shielded area. This required treatment places additional constraints upon construction which further raise costs.

The net threat appearing at any particular equipment port is the vector combination of the effects arising from the penetrating EMP field, the conducted voltages and currents resulting from induced currents on exo-equipment (and exo-facility) collectors, and the secondary EM fields produced by the induced collector currents. At the present time, the relative contribution of each of these effects is not clearly established. Intuitively, however, the long external collectors would appear to be the major contributor if for no other reason than typically they present a large effective antenna aperture.

The earth offers a convenient "sink" for dissipating the energy associated with the currents induced in the conductors leading to the facility. Therefore, major emphasis is usually placed on providing a low resistance connection to earth as close as possible to the point of entrance of collectors into the protected region. A low impedance path is established between the collector and the earth electrode. Then, to protect internal equipment against secondary fields and to minimize current concentration, a heavy shield is placed around the susceptible equipments. If, indeed, the primary contributors to voltages and currents at equipment terminals are the long external conductors, a significant reduction in these fields could be effected by reducing the level of the induced current at the point of entry into the sensitive region. A postulated way of reducing this

current would be to provide alternative, supplemental paths to "drain" the excess collected EMP energy to earth for dissipation prior to reaching the facility. This concept is illustrated by Figure 5. If effective, such a practice could reduce the overall shielding requirements of the facility and thus potentially promises to reduce the cost of EMP hardening. In addition to potential savings in direct costs, i.e., that associated with reducing the need for a heavy metal enclosure, the possible savings in indirect costs may be much greater. These indirect costs refer to those necessary to accommodate conflicts in philosophies, needs and practices between the EMP communities and the lightning protection and EMI communities. Any measures which will make these philosophies, needs and practices more compatible will reduce the total costs of facilities, particularly those in which all three considerations are involved, such as Defense Communications Service facilities.

In view of these possible benefits, an evaluation of supplemental grounding of long external EMP collectors through the use of auxiliary earth electrodes was undertaken. This evaluation considered: (1) the degree of effectiveness of auxiliary earth grounds in reducing the EMP currents induced on long external collectors; (2) the relative EMP energy picked up by external collectors versus that picked up by structural members and internal collectors (in an unshielded facility); (3) the soil and earth electrode system parameters necessary to realize effective auxiliary grounds; (4) methods for establishing preferred locations for the auxiliary grounds; and (5) means for measuring the installed electrodes to confirm that they met the established criteria.

1.2 TECHNICAL APPROACH

Within the context of the above background, an analytical and experimental program was undertaken to accomplish the following goals:

1. Perform appropriate modeling and analysis to assess the relative EMP collection efficiency of internal collectors versus the external collectors of a facility. For the external collectors, ascertain relative effective lengths for both above ground and buried installations.

2. Examine the possible reduction in EMP-induced currents on facility conductors and shields and in the primary earth electrode system achievable through the grounding of collectors at points prior to entering the facility (i.e., at auxiliary earth electrodes). In this assessment, consider:

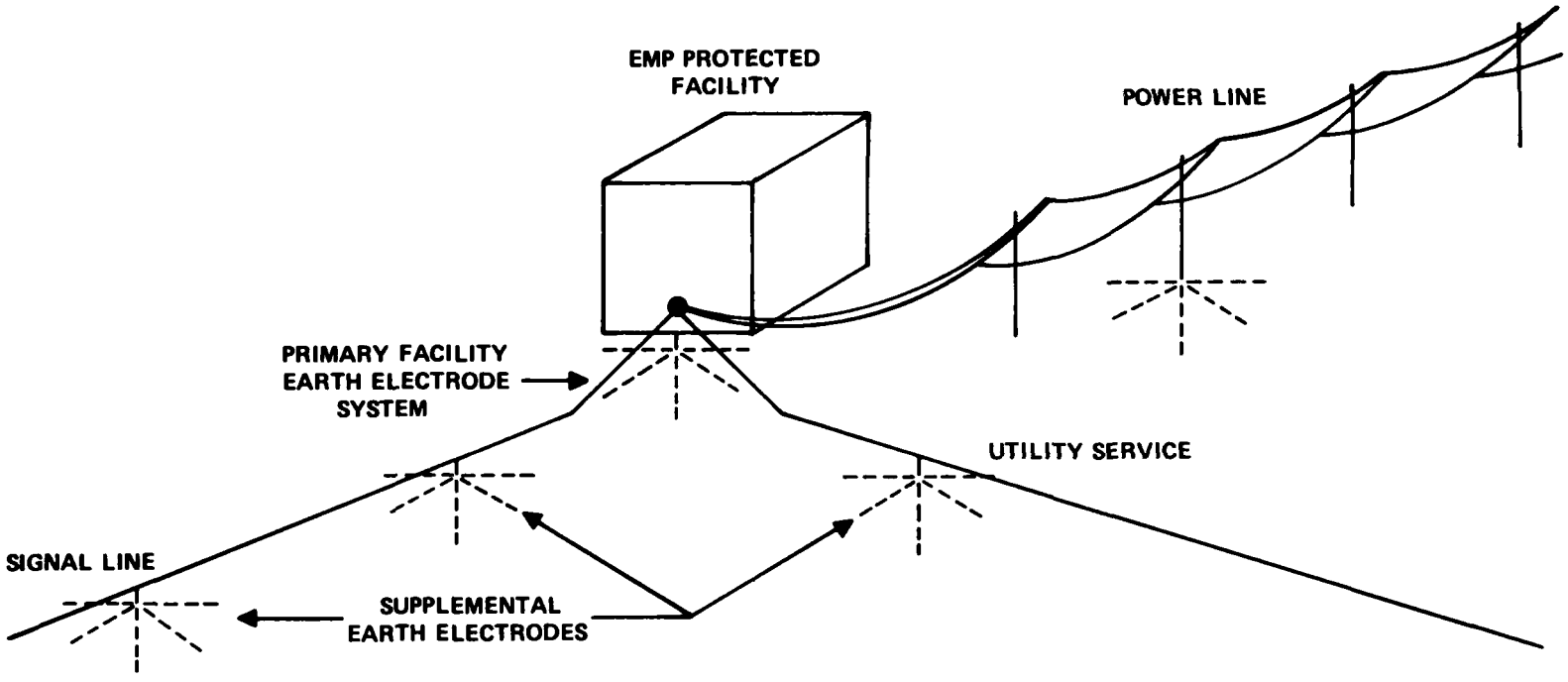

Figure 5. Supplemental grounding concept.

a. The necessary relative resistance and impedance to earth of the primary and auxiliary earth electrode systems;

b. The required earth resistivity parameters and electrode configurations;

c. The degree of reduction in the currents in facility shields, structural members, and primary earth electrode conductors achievable through supplemental grounding of external conductors; and

d. The optimum separation distances between the facility's primary electrode system and the auxiliary grounds.

3. Evaluate candidate techniques for rapidly performing a ground conductivity survey at a site to determine the optimum location for the auxiliary earth electrode systems.

4. Determine the techniques necessary to measure the electrode impedance properties of the auxiliary electrodes after installation. Particular emphasis will be placed on methods usable in the vicinity of pre-existing electrode systems.

In pursuit of these goals, initially, a comprehensive literature survey was made for: (1) existing computer algorithms potentially applicable to the assessment of EMP coupling to collectors, both external and internal, (2) potential approaches to scale modeling for the assessment of collector coupling and the high frequency behavior of buried electrodes, and (3) techniques appropriate for the evaluation of earth electrode systems over frequency ranges compatible with the EMP spectrum. Based on the findings of the literature search, the following specific efforts were undertaken:

1. Development of a computer model capable of permitting an assessment of the EMP response of an extended overhead collector with multiple ground points. An above ground collector was emphasized because it was considered to represent a more severe threat than buried collectors (which enjoy some added protection from the absorbing properties of soil). In order to perform the necessary tradeoff studies, mathematical derivation of an improved algorithm was necessary. This algorithm was implemented on a pair of computers (VAX 11/780 and CYBER 74) and parametric studies were performed.

2. Assessment of techniques for evaluating EMP coupling to internal collectors. The techniques used were analytical modeling using method of moments techniques and experimental determination of the equivalent shielding effectiveness of actual structures over the EMP power spectrum.

3. Identification of an appropriate technique for characterizing the behavior of an earth electrode system (rod, grid, or array) at frequencies sufficient to define its effectiveness for suppression of an EMP. Experimental validation of the selected technique suggests its applicability to field utilization for surveying potential electrode configurations and for evaluating their performance once installed.

1.3 REPORT ORGANIZATION

The activities undertaken and the results achieved on the above efforts are described in the remaining sections of this report. Specifically, Section II discusses the development and utilization of the External Collector Assessment Model (ECAM) while Section III reviews the accomplishments of the internal collector evaluation study. Section IV describes the development of the technique for measuring earth electrode systems at high (to UHF) frequencies and discusses the behavior of various electrode configurations over the frequency range covered by the accepted EMP power spectrum. Overall conclusions and recommendations are set forth in Section V. Supporting analyses and supplementary information are contained in the appendices.

II. EXTERNAL COLLECTOR ASSESSMENT MODEL (ECAM)

2.1 INTRODUCTION

The scenario assumed for the assessment of EMP pickup by external collectors is depicted in Figure 6. An imperfectly shielded facility supplied with electric power from an overhead power line is assumed to represent a worst-case situation in terms of the amplitude of the induced current pulse at the point of penetration into the facility. Other collector configurations, such as those involving twisted or shielded conductors (i.e. signal lines or buried or conduit-encased power lines), are not expected to experience any greater degree of pickup than the overhead, grounded power line. The ground wire commonly associated with overhead power lines, the sheath surrounding armored cable, or the shields of signal cables are all expected to behave similarly under multiple grounding. Thus, the overhead power line with a ground wire was selected as the example on which the influence of supplemental ground connections on EMP pickup was evaluated.

An incremental section (Δx) of transmission line with a perfect ground return can be represented with the circuit diagram shown in Figure 7(a). In this figure, r represents the per unit series resistance, ℓ , the per unit series inductance, g, the per unit shunt conductance and, c, the per unit shunt capacitance. Even where the return is not perfect, i.e., actual earth, the equivalent circuit elements (principally series resistance with a shunt capacitance) can be integrated into these four parameters. However, with the addition of an intentional connection to earth, i.e., ground, the circuit diagram must be modified as shown in Figure 7(b). (Upon evaluation of the relative influence of the various transmission line parameters, it was concluded that the shunt conductance term, g could be deleted without a significant impact on the results.) A reasonable expectation for the equivalent circuit for the down lead and the earth electrode is that of an inductance in series with a parallel resistance and capacitance [3]. Experimental studies [4] have shown that the resistance and capacitance terms representing the earth connection are frequency dependent. This frequency dependency suggests a frequency domain approach as opposed to a time domain approach in spite of the time-limited nature of the incident field, i.e., the EMP. An analytical approach based upon conversion of the EMP waveform to a frequency domain representation, solving for the coupled currents and voltages in the frequency domain, and converting back to a time equivalent waveform was selected as

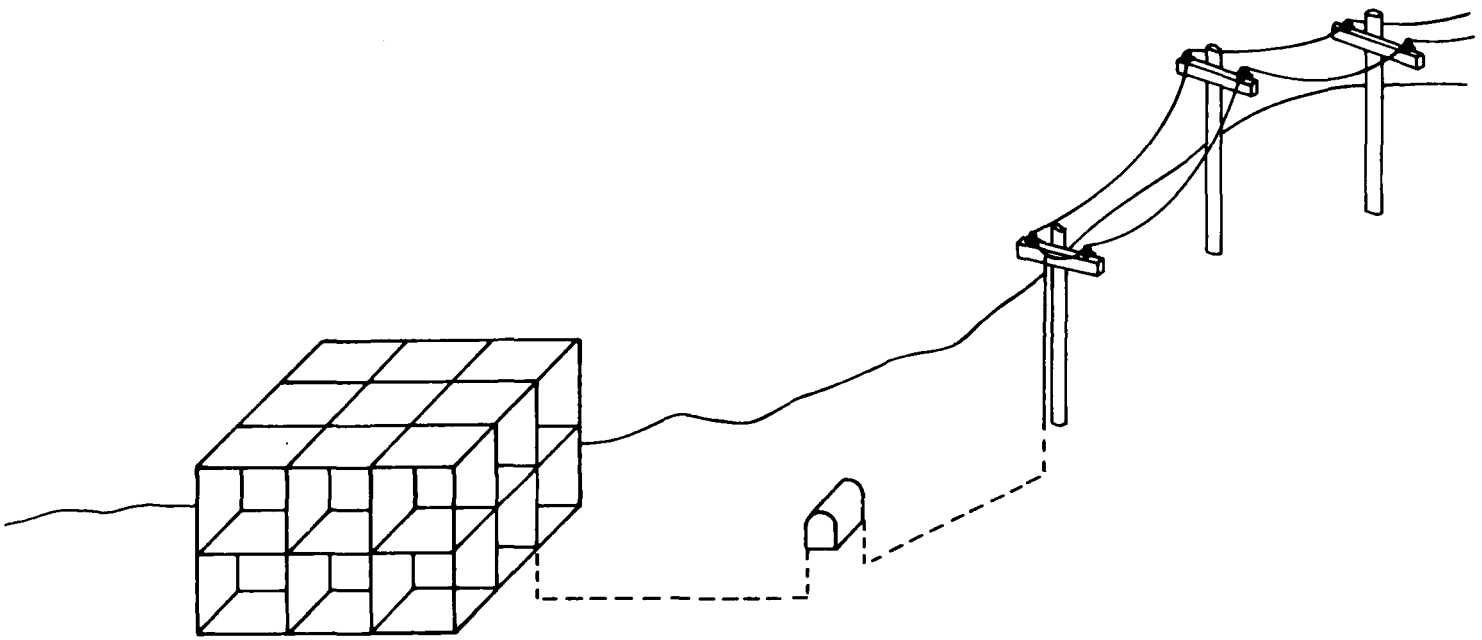

Figure 6. EMP coupling scenario.

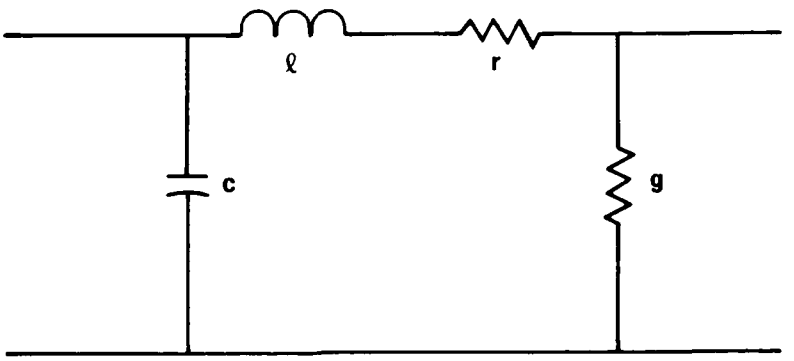

(a) UNIFORM LINE SEGMENT

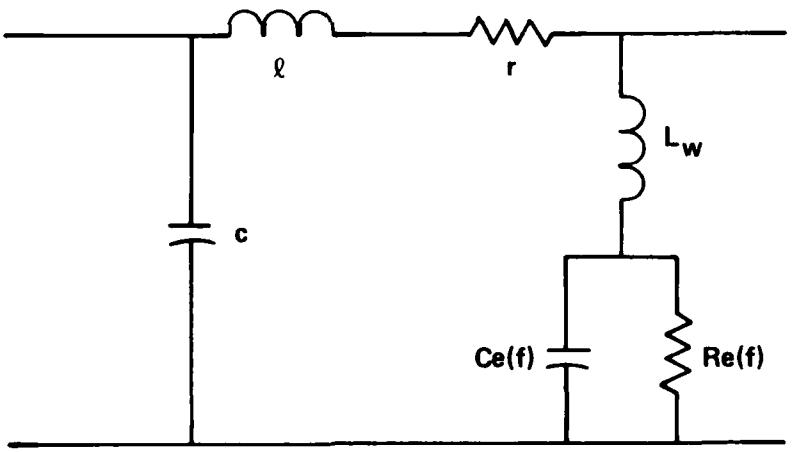

(b) LINE SEGMENT WITH EARTH CONNECTION

Figure 7. Per unit transmission line equivalent circuits.

the most direct. With this approach the transmission line was modeled in the presence of a lossy earth, grounded at various points, and excited by the incident electromagnetic field. This transmission line approach assumes that the TEM mode of propagation primarily determines the amount of current appearing at the end point of the line.

The time waveform and power spectrum for a representative EMP [36] are shown in Figure 8. Notice that frequency components extending into the microwave range are produced by the very fast rise and fall times of the pulse. Because of the exceedingly large bandwidth of the pulse spectrum, forward and inverse Fourier transforms can not be readily performed using a conventional Fast Fourier Transform (FFT). Consequently, an alternate technique, called Filon's method [5], for Fourier transforms was used. This method employs a piecewise linear approximation of the argument function in performing the transform. (For further details on this method, see Appendix A.) The technique was implemented and several test runs were performed to verify its validity for these analyses. The derivation and description of the External Collector Assessment Model (ECAM) which resulted from this approach is described in the following section.

2.2 MODEL DEVELOPMENT

The method for determining the time domain current at the termination of the transmission line when illuminated by an EMP, using the frequency domain transmission line model, may best be illustrated by considering the transmission line as an analogy to an ideal low pass filter, as illustrated in Figure 9. To find the impulse response of the filter, the Fourier transform of the input response is first obtained and multiplied by the filter frequency response, and then the result is inverse transformed to obtain the output time domain response of the filter. A similar approach is taken in the solution of the induced currents on the transmission line. The input time domain EMP field is transformed to the frequency domain using Filon's method, and the induced current on the transmission line is then computed for each given frequency. Finally, the composite of all the discrete frequencies are then inverse Fourier transformed back to the time domain, yielding the time domain representation of the induced current on the line.

The TEM mode formulation for multiconductor transmission lines in the presence of a lossy ground when illuminated by an incident field can be derived from Faraday's Law. If it is assumed that all conductors are perfectly conducting,

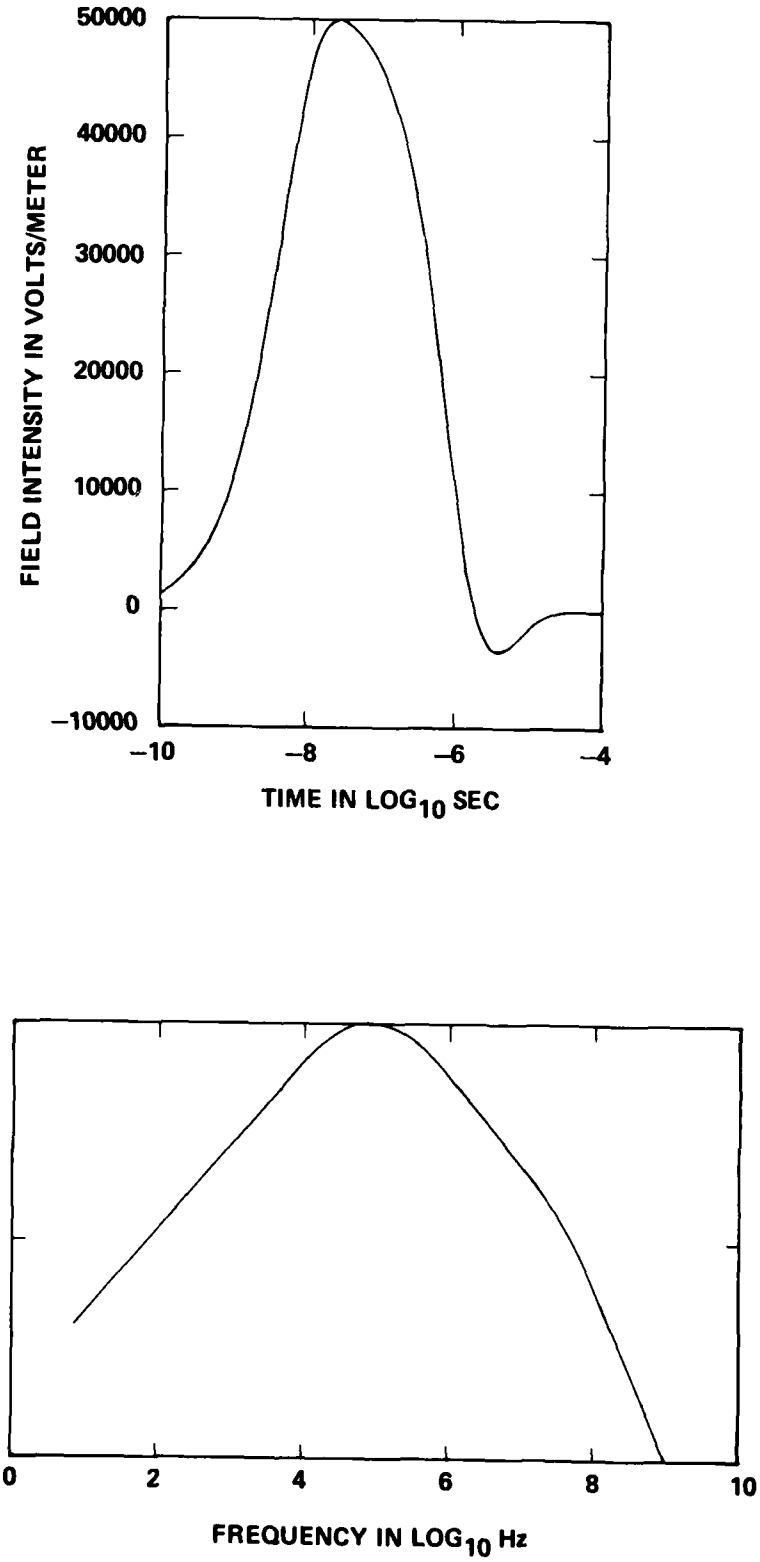

Figure 8. EMP time waveform and power spectrum representations.

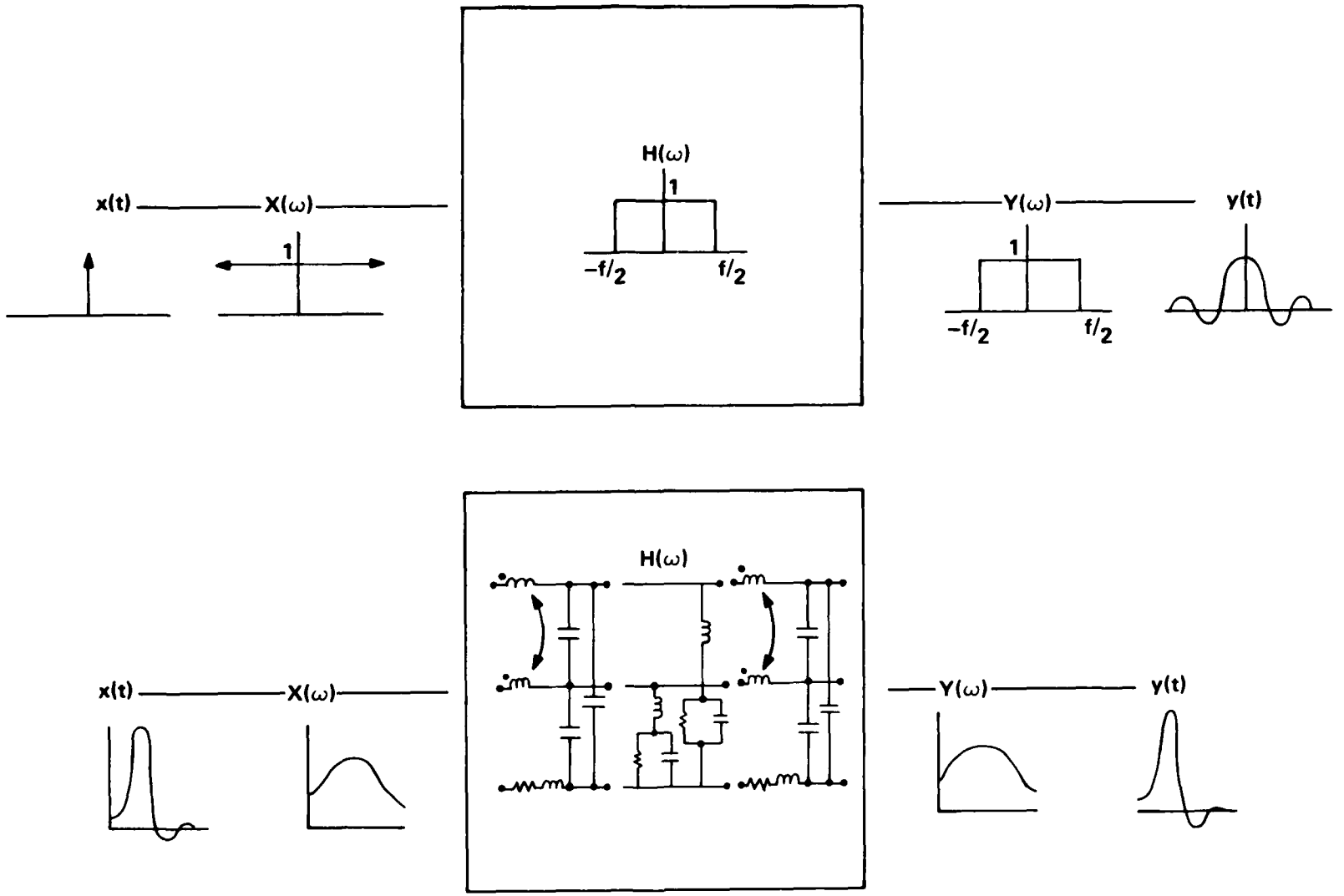

Figure 9. Filter analogy of transmission line analysis problem.

(i.e., r=0) and that the axis of the line is parallel to the x-axis in the rectangular coordinate system, the transmission line equations for an N-conductor uniform line illuminated by an incident field become

$$\frac{\partial \underline{V}(x)}{\partial x} + \underset{\sim}{Z}(\omega)\underline{I}(x) = \underline{V}_s(\hat{x}) \tag{1}$$

and

$$\frac{\partial \underline{I}(x)}{\partial x} + \underset{\sim}{Y}(\omega)\,\underline{V}(x) = \underline{I}_s(\hat{x}) \tag{2}$$

(The derivation of these equations is given in Appendix B.) In Equations (1) and (2), $\underset{\sim}{Z}(\omega)$ and $\underset{\sim}{Y}(\omega)$ are impedance and admittance matrices, respectively, where the element of the i^{th} row and j^{th} column is denoted by $[\underset{\sim}{\ }]_{ij}$. A vector is denoted by $\underline{V}$, where $[V(x)]_i = V_i(x)$ and $V_i(x,t) = V_i(x)e^{j\omega t}$ are the complex valued potentials associated with the i^{th} conductor. The $\underset{\sim}{Z}(\omega)$ and $\underset{\sim}{Y}(\omega)$ matrices are symmetric per-unit-length impedance and admittance matrices, respectively, and can be decomposed into the following matrices:

$$\underset{\sim}{Z}(\omega) = \underset{\sim}{R}_e(\omega) + j\omega\,(\underset{\sim}{L}_e(\omega) + \underset{\sim}{L}) \tag{3}$$

$$\underset{\sim}{Y}(\omega) = j\omega\,\underset{\sim}{C} \tag{4}$$

where each matrix is real and symmetric. $\underset{\sim}{R}_e(\omega)$ and $\underset{\sim}{L}_e(\omega)$ represent the losses introduced by an imperfect (lossy) ground return. $\underset{\sim}{L}$ and $\underset{\sim}{C}$ are independent of frequency and are the per-unit-length external inductance and capacitance matrices, respectively, for a lossless homogeneous medium with perfect earth return and lossless conductors. The $\underset{\sim}{R}_e(\omega)$ and $\underset{\sim}{L}_e(\omega)$ terms are obtained using Carson's Formulas [6] as shown in Appendix C.

Finally, the terms $\underline{V}_s(x)$ and $\underline{I}_s(x)$ are the distributed sources along the line induced by the spectral components of the incident field and are given by:

$$[\underline{V}_s(x)]_i = j\omega\mu \int_o^{d_{io}} [\underline{H}_z^{inc}(y,x)]_i \, dy \tag{5}$$

$$[\underline{I}_s(x)]_i = -\underline{Y} \int_o^{d_{io}} [\underline{E}_y^{inc}(y,x)]_i \, dy \tag{6}$$

The lumped circuit model describing the TEM mode of propagation for an incremental (Δx) section of any multiconductor line in a homogeneous medium is shown in Figure 10. Since the ungrounded line is uniform, all of the Δx length models of the line will be identical.

In Figure 10, the voltage and current at the input end of the Δx section of line are $\underline{V}_i(x)$ and $\underline{I}_i(x)$, respectively. The output voltage and current are represented by $\underline{V}_i(x + \Delta x)$ and $\underline{I}_i(x + \Delta x)$, respectively. The shunt capacitance terms c_{ij}, c_{ii}, c_{jj}, account for the mutual capacitance between the conductors and the ground, and the mutual inductances between conductors are denoted by ℓ_{ij}, ℓ_{jj}. The effects of the incident field are accounted for by the $\underline{V}_s(x)$ and $\underline{I}_s(x)$ terms, where they are distributed sources along the line induced by the incident field. The $\underline{Z}_{ci}(\omega)$ and $\underline{Z}_{cj}(\omega)$ terms represent the losses introduced by an imperfect earth return. The earth loss term, $\underline{Z}_e(\omega)$, can be written as

$$z_e(\omega) = r_e(\omega) + j\omega\ell_e(\omega) \tag{7}$$

where $r_e(\omega)$ is the real part of the earth-correction term and $\ell_e(\omega)$ is the imaginary part.

All parameters are per-unit-length quantities. Therefore, the total value of each parameter for a Δx length model in Figure 10 is the per-unit-length value multiplied by the section length, Δx.

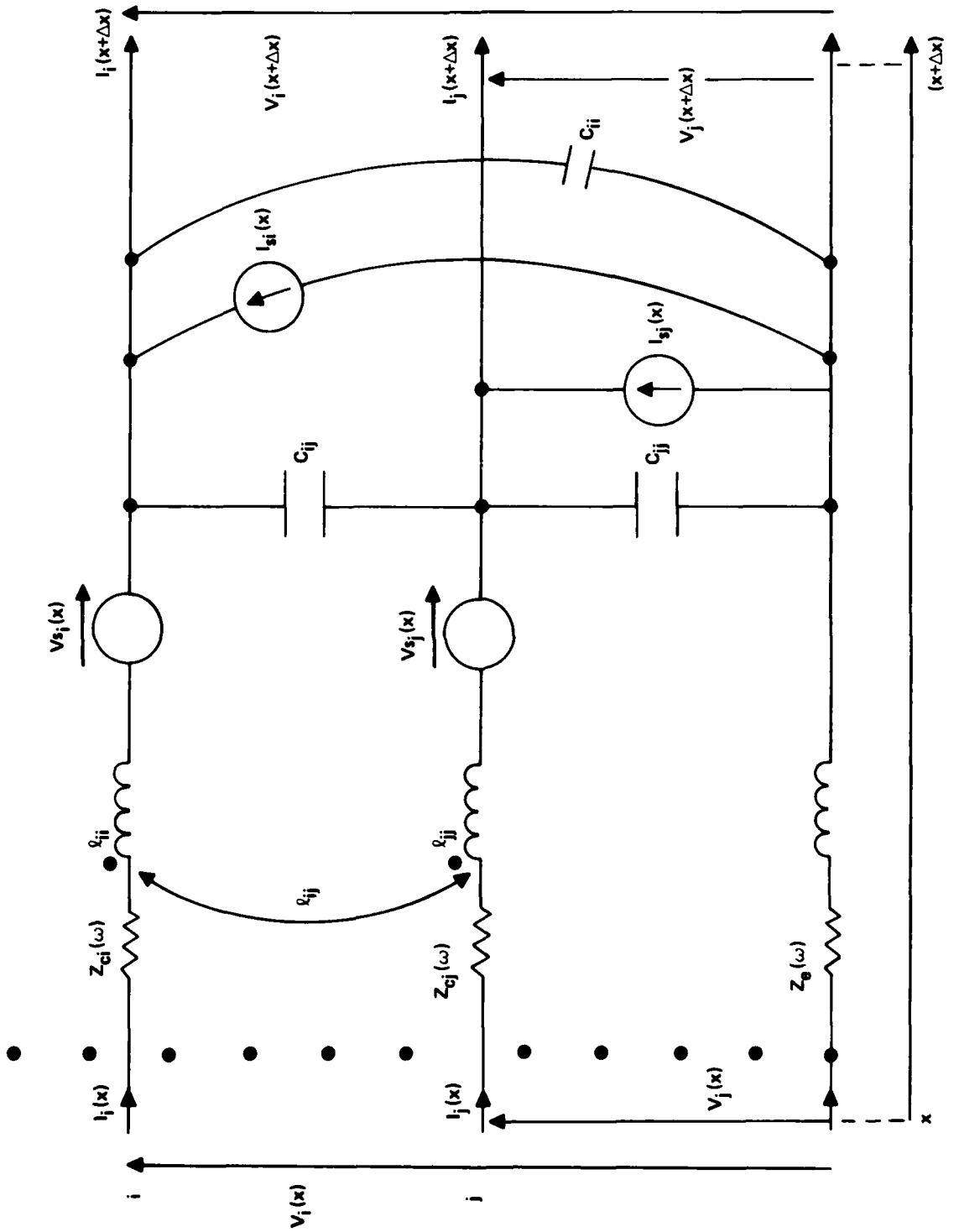

Figure 10. Equivalent circuit of a segment of a grounded multiconductor transmission line in an incident field.

The per-unit-length external inductance matrix for solid, round conductors can be approximated by

$$[L]_{ii} = \frac{\mu_o}{2\pi} \ln\left[\left(\frac{2H_i}{r_{\omega i}}\right)\right] \quad H/m \tag{8}$$

$$[L]_{ij} = \frac{\mu_o}{2\pi} \ln\left[\frac{(D_{ij}^2 + 4H_iH_j)^{1/2}}{D_{ij}}\right] \quad H/m \tag{9}$$

where D_{ij} is the center to center separation of the conductors, H_i is the height of the i^{th} conductor, and r_{wi} is the radius of the i^{th} conductor. It is well known for the case of a homogeneous, free space medium with perfect earth return and lossless conductors that

$$\underset{\sim}{C}\underset{\sim}{L} = \underset{\sim}{L}\ \underset{\sim}{C} = \mu_o\varepsilon_o\underset{\sim}{1}_n \tag{10}$$

thus the per-unit-length external capacitance matrix can be found by

$$\underset{\sim}{C} = \mu_o\varepsilon_o\underset{\sim}{L}^{-1} \tag{11}$$

where the inverse of the matrix $\underset{\sim}{M}$ is denoted by $\underset{\sim}{M}^{-1}$.

Equations (1) and (2) can be rewritten in matrix form as follows:

$$\begin{bmatrix} \frac{\partial \underline{V}(x)}{\partial x} \\ \frac{\partial \underline{I}(x)}{\partial X} \end{bmatrix} = \begin{bmatrix} \underset{n\sim n}{0} & \underset{\sim}{Z} \\ \underline{Y} & \underset{n\sim n}{0} \end{bmatrix} \begin{bmatrix} \underline{\ }(x) \\ \underline{1}\ (x) \end{bmatrix} + \begin{bmatrix} \underline{V}_s\ (x) \\ \underline{I}_s\ (x) \end{bmatrix} \tag{12}$$

where $_n0_n$ is a n x n matrix with zeros in every position.

The set of 2n first-order, complex-valued, ordinary differential equations in Equation (12) are in the form of state variable equations [7]. The solution to this equation which describes the TEM mode of propagation in the transmission line is

$$\begin{bmatrix} \underline{V}(x) \\ \underline{I}(x) \end{bmatrix} = \underset{\sim}{\Phi}(x,x_o) \begin{bmatrix} \underline{V}(x_o) \\ \underline{I}(x_o) \end{bmatrix} + \int_{x_o}^{x} \underset{\sim}{\Phi}(x,\hat{x}) \begin{bmatrix} \underline{V}_s(\hat{x}) \\ \underline{I}_s(\hat{x}) \end{bmatrix} d\hat{x} \quad (13)$$

where $\underset{\sim}{\Phi}(x,x_o)$ is the 2n x 2n complex-valued state transition matrix that is the solution to Equations (1) and (2) when $\underline{V}_s = \underline{I}_s = \underline{0}_n$ and x_o is an arbitrary fixed point along the line. If the line is "abruptly nonuniform," i.e., consists of uniform subsections cascaded together, then Equation (11) for a cascade of N sections becomes

$$\begin{bmatrix} \underline{V}(x_N) \\ \underline{I}(x_N) \end{bmatrix} = \left\{ \underset{\sim}{\Phi}_N(x_N,x_{N-1})\, \underset{\sim}{\Phi}_{N-1}(x_{N-1},x_{N-2}) \cdots \underset{\sim}{\Phi}_2(x_2,x_1) \underset{\sim}{\Phi}_1(x_1,x_0) \right\} \begin{bmatrix} \underline{V}(x_0) \\ \underline{I}(x_0) \end{bmatrix}$$

$$+ \sum_{i=1}^{N-1} \left\{ \underset{\sim}{\Phi}_N(x_N,x_{N-1}) \underset{\sim}{\Phi}_{N-1}(x_{N-1},x_{N-2}) \cdots \underset{\sim}{\Phi}_{i+1}(x_{i+1},x_i) \int_{x_{i-1}}^{x} \underset{\sim}{\Phi}_i(x_i,x) \right\} \begin{bmatrix} \underline{V}_{si}(\hat{x}) \\ \underline{I}_{si}(\hat{x}) \end{bmatrix} d\hat{x}$$

$$+ \int_{x_{N-1}}^{x_N} \underset{\sim}{\Phi}_N(x_N,\hat{x}) \begin{bmatrix} \underline{V}_{sN}(\hat{x}) \\ \underline{I}_{sN}(\hat{x}) \end{bmatrix} d\hat{x} \quad (14)$$

where each uniform section between $x = x_i$ and x_{i-1} is described by

$$\begin{bmatrix} \underline{V}(x_i) \\ \underline{I}(x_i) \end{bmatrix} = \underset{\sim}{\Phi}_i(x_i,x_{i-1}) \begin{bmatrix} \underline{V}(x_{i-1}) \\ \underline{I}(x_{i-1}) \end{bmatrix} + \int_{x_{i-1}}^{x_i} \underset{\sim}{\Phi}_i(x_i,\hat{x}) \begin{bmatrix} \underline{V}_{si}(\hat{x}) \\ \underline{I}_{si}(\hat{x}) \end{bmatrix} d\hat{x} \quad (15)$$

and $\underset{\sim}{\Phi}(x_n, x_o)$ is the overall chain parameter matrix for the cascade of line sections between $x = x_o$ and $x = x_n$. Lumped-element networks at discrete points along the line can also be incorporated by writing their chain parameter matrices and properly placing them in Equation (14). The lumped network shown in Figure 11 was used to model the down conductor and ground rod for the reasons given earlier. This network was placed between two uniform sections of transmission line to model the grounding of the line at various points as shown in Figure 12.

For the line between grounds, the transmission line is uniform and the per-unit-length impedance $\underset{\sim}{Z}(\omega)$ and admittance $\underset{\sim}{Y}(\omega)$ matrices are independent x. In these regions, the state transition matrix, $\underset{\sim}{\Phi}(x_i, x_{i-1})$, can be shown to be a function of only one variable, the difference quantity $(x_i - x_{i-1})$ [7] and thus the chain parameter matrix may be denoted as $\underset{\sim}{\Phi}(x_i - x_{i-1})$. In order to evaluate Equation (14), and thereby solving Equations (1) and (2), the chain parameter matrix $\underset{\sim}{\Phi}(x_i - x_{i-1})$, must be determined for each uniform line section. For multi-conductor lines, Equations (1) and (2) are strongly coupled differential equations, and therefore $\underset{\sim}{\Phi}(x_i, x_{i-1})$ may be found in the following manner: Assume that $\underline{V}_s(x)$ and $\underline{I}_s(x)$ are both zero, then differentiate Equation (2) with respect to x and substitute into Equation (1) to produce the following second order differential equation:

$$\ddot{\underline{I}}(x) = \underset{\sim}{Y}\,\underset{\sim}{Z}\,\underline{I}(x) \tag{16}$$

A solution to Equation (16) may be obtained by a similarity transformation. The particular transform to be used is "modal decomposition" [8]. To use this technique, define a change of variable, $\underline{I}(x) = \underset{\sim}{T}\,\underline{I}_m(x)$, where $\underset{\sim}{T}$ is a nonsingular, complex matrix and $\underline{I}_m(x)$ is a complex-valued vector of mode currents, and substitute into Equation (16) to obtain

$$\ddot{\underline{I}}_m(x) = \underset{\sim}{T}^{-1}\,\underset{\sim}{Y}\,\underset{\sim}{Z}\,\underset{\sim}{T}\,\underline{I}_m(x) \tag{17}$$

(The dots over the variable represent derivatives with respect to the variable in parentheses.)

$$L_w = \frac{\ell\mu}{2\pi} \ell n\left(\frac{2\ell}{a}\right) H$$

$$R_e = \frac{1}{2\pi\ell\sigma} \ell n\left(\frac{2\ell}{a}\right) \Omega$$

$$C_e = \frac{2\pi\epsilon\ell}{\ell n\left(\frac{2\ell}{a}\right)} F$$

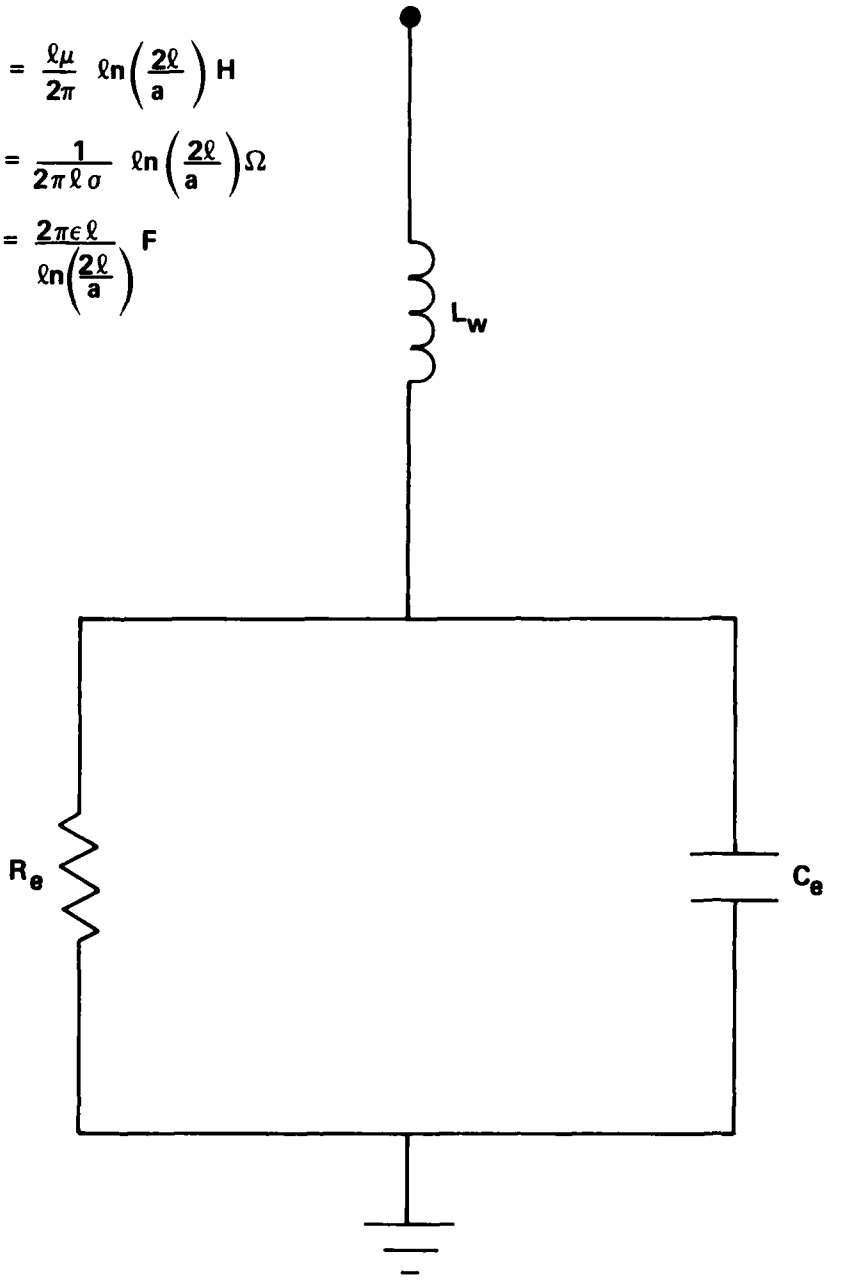

Figure 11. Equivalent circuit model of a ground rod and down conductor.

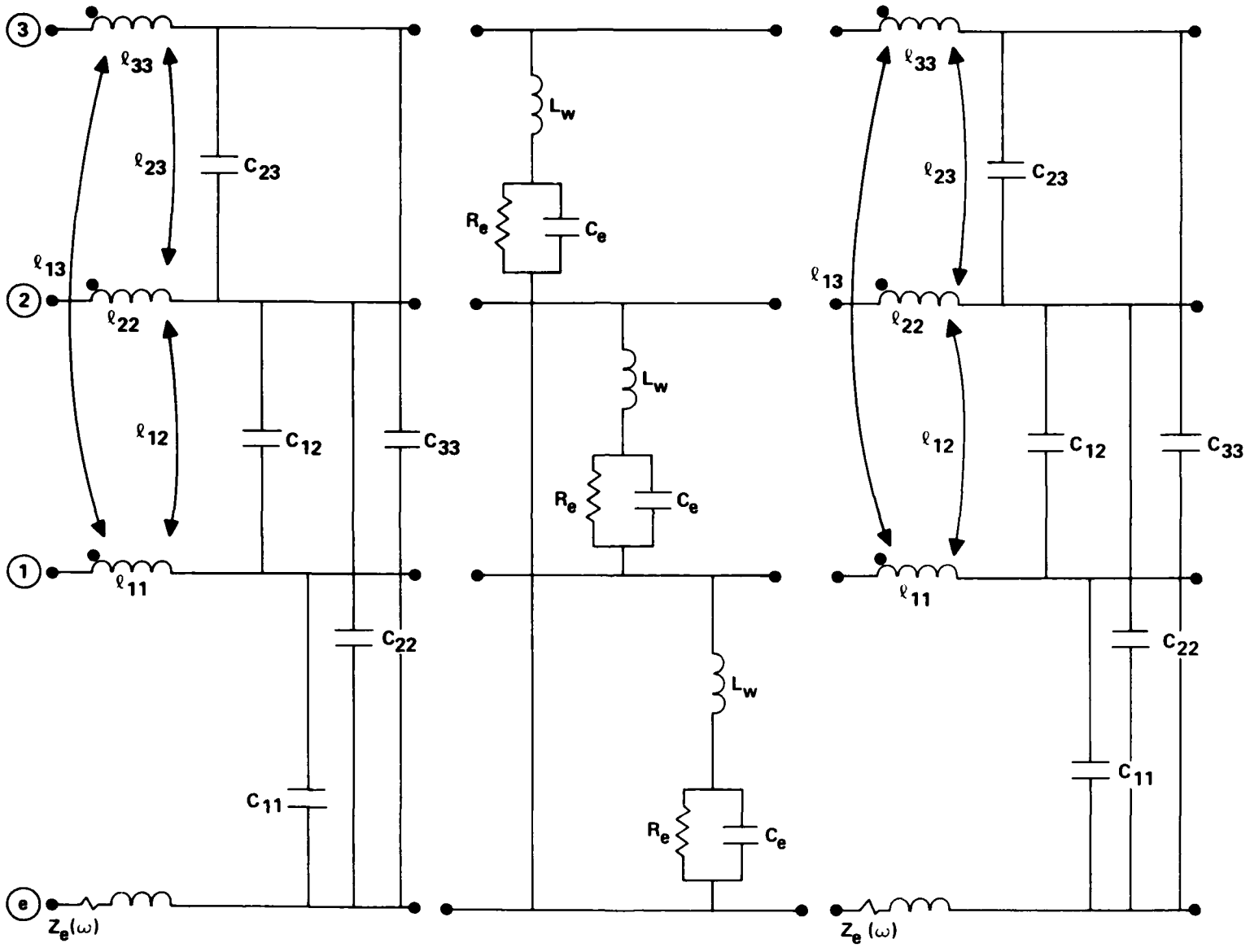

Figure 12. Grounded transmission line model segment.

Next, suppose that there exists a similarity transform, $\underset{\sim}{T}$, that diagonalizes the matrix product $\underset{\sim}{Y}\,\underset{\sim}{Z}$, i.e.,

$$\underset{\sim}{T}^{-1}\,\underset{\sim}{Y}\,\underset{\sim}{Z}\,\underset{\sim}{T} = \underset{\sim}{\gamma}^2 \tag{18}$$

where $\underset{\sim}{\gamma}^2$ is a diagonal matrix. In this case, Equation (17) becomes a set of N uncoupled differential equations with solutions

$$\underline{I}(x) = \underset{\sim}{T}\,\underline{I}_m(x) = \underset{\sim}{T}(e^{-\underset{\sim}{\gamma}x}\underline{I}^+ - e^{\underset{\sim}{\gamma}x}\underline{I}^-) \tag{19}$$

where $e^{\underset{\sim}{\gamma}x}$ is a diagonal matrix with

$$[e^{\underset{\sim}{\gamma}x}]_{ii} = e^{\gamma_i x} \tag{20}$$

$$[e^{\underset{\sim}{\gamma}x}]_{ij} \underset{i\neq j}{=} 0 \tag{21}$$

$\underline{I}^+$ and $\underline{I}^-$ are vectors of complex undetermined constants. These constants will be determined by considering the termination networks of the ends of the line. Since from Equations (1) and (2), $I(x) = -Y\,V(x)$, the voltage may be determined by

$$\begin{aligned}\underline{V}(x) &= -\underset{\sim}{Y}^{-1}\underline{I}(x)\\ &= \underset{\sim}{Y}^{-1}\,\underset{\sim}{T}\,\underset{\sim}{\gamma}(e^{-\underset{\sim}{\gamma}x}\underline{I}^+ + e^{\underset{\sim}{\gamma}x}\underline{I}^-)\\ &= \underset{\sim}{Y}^{-1}\,\underset{\sim}{T}\,\underset{\sim}{\gamma}\,\underset{\sim}{T}^{-1}\{\underset{\sim}{T}(e^{-\underset{\sim}{\gamma}x}\underline{I}^+ + e^{\underset{\sim}{\gamma}x}\underline{I}^-)\}\\ &= \underset{\sim}{Z}\,\underset{\sim}{T}\,\underset{\sim}{\gamma}^{-1}\,\underset{\sim}{T}^{-1}\{\underset{\sim}{T}(e^{-\underset{\sim}{\gamma}x}\underline{I}^+ + e^{\underset{\sim}{\gamma}x}\underline{I}^-)\}\end{aligned} \tag{22}$$

where $\underset{\sim}{\gamma}$ is a diagonal complex-valued matrix with

$$\left[\underset{\sim}{\gamma}\right]_{ii} = \sqrt{\gamma_i^2} \tag{23}$$

$$\left[\underset{\sim}{\gamma}\right]_{ij} \underset{i\neq j}{=} 0 \tag{24}$$

The state transition matrix or chain parameter matrix $\underset{\sim}{\Phi}(x_i, x_{i-1})$ which relates voltages and currents at the two ends of a section of line, in Equation (15), can be obtained by eliminating $\underline{I}^+$ and $\underline{I}^-$ from Equations (19) and (22), yielding

$$\begin{bmatrix} \underline{V}\ (x_i) \\ I\ (x_i) \end{bmatrix} = \underset{\sim}{\Phi}\ (x_i, x_{i-1}) \begin{bmatrix} \underline{V}\ (x_{i-1}) \\ \underline{I}\ (x_{i-1}) \end{bmatrix}$$

$$= \begin{bmatrix} \underset{\sim}{\Phi}_{11}\ (x_i, x_{i-1}) & \underset{\sim}{\Phi}_{12}\ (x_i, x_{i-1}) \\ \underset{\sim}{\Phi}_{21}\ (x_i, x_{i-1}) & \underset{\sim}{\Phi}_{22}\ (x_i, x_{i-1}) \end{bmatrix} \begin{bmatrix} \underline{V}\ (x_{i-1}) \\ \underline{I}\ (x_{i-1}) \end{bmatrix} \tag{25}$$

where $\underset{\sim}{\Phi}_{ij}(x_i, x_{i-1})\ i$, $j = 1,2$ are given by

$$\underset{\sim}{\Phi}_{11}\ (x_i, x_{i-1}) = 1/2\ \underset{\sim}{Y}^{-1}\ \underset{\sim}{T}\ (e^{\underset{\sim}{\gamma}\ (x_i - x_{i-1})} + e^{-\underset{\sim}{\gamma}\ (x_i - x_{i-1})})\ \underset{\sim}{T}^{-1}\ \underset{\sim}{Y} \tag{26}$$

$$\underset{\sim}{\Phi}_{12}\ (x_i, x_{i-1}) = -\ 1/2\ \underset{\sim}{Y}^{-1}\ \underset{\sim}{T}\ \underset{\sim}{\gamma}\ (e^{\underset{\sim}{\gamma}(x_i - x_{i-1})} - e^{-\underset{\sim}{\gamma}\ (x_i - x_{i-1})})\ \underset{\sim}{T}^{-1} \tag{27}$$

$$\underset{\sim}{\Phi}_{21}\ (x_i, x_{i-1}) = -\ 1/2\ \underset{\sim}{T}\ (e^{\underset{\sim}{\gamma}(x_i - x_{i-1})} - e^{-\underset{\sim}{\gamma}\ (x_i - x_{i-1})})\ \underset{\sim}{\gamma}^{-1}\ \underset{\sim}{T}^{-1}\ \underset{\sim}{Y} \tag{28}$$

$$\Phi_{22}\ (x_i, x_{i-1}) = 1/2\ \underset{\sim}{T}\ (e^{\underset{\sim}{\gamma}\ (x_i - x_{i-1})} - e^{-\underset{\sim}{\gamma}(x_i - x_{i-1})})\ \underset{\sim}{T}^{-1} \tag{29}$$

(The details on the similarity transform matrix $\underset{\sim}{T}$ which diagonalizes the matrix product $\underset{\sim}{Y}\ \underset{\sim}{Z}$ given in Equations (3) and (4) can be found in Appendix D). Using the chain parameter matrices in Equation (13) with the $\underset{\sim}{\Phi}_{ij}$ defined in Equations (26) - (29), Equation (13) becomes

$$\begin{bmatrix} \underline{V}(L) \\ \underline{I}(L) \end{bmatrix} = \begin{bmatrix} \underline{\Phi}_{11}(L) & \underline{\Phi}_{12}(L) \\ \underline{\Phi}_{21}(L) & \underline{\Phi}_{22}(L) \end{bmatrix} \begin{bmatrix} \underline{V}(x_o) \\ I(x_o) \end{bmatrix} + \int_o^L \begin{bmatrix} \underline{\Phi}_{11}(L,\hat{x}) & \underline{\Phi}_{12}(L,\hat{x}) \\ \underline{\Phi}_{21}(L,\hat{x}) & \underline{\Phi}_{22}(L,\hat{x}) \end{bmatrix} \begin{bmatrix} \underline{V}_s(\hat{x}) \\ \underline{I}_s(\hat{x}) \end{bmatrix} d\hat{x} \qquad (30)$$

For multiconductor lines, the termination networks can be considered to be linear N-port networks and are characterizable by "Generalized Thevenin Equivalents" as

$$\underline{V}(0) = \underline{V}_o - \underline{\underline{Z}}_o \underline{I}(0) \qquad (31)$$

$$\underline{V}(L) = \underline{V}_L + \underline{\underline{Z}}_L \underline{I}(L) \qquad (32)$$

where $\underline{V}_o$ and $\underline{V}_i$ are complex-valued vectors of equivalent open-circuit port excitation voltages and $\underline{\underline{Z}}_o$ and $\underline{\underline{Z}}_L$ are complex-valued symmetric matrices which represent the termination network at the input and output of the line, respectively.

Expanding Equation (30) and substituting into Equations (31) and (32), the chain parameter matrix formulation incorporating the incident electromagnetic fields becomes the algorithm for the External Collector Assessment Model (ECAM):

$$\left[\underline{\underline{Z}}_L \underline{\Phi}_{22}(L) - \underline{\underline{Z}}_L \underline{\Phi}_{21}(L) \underline{\underline{Z}}_o + \Phi_{11}(L) \underline{\underline{Z}}_o\right] \underline{I}(0)$$

$$= \left[\underline{\Phi}_{11}(L) - \underline{\underline{Z}}_L \underline{\Phi}_{21}(L)\right] \underline{V}(0) - \hat{\underline{V}}_s(L) - \underline{\underline{Z}}_L \hat{\underline{I}}_s(L) \qquad (33)$$

$$\underline{I}(L) = \underline{\Phi}_{21}(L) \underline{V}_o + \left[\underline{\Phi}_{22}(L) - \underline{\Phi}_{21}(L) \underline{\underline{Z}}_o\right] \underline{I}(0) + \hat{\underline{I}}_s(L) \qquad (34)$$

where

$$\hat{\underline{V}}_s(L) = \int_0^L \underline{\Phi}_{11}(L,\hat{x})\,\underline{V}_s(\hat{x}) + \underline{\Phi}_{12}(L,\hat{x})\,\underline{I}_s(\hat{x})\;\; d\hat{x} \tag{35}$$

$$\hat{\underline{I}}_s(L) = \int_0^I \underline{\Phi}_{21}(L,\hat{x})\,\underline{V}_s(\hat{x}) + \underline{\Phi}_{22}(L,\hat{x})\,\underline{I}_s(\hat{x})\;\; d\hat{x} \tag{36}$$

(See Appendix E for details on the calculation of $\hat{\underline{V}}_s(L)$ and $\hat{\underline{I}}_s(L)$.

To use ECAM to calculate the current at the output termination of a multiconductor transmission line excited by an incident field, first determine $\underline{I}(0)$ in Equation (33) and substitute into Equation (34) and solve for $\underline{I}(L)$. Thus, at each frequency given by Filon's decomposition of the EMP, the termination current may now be determined. Upon determination of these various currents, the time domain representation of the termination current is calculated by performing the inverse Fourier transform with Filon's method.

2.3 USE OF ECAM TO EVALUATE THE EFFECTS OF SUPPLEMENTAL GROUNDS ON EXTERNAL COLLECTORS

ECAM was programmed on a VAX 11/780 computer. (Special care was taken to check out each separate section of the program because no data existed against which program results could be compared.) Initial verification runs of the behavior of a transmission line over a perfect ground plane were promising in terms of the relative peak currents and the late time (trailing edge) response. Early time (leading edge) induced pulse shapes were incorrect, however. Subsequent refinement in the frequency-to-time domain conversion process yielded plausible pulse shapes. To illustrate, Figure 13 compares the time response produced by ECAM (upper graph) with those reported by others [9]. The results agree closely both in relative magnitudes and in general waveshape.

Several test cases were run and the results examined. Figure 14(a) shows the computed current response of a 50 m line over a perfectly conducting ground plane short circuited at both ends, while Figure 14(b) shows the response of the same line over a lossy ground plane. It can be seen from these two figures that the current induced in the line is greater over a lossy ground plane than over a perfect ground plane; this effect can be attributed to the influence of reflections from the imperfect ground plane.

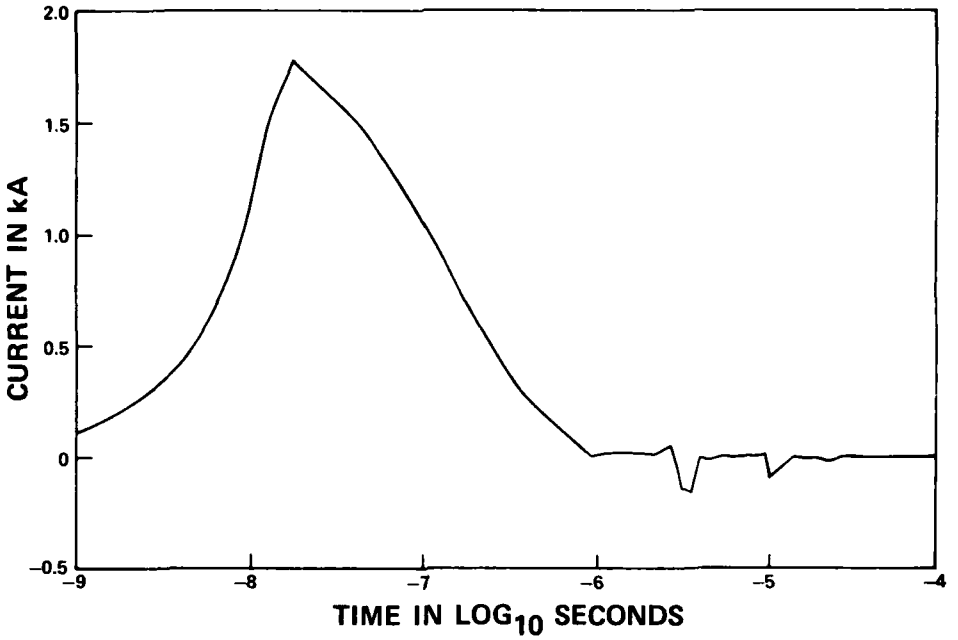

(a) ECAM RESULTS.

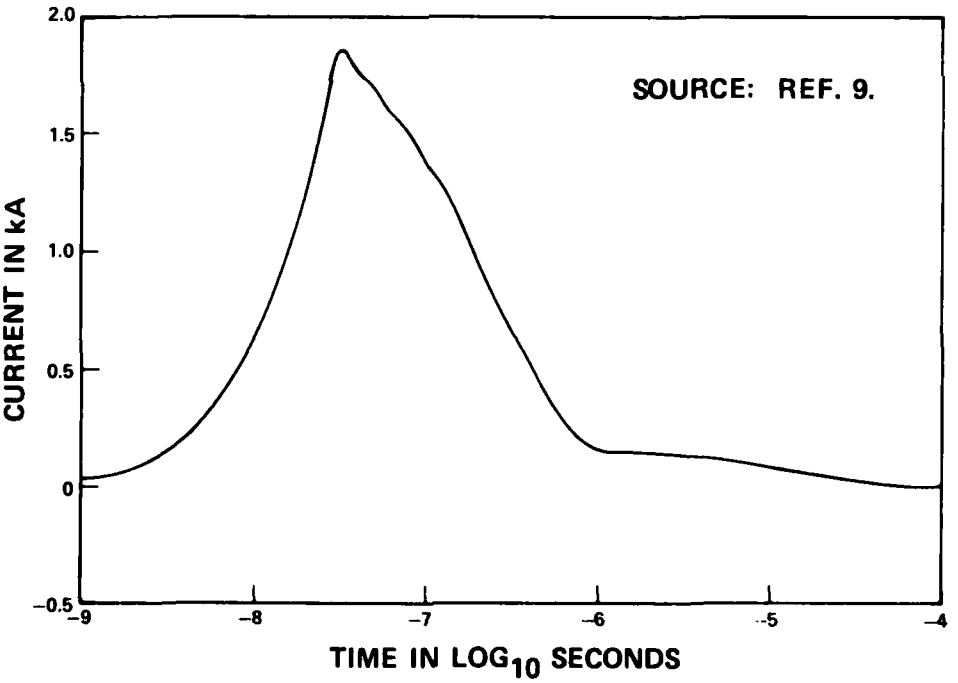

(b) MARABLE, et al., RESULTS.

Figure 13. Comparative results of computed induced currents for an infinitely long wire, 10 meters high.

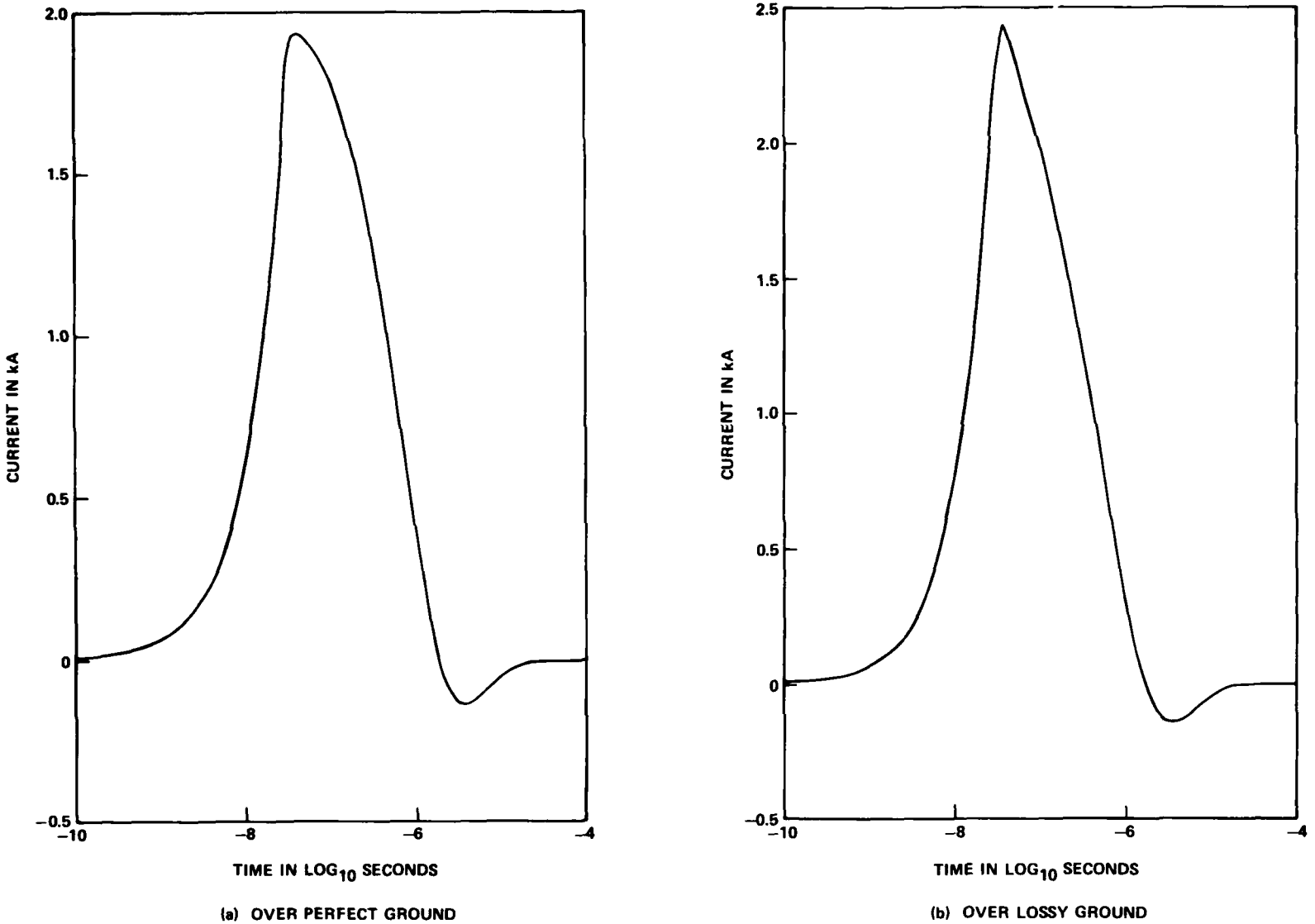

Figure 14. Computed EMP current response of a 50 meter line short circuited at both ends.

Figure 15(a) shows the response of a 50 m line over a lossy ground with a short circuit at the output and a 100 ohm input, while Figure 15(b) shows the same line with an additional ground point at the center. For this case, the additional ground has no effect on the induced current pulse amplitude and only slightly alters the pulse shape.

Figures 16(a) and 16(b) compare the responses of a 10 m long line with that of a 500 m line, both over lossy ground with 100 ohms input impedance and short circuited at the output. It can be seen that a slight increase in pulse current amplitude does occur in going from 10 m to 500 m in length.

Next, the peak amplitudes of the induced currents were determined for several conditions of line length, height above ground, and number of grounding points. For each condition examined, line parameters of wire radius, input impedance and output impedance were maintained constant at 200 mils, 100 ohms and 500 ohms, respectively. Figure 17 shows the behavior of peak pulse amplitude as a function of transmission line length. (For this series of calculations, no ground connections were assumed.) Note that for this particular case of a 10 meter high line over a lossy ground the peak current increases rapidly with length up to about 50 meters. (Figure 18 shows the detailed behavior below 50 m.) Beyond 50 m (and up to 1000 m), the peak current remains in the vicinity of 1200 A except for an additional rise of 300A at approximately 500 m. (This "peak" is probably related to a pseudo-resonant length of the transmission line.)

Figure 19(a) shows the impact of a number of ground points equally spaced over a 50 meter length of line at various line heights from 1 meter to 15 meters. It can be observed from this figure that the effects of supplemental grounds are more pronounced as the height of the line above the earth increases. Figure 19(b) details the effects on peak induced current from increasing the number of grounding points on the 50 m long, 10 m high line. A reduction in peak current of approximately 2:1 is achieved in going from 0 grounds to 50 grounds.

Figure 20 shows the influence of a fixed number of grounding points evenly distributed over varying lengths of lines. The behavior of the 10 meter long line (height also equal to 10 meters) implies that grounding points 1 meter apart (10 meters long divided by 10 grounding points) may be required to make a noticable impact on the amplitude of the EMP-induced current. Specifically, Figure 21 shows the behavior of the induced peak current with various numbers of grounds uniformly distributed over a 50 meter length. Notice that 50 grounds 1 meter apart produce a 53 percent reduction in the peak current amplitude induced on the line with 5

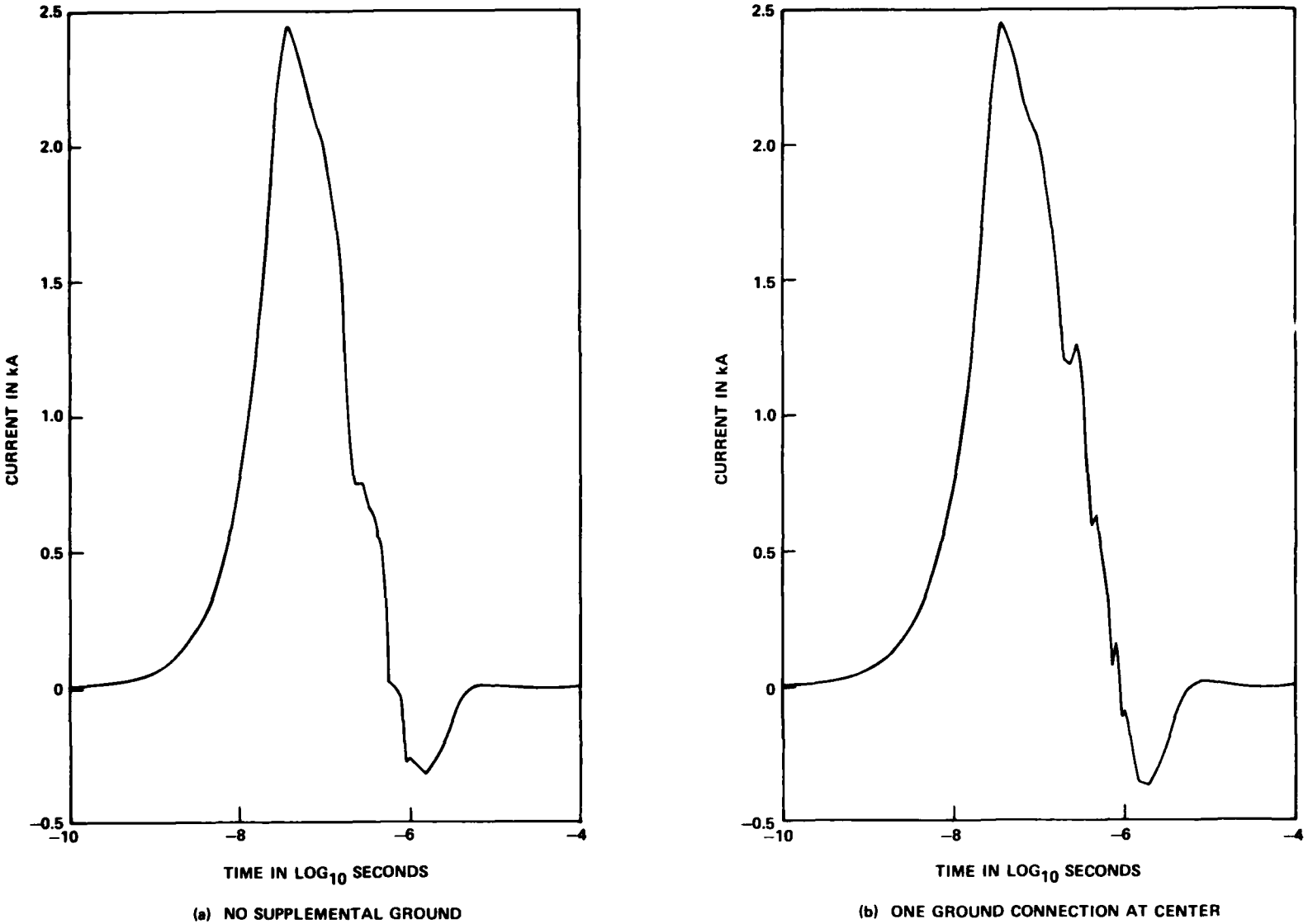

Figure 15. Computed EMP current response of a 50 meter line over lossy ground (line input terminated in 100 ohms and output short circuited).

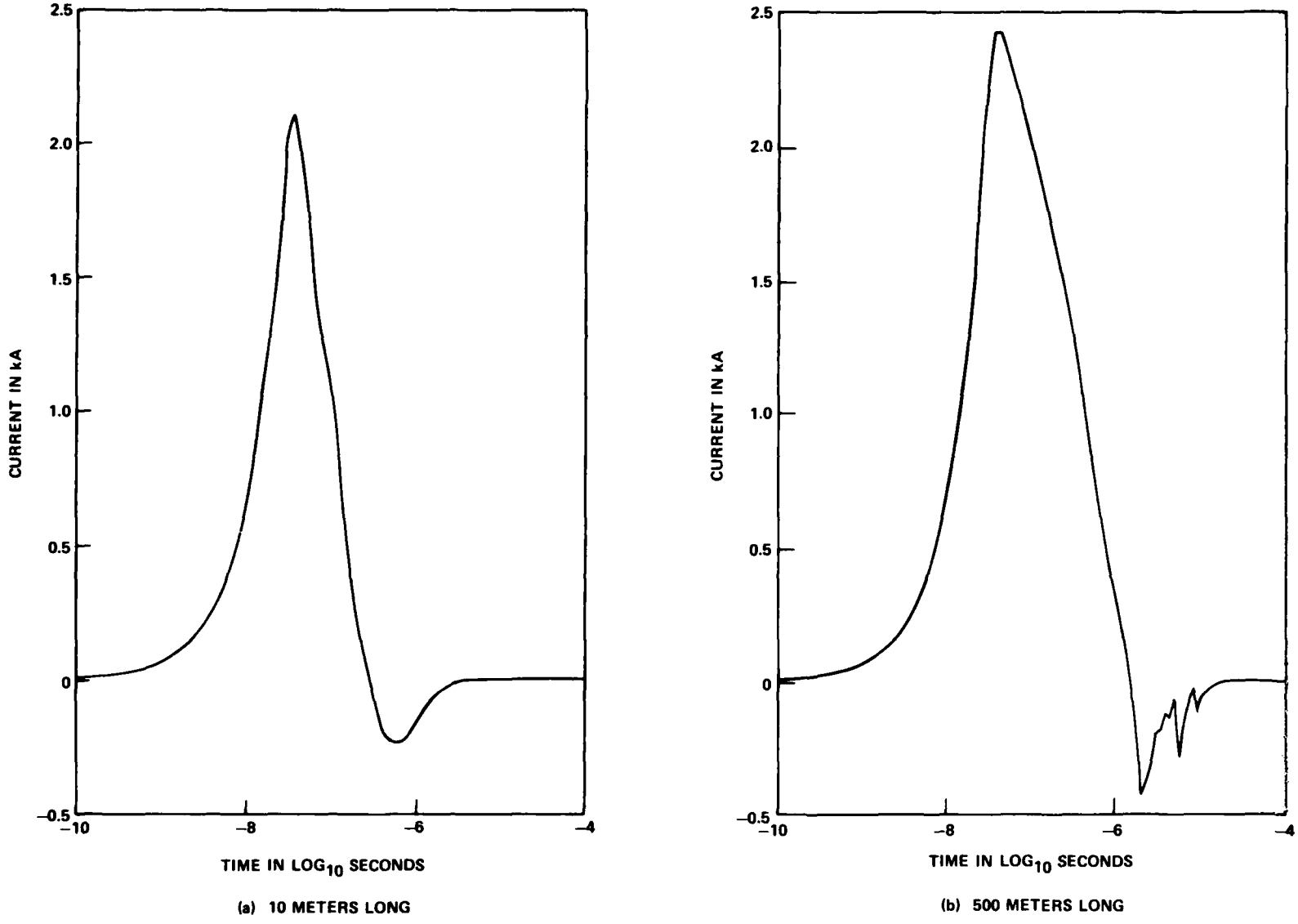

Figure 16. Computed EMP current response of two lengths of line over lossy ground (line input terminated in 100 ohms and output short circuited).

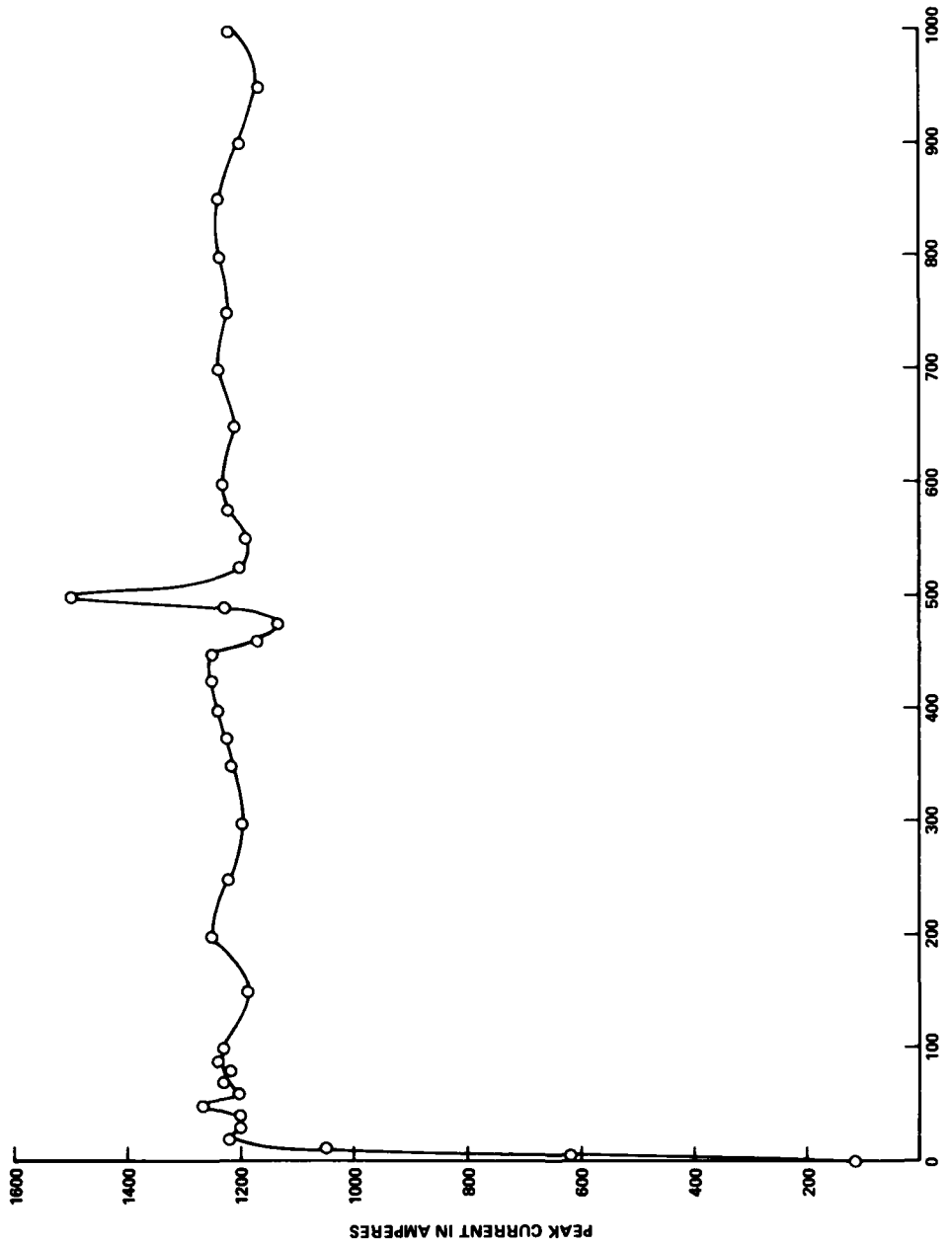

Figure 17. Peak EMP-induced current as a function of line length (no supplemental grounds).

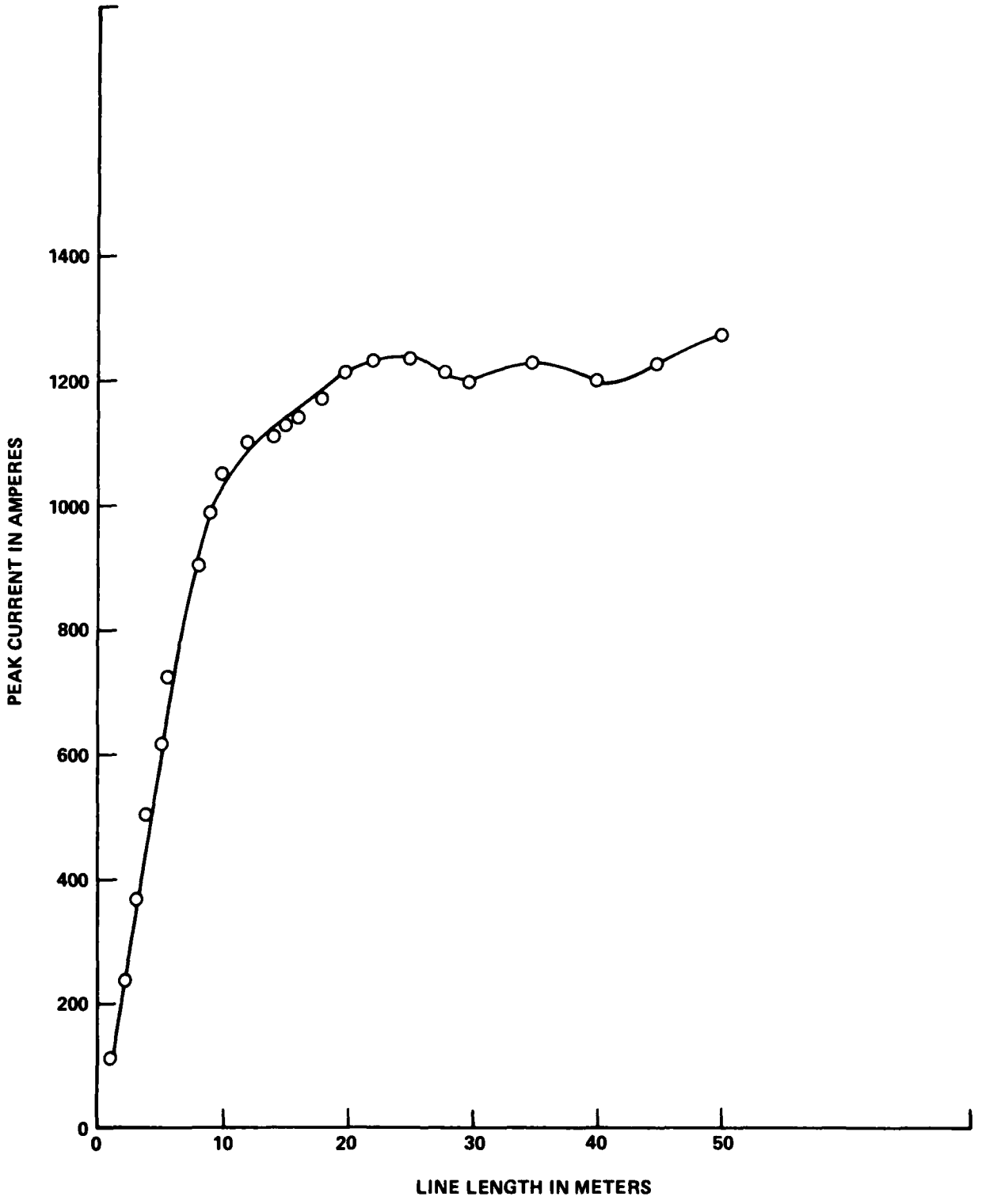

Figure 18. Details of 0-50 meter portion of Figure 17.

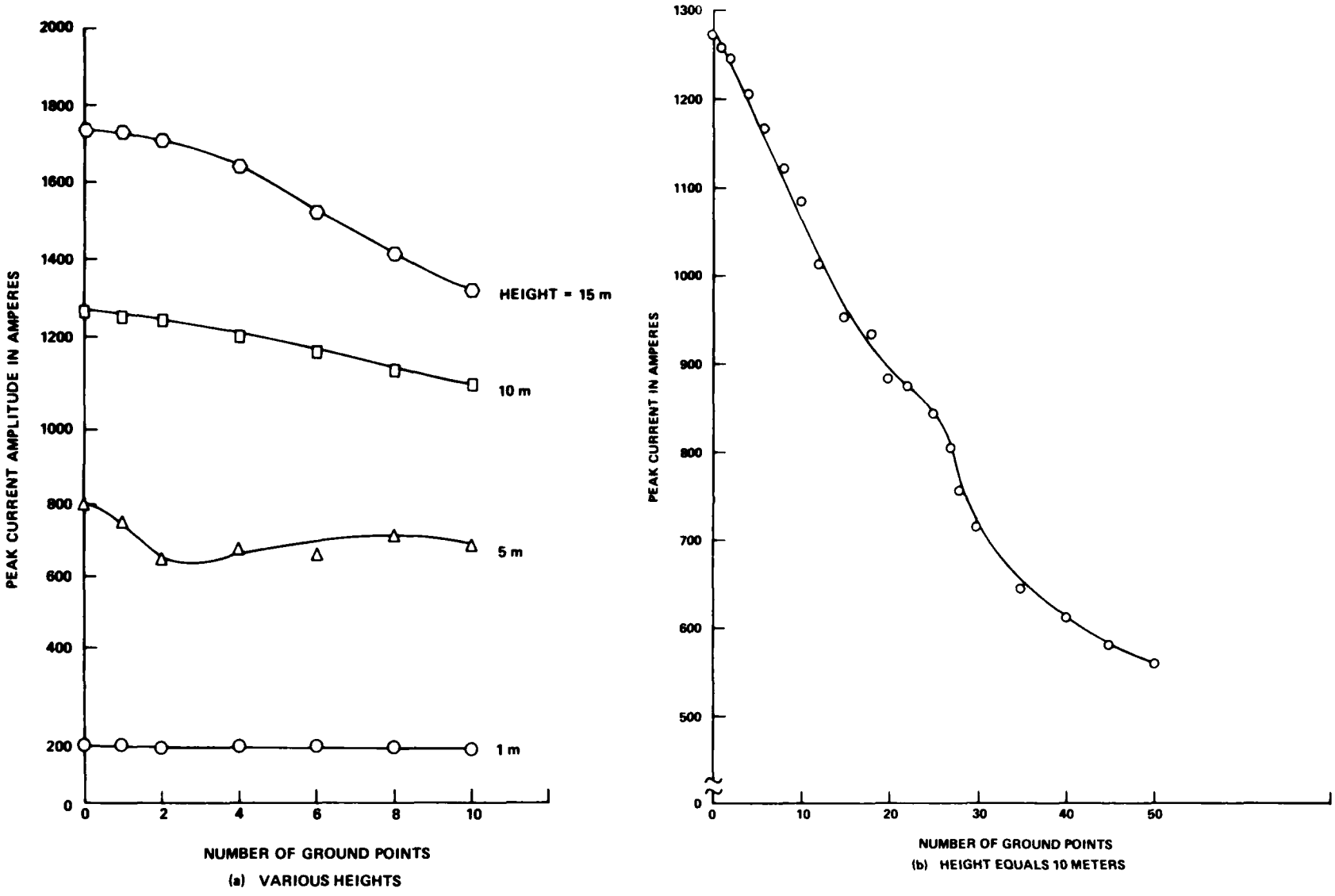

Figure 19. Peak EMP-induced current as a function of number of supplemental grounds on a 50 meter line.

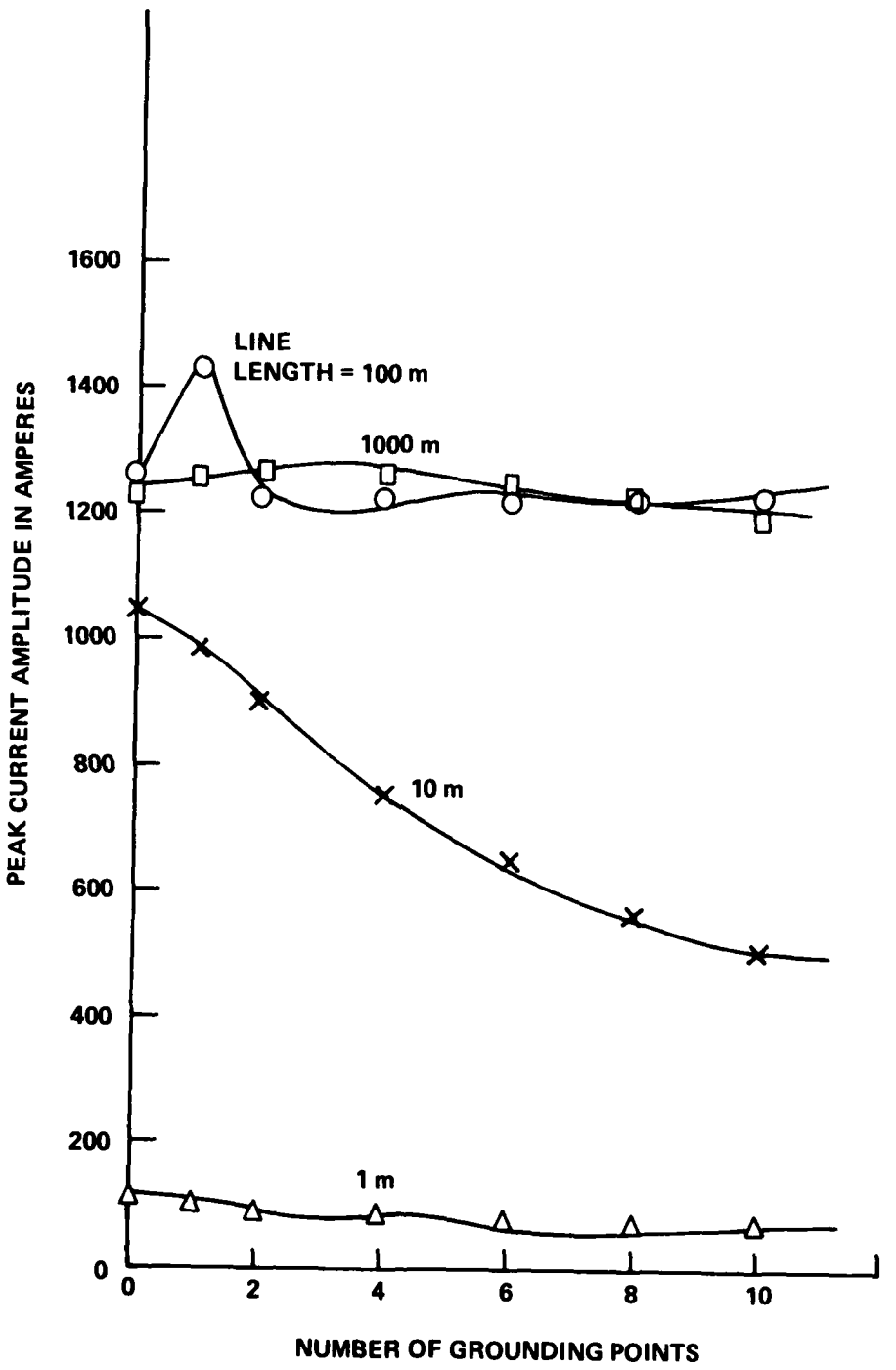

Figure 20. Peak EMP-induced current as a function of number of supplemental grounds for various lengths of transmission line.

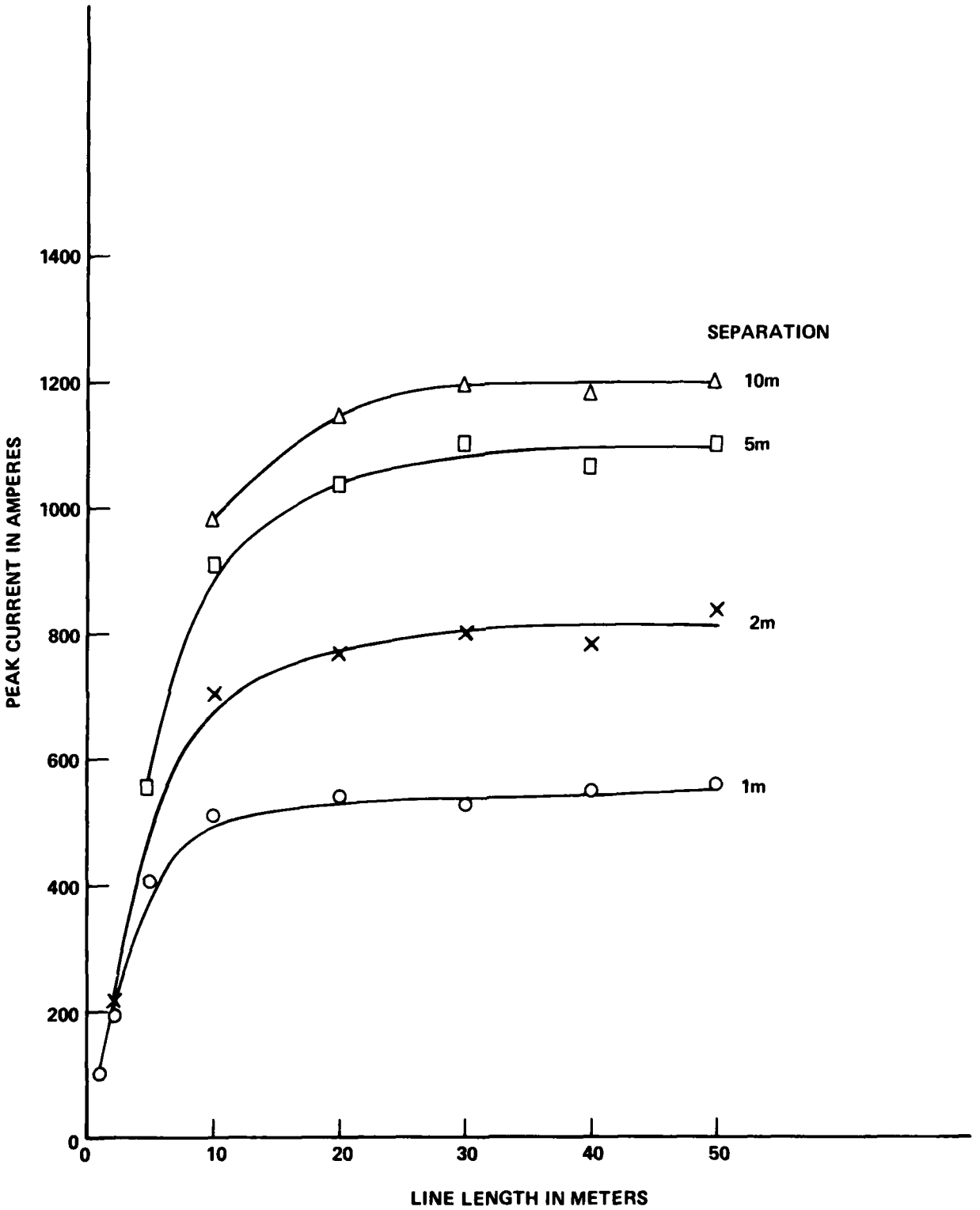

Figure 21. Peak EMP-induced current as a function of uniformly distributed grounds.

grounds 10 meters apart. Figure 22 extends this evaluation to consider the effects of realistically separated grounding points on longer lines. Ground connections separated by 10 meters and 20 meters over a 350 meter length and a 500 meter length, respectively, are compared in this figure. Note that the differences in the peak induced current levels are less than 10 percent for lengths greater than 50 meters.

These results imply that control of the EMP-related current on external collectors at the facility penetration point is most receptive to the installation of supplemental grounds within the first 50 meter portion of the line adjacent to the facility. They suggest that the penetrations of long, overhead collectors (power lines, signal lines, etc.,) should be handled in the manner illustrated in Figures 23 and 24. Figure 23 shows the implied manner of treating a power line penetration. The essential features of this method are:

- o The physical entrance point is located some 30 to 50 m from the main facility.
- o The power transformer is enclosed in a solid metal shield (which could be the intrinsic housing).
- o Power conductor routing from the transformer to the facility is inside buried solid metal conduit/pipe. Initimate contact between the conduit and the soil should be maintained throughout its length. The facility's shielding boundary is continued to the remote entrance point via the metallic conduit and transformer enclosure.
- o A low impedance ground (preferably a grid or counterpoise) should be provided for the transformer.
- o The cable conduit should be well bonded to the transformer and building grounding networks.
- o Surge arrestors appropriate for lightning and EMP should be provided on the primary and secondary sides of the transformer.

Figure 24 shows a similar treatment for signal line entrances. Installation principles are the same as for power line penetrations. Effective lightning and EMP protection including surge arrestors along with inductive and capacitive filters must be applied to each collector.

In summary, the preliminary results of the external EMP collector analysis effort indicate that:

(1) A direct relationship between induced current amplitude and line length holds only up to lengths of 50 m or so. Beyond 50 m, only secondary relationships with length were observed.

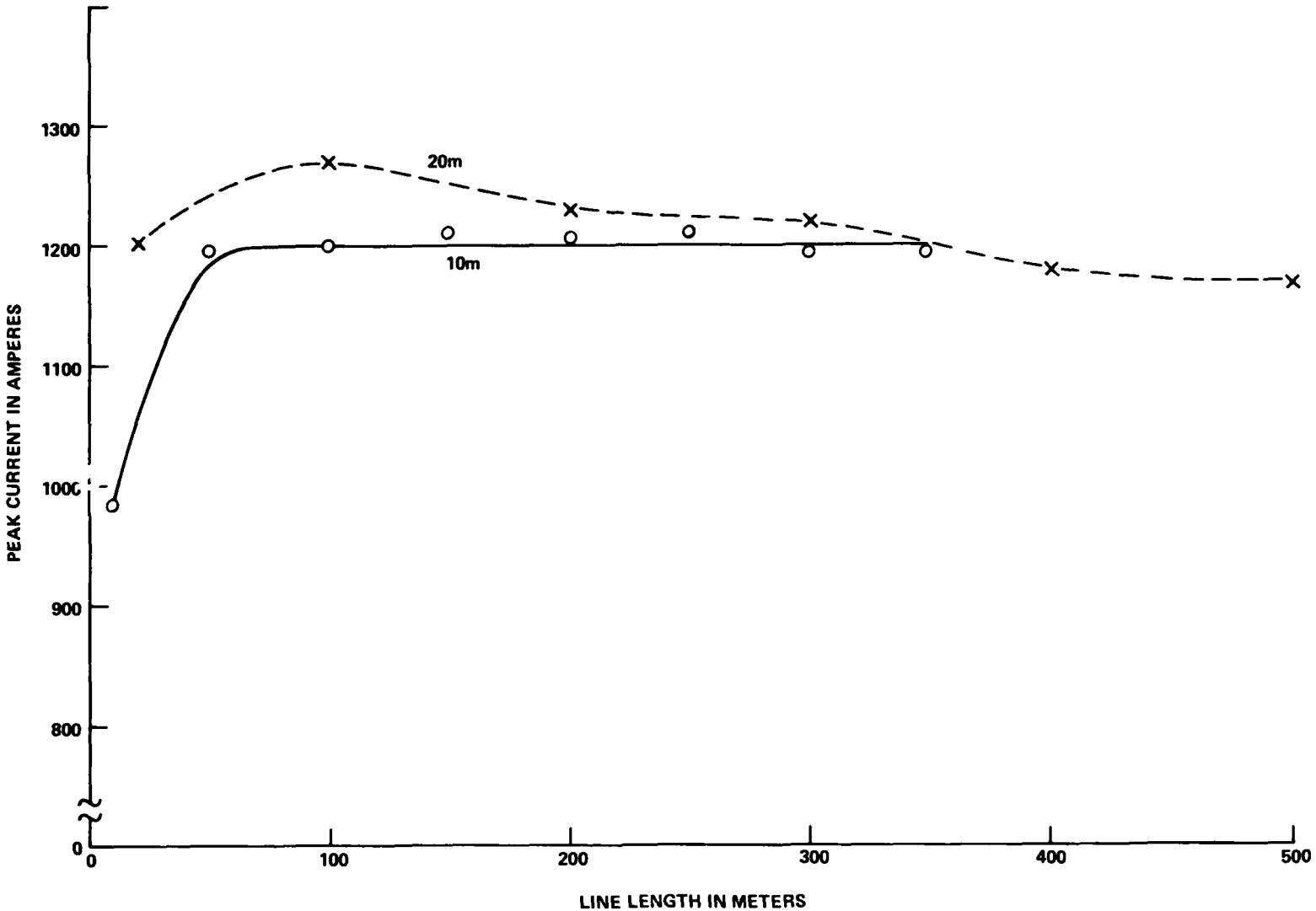

Figure 22. Peak EMP-induced current versus line length for uniformly spaced supplemental grounds.

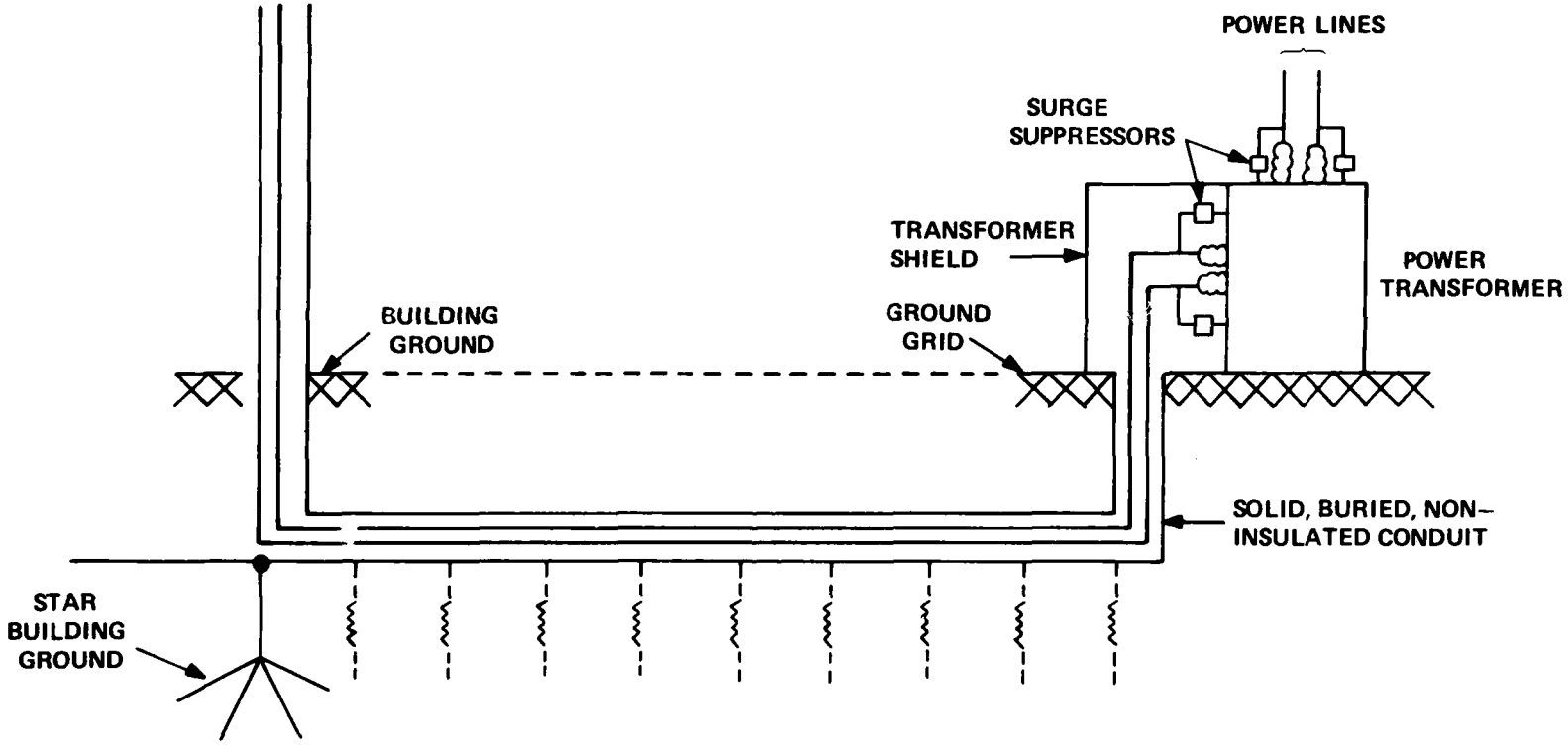

Figure 23. Candidate power line penetration treatment.

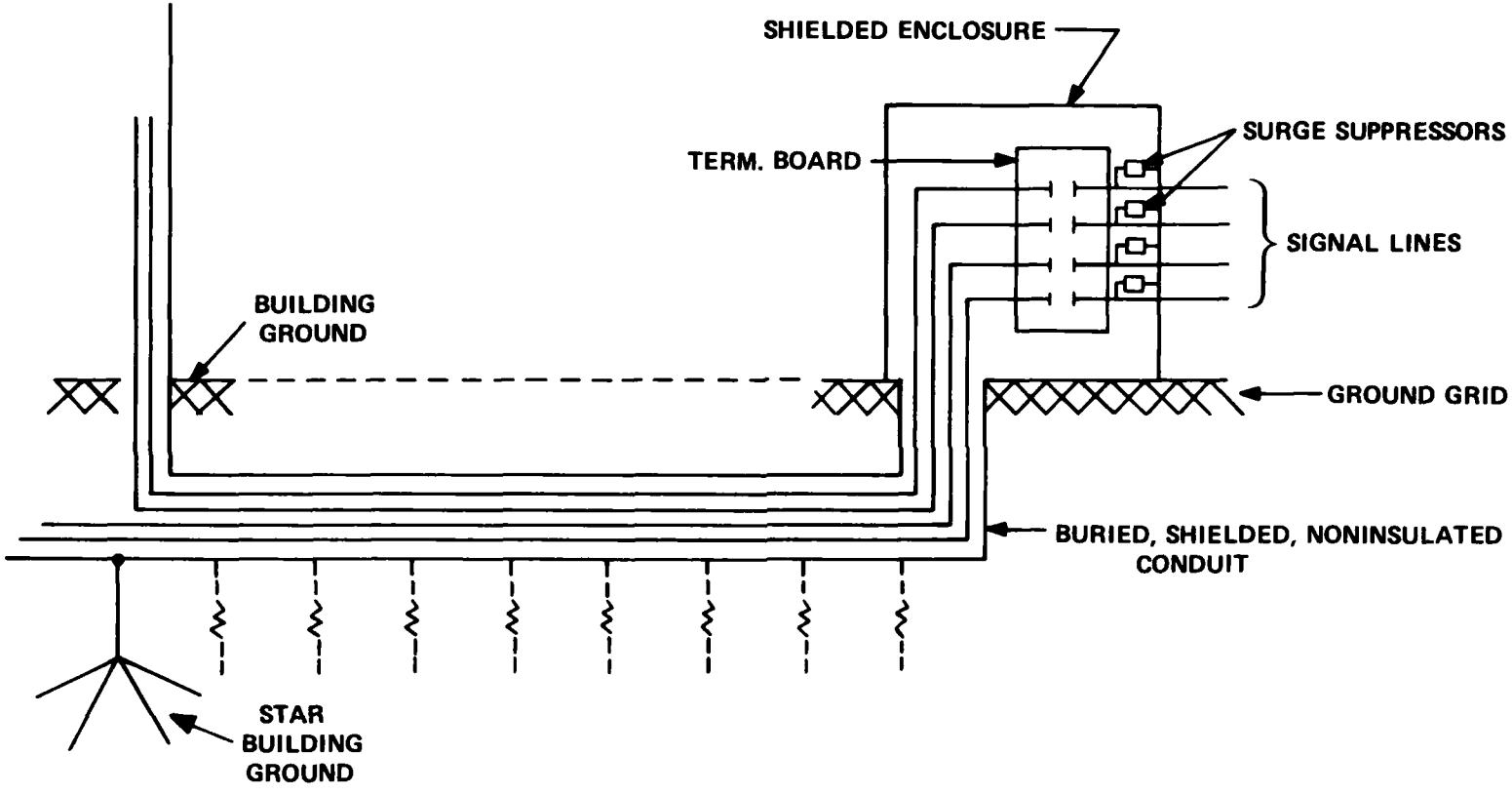

Figure 24. Candidate signal line penetration treatment.

(2) Except possibly for short line lengths, multiple grounds exhibit only a secondary influence on the level of EMP pickup by overhead power lines.

(3) Remote locations of external collector penetrations into a protected facility may be desirable.

III. INTERNAL COLLECTOR INVESTIGATION

3.1 INTRODUCTION

Protection against failure due to EMP-induced currents only on external collectors leading into the structure may not be sufficient. The building itself, with its internal wiring, can also act as a collector of EMP-induced currents. These currents can inductively couple to sensitive equipment with sufficient magnitude to lead to failure or upset. Indeed, the internally-produced currents could (a) be of much greater magnitude than those induced externally so that the external sources are of lesser significance, (b) be of such magnitude that the total effect of the external and internal collectors must be considered, or (c) be of insignificant magnitude.

The EMP pickup of internal collectors versus that of external collectors was addressed because extensive efforts may be applied to the formulation and implementation of hardening measures for external collectors only to find that the levels of EMP-related energy appearing at equipment terminals from pickup by internal collectors are greater than those from external collectors, even without hardening. The relative severity of the EMP threat from external collectors versus that from internal collectors is of particular concern to many types of facilities. Those types of facilities that do not normally incorporate an intrinsic metal shield as part of their construction pose a unique challenge. This is not to say that the typical "unshielded" structures provide no protection whatsoever. In fact, considerable experience exists to show that normal commercial/industrial buildings do attenuate those radio frequency signals which fall within the EMP spectrum. Thus, even without the presence of a solid metal shield, internal collectors in most facilities can expect to enjoy some protection from an EMP. Unfortunately, the extent of this protection cannot yet be quantified. Such quantification is necessary for effective utilization of the "zonal" approach to hardening [10], [11]. Zonal hardening depends upon certain degrees of protection being assignable to particular barriers. Thus, two major reasons for seeking to gain a greater understanding of the EMP response of internal collectors are:

(1) To examine the relative pickup between internal and external collectors in order to see where suppression emphasis needs to be placed, and

(2) To quantify the relative protection offered by the intrinsic facility.

For these reasons, a preliminary investigation into the problem of EMP coupling to internal collectors was conducted. This investigation employed both an analytical effort and an experimental effort. The analytical effort sought to evaluate the EMP response of a straight conductor inside a simplified array* of conductors with the aid of an existing computer model based on the method of moments technique. The experimental effort focused on measuring the shielding effectiveness of two available structures at selected frequencies within the EMP spectrum.

3.2 ANALYTICAL ASSESSMENT OF INTERNAL COLLECTOR COUPLING

A search of the literature produced two computer models seemingly applicable to the analysis of EMP coupling to internal collectors. These two models are:

(1) Time Domain Electromagnetic Response of Thin Wire Structures (TWTD) [12], and

(2) Three Dimensional EMP Time-Domain Finite Difference Code (THREDE) [13]

The first of these was chosen for use because it had been reportedly applied to the analysis of large structures [12], was readily obtainable, and was compatible with available computers (a DEC VAX 11/780 and a CDC CYBER 74). As described in the reference, TWTD utilizes a Gaussian waveform. Thus, the first step in the implementation of the model was to modify it to accept an incident EMP waveform defined as a four-term exponential (see Equation (A-8) in Appendix A). The next steps were to implement the model on the VAX 11/780 computer and to design a series of test cases for evaluation.

The test cases are shown in Figure 25. The representation of a collector inside a facility is that of a single wire inside a wire mesh cage. This internal wire is not physically connected to any other part of the mesh. The number of

*Any mathematical model of field penetration into structures must necessarily represent a simplified version of what is otherwise a very complicated problem. Because of the complexity and variation of the internal structure of buildings, it is extremely difficult to develop an all-encompassing mathematical theory that accounts for all circumstances. However, the approach taken assumed that the fundamental collector properties of such structures could be analyzed.

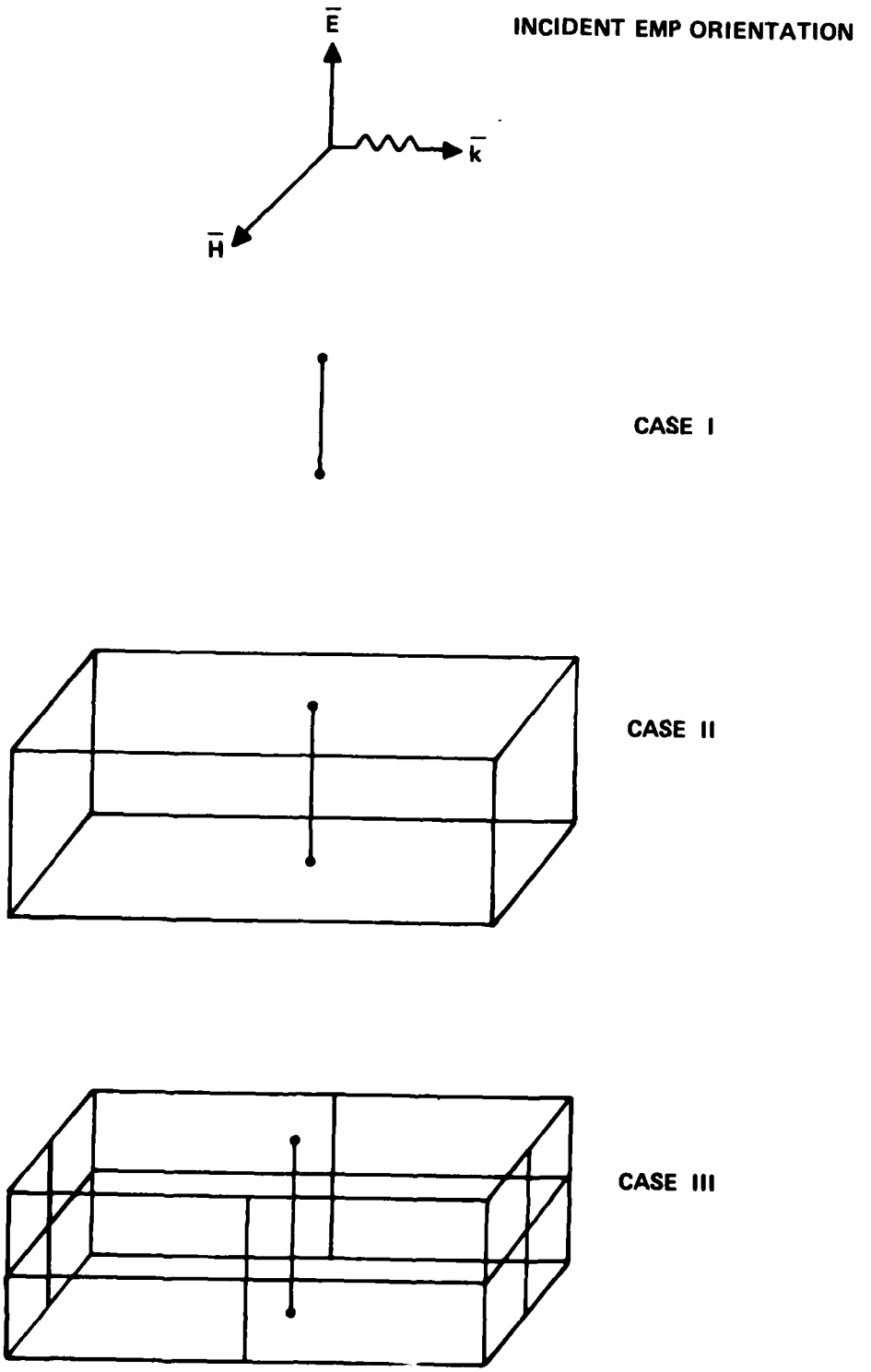

Figure 25. Test cases for the analysis of internal collectors.

wires forming the mesh can be increased or decreased so that different levels of shielding can be examined. The shielding effectiveness of the mesh is determined by comparing the magnitude of current induced on the internal wire to the current induced on the same wire with no mesh present.

For verification of the modified TWTD code, an initial experiment was designed to determine the current induced on a single wire with no wire mesh present. A wire, 1.5 m in length, and 0.0029 m in radius, was illuminated by the EMP polarized in the direction of the wire. The wire was divided into 40 zones and the 20th and 21st zones were loaded with 50 Ω resistances. The resulting induced current is given in Figure 26. The damped oscillating current is an expected result.

The practical limitation to the size of a structure that can be analyzed with TWTD is determined by the highest frequency component of the EMP for which meaningful data is desired. To use the code, the user must supply a time sampling increment, Δt, which is determined by this highest frequency component. The sampling criterion imposed by the code is that there be approximately 12 samples/cycle at the highest frequency. An initial estimate for Δt was based upon the assumption that EMP spectral components more than 90 dB down from the peak should contribute negligibly to the induced current. From Figure 8, it can be seen that all components above 667 MHz fall in this category. Thus, 667 MHz was selected as the highest frequency of interest. Applying the 12 sample/cycle requirement produces a Δt of 1.25×10^{-10} seconds. (The response of Figure 26 resulted from utilizing $\Delta t = 1.25 \times 10^{-10}$ sec.)

For more complex structures, however, small time increments incur unacceptably large computer memory and run time requirements. Therefore, an ability to use large time increments was considered highly desirable. Unfortunately, upon examination of preliminary results with large time increments, it was found that as Δt was increased to 5×10^{-10} seconds (representing a highest frequency component of 167 MHz) the EMP-induced current exhibited unbounded oscillations as time increased (a condition obviously not possible with a time-limited input). Consequently, all of the test cases were evaluated with $\Delta t = 1.25 \times 10^{-10}$ seconds.

Such a small value of Δt places a severe limitation on the size of a structure that is practical to run with TWTD. In fact, it is necessary that $D \leq c\Delta t$, where D is the longest zone in any zoning scheme of the structure, and c is the speed of light in a vacuum. For $\Delta t = 1.25 \times 10^{-10}$ seconds, $D \leq .0375$ m. Thus, a single wire 1 m long requires approximately 27 zones. (It is evident that a typical structure

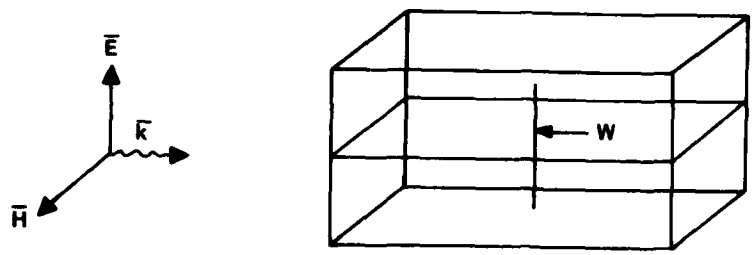

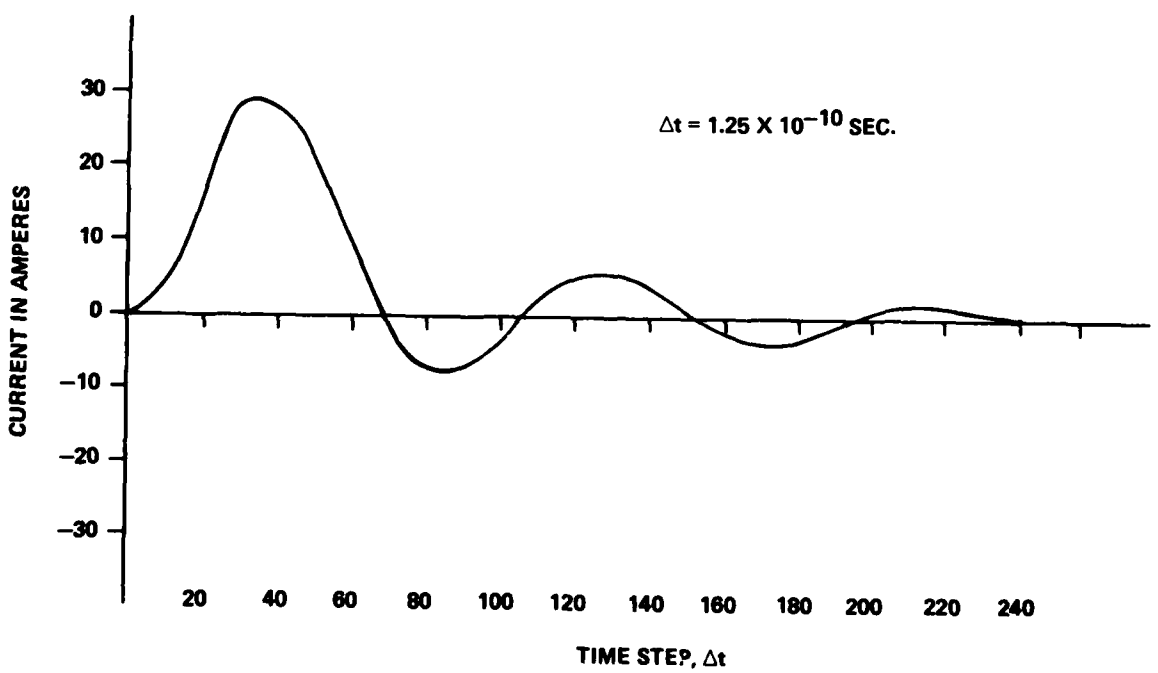

Figure 26. Calculated current response of a 1.5 m internal collector.

of realistic dimensions and complexity will require an extensive amount of computer time and memory.)

For these reasons, only the analysis of structures of small dimension was attempted. The dimensions of the wire cage of the test cases were chosen to be 0.2 m x 0.1 m x 0.05 m in length, width and height, respectively, with an internal wire of length 0.05 m centered vertically inside the cage. The wire radius was 0.0003 m. The incident EMP was assumed vertically polarized parallel to the internal collector. Each 0.1 m section of wire in the cage was divided into three zones. The 0.05 m and 0.025 m sections were divided into two zones and one zone, respectively.

The computed responses of the 0.05 m "internal collector" are shown in Figure 27 for the one unshielded and two shielded cases. Notice that the early time responses of the induced currents are well behaved. In all three cases, however, oscillations begin around the 30th time step, or around 3.75 nanoseconds.

Since the preliminary results of Figure 26 had indicated that the resulting currents seemed to be more stable with longer wire lengths, it was decided to test a larger structure. For this test, a 0.5 m x 0.5 m x 0.5 m cage with a vertically centered 0.5 m wire was run. Again, the EMP was vertically polarized. Each 0.5 m segment was divided into 14 zones. The results, compared to an unshielded wire of the same length, are given in Figure 28. Computer memory space limited the number of time steps to 58, but the results do show decaying oscillatory behavior. The initial peak currents occur at about 2.5 nanoseconds, and the shielded wire shows an attenuation in the peak current level of 1.68 dB with respect to the unshielded wire.

These results indicate that more work is necessary in order to make TWTD a useful tool for EMP analysis of internal collectors. Indeed, the severe limitation placed on the size of structures that can be analyzed with TWTD may limit its usefulness. Also, these results indicate that convergence criteria for the modified (four-term exponential) TWTD code have not been fully characterized. These criteria may well be different than those described for the unmodified code. The usefulness of TWTD for analyzing EMP coupling to internal collectors will depend on the upper limit of the structural size capability of the program and the severity of the conditions necessary for convergence.

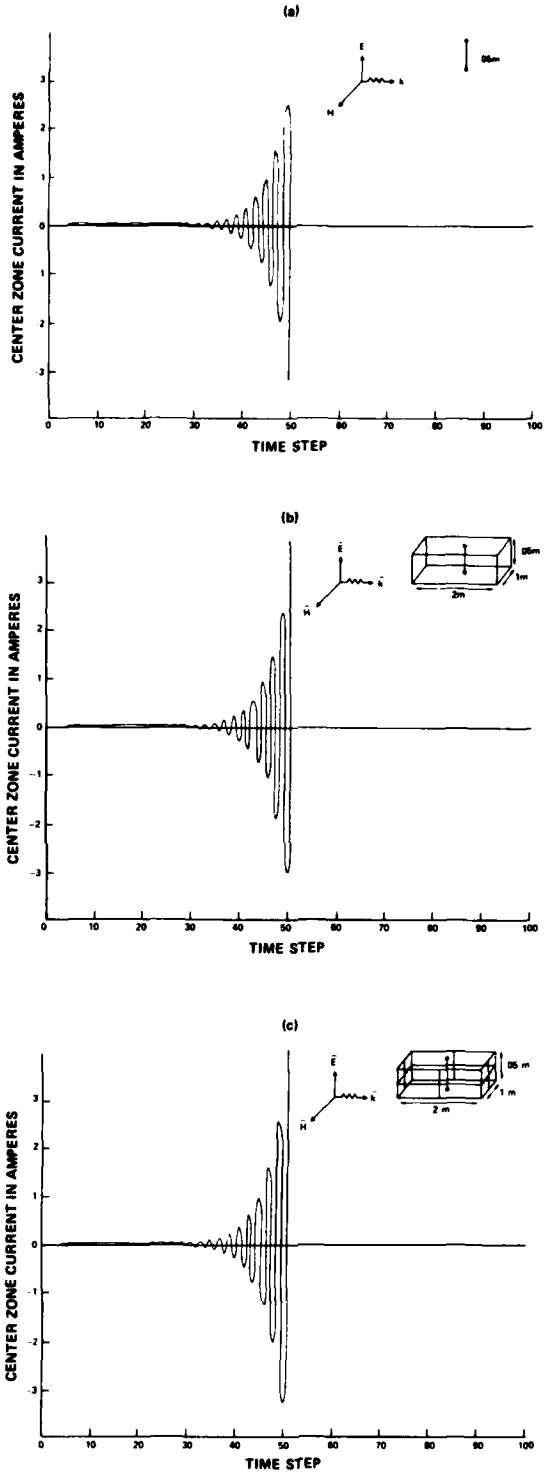

Figure 27. Calculated current response of 0.05 m internal collector for three different shielding conditions.

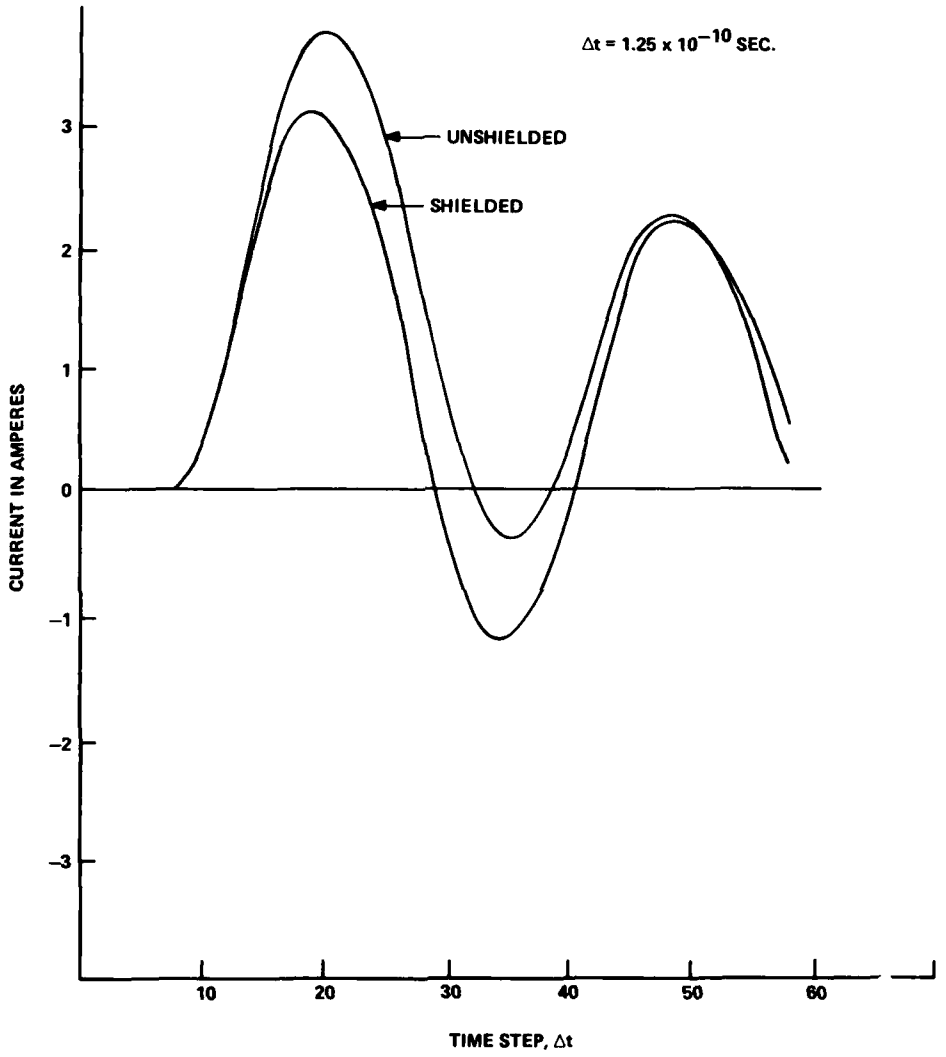

Figure 28. Calculated (center zone) current response of a shielded versus an unshielded 0.5 m conductor.

3.3 EXPERIMENTAL INVESTIGATION OF STRUCTURAL SHIELDING AT EMP FREQUENCIES

The degree of coupling to an internal collector will be influenced by the shielding effectiveness of the surrounding structure. To obtain an estimate of this influence, measurements of the attenuation of EM fields into two buildings were performed in order to see if any insight could be gained into the shielding properties of "typical" structures over a frequency range representative of the EMP power spectrum. The field strengths of locally available commercial broadcast sources from 0.59 MHz to 660 MHz were measured externally to the structures and at selected locations within. These measurements were made in two buildings located on the Georgia Tech campus. Each building is of steel and masonry (brick veneer over concrete blocks) construction. Building No. 1 consists of three floors, while Building No. 2 contains four floors. (See Figure 29 for generalized layouts and for relative locations of the radiating sources.)

For each building, reference field levels were measured on the roof for each selected emitter. (The reference levels were taken as the average at two roof locations.) Then, at various interior locations on each floor, the field strength levels of each emitter were again measured. Identical antennas were used in each case and signal substitution methods using calibrated signal sources were employed to indicate the relative signal levels at each frequency. At each location, the pickup antenna was rotated until a maximum signal level was obtained. The difference between the field level measured on the roof and at an interior location was defined as the relative shielding effectiveness of the structure at that point.

Interior test sites were distributed around the periphery of the buildings approximately 5 to 6 meters from the outside wall. Also, a location near the center of each building was chosen for measurement. In this way, knowing the direction of the transmitter, the effects on attenuation of the field of longer path lengths through the building could be observed.

The data from the measurements are presented in Tables 1 and 2. In all cases the data are given as the attenuation (in dB) observed at the location nearest the source (N), at a central location (C), and at a point farthest from the source (F). The data indicate that the greatest attenuation is, in general, on the ground floor and decreases on the higher floors. This characteristic appears to hold throughout the range of frequencies measured. This result is in agreement with Rice [14], whose measurements at 35 and 150 MHz found the greatest attenuation on the lowest level. Rice also found overall average local losses for 11 buildings in New York

Table 1. Signal Attenuation in dB as Measured at Selected Locations in Building No. 1.

Source		Location*									
Freq. MHz	Identifier	R**	GN	GC	GF	1N	1C	1F	2N	2C	2F
.59	WPLO	70	34	49	-	12.5	42	31	14	25	24
.86	WAEC	63.5	45.5	45.4	36.5	25.5	37.5	19.5	9.5	23.5	19.5
1.33	WIGO	66	38	43	27	15	40	33	14	26	20
32.6	---	50.5	-	37.5	-	-	38.5	-	-	29.5	-
55	CH 2	34.5	32.5	41.5	23.5	9.5	19.5	32.5	2.5	17.5	2.5
77	CH 5	25.5	33.5	48.5	22.5	20.5	45.5	30.5	17.5	28.5	19.5
91	WREK	11	36	30	25	20	19	37	22	13	18
98	WSB	29.5	22.5	32.5	-	13.5	18.5	12.5	19.5	13.5	9.5
162	WEATHER	39	-	31	-	-	22	-	-	16	-
198	CH 11	32	28	26	26	12	23	18	3	12	14
485	CH 17	16.5	30.5	28.5	-	26.5	28.5	33.5	18.5	18.5	26.5
660	CH 46	38.5	34.5	39.5	-	9.5	24.5	34.5	14.5	28.5	18.5

*G, 1 and 2 refer to ground, first and second floor. N, C, and F refer to the location nearest, central and farthest from the source. Locations N and F are always on the periphery.

**The value R is the field strength taken on the roof as a reference level.

Table 2. Signal Attenuation in dB as Measured at Selected Locations in Building No. 2.

Source		Location*												
Freq. (MHz)	Identifier	R**	GN	GC	GF	1N	1C	1F	2N	2C	2F	3N	3C	3F
.59	WPLO	68	37	62	-	24	53	25	19	47	22	19	32	19
.86	WAEC	62	25	44	-	17	48	21	18	47	19	11	30	22
1.34	WIGO	66	-	54	21	22	54	23	28	44	21	33	30	14
32.6	-	39	-	38	-	-	31	-	-	34	-	-	29	-
55	CH 2	20	45	42	50	28	30	30	34	23	19	19	20	25
77	CH 5	27	31	32	49	10	30	9	0	25	12	-3	24	8
91	WREK	10	27	28	51	10	21	26	-2	17	34	5	16	20
98	WSB	22	34	32	36	13	26	19	12	23	27	5	15	17
162	WEATHER	33	-	26	-	-	36	-	-	26	-	-	17	-
198	CH 11	30	24	28	35	10	20	18	-2	12	18	4	11	11
485	CH 17	14	40	43	50	24	40	32	13	26	35	21	21	37
660	CH 46	36	40	40	39	25	29	23	11	27	21	20	23	14

*G, 1 and 2 refer to ground, first and second floor. N, C and F refer to the location nearest, central and from the source. Locations N and F are always on the periphery.

**The value R is the field strength taken on the roof as a reference level.

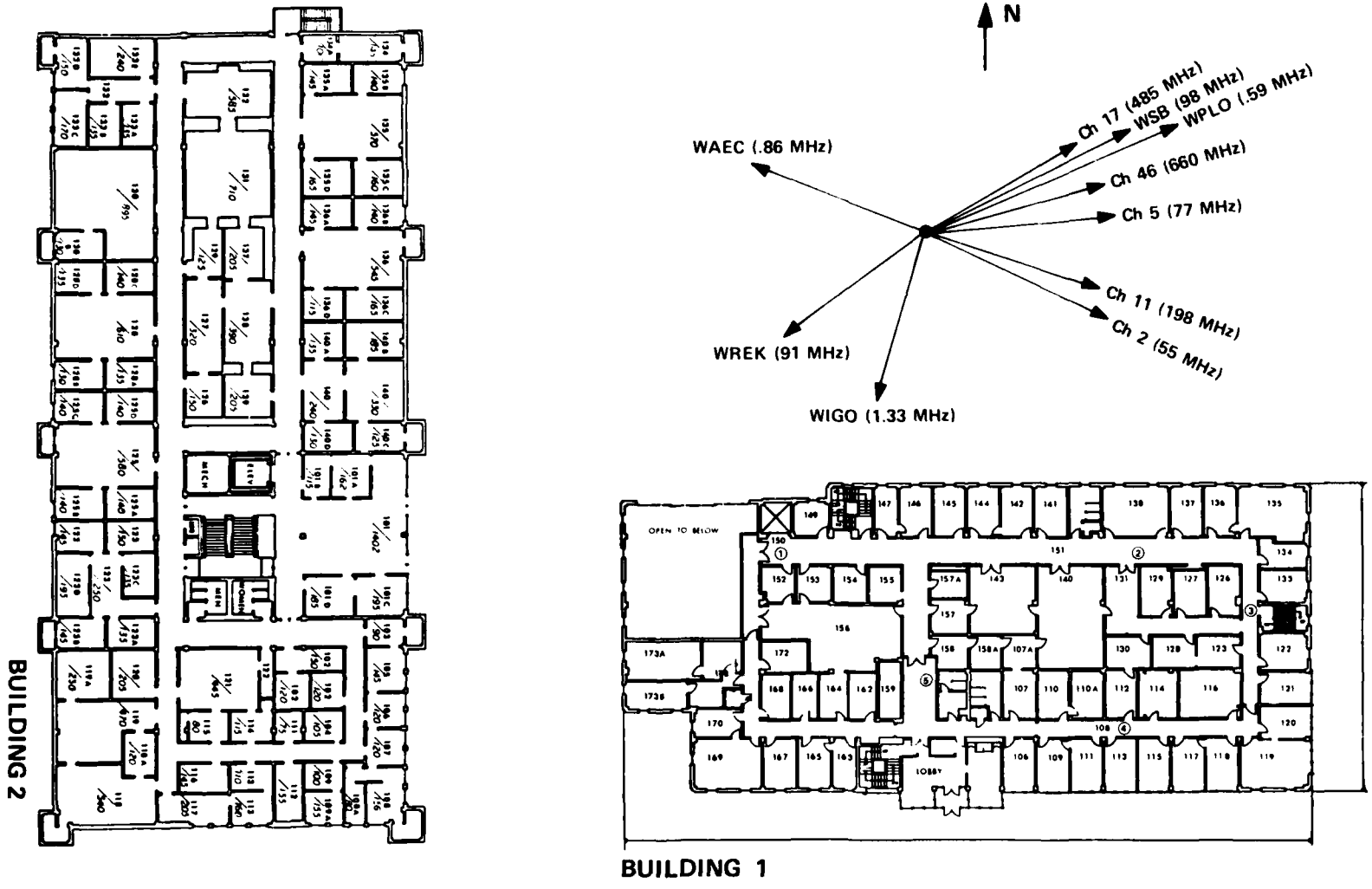

Figure 29. Relative source locations for structural shielding effectiveness measurements.

City to be about 20 dB at 150 MHz and 25 dB at 35 MHz. Local loss means that the signal strength (in dB) measured on the main street level floor of the building as compared to the signal strength in the street adjacent to the building.) The first floor (street level) overall averages for the two buildings measured were about 35 dB at 32.6 MHz and 20 dB at 162 MHz. It must be remembered that the data of Tables 1 and 2 are relative to the signal strength recorded on the roofs of the buildings.

From Figure 29, the relative path lengths that the signal must travel to reach the measuring point inside the building can be noted. Specifically, Figure 30 shows the attenuation at all frequencies as the measuring point is moved around the periphery of the first floor of the building (see Building No. 1 floor plan, Figure 31, for exact locations of measurement points). For some of these locations, the attenuation dependence on path length is clear. For instance, at 55 MHz (whose source lies to the southeast), the attenuation should be least at Position 3, intermediate at Position 5 and greatest at Position 1. Attenuation at these locations is 9.5, 19.5, and 32.5 dB, respectively. At frequencies of 485 MHz and 660 MHz, more attenuation with longer path length is noted. With the exception of 91 MHz*, every measurement shows greater attenuation of the signal at the center of the building than at the periphery. However, at 6 frequencies (0.59, 0.86, 1.33, 77, 98, and 198 MHz), the longest path length shows a lower attenuation than the center. Of course, in an urban environment, multiple reflections of the signal by nearby objects could account for low attenuation at any peripheral location.

In Figure 32, the comparison between the attenuation on the first floor at the central location of Building No. 1 and Building No. 2 is presented. In general, the attenuation is greater for Building No. 2. (The solid lines of Figure 32 represent the best fit curve from linear regression.) Note that differences are evident in the shielding effectiveness of the two buildings. The only significant physical differences between the two structures are their sizes (Building No. 1, 76 m x 33 m; Building No. 2, 58 m x 30 m') and their orientations (see Figure 29). The two buildings are approximately 122 m apart.

In Figure 33, the attenuation in the central location in Building No. 1 is given for various floors. The solid lines (linear regression fit) indicates that the attenuation, in general, is greatest on the ground floor, intermediate on the first floor, and lest on the second floor. (This trend is in agreement with that published by Rice.) In particular, note that, over the frequencies containing most

*The 91 MHz source is the campus radio station located close by.

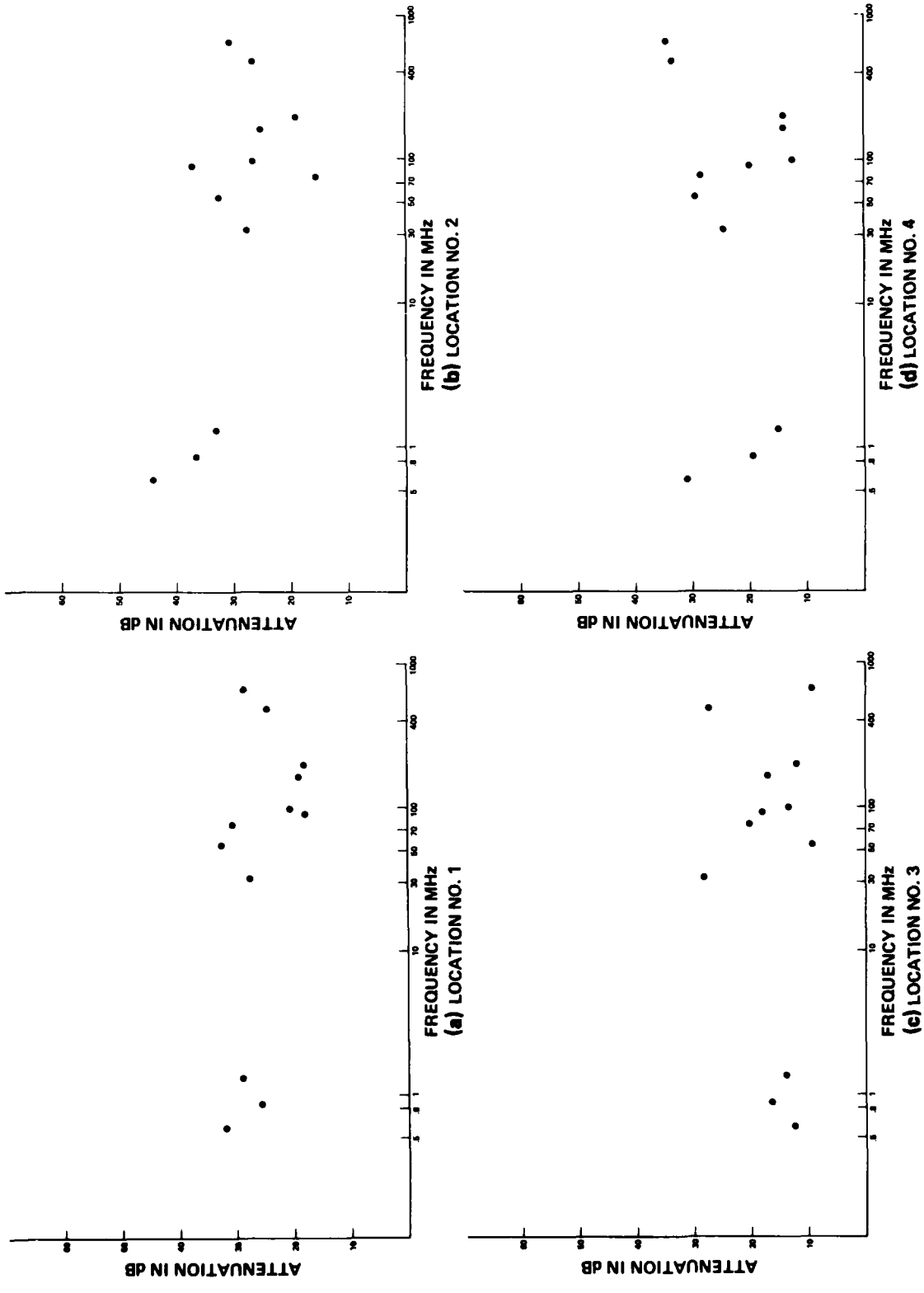

Figure 30. Measured shielding effectiveness at selected locations in Building No. 1. (Cont'd.)

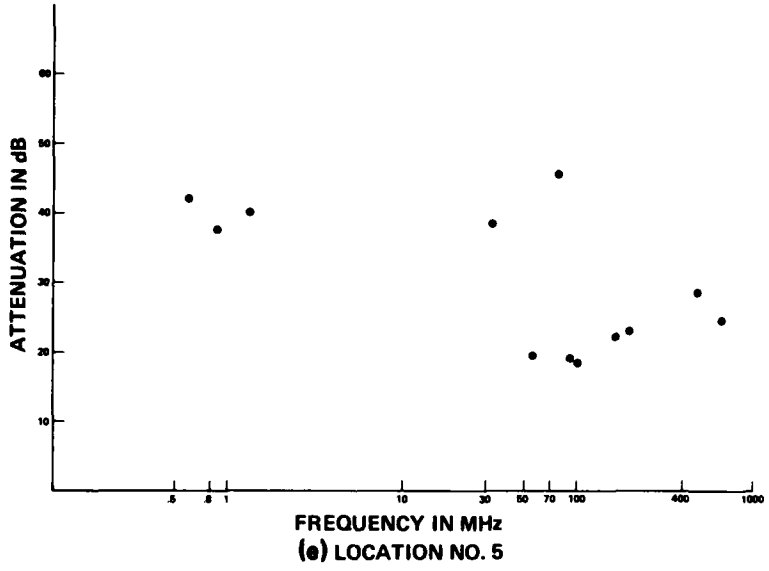

Figure 30 (Cont'd.) Measured shielding effectiveness at selected locations in Building No. 1.

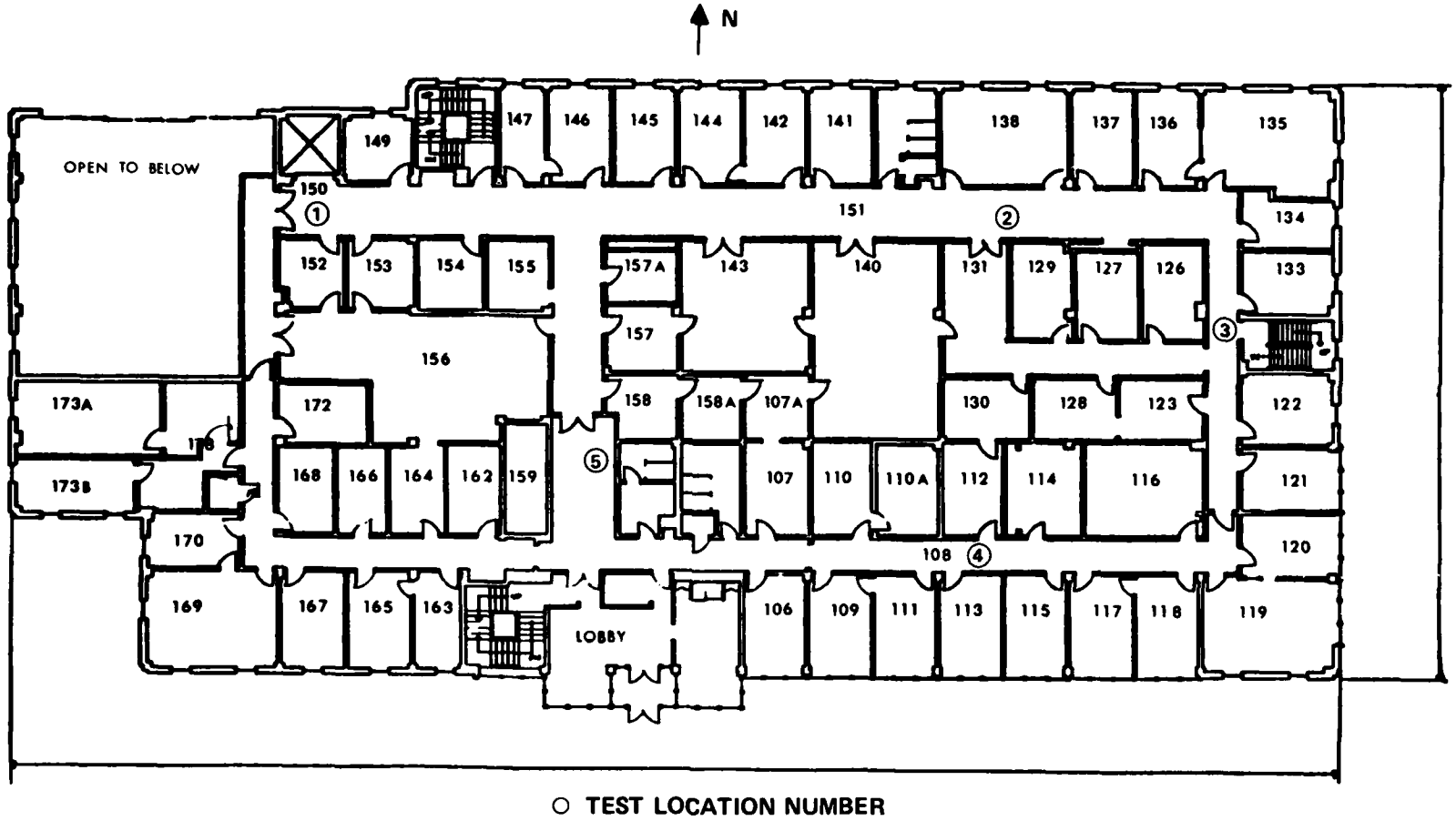

Figure 31. Floor plan of Building No. 1 showing relative locations for measurements shown on Figure 30.

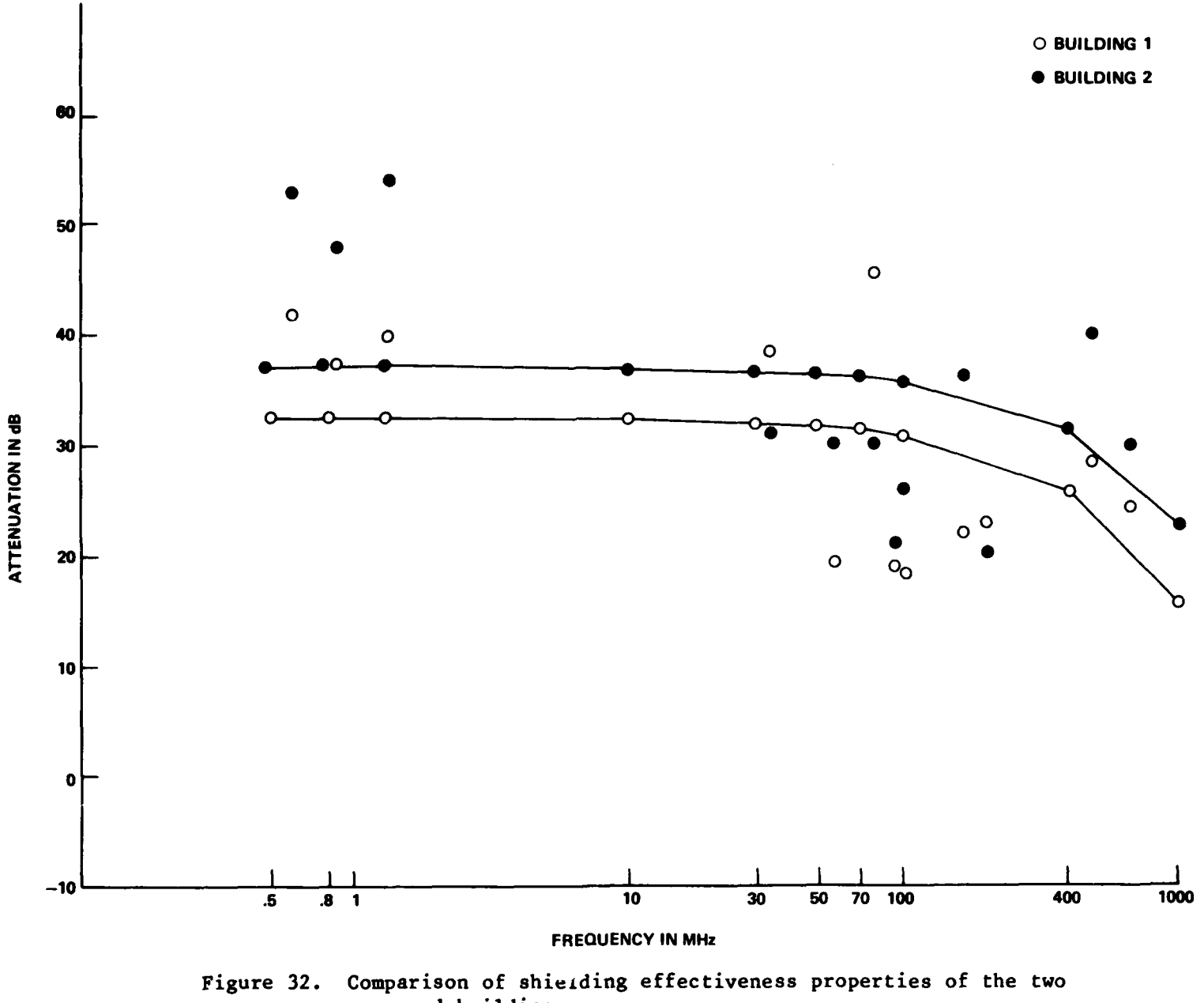

Figure 32. Comparison of shielding effectiveness properties of the two measured buildings.

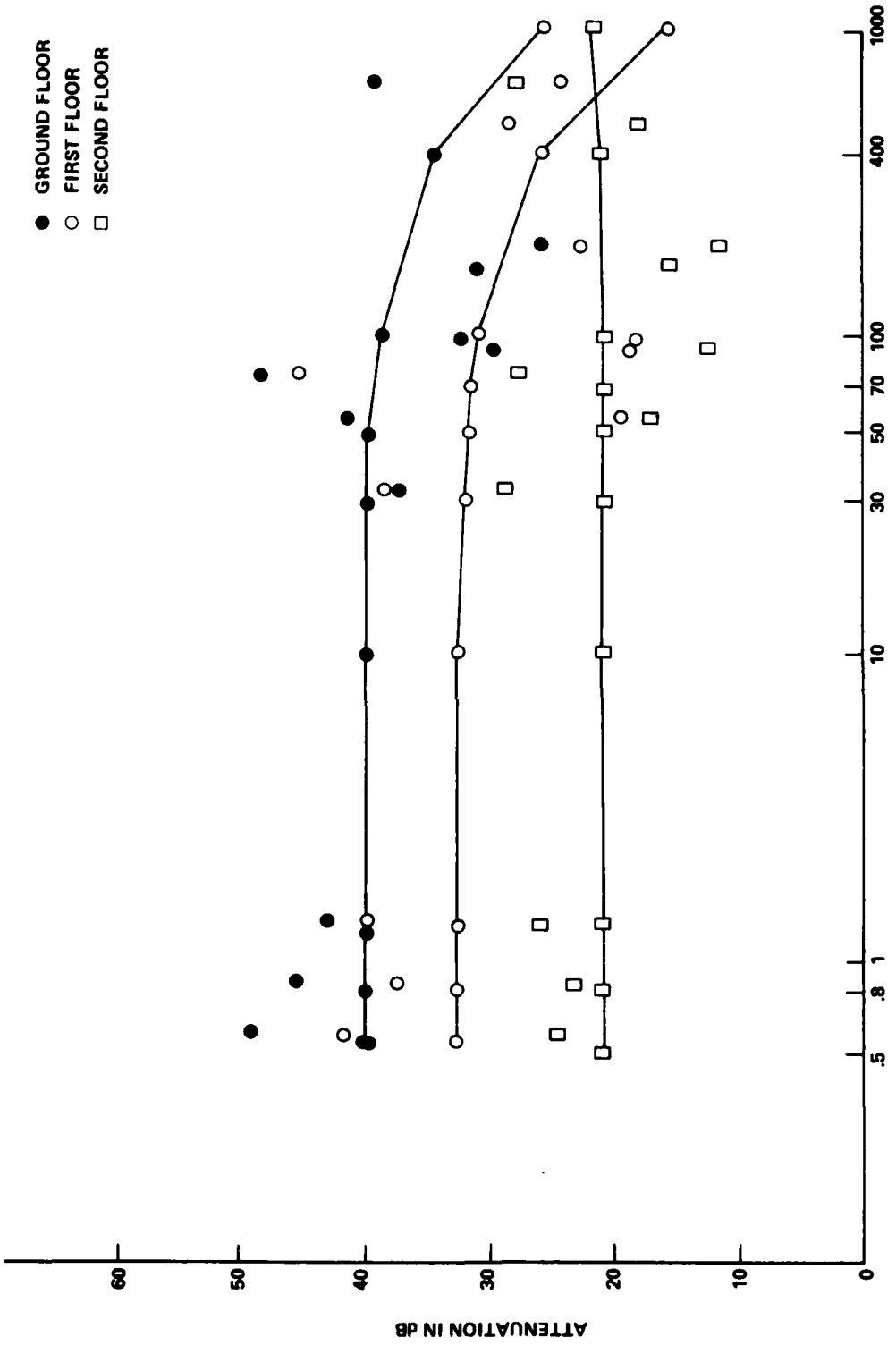

Figure 33. Shielding effectiveness versus floor level for Building No. 1.

of the energy of an EMP ($<$100 MHz), a general attenuation of from 20 to 40 dB is offered by this "typical" structure.

It is postulated that, with adequate data of the above described type, structures can be considered as generalized filtering functions which can be used to operate on an incident EMP to evaluate the relative pickup by internal conductors. Because of the heterogeneous nature of typical structures, a statistical description of shielding effectiveness is perhaps the only meaningful approach. The data gathered to date is not sufficient for statistical analyses, however. Additional measurements of these kinds are therefore suggested.

IV. EARTH ELECTRODES FOR EMP GROUNDING

4.1 INTRODUCTION

As an adjunct to the collector assessment study, an investigation was conducted into the properties of earth electrode systems over a frequency range covering a major portion of the EMP power spectrum (see Figure 8). Since this power spectrum extends well into the UHF region, conventional low frequency (less than 100 Hz) measurement techniques are not adequate to describe the electrode system's response to an EMP. Therefore, initial emphasis was placed on the development of a measurement technique that could be used to both (1) assess the performance of a given electrode and (2) conduct a site survey to determine the best location for electrodes. Then the technique was used to evaluate the performance of various common electrode configurations.

The response of an earth electrode to an EMP is determined by the properties of the soil and the electrical characteristics of the particular geometrical configuration [15]. Thus, the first step in establishing an adequate ground is to determine the dielectric properties (conductivity, permittivity, and permeability) of the soil. (This step is important because it dictates the geometrical configuration (i.e., number of ground rods, method of interconnection, etc.) required to establish a good ground in a given area.)

Historically, soil parameter identification started with a laboratory analysis of soil samples and then moved to sophisticated on-site analyses of the soils and underlying strata at the planned location. Recent advances in on-site techniques have been made (see Appendix F for a detailed discussion of various techniques, both recent and traditional). One of these, the Resonant Linear Antenna Method [16] appears to be the most suitable for EMP grounding studies. (The method is accurate over a broad frequency range, is easily transportable, and is generally in use by geophysicists for geological surveying.) From the input admittance and the geometry of a probe antenna, the soil parameters can be calculated. This method requires only a resonant monopole antenna, a signal source covering the desired frequency range, and a display device complete with necessary coaxial voltage and current probes. An adaption of this technique was employed to examine the behavior of selected earth electrodes up to frequencies reflective of fast risetime responses applicable to EMP waveforms. Traditionally, the grounding of power circuits (25-60 Hz) [17] and grounding for lightning protection (impulse)

[18], [19], [20] was the primary concern for structures and power lines. Thus, many studies were performed to determine the volt-ampere characteristics of a driven ground rod using direct current or low frequency (< 100 Hz) alternating current instruments to determine power frequency properties [21], [22]. Impulse generators were used to determine the response to lightning strokes [23]. The typical impulse generator was capable of producing 50 kilovolts and 800 amperes. From these tests, a resistive, inductive and capacitive (RLC) model of a ground rod was developed [24] (Figure 34) that reflected the geometry of the rod, the soil parameters [25], and the climatic conditions at the time of the test [26], [27].

The rise time of the typical EMP is much faster than the rise time of a lightning pulse, however. Thus, a new technique for measuring ground electrode impedances was necessary. After careful consideration of existing instrumentation capabilities and upon evaluation of the EMP power spectrum, it was determined that a technique capable of displaying the response of an electrode system up to 500 MHz would be appropriate. To cover the entire frequency range from DC up to 500 MHz, three different measurement techniques must be used. The three frequency ranges covered by each are: (1) low (DC to 100 Hertz), (2) medium (100 Hertz to 500 kilohertz), and (3) high (500 kilohertz to 500 megahertz). The design and construction of a standardized test probe along with a description of the test techniques for these three frequency regions are discussed in the next sections.

4.2 STANDARD TEST PROBE

For the standardized test probe, a rod of 1.25 cm (0.5 inches) in diameter and 81 cm (32 inches) in length was chosen. (Brass was used although steel, copper, or any other metal of sufficient strength is adequate.) This length is long enough to provide effective soil contact but not so long as to require extensive work to place the rod in the ground.

An adapter was then constructed to interface the ground rod to the test instruements (see Figures 35 and 36). The adapter consists of a tapered coaxial line transition with a male type N connector on the top. The taper maintains 50 ohms impedance down to the point of attachment to the rod. (The impedance characteristics of the connector from 0.5 to 500 megahertz are shown in Figure 37.) The adapter is fastened to the ground rod via a threaded connection.

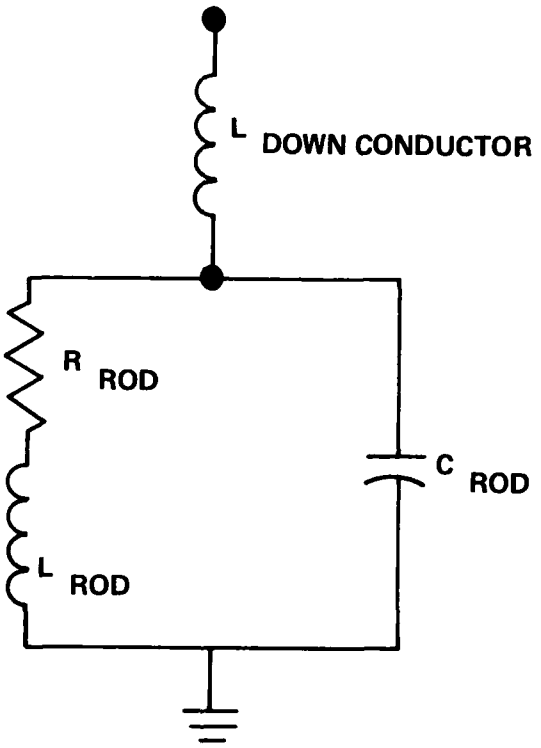

Figure 34. Ground rod model.

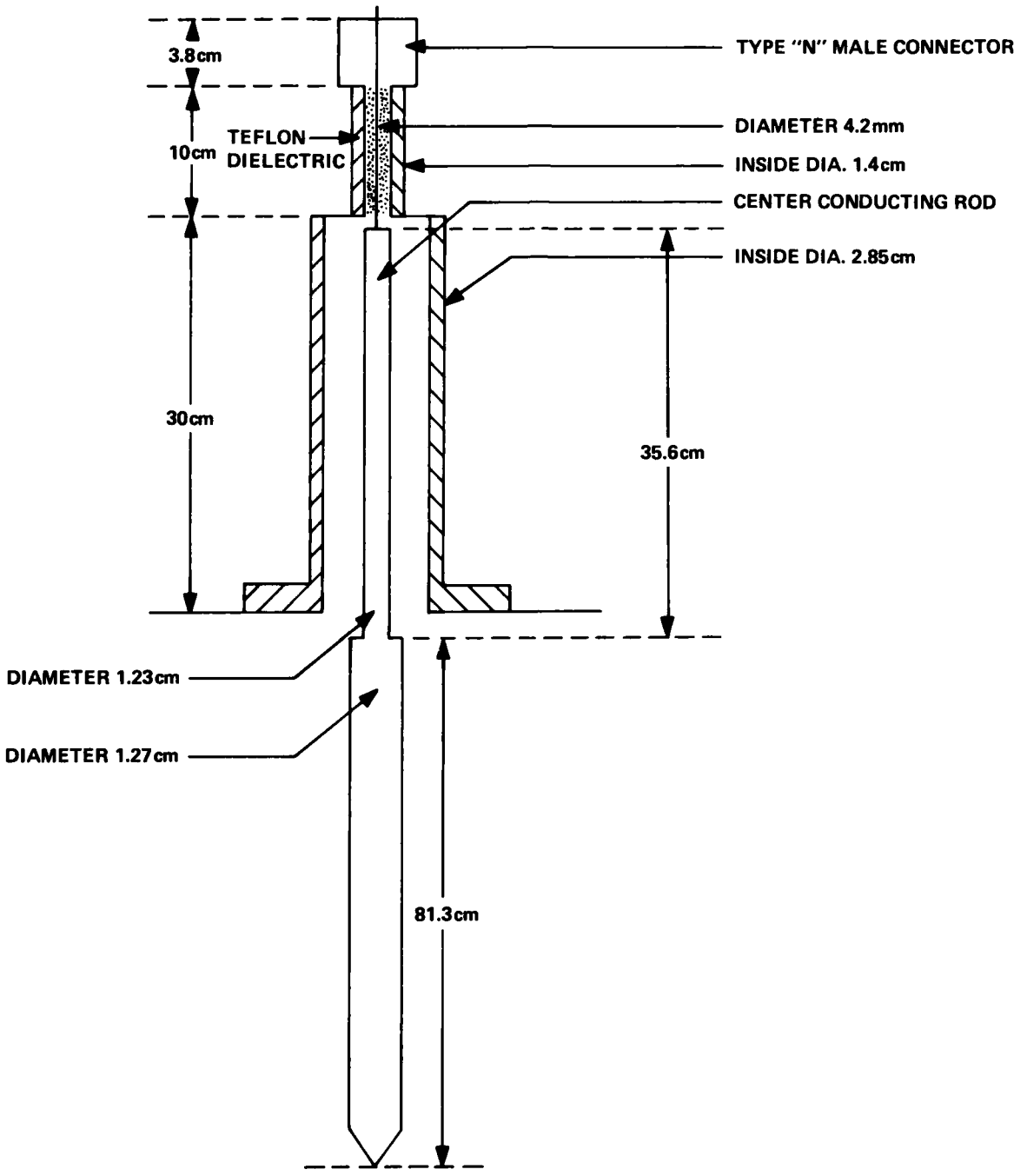

Figure 35. Standard test probe details.

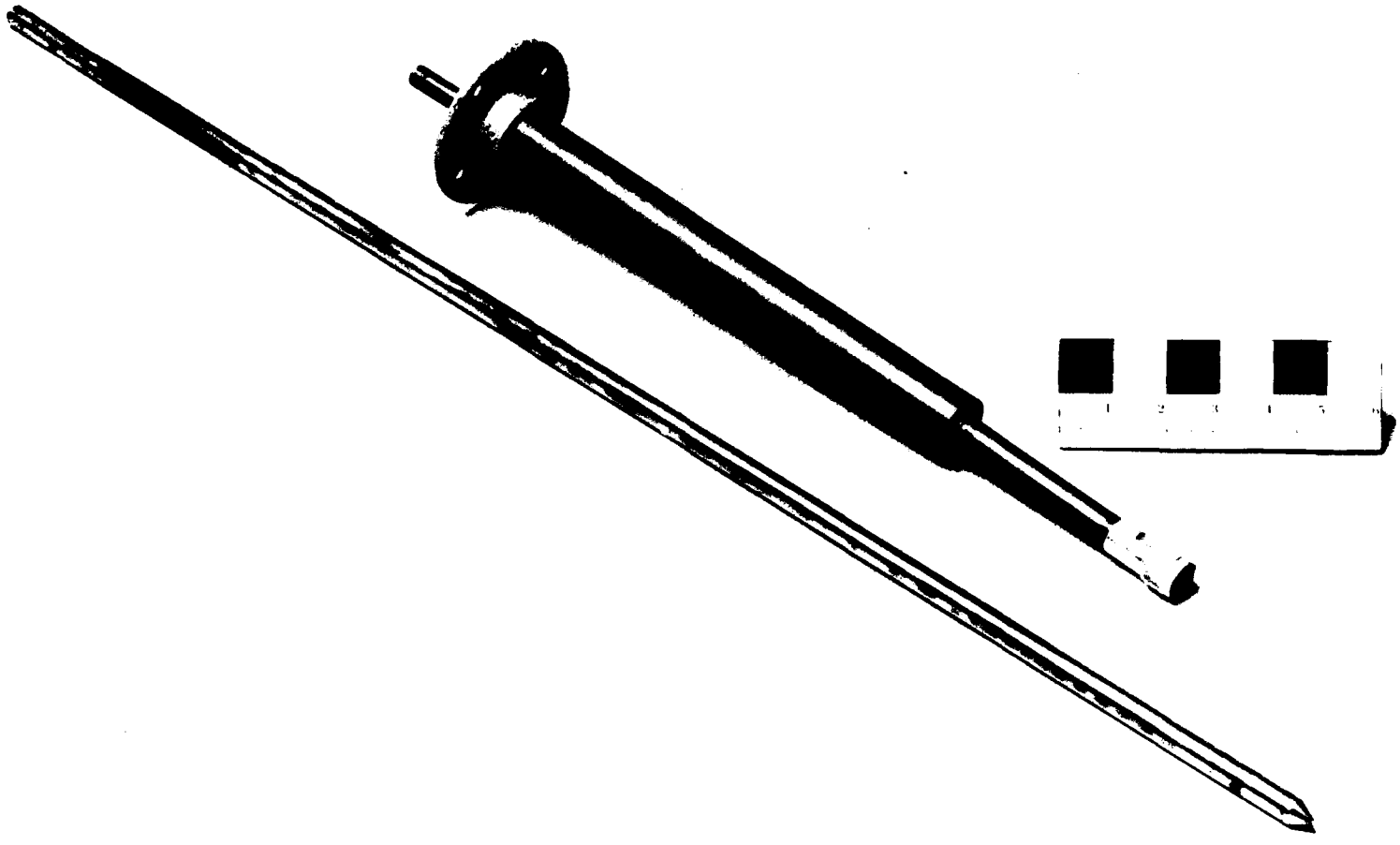

Figure 36. Photograph of standard test probe.

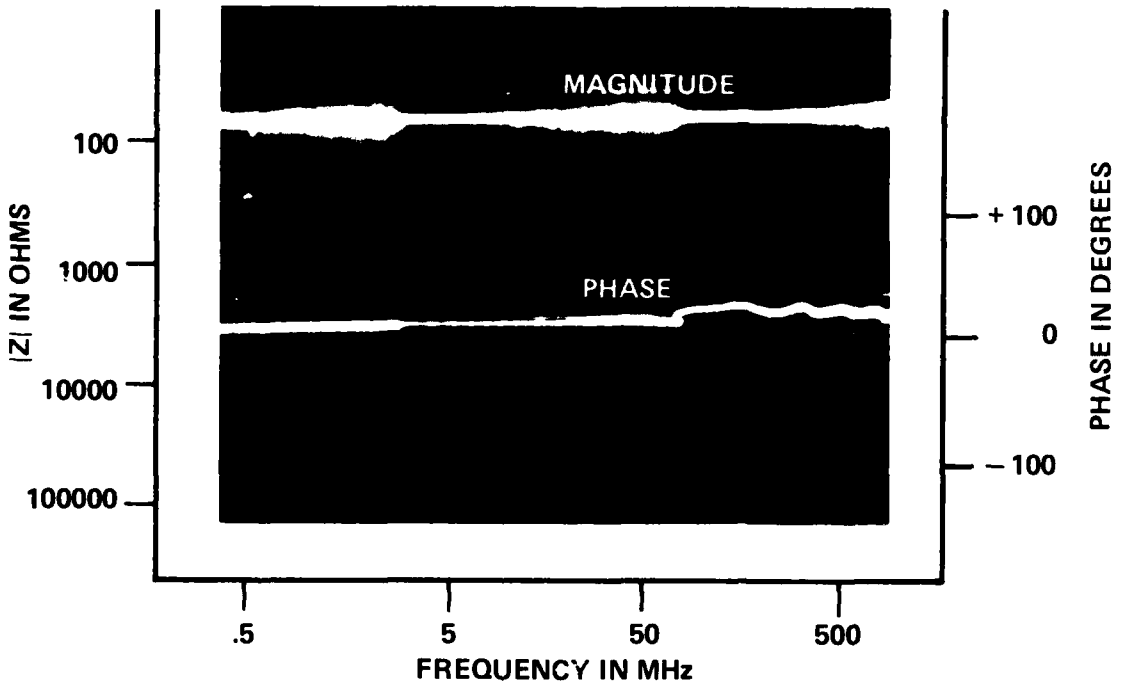

Figure 37. Connector input impedance.

4.2.1 High Frequency Measurements

The high frequency impedance characteristics of the test probe were measured with the aid of a General Radio 1710 RF Network Analyzer. The analyzer was connected to the type N connector as shown in Figure 35, calibrated (Figure 38), and an impedance plot of the probe in earth was photographed (see Figure 39). It is noted that there is a great deal of ringing associated with both the magnitude and phase of the rod impedance. The ringing is due to the non-uniform imaging of the rod with the soil, the inductance and capacitance of the test leads to earth, and the standing waves at the surface [28]. By increasing the reference plane area of the probe, the standing waves and reflections were reduced, yielding a more acceptable plot of the ground rod impedance. The reference plane area was increased by attaching auxiliary grounds and an aluminum plate to the test connector shield (see Figure 40). A series of plots, Figures 41 to 46, were taken with different auxiliary grounds. The figures reveal that the rod impedance ringing decreased and displayed an overall capacitive nature at high frequencies as expected. These results indicated that this approach can be used to determine the impedance of the reference probe up to frequencies of 500 MHz. From this impedance characteristic, determination of the equivalent circuit of the probe can be made [29].

A computer run was made to calculate the input impedance of the equivalent ciruit (Figure 34) with the test rod geometry and soil conditions of the particular test area. The input impedance of the ground rod equivalent circuit is given by:

$$Z = \frac{Z_L Z_C}{Z_L + Z_C} \tag{37}$$

where

$$Z_L = R + j\omega L$$

$$Z_C = \frac{1}{j\omega c}$$

$$R = \frac{\rho}{2\pi\ell} \ell n \left(\frac{2\ell}{a}\right) \text{ ohms}$$

$$L = 2\ell \ell n \left(\frac{2\ell}{a}\right) 10^{-7} \quad H$$

$$C = \frac{\epsilon_r \ell}{2\ell n \left(\frac{2\ell}{a}\right)} \frac{10^{-9}}{9} \quad F$$

ℓ = length of rod

a = radius of rod

$\rho = 97.67\ \Omega$ m

$10 \leq \epsilon_r \leq 13$

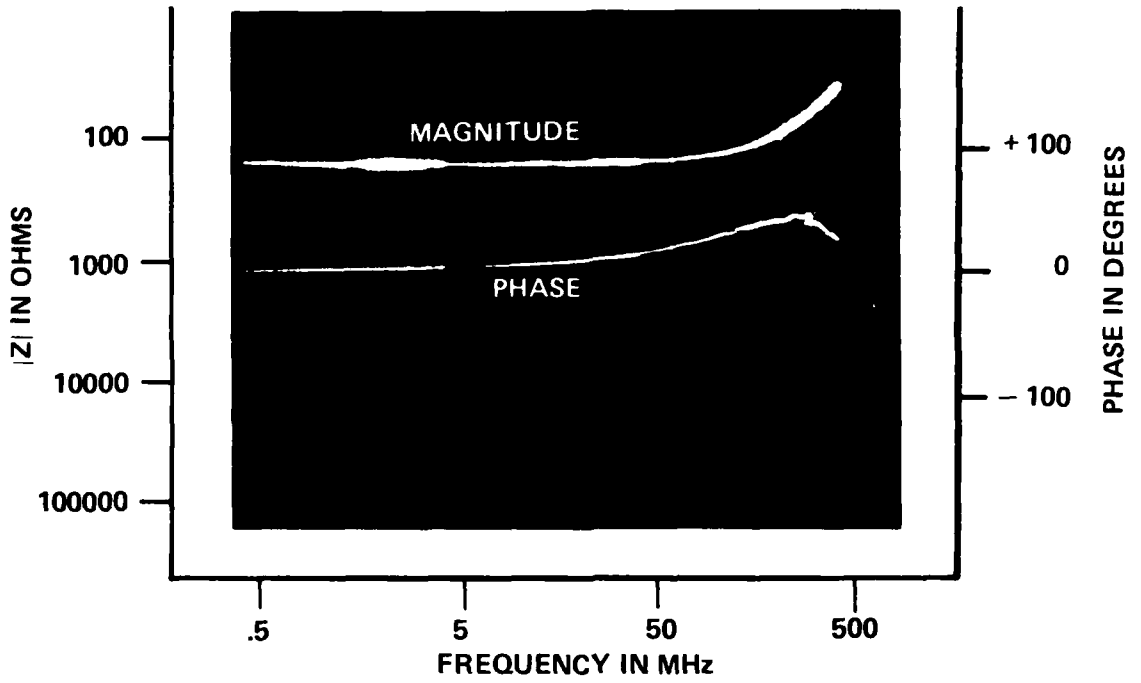

Figure 38. Connector output impedance for calibrated 100 ohm load.

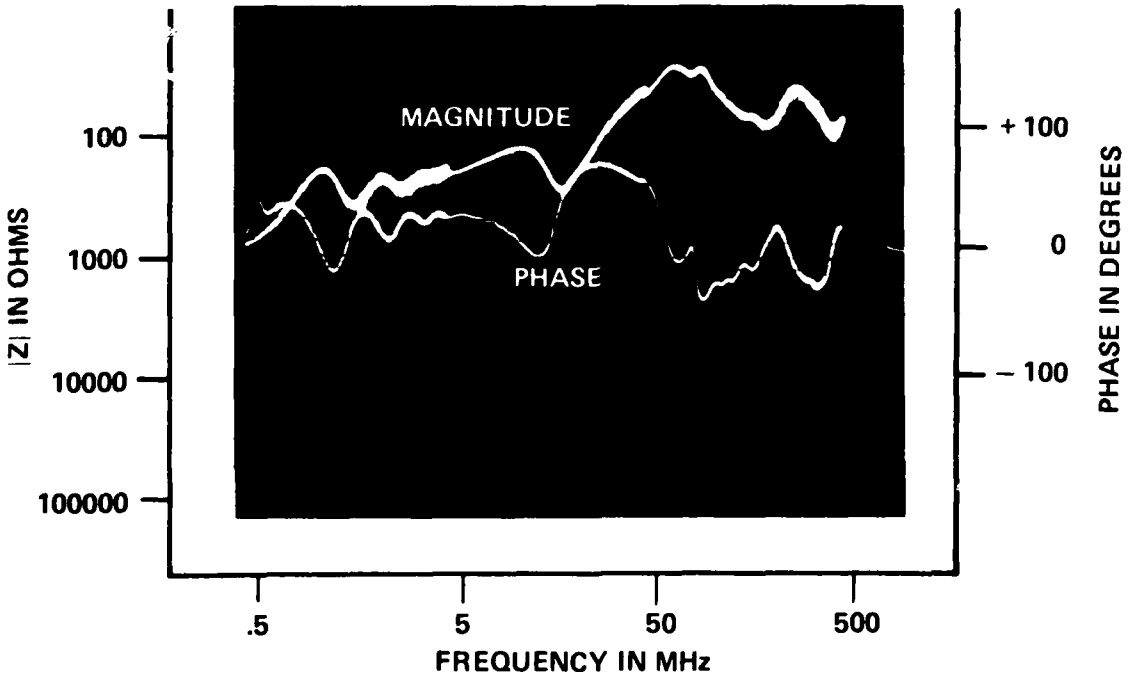

Figure 39. Simple ground rod impedance.

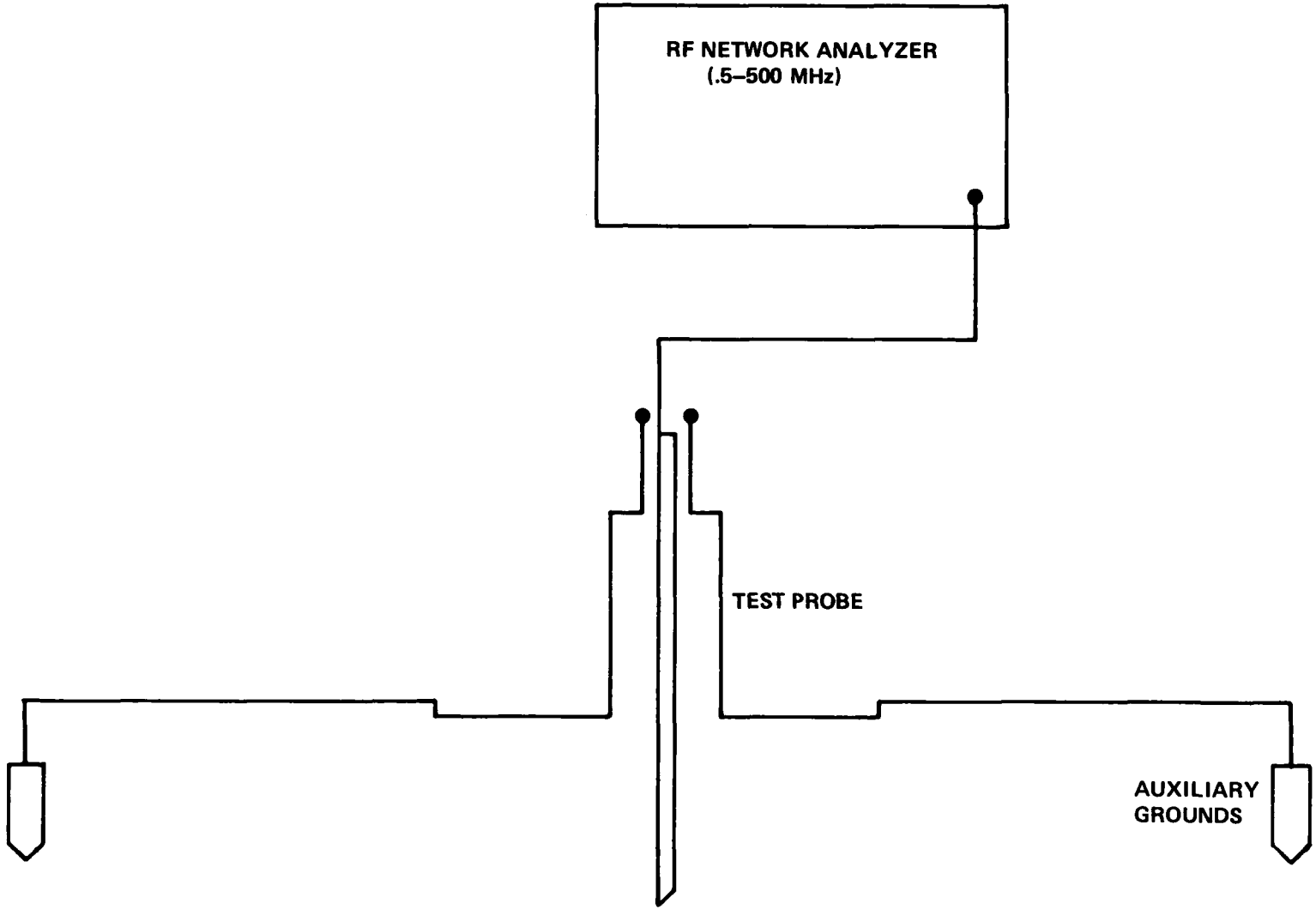

Figure 40. Test setup for high frequency measurements.

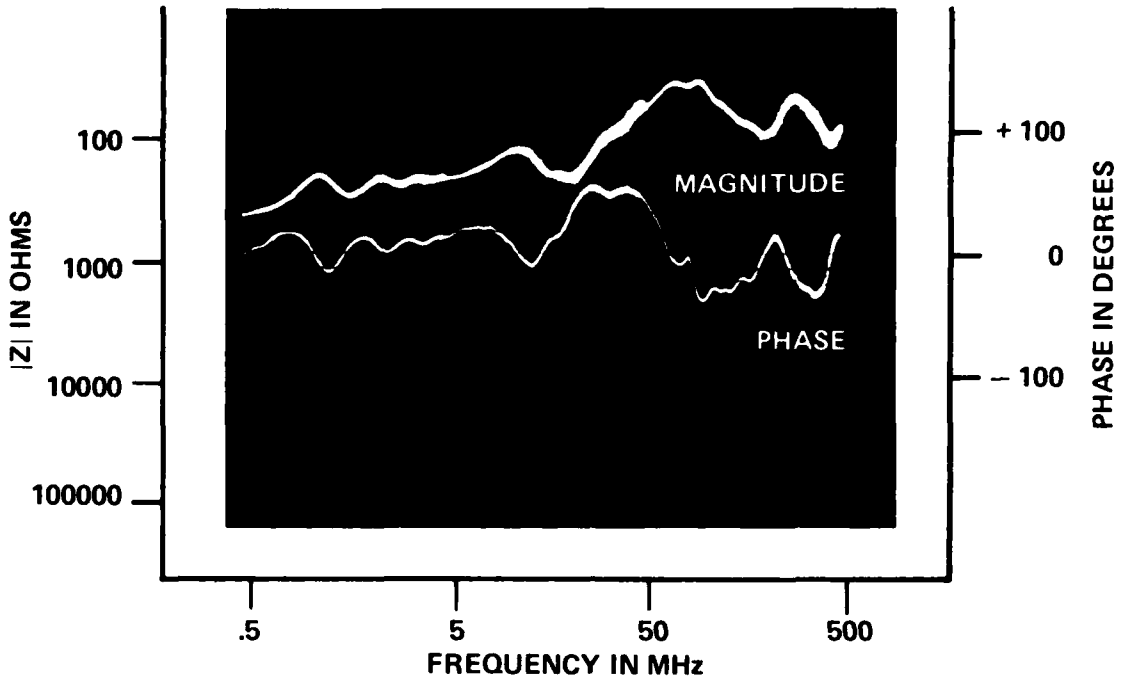

Figure 41. Impedance of ground rod and one auxiliary ground.

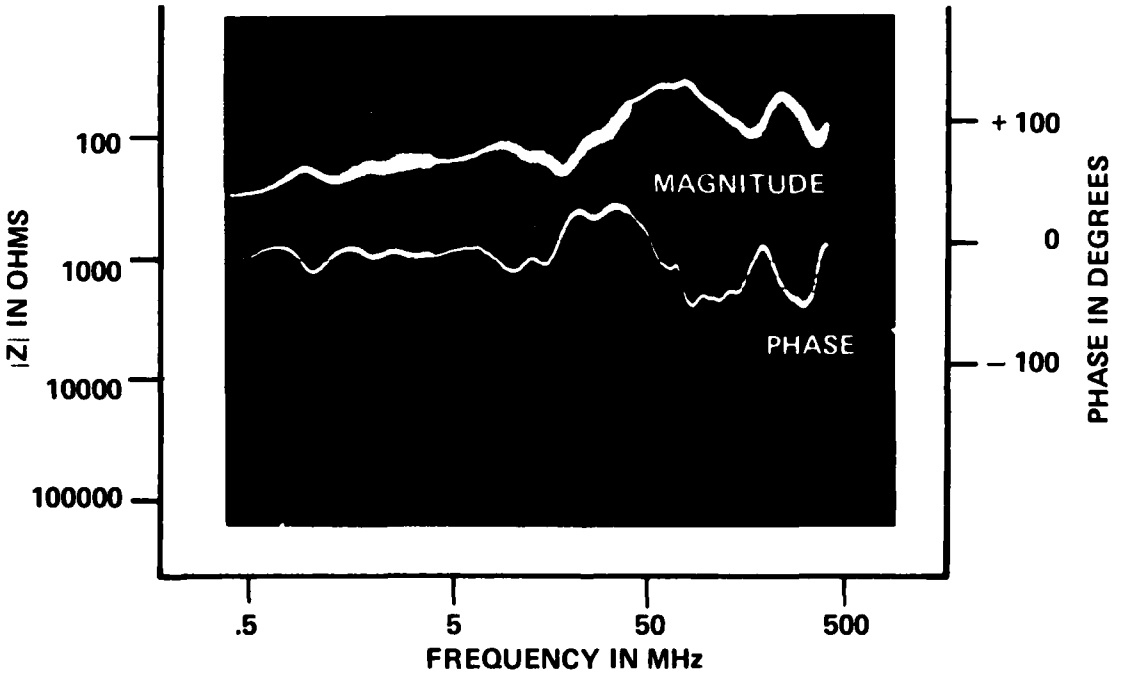

Figure 42. Impedance of ground rod and two auxiliary grounds.

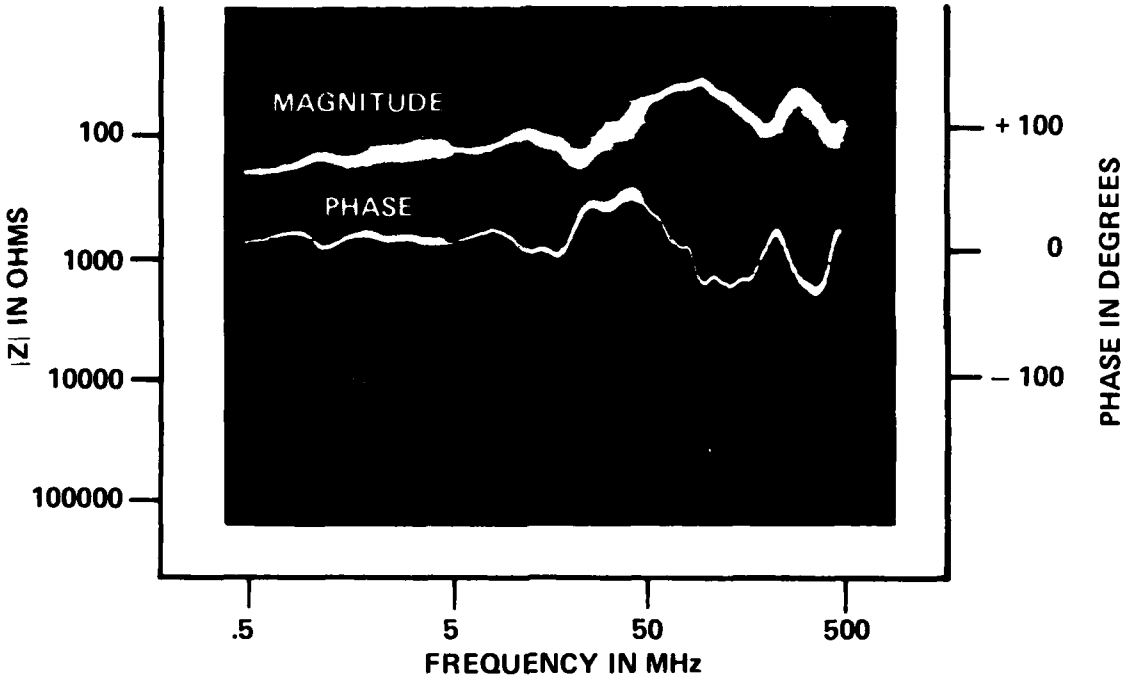

Figure 43. Impedance of ground rod and three auxiliary grounds.

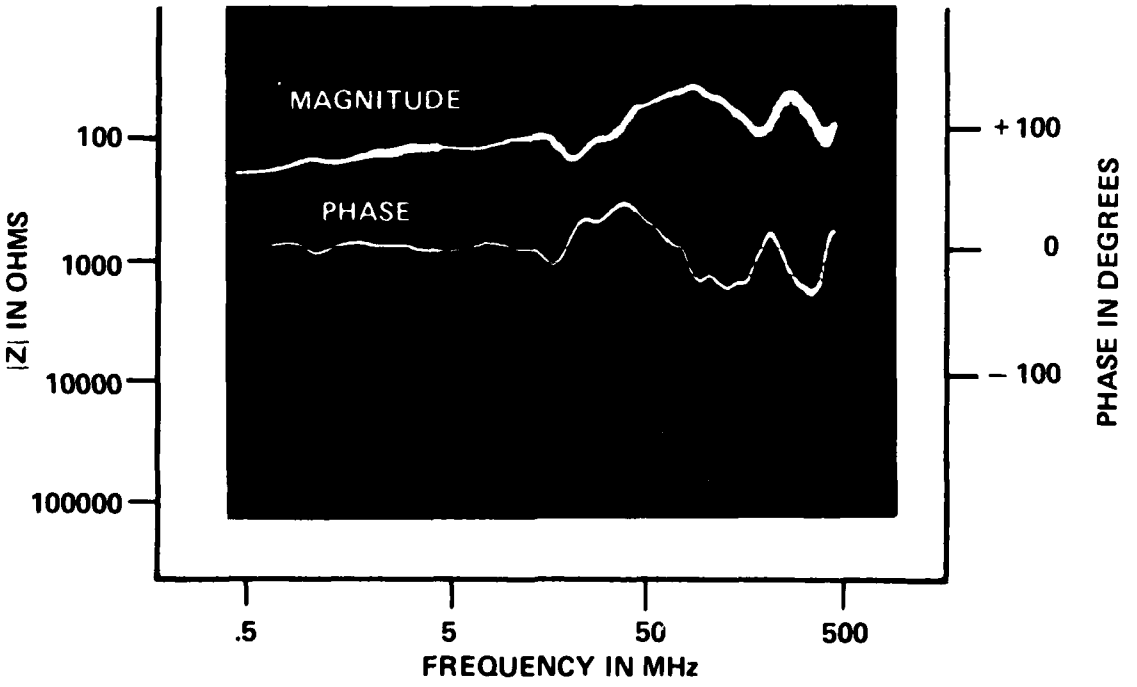

Figure 44. Impedance of ground rod and four auxiliary grounds.

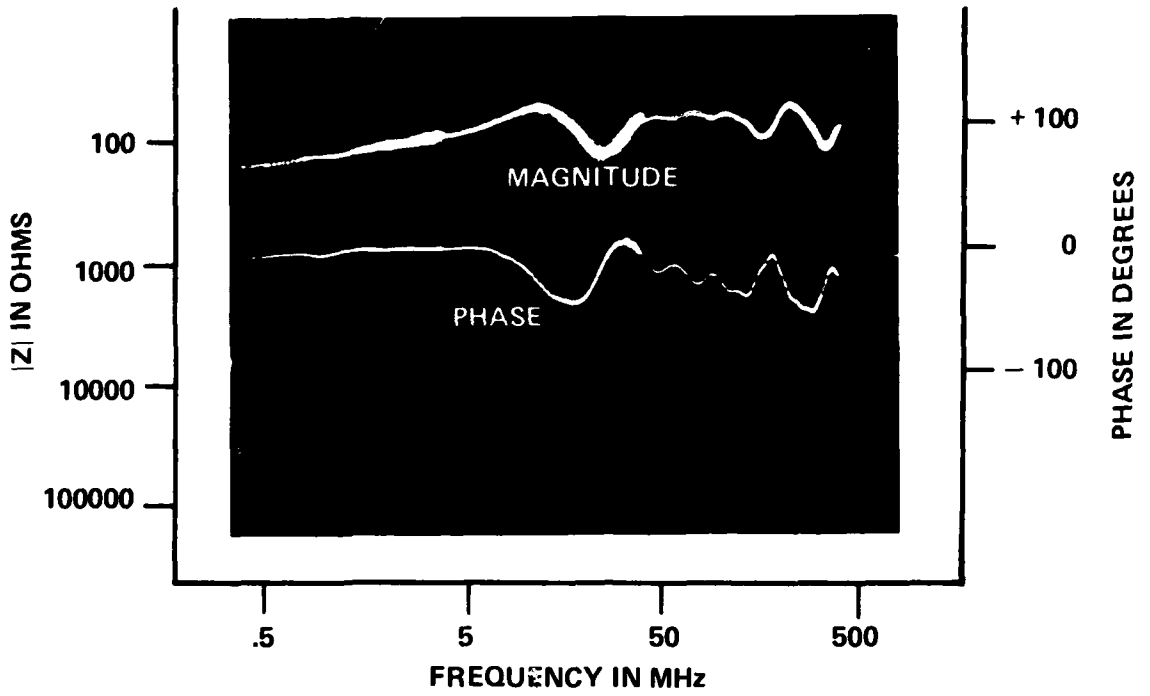

Figure 45. Impedance of ground rod, four auxiliary grounds, and an aluminum ground plate.

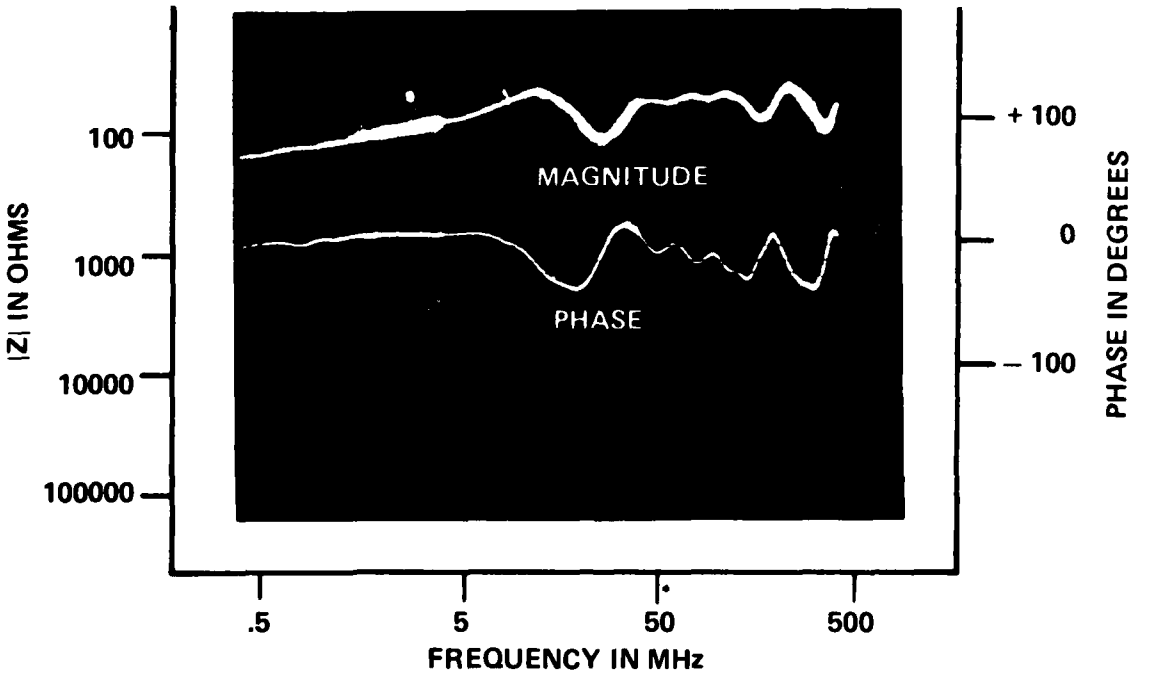

Figure 46. Impedance of ground rod, four auxiliary grounds, and a buried aluminum ground plate.

A graph of the results is shown on Figure 47. For this second order system, the resonant frequency is approximately 15 megahertz. The response of the final test configuration (Figure 46) reveals a resonance around 8 to 9 megahertz with ringing from 100 to 500 megahertz.

4.2.2 Low Frequency Measurements

The impedance of an earth electrode at low frequencies is dominated by the properties of the soil. Analytically the resistance of a ground rod can be determined if the soil resistivity, ρ, and the rod geometry are known, i.e.,

$$R = \frac{\rho}{2\ell} \ell n \frac{2\ell}{a} \text{ ohm} \qquad (38)$$

where ℓ = length of the rod and a = its radius.

Experimentally the ground rod resistance was accurately measured by the Fall-of-Potential Method (see Figure 48) [30]. This is a simple voltage drop measurement relating the current injected to the resistance of the probe (ground rod). (The injected current usually has a frequency of 70 to 100 hertz so as not to be confused with stray 60 hertz ground currents.) The ground probe resistance was found by recording the resistance on a Biddle Meggar-Earth Tester* as distance, d (distance between the ground rod and probe C_2), was varied. The potential probe, P_2, must be placed 62% of d, between the ground rod and probe C_2. By using this method a plot was made of ground rod resistance versus separation distance, d (see Figure 49). From this graph the test ground rod resistance was determined to be 107 ohms.

The four probe technique can also be used to find soil resistivity, ρ. The resistivity of the soil at the test site was measured using the test setup shown in Figure 50.

It was determined to be 97.67 ohm-meter. With this resistivity, the resistance of the ground rod should be 98.6 ohms, which is within 10% of the Fall-of-Potential Method. (This result is considered to represent reasonable accuracy, given the high degree of dependence of the tests on environmental conditions.)

---

* James G. Biddle Co., Plymouth Meeting, PA 19462

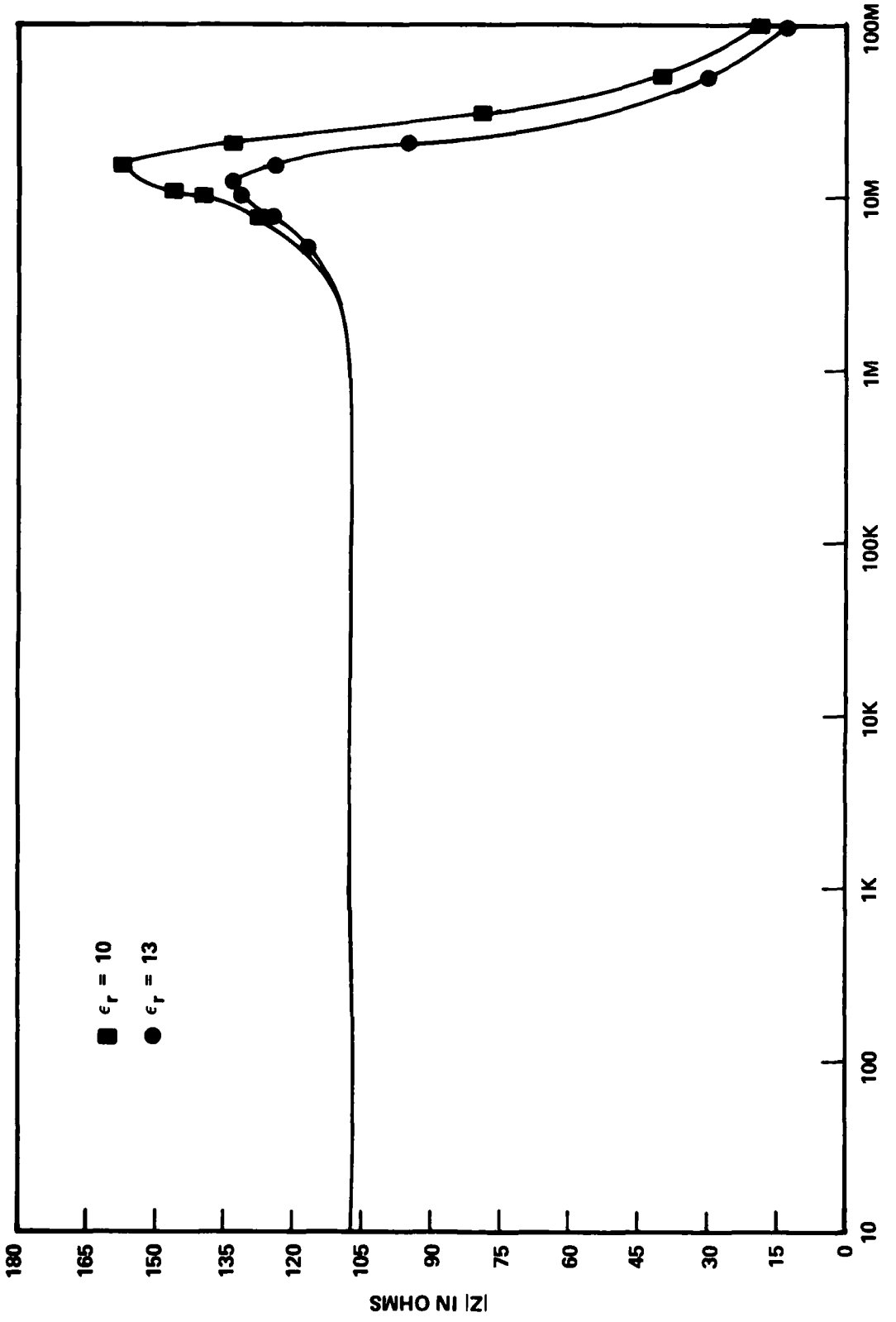

Figure 47. Computer simulation of impedance of ground electrode model.

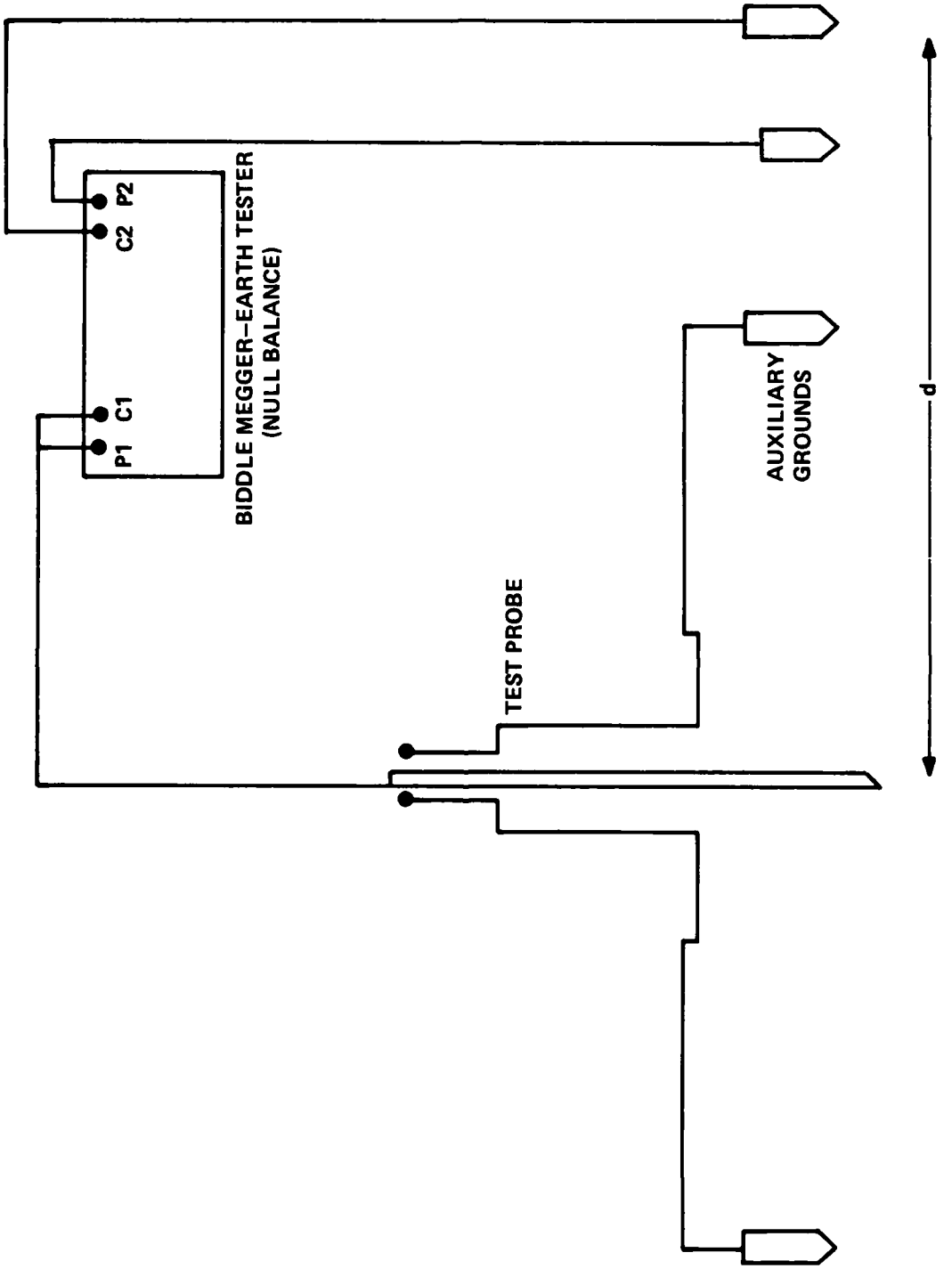

Figure 48. Test setup for low frequency measurements.

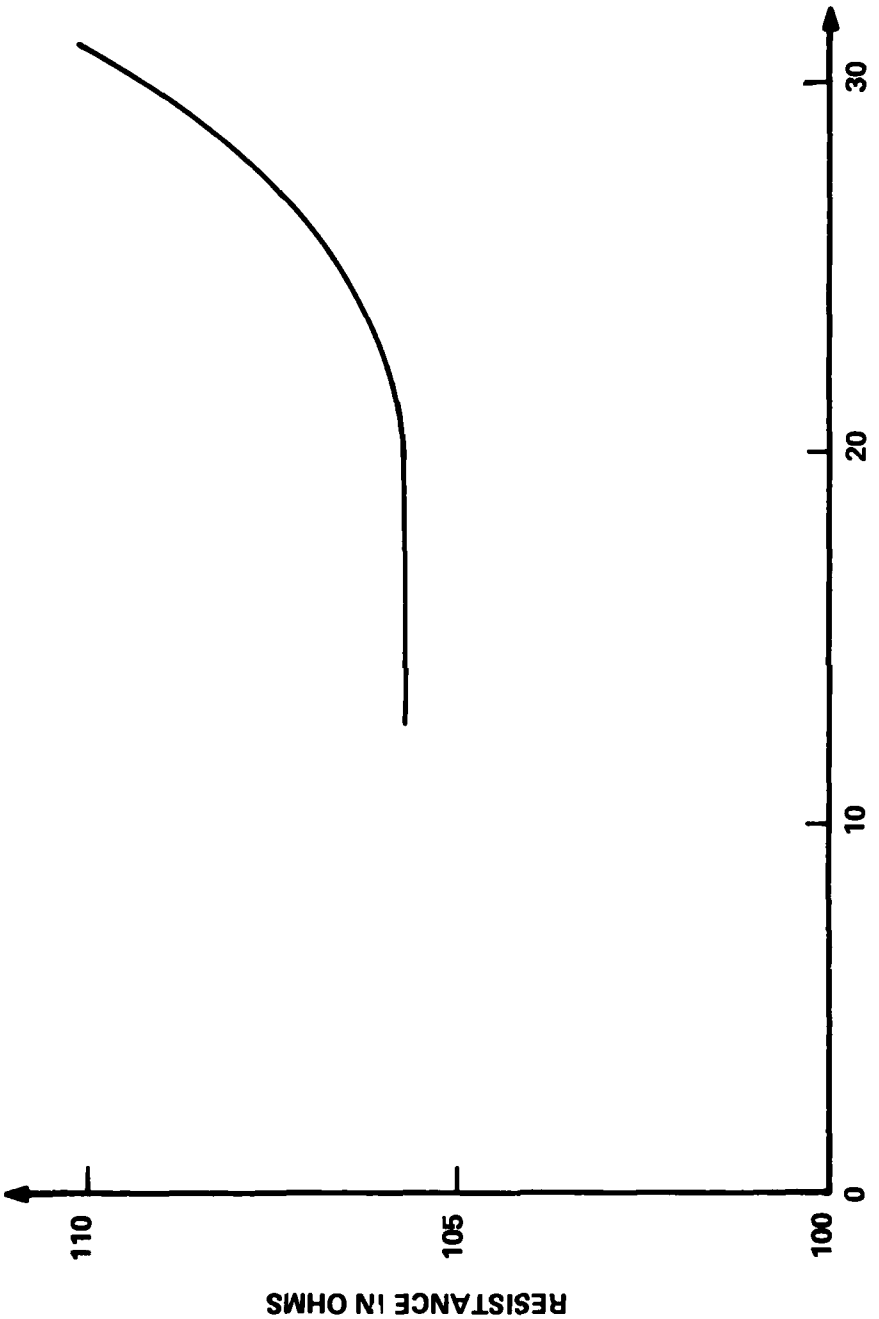

Figure 49. Test probe resistance characteristic.

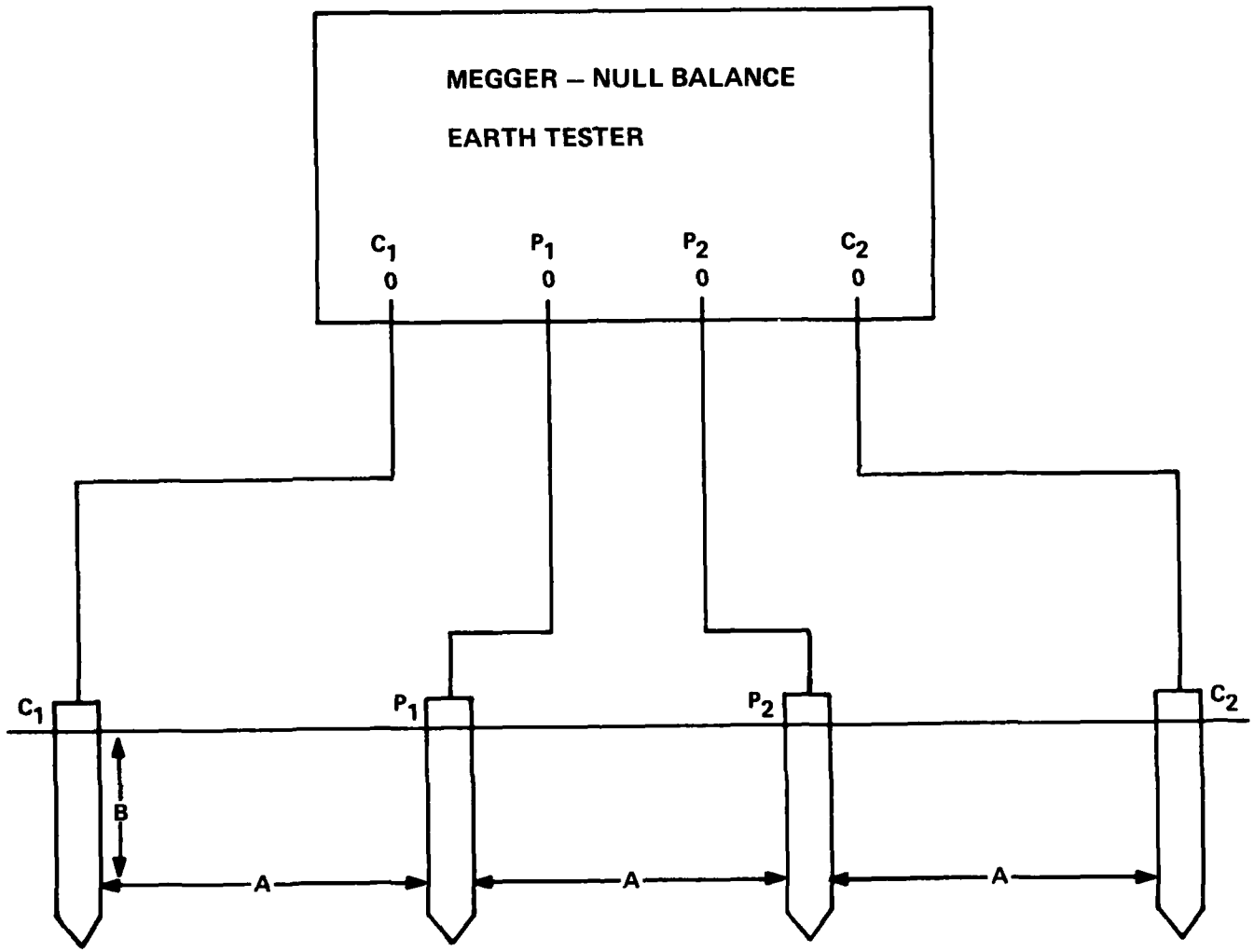

Figure 50. Soil resistivity measurement setup.

4.2.3 Mid-Frequency Measurements

The mid-frequency range, 100 hertz to 500 kilohertz, impedance measurement proved to be the most difficult to obtain because of instrumentation limitations. Most off-the-shelf impedance measuring devices require that the object of the test not be grounded. (Specifically the HP 4800A Vector Impedance Meter has "DO NOT GROUND" printed under the input terminals.) Therefore, measuring the impedance of a grounded rod proved impossible with this type of instrument.

An approach was developed which relied strictly on network theory and the fact that the magnitude of the impedance is equal to the ratio of the magnitude of the voltage across and the current through the rod. Several attempts were made to obtain a suitable measurement. Since most oscilloscopes use "ground" as a reference and have a high impedance input, there was no problem with making voltage measurements on the source end of the ground rod. A problem arose in trying to measure the current into the ground rod, however. The first try was to measure the voltage drop across a one ohm resistor in series with the ground rod. Problems were encountered when the oscilloscope probe shield was connected to the terminal of the resistor thereby adding another "ground" to the circuit. Attempts were made to isolate the oscilloscope from ground, but this only served to increase the noise in the measurement. Obviously, a method of measuring the current was needed which would provide isolation from ground and provide noise reduction.

An HP current probe and amplifier provided just such a solution (see Figure 51). This test setup worked well in measuring the ground rod impedance over the mid-frequency range. The results match the low and high frequency impedance measurement of the rod and allowed measurements of impedance over the low end of the EMP spectrum. Figure 52 is a plot of the test probe impedance to ground using the mid-frequency setup. The highest frequencies are compared to the high frequency test and the results are within the measurement error.

The test procedure consisted of varying the frequency of the HP 651A Test Oscillator, while maintaining constant output voltage, and measuring the voltage at the terminal of the ground rod and the current through the lead to the ground rod. The test probe configuration was the same as for the high frequency measurements technique. The ground plate and auxiliary ground points were used to provide an effective reference contact with the soil.

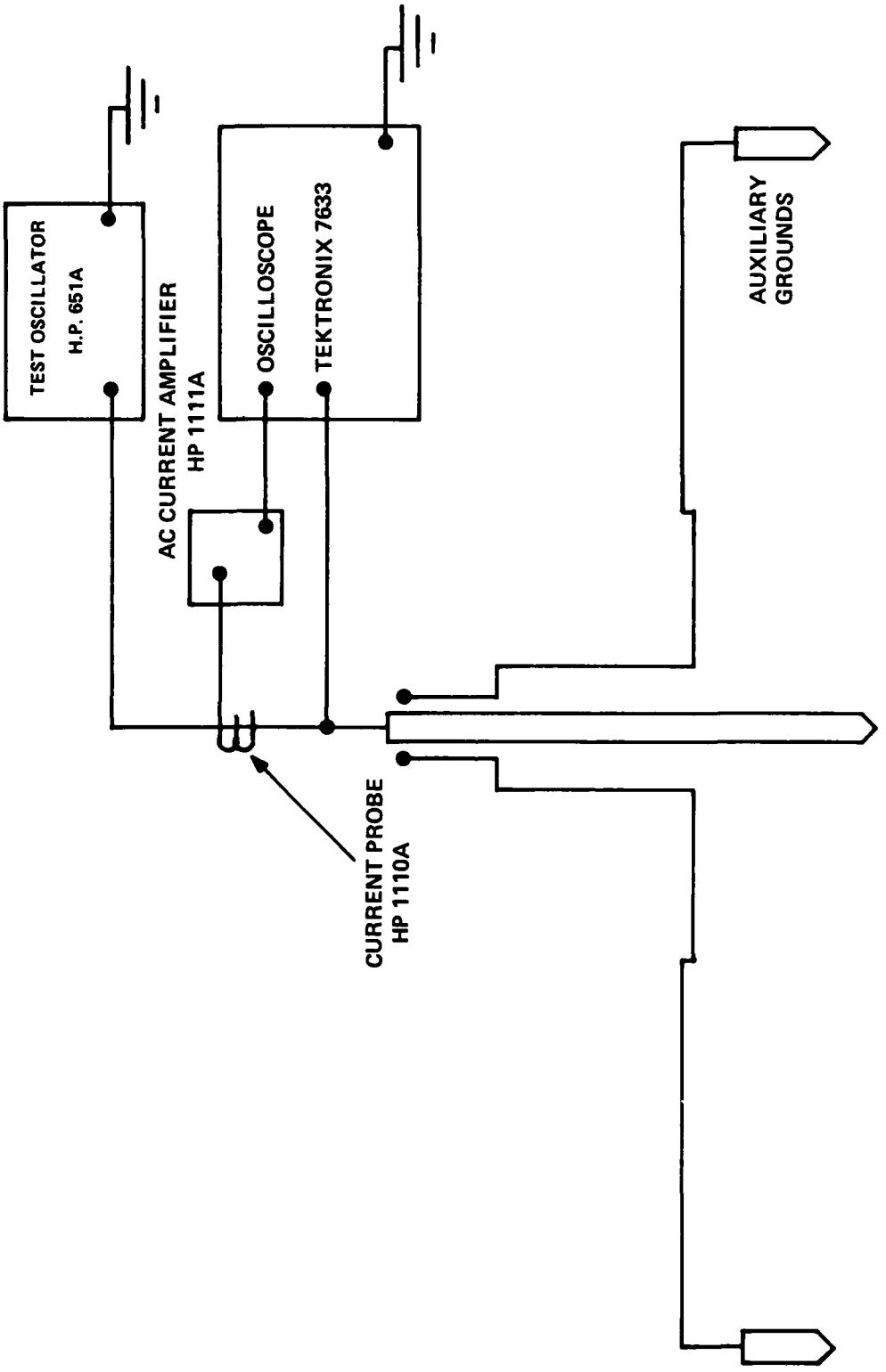

Figure 51. Test setup for mid-frequency measurement.

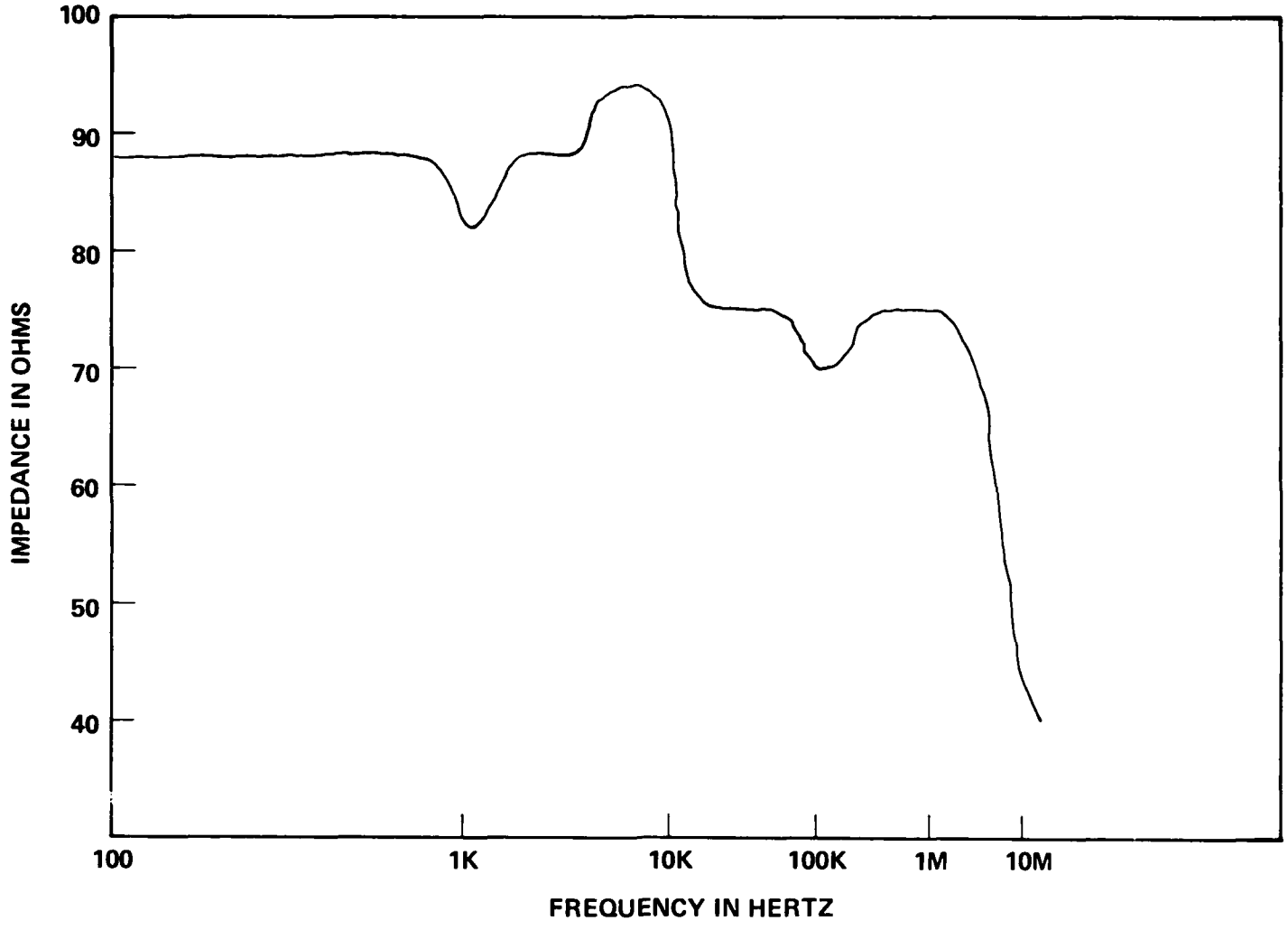

Figure 52. Mid-frequency ground electrode impedance behavior.

AD-A131 255 SUPPLEMENTAL GROUNDING OF EXTENDED EMP COLLECTORS(U) 2/2
GEORGIA INST OF TECH ATLANTA ENERGY AND MATERIAL
SCIENCES LAB H W DENNY ET AL. 31 JAN 82 DNA-5940F
UNCLASSIFIED DNA001-80-C-0294 F/G 20/14 NL

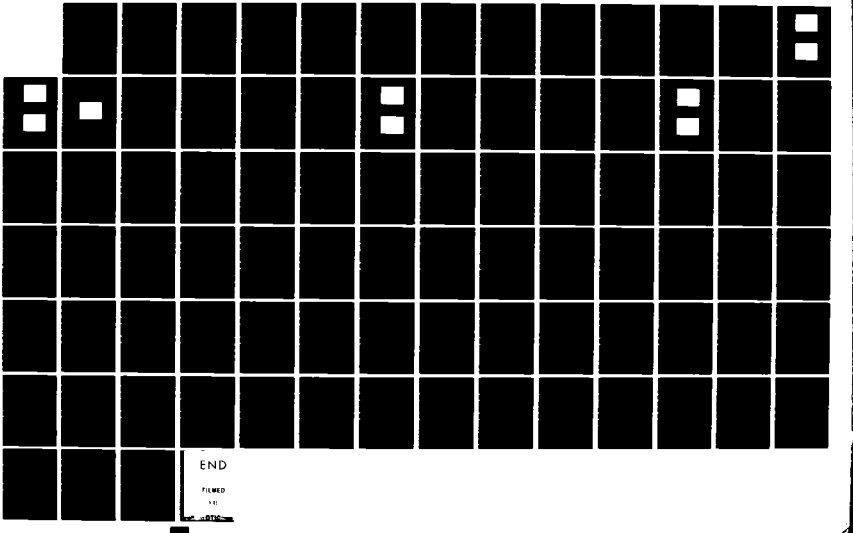

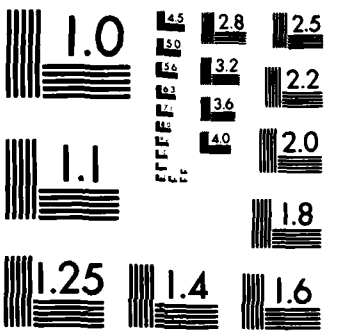

4.3 EVALUATION OF GROUND ELECTRODES

There are times when a single ground rod does not offer an adequately low impedance path to earth, and another configuration will be required to provide a lower impedance path to earth. Electric utilities use this approach in substation grounding whereby they use a ground mat (a combination of rods and wires) to effectively ground an entire area. By connecting ground rods in parallel, the overall impedance can be lowered. This is a well understood practice for low frequency grounding. The purpose of the grid is primarily to lower the step-and-touch potential between any two step and touch points in the area when large fault currents are flowing. This principle is presumed to hold true for lightning strokes although utilities are constantly trying to upgrade their tower grounding techniques [31] to handle the high frequency as well as high currents of lightning. A good reference for substation grounding techniques is the IEEE "Guide for Safety in Alternating-Current Substation Grounding," [3]. This guide tells how to calculate and measure ground rod impedance. Section 23 of the guide is devoted to Model Testing [32]. Model testing has been employed to determine ground resistance and potential gradient patterns of different grounding configurations because modeling allows the various parameters to be controlled. This control allows a comparison of different grounding schemes to be made. The model usually consists of scaled (1:20) ground rods and wires, submerged in a tank of water. The resistance measurements are made by the standard Fall-of-Potential method described previously. The scaling factors are used to relate the test measurements to various conditions of fault current and earth resistivity. It was assumed that this technique could be coupled with scale modeling techniques for electromagnetic systems [33]. Scale modeling techniques have been effectively used for the measuring patterns of low frequency buried antennas [34]. Thus, scale modeling was used to assist in the measurement of high frequency impedance characteristics of different electrode configurations.

4.3.1 The Scale Models

The development of a scale model to accurately predict results of an electromagnetic system requires that strict attention be paid to the four scaling factors:

ρ = the scale factor for length

γ = the scale factor for time

α = the scale factor for electric intensity

β = the scale factor for magnetic intensity

If these parameters are accounted for when deriving the model, then an absolute model of the system can be developed.

The scale factor for length will determine the physical size of the model. Since the purpose was to measure ground rods and wires, a value of p was chosen which would allow multiple rods to be placed in a relatively small box of soil. The physical limitations were the size of the box and the quantity of earth required to fill it. The typical ground rod is approximately 3 to 4 meters in length and 1.0 to 2.5 cm in diameter. Noting that the model length, ℓ_m, will vary as

$$\ell_m = \frac{\ell}{p} \tag{39}$$

then a model length of 4 cm can be used if p = 100. It was felt that 4 cm would be a convenient length because the box of soil could be 15 cm in depth and not cause fringing problems. Therefore, a 100 to 1 length scale factor was chosen.

The soil parameters for the experiment will vary with the model scale factors by the following relationships:

$$\sigma_m = \frac{p\alpha}{\beta}\sigma \tag{40}$$

$$\varepsilon_m = \frac{p\alpha}{\beta\gamma}\varepsilon \tag{41}$$

$$\mu_m = \frac{p\beta}{\alpha\gamma}\mu \tag{42}$$

The impedance of the model will vary with the scale factors of the E and H fields:

$$Z_m = \frac{\beta}{\alpha} Z \tag{43}$$

Note in Equation (43) that the model impedance is not an explicit function of physical or time scaling. Therefore, the network analyzer could be used to measure the impedance with the E and H scale factors equal to 1.0. This approach facilitated measurements because the impedance of the ground network could be read directly off the analyzer screen.

The model soil is a 325 Mesh Silica mixed with granulated graphite in a 7 to 5 mixture. The relative dielectric constant and the conductivity was determined to be 11.3 and 0.12 mho per meter, respectively. This mixture was placed in a copper lined styrofoam box to a depth of about 15 cm. A copper ground plate with a cut-out for the ground test samples was placed on top of the soil (see Figures 53 and 54).

The ground test sample configurations were chosen to conform with commonly used geometries. These configurations were numbered from one to five as follows:

No.	Configuration	Figure
1.	Single Ground Rod	55
2.	Two Parallel Rods	56
3.	Three Parallel Rods (triangular)	57
4.	Eight Parallel Rods (star)	58
5.	Eight Parallel Rods (loop)	59

The construction of the ground rod assemblies began with a square plastic plate for support. A copper plate was glued to the top of the plastic plate and a hole was drilled through the two plates. A BNC connector was then placed over the hole, and the shield was soldered to the copper plate. A 4 cm long, #32, 0.127 cm wire was then soldered to the BNC connector (see Figure 55). The size of the plates was chosen to correspond to the cutout in the copper ground plate of the test box as shown in Figure 54.

The test samples with two or more ground rods have a spacing between rods approximately equal to the length of the rods. (This distance was difficult to control during the actual experiment because of the flexibility of the small diameter wire.)

4.3.2 Configuration Tests and Results

The general test setup is shown in Figure 60. The network analyzer probe was connected to the BNC connector of the sample after the sample had been carefully placed in the soil. Care was taken when the sample was placed in the soil to avoid bending the thin ground rods. Such bending was found to lead to erroneous measurements because the capacitance of the circuit would change with relative position of the rods. In addition, uncorrelated measurements were noted to arise

from variations in soil density. To overcome this problem, the soil was first stirred to loosen it up for the insertion of the ground rods, and then small weights were placed on top of the samples to provide uniform packing of the soil. With this procedure, the experiments were repeatable.

The object of the tests was to determine the impedance characteristics of different ground rod configurations at high frequencies and compare the results with those at low frequency (DC). The DC resistance for different configurations, all other conditions held constant, should vary with the Geometric Mean Distance, A, of the sample [35], i.e.,

$$R = \frac{\rho}{2\pi\ell} \ln \frac{2\ell}{A} \text{ ohms} \tag{44}$$

where

$$A = (a\, S_2\, S_3 \ldots S_n)^{1/n} \tag{45}$$

a = radius of rod

S_i = distance from rod 1 to rod i

Several DC tests were run to determine if the test samples followed this accepted theory. Figure 61 displays a very good correlation between the tests and theory. By adding ground rods of the proper spacing, the effective resistance to ground was lowered.

The high frequency impedance of an earth electrode system should vary as the square root of L/C, where L is the inductance and C is the capacitance of the particular configuration. These parameters vary with Geometric Mean Distance, A, as follows:

$$L = 2\ell \ln \frac{2\ell}{A} \; 10^{-7} \text{ H} \tag{46}$$

and

$$C = \frac{\varepsilon_r \ell}{2\ell n(\frac{2\ell}{A})} \times \frac{10^{-9}}{9} \text{ F} \tag{47}$$

where ℓ = length of rod

ε_r = relative dielectric constant of soil

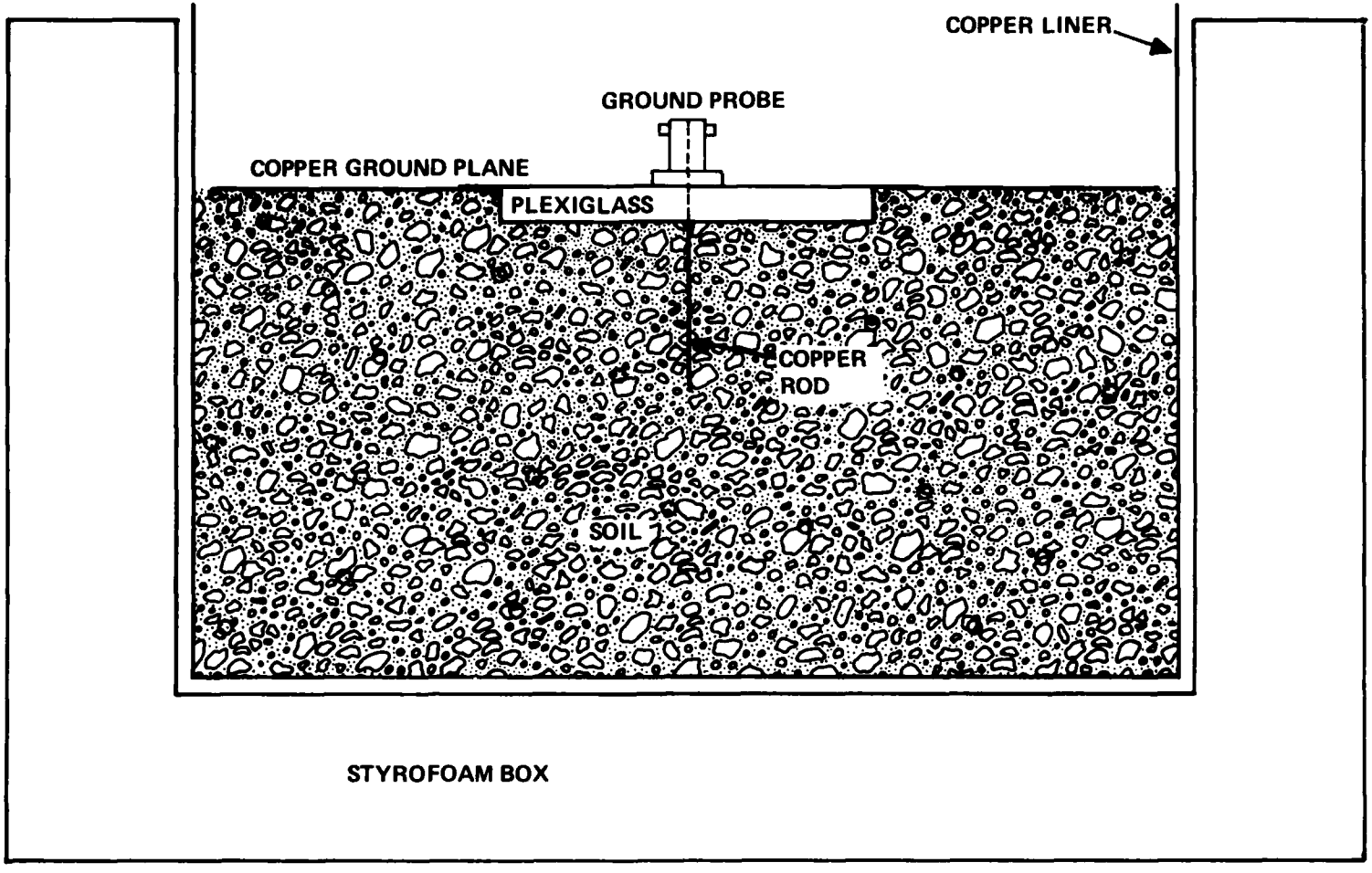

Figure 53. Test box for ground electrode model - cutaway view.

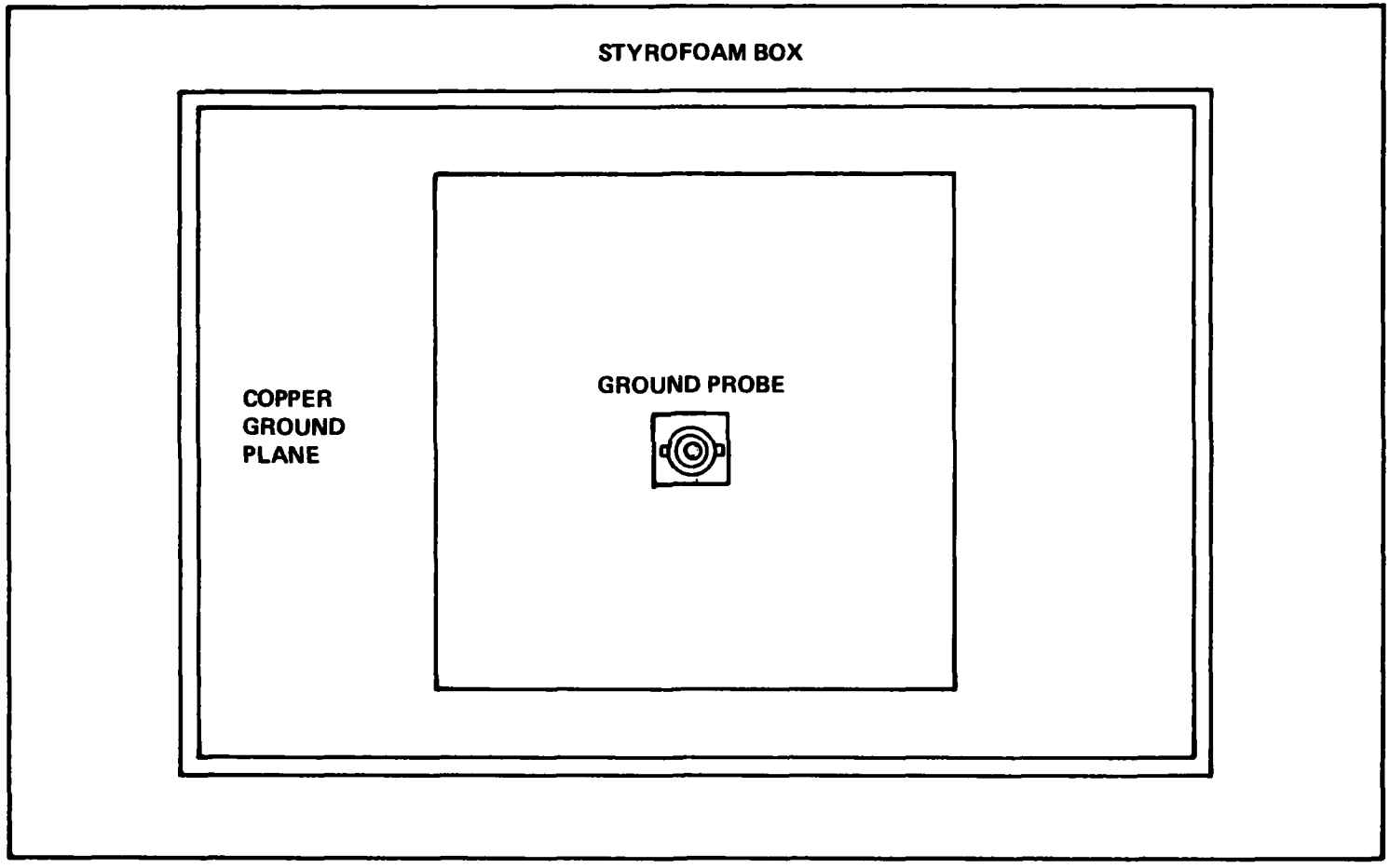

Figure 54. Test box for ground electrode model - top view.

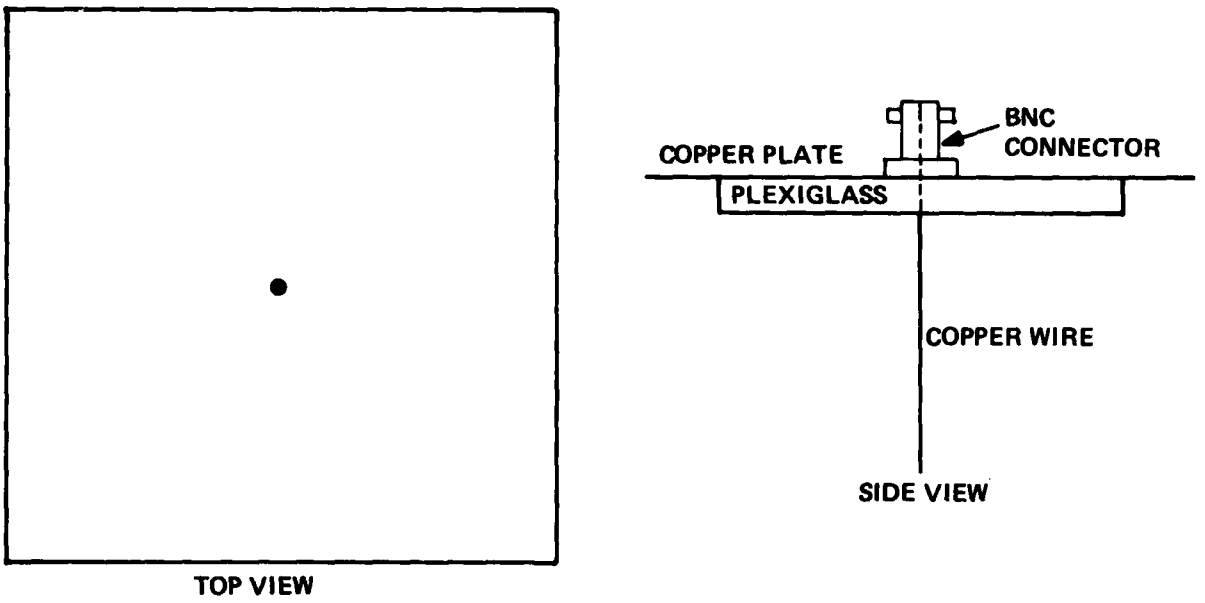

Figure 55. Single ground rod model.

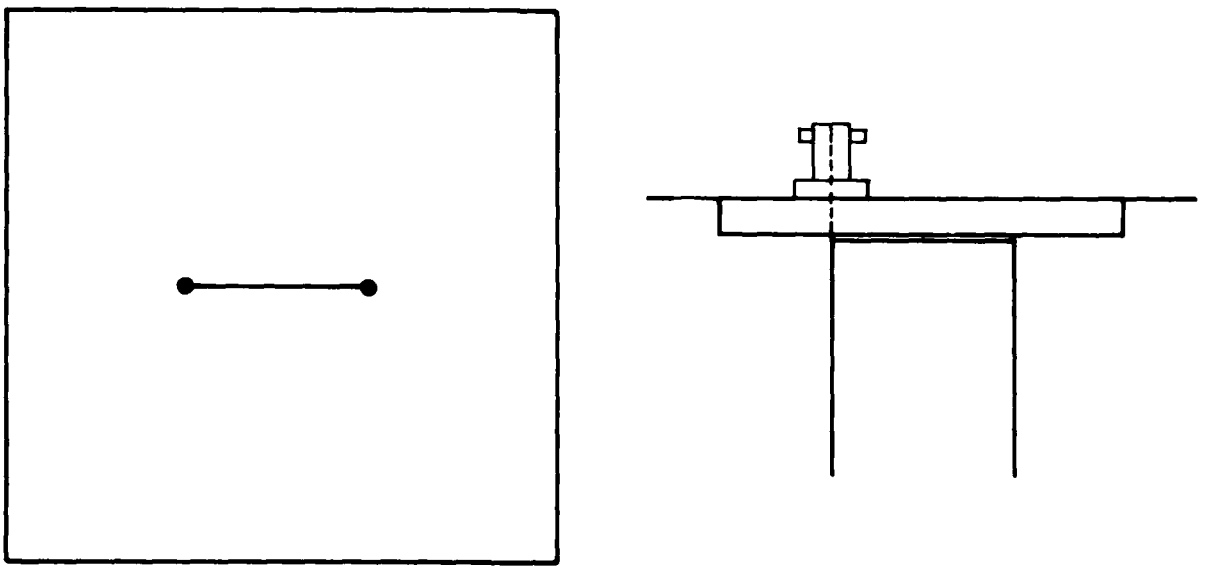

Figure 56. Two parallel rod model.

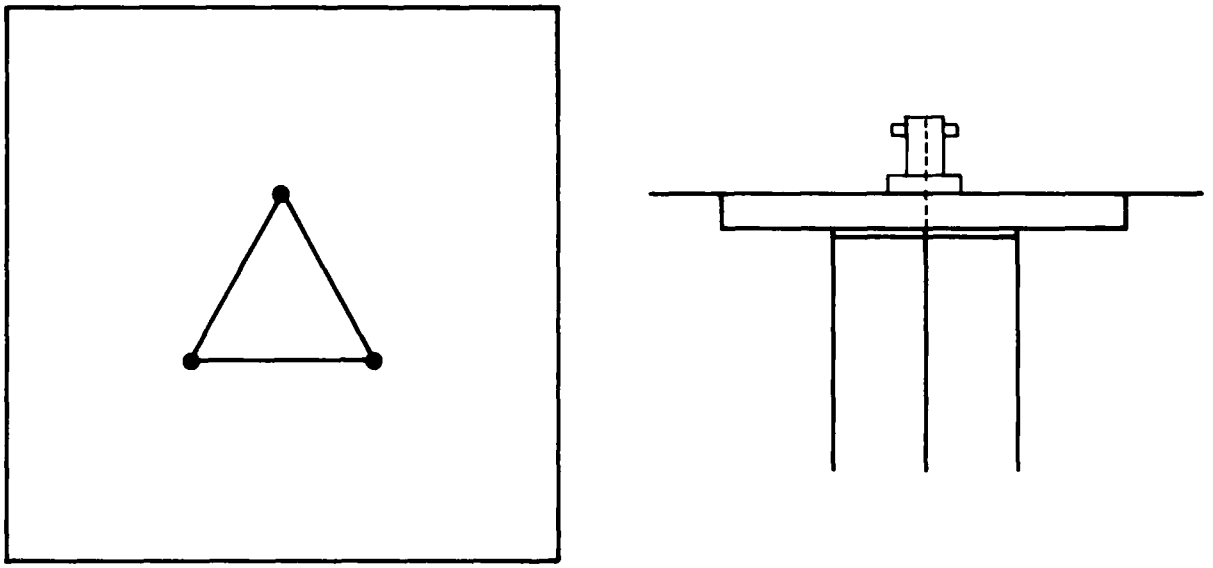

Figure 57. Three parallel rod model.

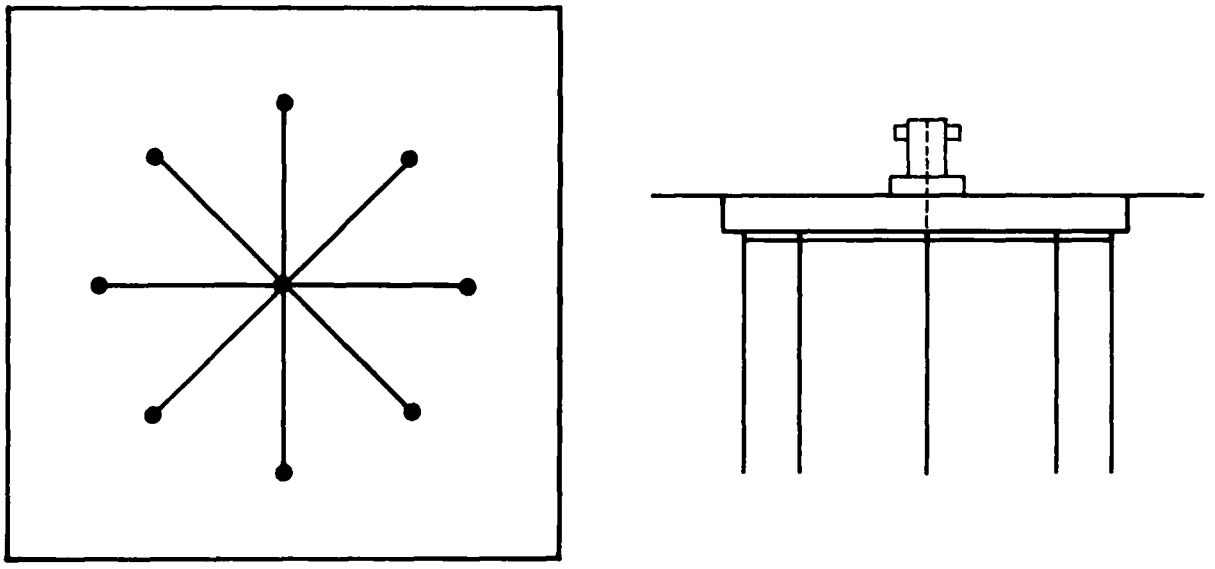

Figure 58. Eight parallel rod (star) model.

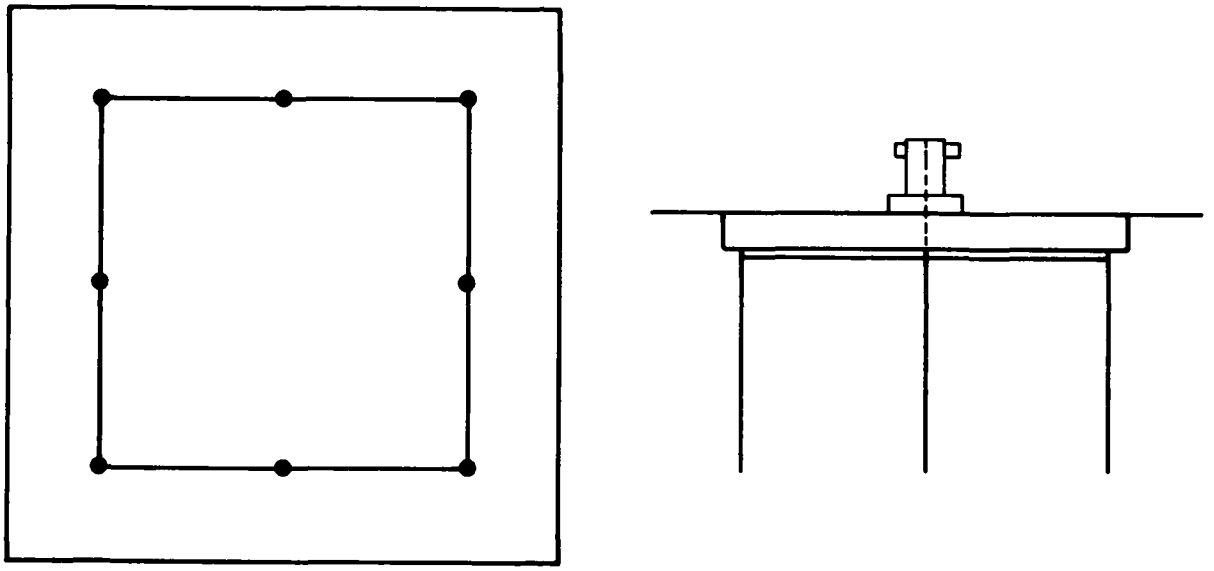

Figure 59. Eight parallel rod (loop) model.

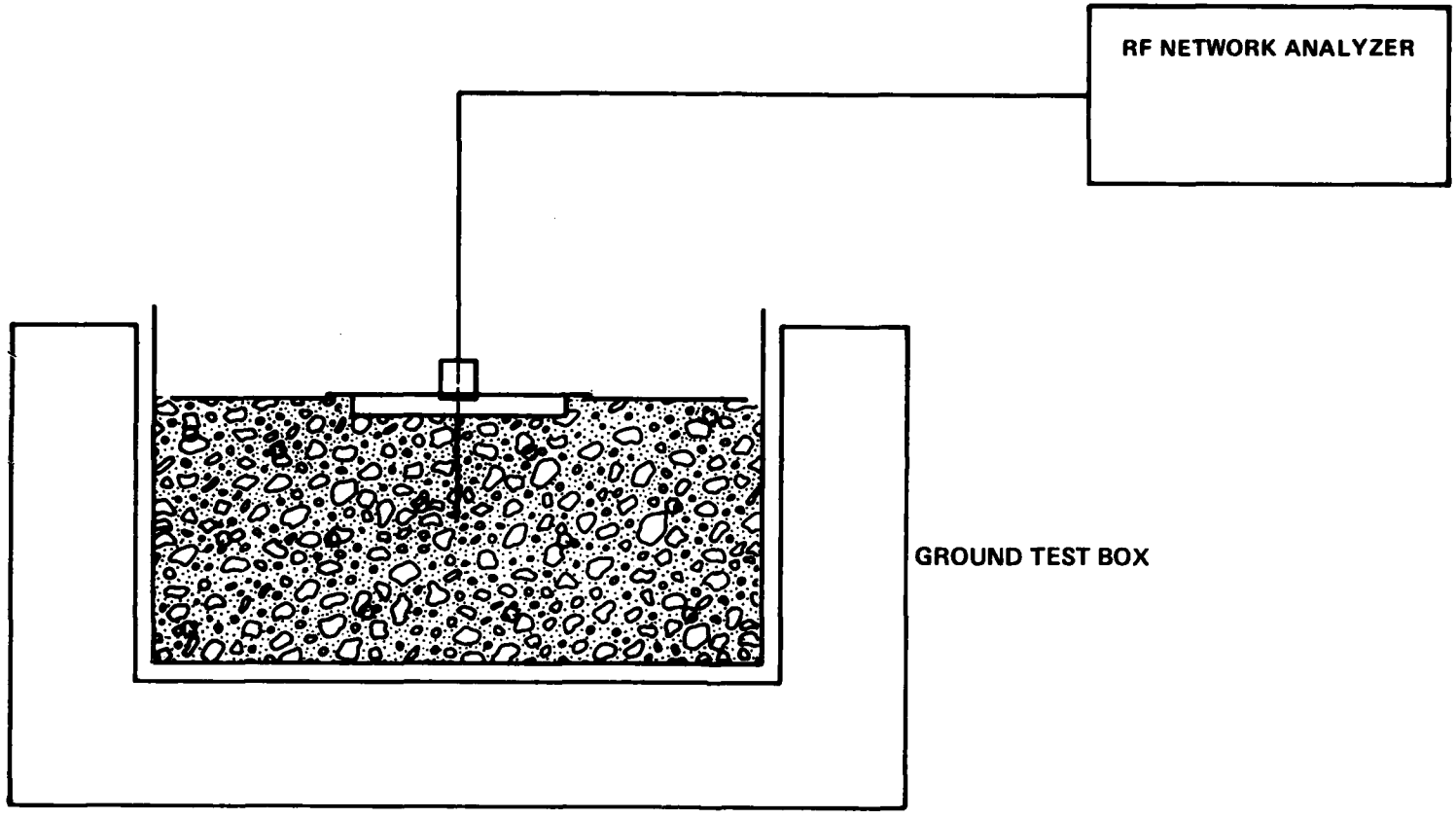

Figure 60. Test setup for model impedance measurement.

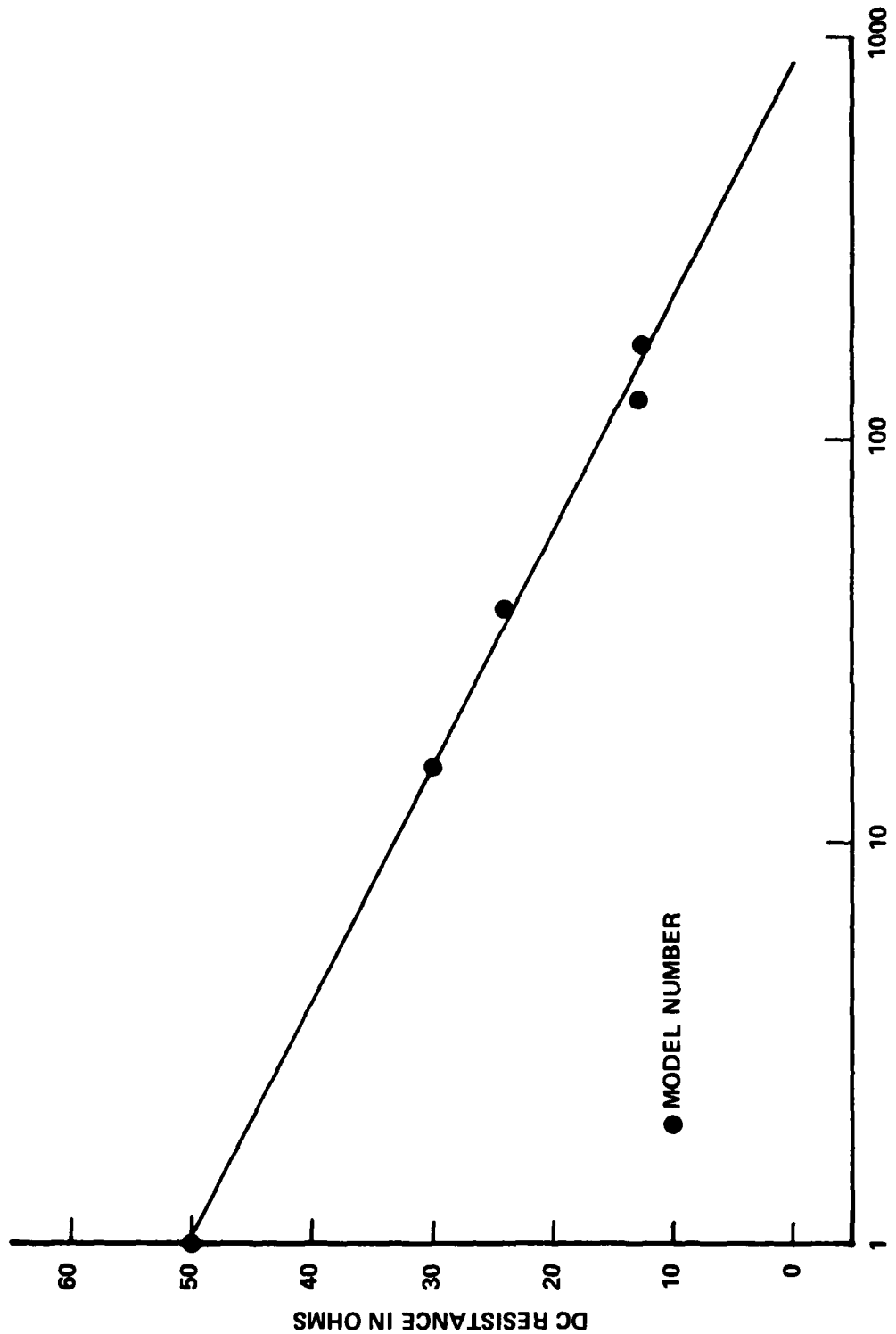

Figure 61. Behavior of electrode resistance with relative area.

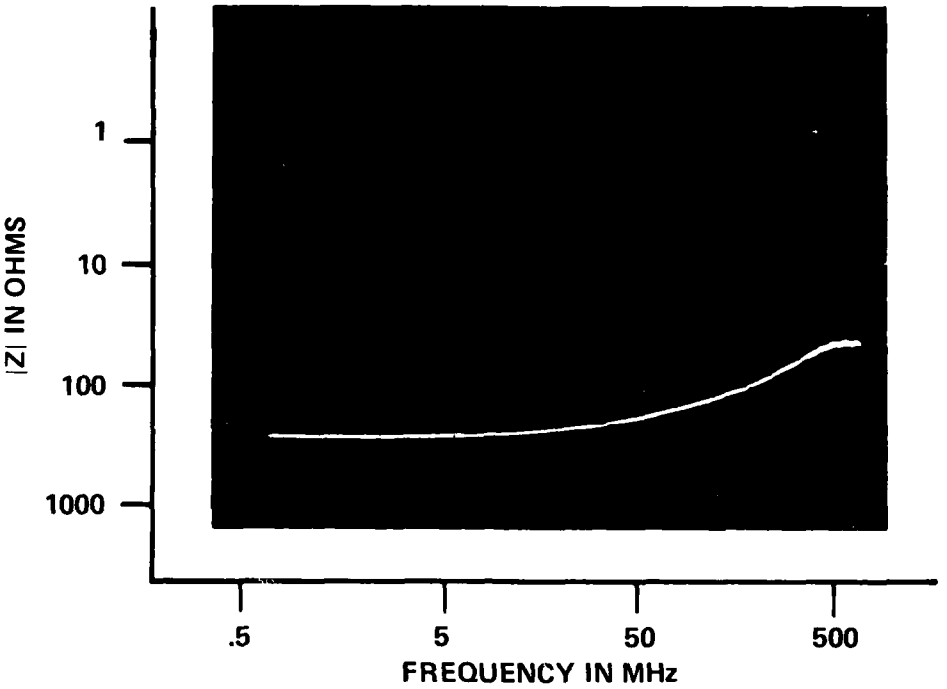

Figure 62. Single ground rod impedance behavior.

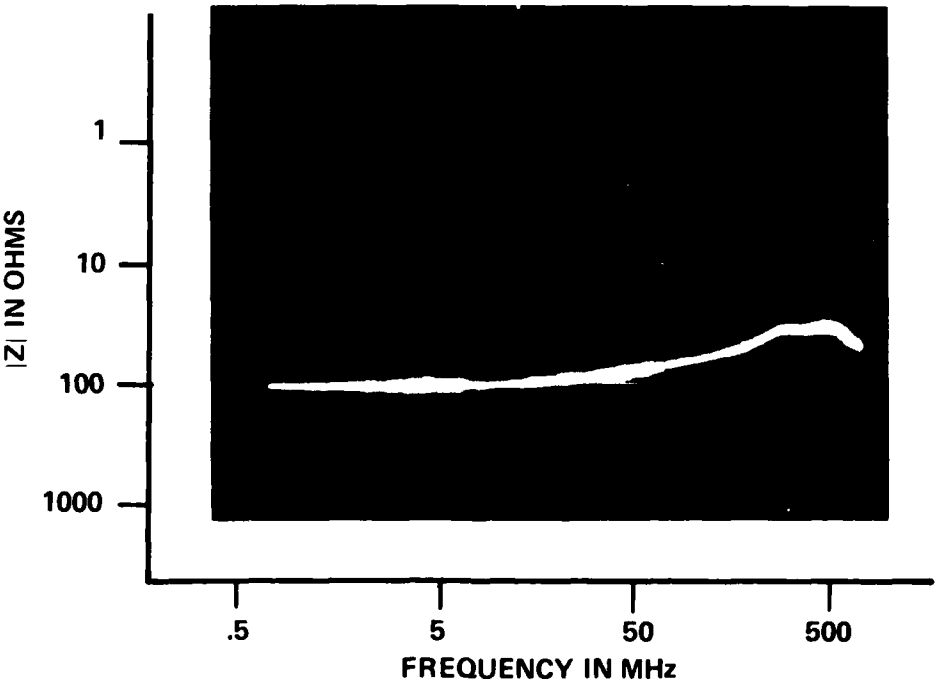

Figure 63. Two parallel rod impedance behavior.

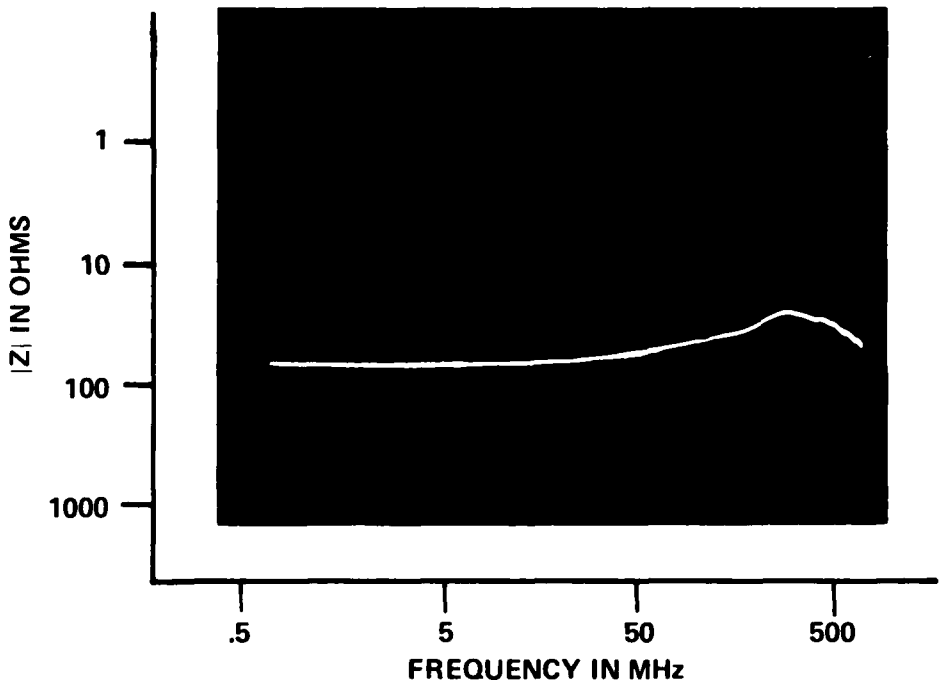

Figure 64. Three parallel rod impedance behavior.

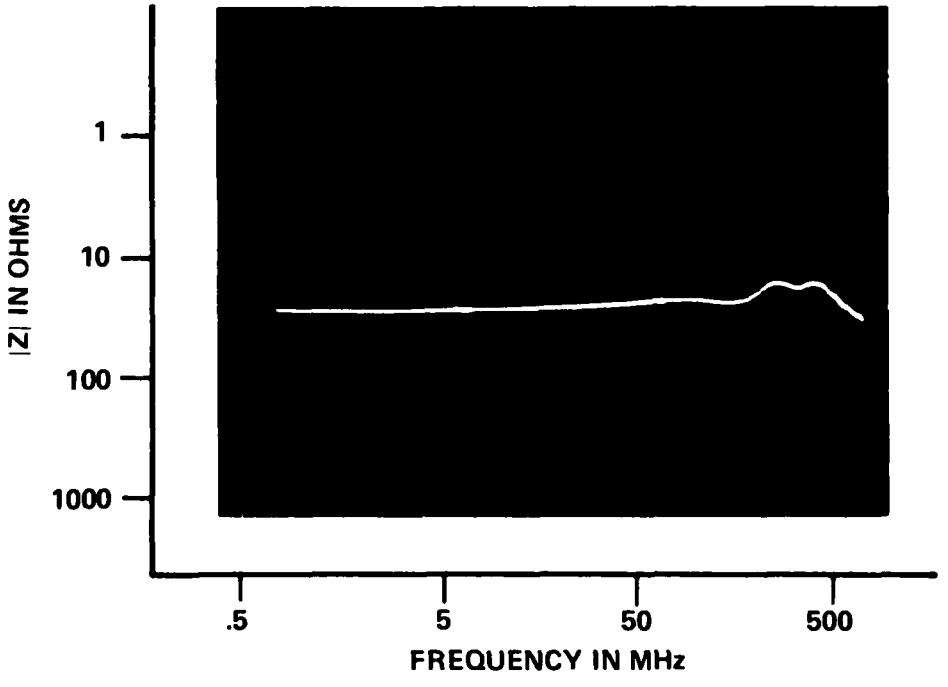

Figure 65. Eight parallel rod (star) impedance behavior.

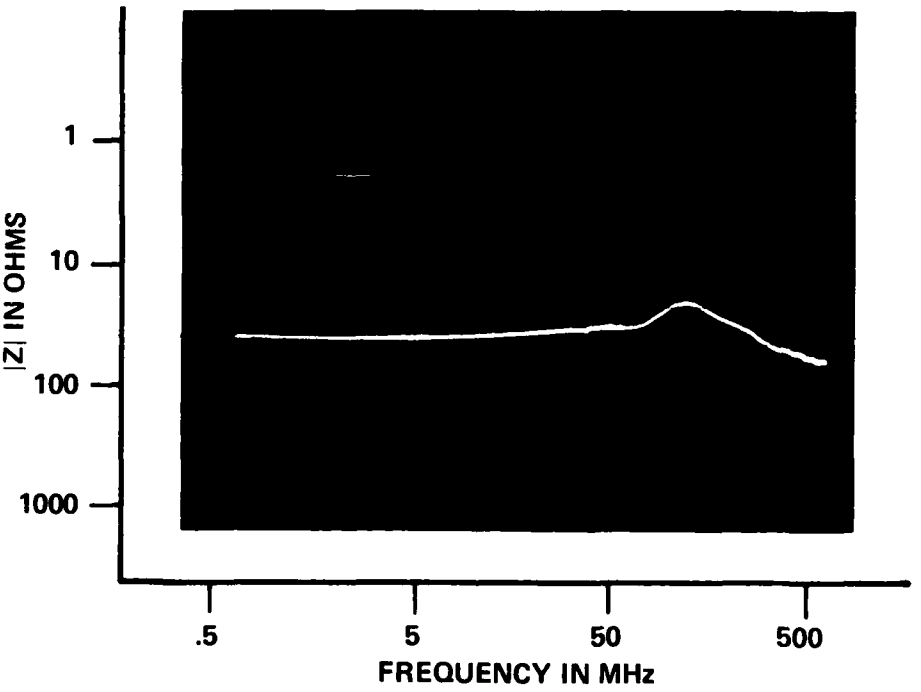

Figure 66. Eight parallel rod (loop) impedance behavior.

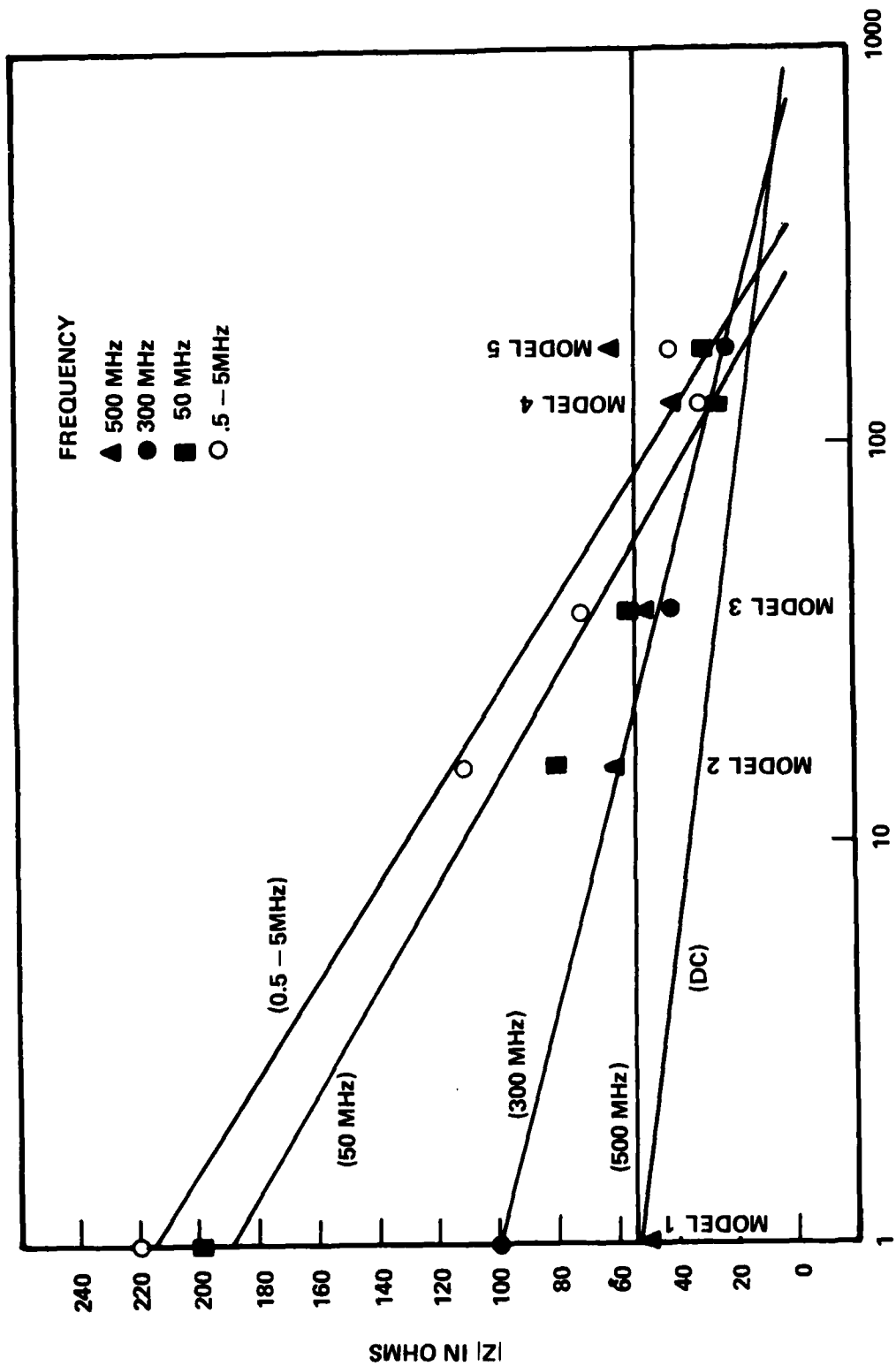

Figure 67. Behavior of model impedances at various frequencies.

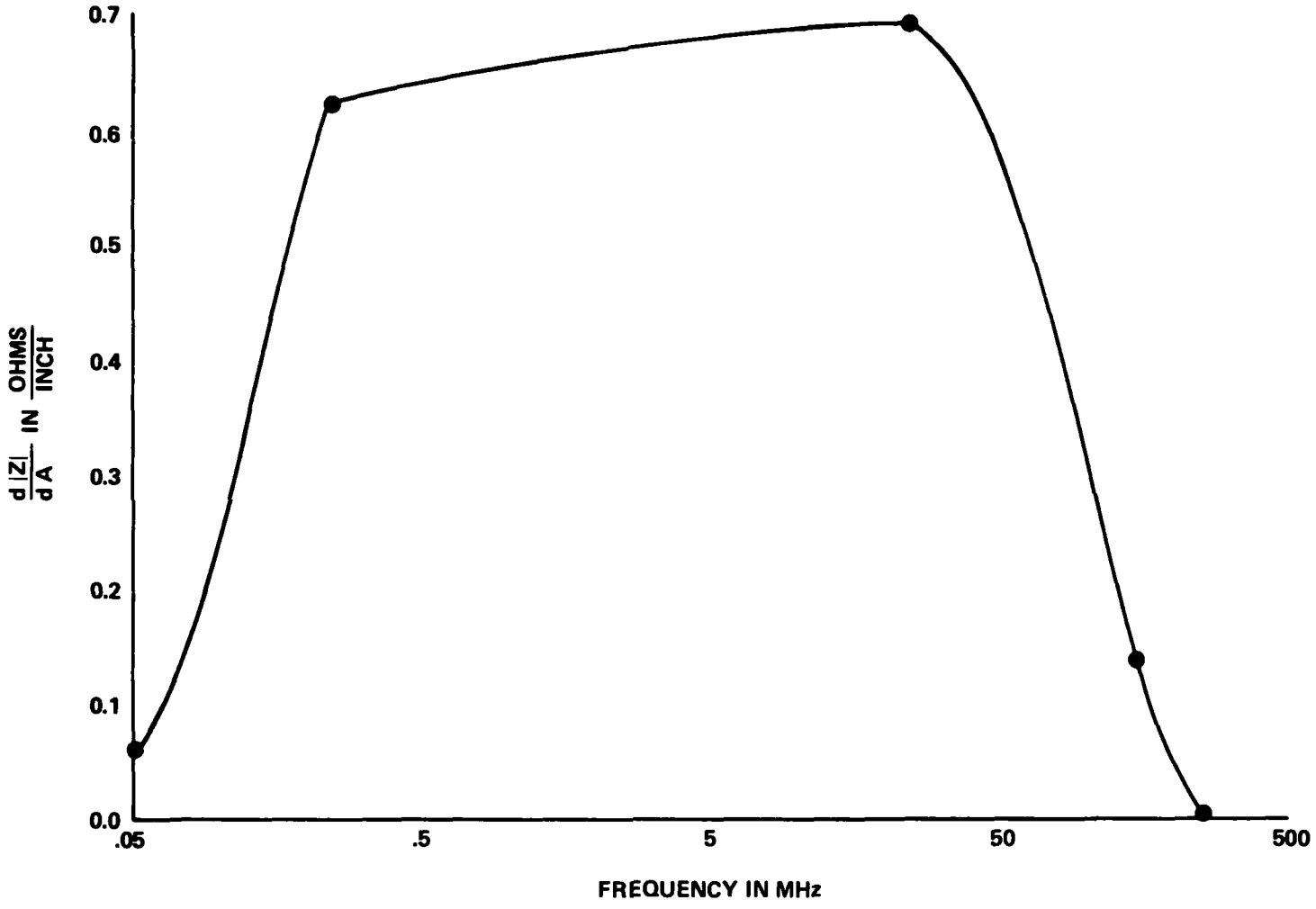

Figure 68. Marginal impedance per geometric mean distance of model.

Therefore, the impedance, Z, will vary with the Geometric Mean Distance, A:

$$Z \simeq \frac{60}{\sqrt{\varepsilon_r}} \quad \ell n \ (\frac{2\ell}{A}) \quad \text{ohms} \tag{48}$$

Testing was performed from 0.5 to 500 megahertz to determine if this hypothesis was true. The results are shown by the photographs in Figures 62 to 66 and are plotted on Figure 67. Examination of the figures reveals that the impedance does decrease with increasing Geometric Mean Distance for frequencies up to at least 300 megahertz. At 500 megahertz the impedance is relatively constant regardless of the ground rod area. It should be noted that the benefits of significant increases in area are limited, particularly at frequencies above 100 megahertz. The range of frequencies between 500 kilohertz and 100 megahertz enjoys the most benefit from increasing the area (see Figure 68). At frequencies above 100 megahertz, the conductor-soil interface evidently predominates, giving little change in impedance for increases in area. At DC the impedance (resistance) is strictly determined by rod contact area which is inversely proportional to the length of the ground system.

To examine this argument more closely, it was decided to remove the rods and leave the ground wires on Models 4 and 5, forming new Models 6 and 7 (see Figures 69 and 70), respectively. The same impedance tests were performed on Models 6 and 7, (Figures 71 and 72) and the results compared to Models 4 and 5 (see Figures 73 and 74). The figures reveal that as frequency is increased the impedance of the "rodless" sample approaches that of the sample with rods. Thus, for any frequency greater than approximately 300 megahertz, surface contact with earth will yield as good a ground as is obtainable. (The impedance to ground will be determined by the soil parameters at the point of contact.)

The above models represent only the external, below ground grid and rod structures. Most facilities, however, use a ground plate or ground bus that runs throughout the facility to which all equipment grounds are tied. There is a need to measure the impedance looking into this ground configuration [36] because this is the "ground" that internal equipment will see. To simulate the facility ground bus, Models 6 and 7 were further rewired so as to connect all the ground points together (multi-point ground) above the ground plate as shown in Figures 75 and 76.

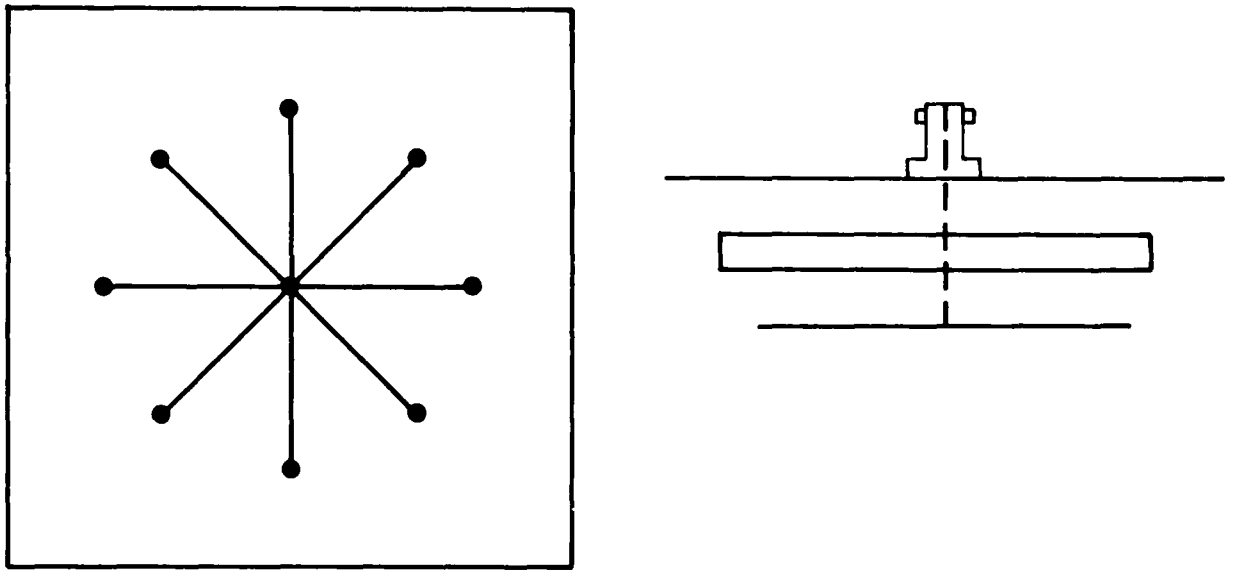

Figure 69. Model 6 - Star with no ground rods.

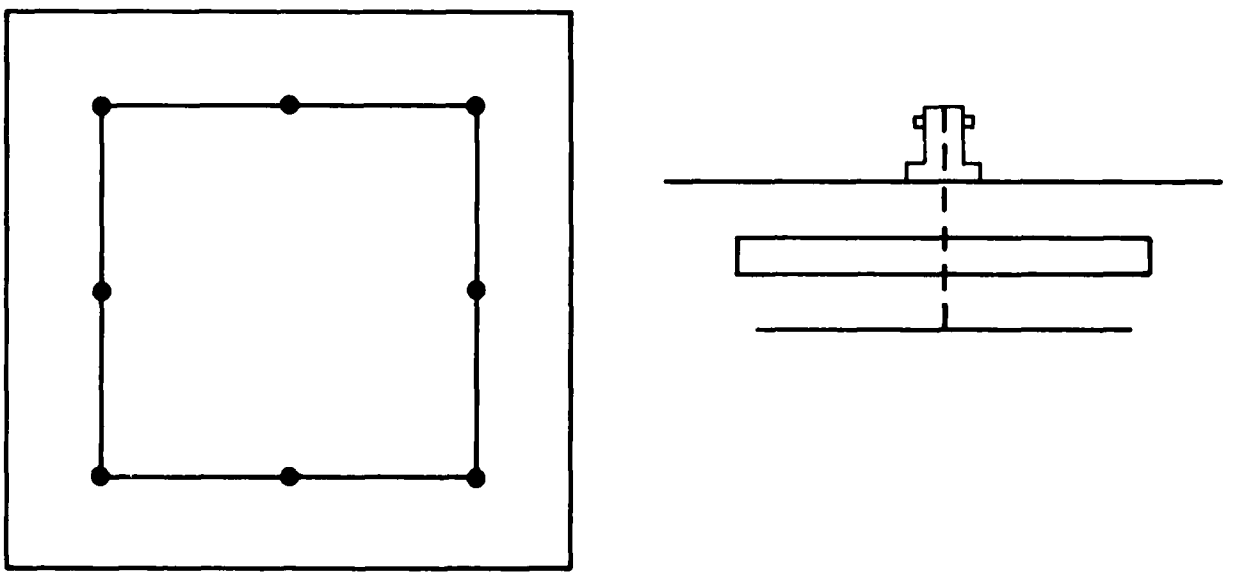

Figure 70. Model 7 - Loop with no ground rods.

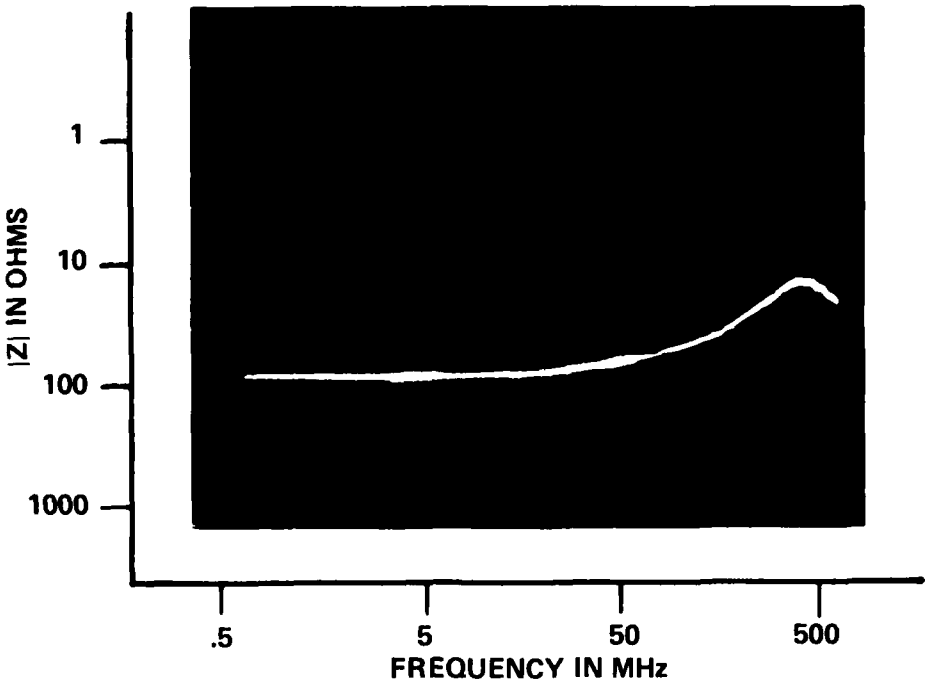

Figure 71. Model 6 impedance behavior.

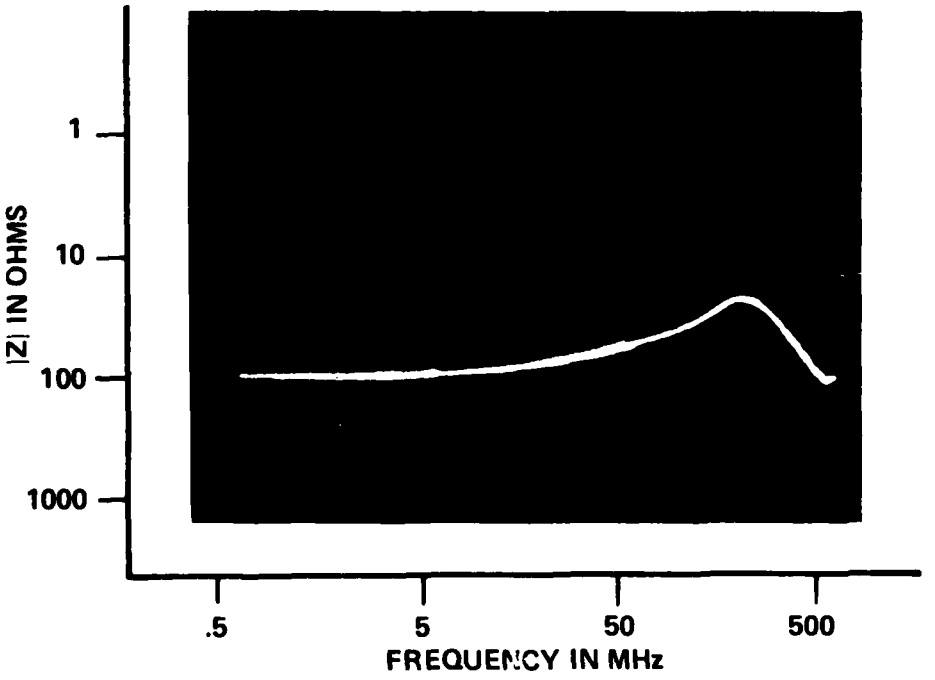

Figure 72. Model 7 impedance behavior.

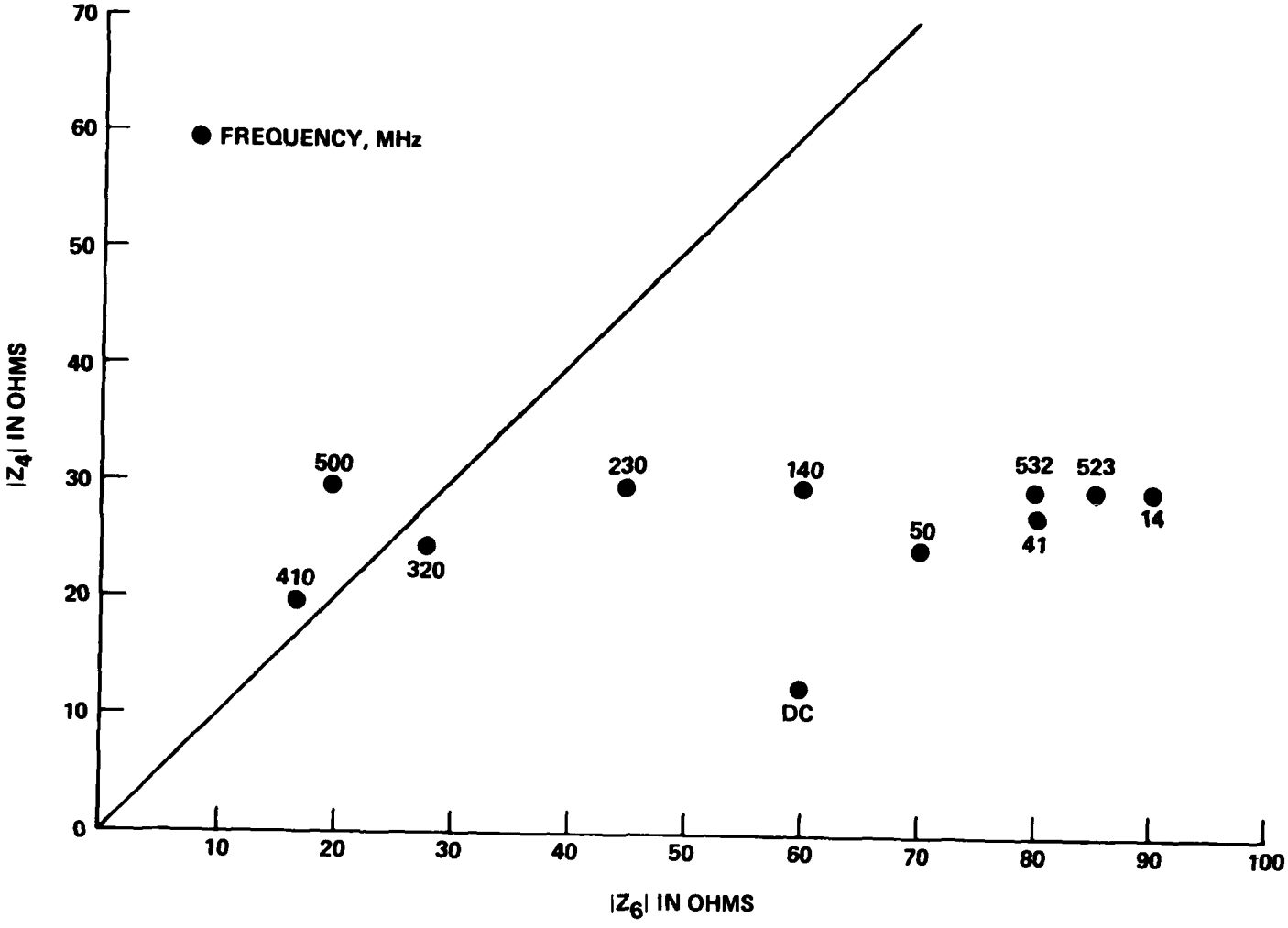

Figure 73. Comparison of Model 4 and Model 6 impedances at various frequencies.

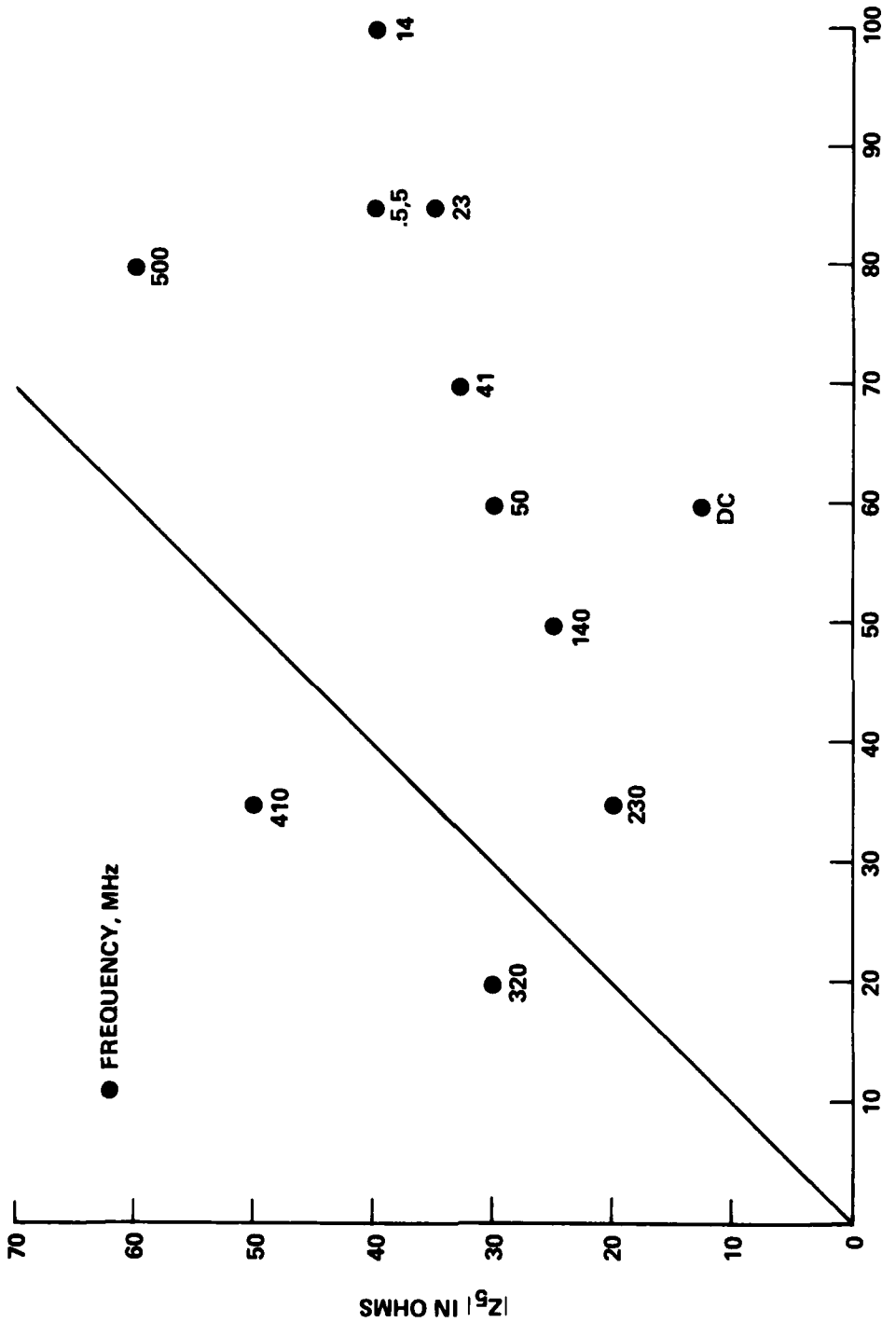

Figure 74. Comparison of Model 5 and Model 7 impedances at various frequencies.

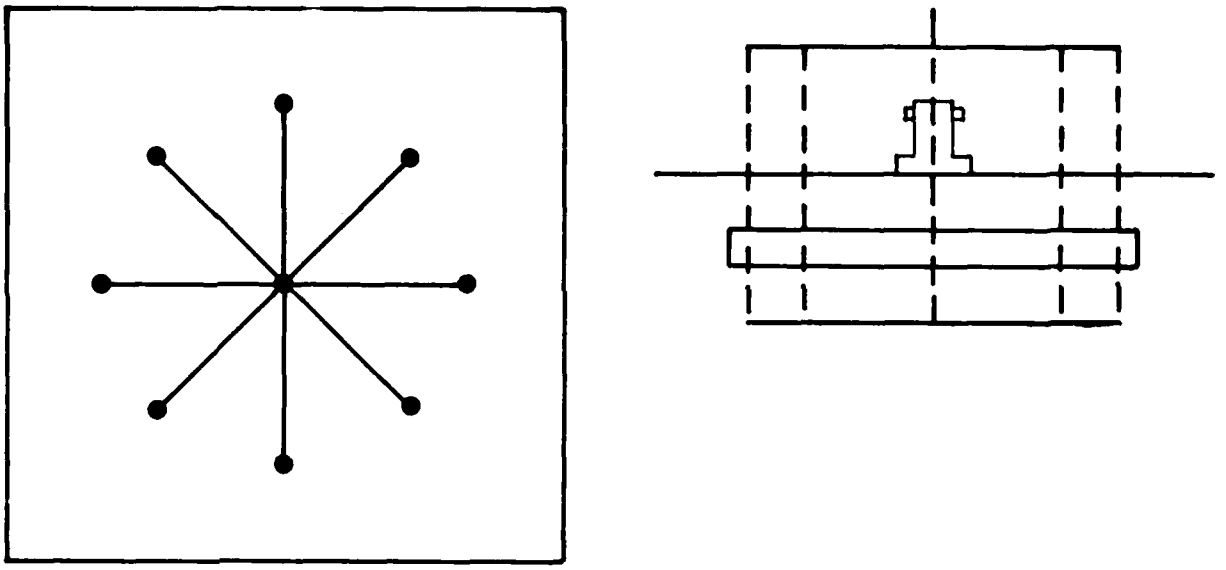

Figure 75. Model 8 - Model 6 with shorted ground connections.

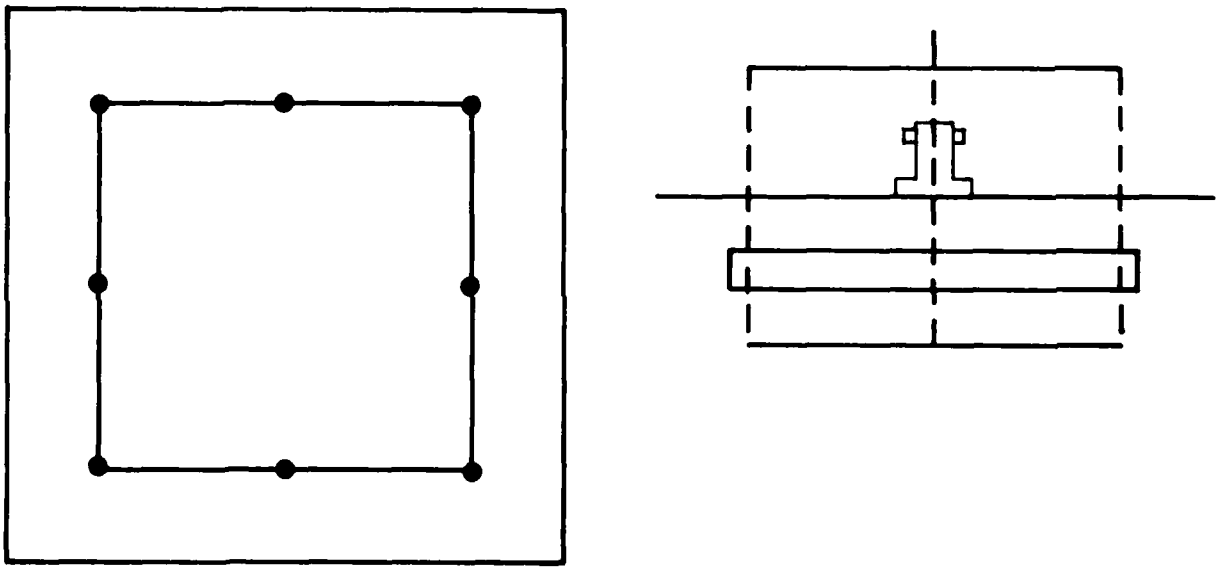

Figure 76. Model 9 - Model 7 with shorted ground connections.

The models thus created were numbered 8 and 9, respectively. These models were connected to the network analyzer and the impedance plots (Figures 77 and 78) were taken. The photos exhibit the resonance characteristics of a series RLC circuit. The added inductance of the above ground wires has added appreciable series inductance to the circuit. Thus, as viewed from the equipment point of termination of a ground lead, the benefits offered by an earth ground may be negated by the inductance of the connecting lead.

4.4 OBSERVATIONS

An earth electrode system behaves like a second order, parallel, RLC network. It's low frequency (DC and power frequencies) impedance is predominantly determined by the resistivity of the soil and the length of the conductors. The high frequency (up to 500 MHZ) impedance of the electrode is governed primarily by the soil's dielectric properties.

The impedance of an earth electrode system is inversely proportional to its geometric mean distance. This proportionality tends to disappear above 300 MHz. Above this frequency, there appears to be no benefit to be derived from increasing the ground system area.

Ground rods appear to be unimportant in so far as the behavior of an electrode system at RF (fast rise and fall times) is concerned. The contact of the electrode appears to be the primary factor in determining effectiveness.

For determining the best location for an earth electrode, the Resonant Antenna method is the most promising candidate for performing rapid ground conductivity and dielectric surveys. This method is portable, does not disturb the site, and accurately indicates performance over the frequency range occupied by the EMP power spectrum. This method should be supplemented with the standard Fall-of-Potential method to determine the low frequency (or DC) resistance of an electrode. High frequency measurements can be made with an RF Network Analyzer.

A typical approach to the establishment of auxiliary grounds would be to survey candidate sites with the Resonant Linear Antenna method. The local soil parameters will dictate the most appropriate ground configuration. After the electrodes are installed, they should be verified at DC by the classical Fall-of-Potential method, and their high frequency performance should be confirmed with a portable RF Network Analyzer.

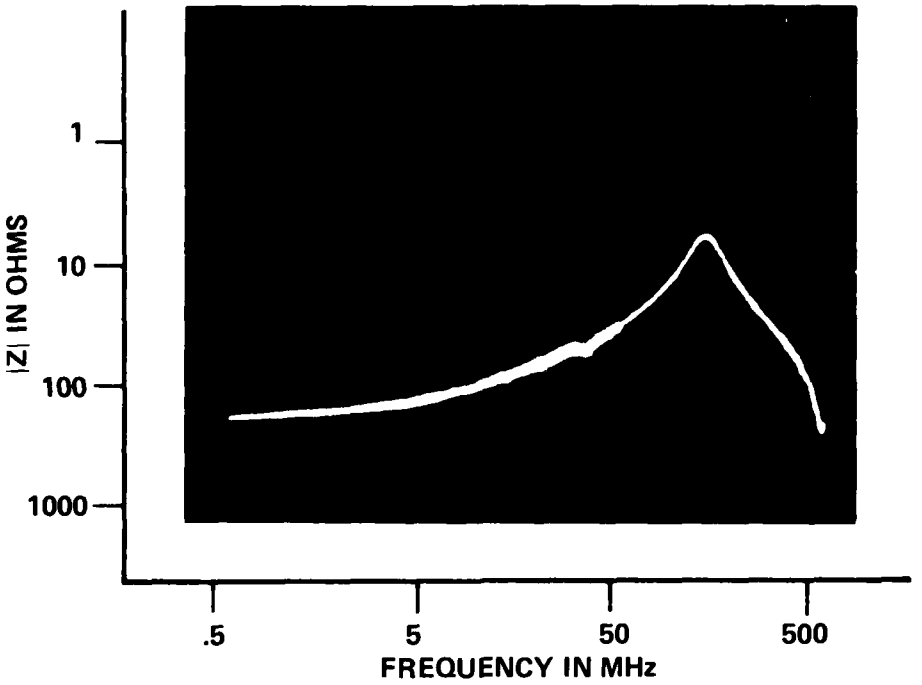

Figure 77. Model 8 impedance behavior.

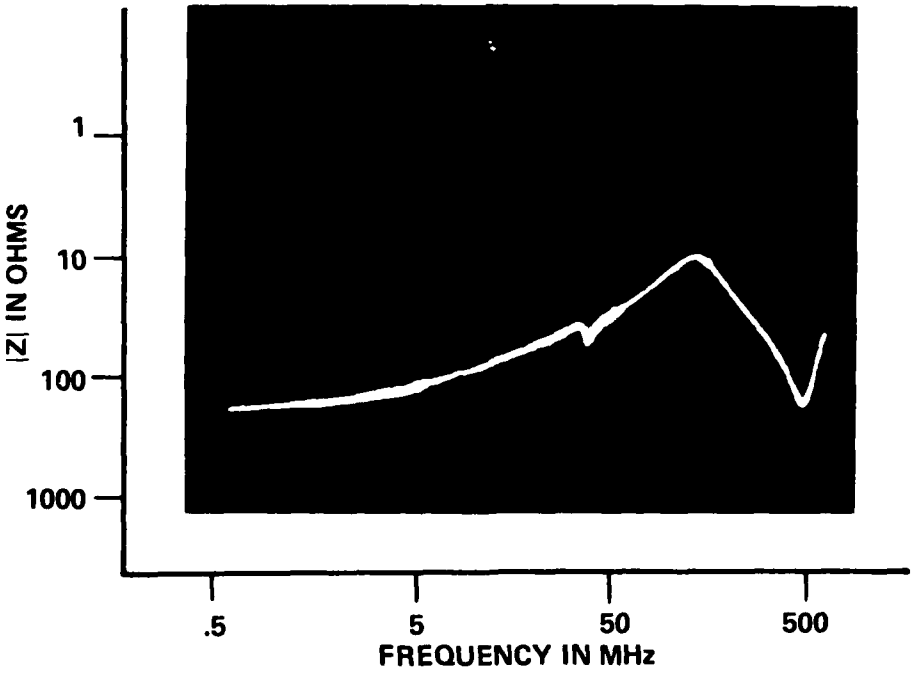

Figure 78. Model 9 impedance behavior.

V. CONCLUSIONS AND RECOMMENDATIONS

The External Collector Assessment Model (ECAM) can be effectively applied to the evaluation of EMP pickup of an overhead power line under various conditions of line length, line spacing, and number of grounding points. The results indicate that supplemental grounds exert a primary influence on the level of induced current only when they are placed within some 30-50 m of the line termination, i.e., the facility penetration point. At greater distances, supplemental grounds do exhibit a detectable effect but it is not considered sufficient to justify the associated effort and expense. The close-in effects, however, suggest that the "point of penetration" should be remotely located from the protected facility with surge suppression applied at the remote location and the intervening conductors routed underground in metal conduit.

The results from the preliminary investigation of internal collector coupling were inconclusive. Those obtained with an available method of moments code strongly suggest that considerably more developmental work is going to be required if an analytical aproach is to be used. The limited results that were achieved suggest that internal collector pickup should be evaluated relative to potential effects from external collector pickup. A more promising approach for quantifying the level of internal collector pickup is that of experimental determination of the nominal shielding effectiveness of a typical, "unshielded" facility. Preliminary results suggest that indeed the inherent protective properties of typical construction may be usable and may be quantifiable. If such proves to be the case in actual operational facilities, a networks approach is suggested to the determination of the voltage and current levels on internal collectors from an EMP event (or any other electromagnetic threat).

Although extensive supplemental grounds on external collectors are not suggested, earth electrode systems do play a viable role in the protection of a facility from an EMP (or other impulsive phenomenon, such as lightning). Therefore, the earth electrode measurement approach described herein should prove useful in determining those constitutive parameters necessary for electrode design, for surveying a candidate site for the preferred electrode location, and for evaluating the performance of an installed electrode, whether full size or scaled. It utilizes current state-of-the-art instrumentation, which would have to be appropriately ruggedized for in-field use.

In view of the promising results of the external collector assessments, it is recommended that these assessments be extended to accommodate the effects of

nonlinear devices, i.e., surge suppressors. Further, validation of the analytical results through scale model tests (using TEM mode wave launchers) should be undertaken to confirm the penetration treatments suggested.

Additional experimental work on the shielding effectiveness of typical structures is recommended to support tradeoff decisions as to the level of supplemental shielding required for a given installation. Analytical verification of certain simplified geometries may be in order to confirm experimental findings.

VI. REFERENCES

1. Lightning Protection Code 1968, NFPA 78, National Fire Protection Association, Boston, MA.

2. Volcik, L., Martin, T. A., Mindel, I. N., "Shielded Enclosure Test Bed Requirement", DNA 5341F, Contract No. DNA 001-79-C-205, IIT Research Institute, Chicago, IL, April 30, 1980.

3. IEEE Guide for Safety in Alternating-Current Substation Grounding, IEEE Std. 80-1961, IEEE New York, NY.

4. Messier, M. A., "The Effect of Ground Reflections on Observed EMP Waveforms," DNA 3370T, Contract No. DNA-001-73-C-0118, Mission Research Corporation, Santa Barbera, CA, September 11, 1974.

5. Dudley, D. G., "Numerical Inversion of the Fourier Transforms A Combination Trapezoidal and Filon Technique," UCRLOS1878, California University, Livermore, CA, 1975.

6. Carson, J. R., "Wave Propagation in Overhead Wires with Ground Return," Bell System Technical Journal, Vol. 5, Oct. 1926, pp. 538-554.

7. Paul, C. R., "Applications of Multiconductor Transmission Line Theory to the Prediction of Cable Coupling, Volume I, Multiconductor Transmission Line Theory," RADC-TR-76-101, Contract No. F30602-72-C-0418, Rome Air Development Center, Griffiss AFB, NY, April 1976.

8. Paul, C. R., "Modal Decomposition for Power Transmission Lines with Imperfect Earth Return," Proceedings of the IEE (London), Vol. 124, July 1971, pp. 647-648.

9. Marable, J. H., et. al., "Power System EMP Protection," AFWL EMP Interaction Note 246, Kirtland AFB, Albuquerque, NM, May 1975.

10. DNA EMP (Electromagnetic Pulse) Handbook, Volume 1 - Design Principles DNA 2114H-1, General Electric Company - TEMPO DASIAC, 816 State Street, Santa Barbara, CA 93102.

11. Vance, E. F., "Electromagnetic-Interference Control," IEEE Transactions on Electromagnetic Compatibility, Vol. EMC-22, No. 4, November 1980, pp. 319-328.

12. Landt, J. A., Miller, E. K. Van Blaricum, M., "WT-MBA/LLL1B: A Computer Program for the Time Domain Electromagnetic Response of Thin-Wire Structures," AWFL EMP - Interaction Note 210, Kirtland AFB, Albuquerque, NM, May 6, 1974.

13. Holland, R., "THREDE: A Free-Field EMP Coupling and Scattering Code," IEEE Transactions on Nuclear Science, Vol. NS-24, Dec. 1977, pp. 2416-2421.

14. Rice, L. P., "Radio Transmission into Buildings at 35 and 150 Mc.", Bell System Technical Journal, Jan. 1959, pp. 197-210.

15. Electromagnetic-Pulse Handbook for Electric Power Systems, Stanford Research Institute, Palo Alto, CA, February 4, 1975.

16. Smith, G. S., and King, R. W. P., "The Resonant Linear Antenna as a Probe for Measuring the In Situ Electrical Properties of Geological Media", Journal of Geophysical Research, Vol. 79, No. 17, June 10, 1974, pp. 2623-2628.

17. Towne, H. M., "Impulse Characteristics of Driven Grounds", General Electric Review, Vol. 31, No. 11, November 1928, pp. 605-609.

18. Bellaschi, P. L., "Impulse and 60 Cycle Characteristics of Driven Grounds", AIEE Transactions, Vol. 60, March 1941, pp. 123-128.

19. Bellaschi, P. L., Armington, R. E., and Snowden, A. E., "Impulse and 60-Cycle Characteristics of Driven Grounds II", AIEE Transactions, Vol. 61, 1942, pp. 349-363.

20. Eaton, J. R., "Impulse Characteristics of Electrical Connections to the Earth," General Electric Review, Vol. 47, October 1944, pp. 41-50.

21. Curdts, E. B., "Some of the Fundamental Aspects of Ground Resistance Measurements", AIEE Transactions, Communications and Electronics, Vol. 77, No. 39, November 1958, pp. 767-770.

22. Duke, C. A., and Smith, L. E., "The Technique and Instrumentation of Low-Impedance Ground Measurement", AIEE Transactions, Communications and Electronics, Vol. 77, No. 39, November 1958, pp. 767-770.

23. Gaddy, O. L., "A Simple Method of Measuring Fractional Millimicrosecond Pulse Characteristics," IRE Transactions on Instrumentation, Vol. 1-9, No. 3, December 1960, pp. 326-333.

24. Mukhedkar, D., Gervais, Y., and De Jean, J. P., "Modeling of a Grounding Electrode", IEEE Transactions on Power Apparatus and Systems. Vol. PAS 92, No. 1, January-February 1973, pp. 295-297.

25. Mukhedkar, D., and Dawalibi, F., "Ground Electrode Resistance Measurements in Non-Uniform Soils", IEEE Transactions on Power Apparatus and Systems, Vol. PAS-93, 1973, pp. 109-115.

26. Scott, L. D., and Smith, G. A., "Measurement Techniques for Antennas in Dissipative Media", IEEE Transactions on Antennas and Propagation, Vol. AP-21, No. 4, July 1973, pp. 499-507.

27. Mukhedkar, D., Gervais, Y., and Dawalibi, F., "Modeling of Potential Distribution Around a Grounding Electrode", IEEE Transactions on Power Apparatus and Systems, Vol. PAS-92, No. 4, July-August 1973, pp. 1455-1459.

28. Lee, K. M., and Smith, G. S., "Measured Properties and Insulated Antennas in Sand", IEEE Transactions on Antennas and Propagation, Vol. AP-23, No. 5, September 1975, pp. 664-70.

29. Lytle, R. J., "Properties of the Ground Inferred from Electromagnetic Measurements", IEEE Transactions on Antennas and Propagation, Vol. AP-27, No. 6, November 1979, pp. 899-902.

30. Denny, H. W., Holland, L. D., Robinette, S. L., and Woody, J. A., "Grounding, Bonding, and Shielding Practices and Procedures for Electronic Equipments and Facilities," Volume 1, Final Report, Contract DOT-FA72WA-2850, Engineering Experiment Station, Georgia Institute of Technology, December 1975, AD A022 332.

31. Rogers, E. J., "Impedance Characteristics of Large Tower Footings to a 100 s Square Wave of Current", IEEE Transactions on Power Apparatus and Systems, Vol. PAS-100, No. 1, January 1981, pp. 66-71.

32. Armstrong, H. R., "Grounding Electrode Characteristics from Model Tests," AIEE Transactions, Vol. 72, Part II, pp. 1301-6,1953.

33. Sinclair, G., "Theory of Models of Electromagnetic Systems," Proceedings of the IRE., November, 1948, pp. 1364-1370.

34. Jenkins, H. H., "Study and Evaluation of Buried Dipole Antennas", Final Report, Contract No. DAAB07-74-C-0103, Engineering Experiment Station, Georgia Institute of Technology, May 1975.

35. Rudenberg, R., Electrical Shock Waves in Power Systems, Harvard University Press, Cambridge, Massachusetts, 1968.

36. "EMP Protection for Emergency Operating Centers," TR-61A, Defense Civil Preparedness Agency, Washington, D.C., July 1972.

APPENDIX A

FILON'S METHOD FOR TIME-FREQUENCY DOMAIN CONVERSIONS

In order to use the frequency domain model of the transmission line to determine the EMP coupling to the line, an accurate and efficient method of transforming from the time domain to the frequency domain and vise versa was necessary. Because of the exceedingly large bandwidth of the EMP power spectrum, conventional methods were too inefficient. A method called "Filon's Method" proved effective. The method is based on a piecewise linear approximation of the argument function. The purpose of this appendix is to summarize the essential features of this method.

The Fourier Integral may be written as

$$F(\omega) = \int_{-\infty}^{\infty} f(t)\ e^{-j\omega t}\ dt \qquad \text{(A-1)}$$

while the Inversion Integral may be written as

$$f(t) = \frac{1}{2\pi} \int_{-\infty}^{\infty} F(\omega)\ e^{j\omega t}\ d\omega \qquad \text{(A-2)}$$

If f(t) in Equation (A-1) is sufficiently smooth, then straight line segments may be used to approximate (piecewise-linearly) f(t) by

$$f(t) \cong \sum_{i=1}^{N} a_i t + b_i \qquad \text{(A-3)}$$

where, as given in Figure (A.1),

$$a_i = \frac{f(t_{i+1}) - f(t_i)}{t_{i+1} - t_i}$$

$$b_i = f(t_i) - a_i t_i$$

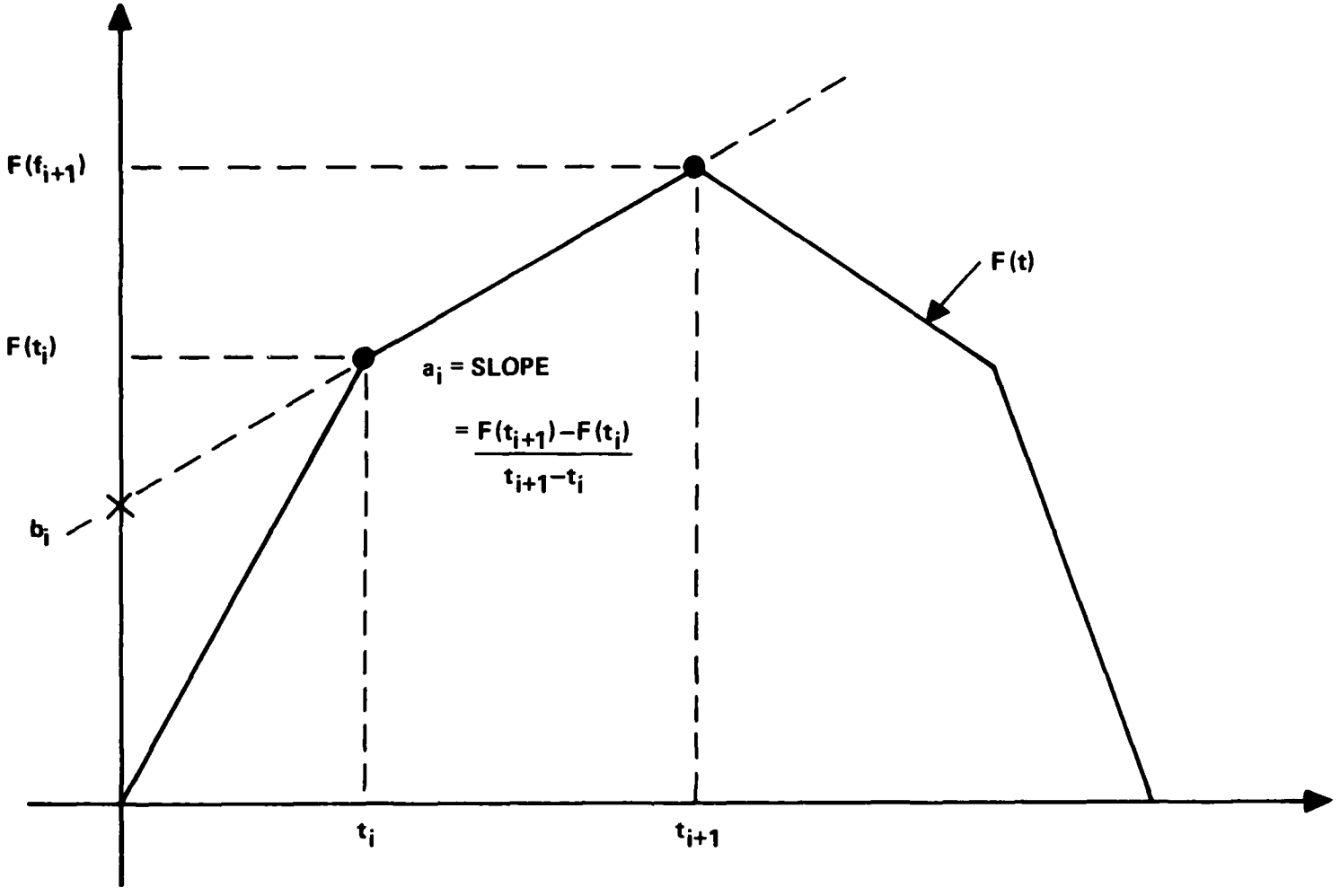

Figure A-1. Piecewise-linear approximation of a time function, F(t).

Differentiating f(t) twice, one obtains

$$f''(t) \tilde{=} \sum_{i=1}^{N} a_i \, \delta(t - t_i) \qquad \text{(A-4)}$$

where δ (t) is the dirac delta function. However, it is known that differentiating Fourier transforms twice yields:

$$f''(t) = (j\omega)^2 \, F(\omega) \qquad \text{(A-5)}$$

Substituting Equations (A-4) and (A-5) into Equation (A-1), produces

$$-\omega^2 \, F(\omega) \tilde{=} \int_{-\infty}^{\infty} \sum_{i=1}^{N} a_i \, \delta(t - t_i) \, e^{-j\omega t} \, dt \qquad \text{(A-6)}$$

which can be reduced to

$$F(\omega) \tilde{=} -\frac{1}{\omega^2} \sum_{i=1}^{N} a_i \, e^{-j\omega t_i} \qquad \text{(A-7)}$$

Using this equation, the Fourier Transform of a smooth time function f(t) may be easily calculated.

This method was used to transform the incident EMP field from the time domain to the frequency domain. To illustrate, the EMP incident field is commonly represented as a four term exponential as follows:

$$E(t) = E_o \left[e^{-\alpha t} - e^{-\beta t} - A(e^{-\alpha t} - e^{-\delta t})\right] \qquad \text{(A-8)}$$

where

$E_o = 5 \times 10^4 / .9646$ V/m

$\alpha = 1.5 \times 10^6$

$$\beta = 2.6 \times 10^{8}$$

$$\alpha = 2.0 \times 10^{5}$$

$$\delta = 5.0 \times 10^{5}$$

$$A = (\alpha^{-1} - B^{-1})/(\alpha^{-1} - \delta^{-1})$$

and t is defined in seconds.

(The time domain representation of this incident field and its transformed frequency spectrum are shown in Figure 8.)

The transmission line program was run for 211 discrete frequencies, where an incident plane wave is impinged upon the line at the given frequency of the calculated amplitude and phase. The frequency domain output of the program then was transformed back to the time domain by the way of the inversion integral.

The piecewise linear approximation method used in the forward integral was also used in the inverse transformation to obtain f(t) from the real and imaginary parts of $F(\omega)$. Since f(t) is known to be a real time causal function, then f(t) can be determined in terms of the real or imaginary part of its Fourier transform*

$F(\omega) = R(\omega) + i\, X(\omega)$

$$f(t) = \frac{2}{\pi} \int_{o}^{\infty} R(\omega) \cos \omega t \, d\omega = -\frac{2}{\pi} \int_{o}^{\infty} X(\omega) \sin \omega t \, d\omega \qquad \text{(A-9)}$$

Therefore, since either the real or the imaginary parts of the transform may be used, the imaginary part $X(\omega)$ was selected. Thus f(t) can be determined by evaluating the following:

$$f(t) = -\frac{2}{\pi} \int_{o}^{\infty} X(\omega) \sin \omega t \, d\omega \qquad \text{(A-10)}$$

where $X(\omega)$, the imaginary part of the Fourier transform, is piecewise linearly approximated by

$$X(\omega) = \sum_{k=1}^{N} c_k \omega + d_k \qquad \text{(A-11)}$$

*A. Papoulis, The Fourier Integral and Its Applicattions, McGraw-Hill, New York, NY,(1962), pp. 53-59.

where

$$c_k = \frac{F(\omega_{k+1}) - F(\omega_k)}{\omega_{k+1} - \omega_k}$$

$$d_k = F(\omega_k) - c_k \omega_k$$

Thus, analogously with the forward (i.e., time-to-frequency) transformation, the frequency function is piecewise-linearly approximated. Then Equation (A-11) is substituted into Equation (A-10) and integration is performed to obtain:

$$f(t) = -\frac{2}{\pi} \sum_{k=1}^{N} c_k C(t) - d_k D(t) \qquad \text{(A-12)}$$

where

$$C(t) = -\frac{\omega_{k+1}}{t} \cos \omega_{k+1} t + \frac{1}{t^2} \sin \omega_{k+1} t$$

$$+ \frac{\omega_k}{t} \cos \omega_k t - \frac{1}{t^2} \sin \omega_k t$$

and

$$D(t) = -\frac{1}{t} \cos \omega_{k+1} t + \frac{1}{t} \cos \omega_k t$$

Using Equation (A-7) for the forward (time-to-frequency) Fourier transform and Equation (A-12) for the inversion (frequency-to-time) transform, Fourier transformations for time functions with exceedingly large bandwidths may be performed.

APPENDIX B

DESCRIPTION OF MULTICONDUCTOR TRANSMISSION LINE BEHAVIOR WHEN ILLUMINATED BY AN INCIDENT FIELD IN THE PRESENCE OF A LOSSY GROUND

The purpose of this appendix is to derive the transmission line equations for a uniform line consisting of N perfect conductors at a given height above a lossy ground when the line is excited by an incident electromagnetic field*. The equations can be developed from Faraday's law in integral form, which can be expressed as

$$\int_{C_i} \underline{E} \cdot \underline{d\ell} = -j\omega\mu \int_{S_i} \underline{H} \cdot \hat{n}\, da \qquad \text{(B-1)}$$

where S_i is a flat, rectangular surface in the x-y plane between the i^{th} wire and the ground plane and between x and $x + \Delta x$ as shown in Figure B-1. The unit normal n is z directed, the surface differential is defined as da = dxdy and C_i is a closed contour encircling S_i in a counter-clockwise direction. Equation (B-1) can then be rewritten as**

$$\int_0^{d_{io}} \left[E_{ti}(y, x + \Delta x) - E_{ti}(y,x)\right] dy - \int_x^{x+\Delta x} \left[E_{\ell i}(d_{io}, x) - E_{\ell i}(0, x)\right] dx$$

$$= -j\omega\mu \int_x^{x+\Delta x} \int_0^{d_{io}} H_{ni}(y,x)\, dy\, dx \qquad \text{(B-2)}$$

where E_{ti} is the component of the total electric field (incident plus scattered) transverse to the line axis and lying along a straight line between the conductor and the ground plane; $E_{\ell i}$ is the component of total electric field along the longitudinal axis of the line; H_{ni} is the component of total magnetic field perpendicular to the plane formed by the wire and ground.

*C. R. Paul, "Applications of Multiconductor Transmission Line Theory to the Prediction of Cable Coupling, Volume VI, A Digital Computer Program for Determining Terminal Currents Induced in a Multiconductor Transmission Line by an Incident Electromagnetic Field." Technical Report, RADC-TR-76-101, Rome Air Development Center, Griffiss AFB, NY, February 1978.

**In integrating from y = 0 to $y = d_{io}$, it is assumed that $r_{wi} << d_{io}$, i.e., the wire may be replaced by a filament.

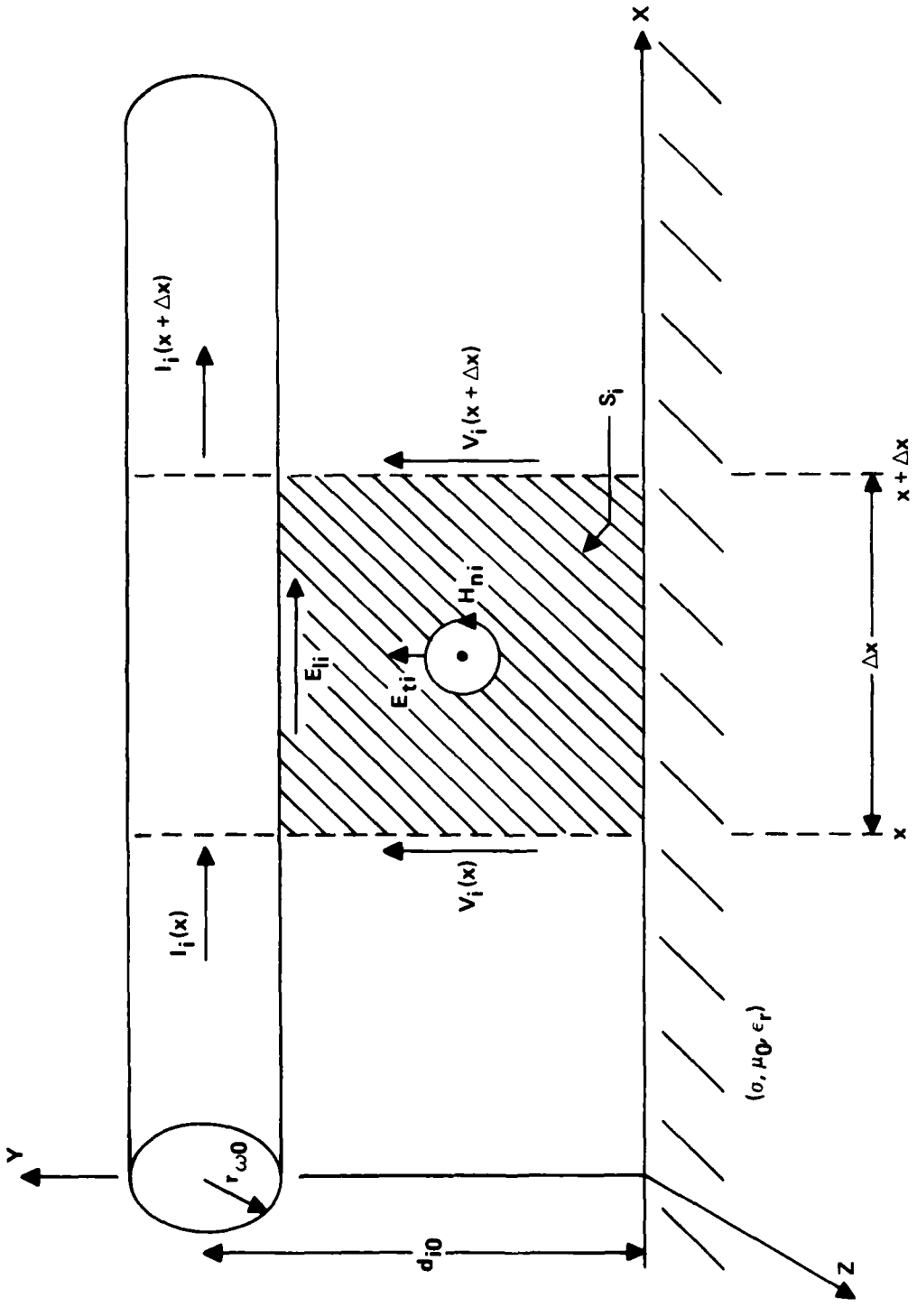

Figure B-1. Incremental transmission line model.

The voltage between the i^{th} wire and the ground may be defined as

$$V_i(x) = -\int_o^{d_{io}} E_{ti}(y, x)\, dy \qquad \text{(B-3)}$$

Thus,

$$\frac{-dV_i(x)}{dx} = \lim_{\Delta x \to o} \frac{1}{\Delta x} \int_o^{d_{io}} \left[E_{ti}(y, x + \Delta x) - E_{ti}(y, x)\right] dy \qquad \text{(B-4)}$$

Since the wires are assumed to be perfect conductors ($E_{\ell i}(d_{io},x) = 0$), then Equation (B-2) becomes

$$\frac{dV_i(x)}{dx} - \lim_{\Delta x \to o} \frac{1}{\Delta x} \int_x^{x+\Delta x} E_{\ell i}(0,x) = j\omega\mu \int_o^{d_{io}} H_{ni}(y)dy \qquad \text{(B-5)}$$

The second term of Equation (B-5) needs to be evaluated using L'Hospital's Rule, i.e.

$$\lim_{\Delta x \to o} \frac{1}{\Delta x} \int_x^{x+\Delta x} E_{\ell i}(0,x)dx = \lim_{\Delta x \to o} \frac{\frac{d}{d\Delta x} \int_x^{x+\Delta x} E_{\ell i}(0, x)\, dx}{\frac{d}{d\Delta x}(\Delta x)} \qquad \text{(B-6)}$$

The numerator of Equation (B-6) may then be evaluated using Leibnitz's Rule:

$$\frac{d}{d\Delta x} \int_x^{x+\Delta x} E_{\ell i}(0, x)\, dx = \int_x^{x+\Delta x} \frac{\partial E_{\ell i}(0,x)}{\partial \Delta x}\, dx$$

$$+ (1)\, E_{\ell i}(x + \Delta x) - (0) E_{\ell i}(x) = E_{\ell i}(x + \Delta x) \qquad \text{(B-7)}$$

Substituting Equation (B-7) into Equation (B-6) and Equation (B-6) back into Equation (B-5) produces

$$\frac{dV_i(x)}{dx} - E_{\ell i}(x) = j\omega\mu \int_o^{d_{io}} H_{ni}(y)\, dy \qquad \text{(B-8)}$$

The total $\underline{H}_n$ field can now be separated into two parts:

$$\underline{H}_n = \underline{H}_n^{scat} + \underline{H}_n^{inc} \qquad \text{(B-9)}$$

where $\underline{H}_n^{scat}$ is the scattered magnetic field and $\underline{H}_n^{inc}$ is the incident field.

The longitudinal electric field, $\underline{E}$ (x), represents the losses in the earth and can be expressed as

$$\underline{E}_\ell(x) = \underset{\sim}{Z}_g \underline{I}_1(x) \qquad \text{(B-10)}$$

where

$$\underset{\sim}{Z}_g = \underset{\sim}{R}_e + j\omega \underset{\sim}{L}_e \qquad \text{(B-11)}$$

and

$$\underline{I}_1(x) = -\underline{I}(x) \qquad \text{(B-12)}$$

The ground impedance term $\underset{\sim}{Z}_g$ is made up of the ground resistance term $\underset{\sim}{R}_e$ and the ground inductance term, $\underset{\sim}{L}_e$, which can be calculated using Carson's Formula's*.

*Carson, op. cit., Reference 6.

Substituting Equation (B-12) into Equation (B-10) and using Equation (B-9), Equation (B-8) becomes

$$\frac{\partial \underline{V}(x)}{\partial x} + \underset{\sim}{Z}_g \underline{I}(x) = + j\omega\mu \int_o^{d_{io}} H_{ni}^{\text{scat}}(y, x)\, dy + j\omega\mu \int_o^{d_{io}} H_{ni}^{\text{inc}}(y)\, dy \qquad \text{(B-13)}$$

The scattered flux passing between the conductor and the ground plane is directly related to the scattered magnetic field and the per-unit-length inductance matrix $\underset{\sim}{L}_1$ by

$$\phi_i^{\text{scat}}(x) = -\int_o^{d_{io}} \mu H_{ni}^{\text{scat}}(y)dx = [\underset{\sim}{L}\, \underline{I}(x)]_i \qquad \text{(B-14)}$$

Upon substituting Equation (B-14) into Equation (B-13), the transmission line voltage equation is obtained for the line excited by an incident field in the presence of a lossy earth as

$$\frac{d}{dx} \underline{V}(x) + \underset{\sim}{Z}_T \underline{I}(x) = \underline{V}_s(x) \qquad \text{(B-15)}$$

where

$$\underset{\sim}{Z}_T = j\omega \underset{\sim}{L} + \underset{\sim}{Z}_g \qquad \text{(B-16)}$$

and

$$V_{si}(x) = j\omega\mu \int_o^{d_{io}} H_{ni}^{\text{inc}}(y)\, dy \qquad \text{(B-17)}$$

The transmission line current equation may be derived using Amperes' Law in differential form

$$\nabla \times \underline{H} = j\omega\varepsilon\underline{E} + \underline{J} \qquad \text{(B-18)}$$

Assuming a source free region and allowing only the TEM mode of propagation, Equation (B-18) becomes

$$\underline{E}_y = \frac{1}{j\omega\varepsilon}\left[\frac{\partial \underline{H}_x}{\partial z} - \frac{\partial \underline{H}_z}{\partial x}\right] \qquad \text{(B-19)}$$

where E_y consists of a scattered electric field component and an incident field component and is written as

$$\underline{E}_t(y, x) = \underline{E}_y(y, x) = \underline{E}_y^{\,scat}(y, x) + \underline{E}_y^{\,inc}(y, x) \qquad \text{(B-20)}$$

Substituting Equation (B-19) into the voltage definition (Equation B-3) produces

$$V_i(x) = \frac{-1}{j\omega\varepsilon}\int_o^{d_{io}}\left[\frac{\partial H_{zi}^{\,scat}(y, x)}{\partial x} + \frac{\partial H_{zi}^{\,inc}(y, x)}{\partial x} - \frac{\partial H_{xi}^{\,scat}(y, x)}{\partial z} - \frac{\partial H_{xi}^{\,inc}(y, x)}{\partial z}\right] dy \qquad \text{(B-21)}$$

Using the definition in Equation (B-14), Equation (B-21) becomes

$$V_i(x) = \frac{-L}{j\omega\mu\varepsilon} \frac{d}{dx} \left[\underline{I}(x)\right] - \frac{1}{j\omega\varepsilon} \int_o^{d_{ic}} \frac{\partial}{\partial z} H_{xi}^{scat}(y,x)$$

$$- \int_o^{d_{io}} E_{ti}^{inc}(y, x)\, dy \qquad \text{(B-22)}$$

If it is assumed that there are no transverse components of current on the wire or the ground plane, then $\underline{H}_x^{scat}(y,x) = 0$ and Equation (B-22) becomes

$$\frac{\partial I_i(x)}{\partial x} + j\omega\varepsilon \underset{\sim}{L}^{-1} \underline{V}(x) = -j\omega\mu\varepsilon \underset{\sim}{L}^{-1} \int_o^{d_{io}} E_{ti}(y, x)\, dy \qquad \text{(B-23)}$$

Since

$$\underset{\sim}{C} = \mu\varepsilon \underset{\sim}{L}^{-1} \qquad \text{(B-24)}$$

then Equation (B-23) becomes

$$\frac{\partial}{\partial x} \underline{I}(x) + \underset{\sim}{Y}\, \underline{V}(x) = \underline{I}_s(x) \qquad \text{(B-25)}$$

where

$$\underset{\sim}{Y} = j\omega \underset{\sim}{C} \qquad \text{(B-26)}$$

and

$$\underline{I}_s(x) = - \underset{\sim}{Y} \int_o^{d_{io}} \underline{E}_t(y, x)\, dy \qquad \text{(B-27)}$$

Thus, Equations (B-15) and (B-25) are the first order voltage and current transmission line differential equations for a transmission line in the presence of a lossy ground when impinged upon by an incident electromagnetic field.

APPENDIX C

DETERMINATION OF THE EARTH RETURN PARAMETERS

The problem of wave propagation along a transmission system composed of an overhead wire parallel to the surface of the earth was first solved by Carson in 1926*. The contribution of the resistance $\underset{\sim}{R}_e$ and reactance $\underset{\sim}{X}_e$ due to the earth-return path was calculated using the infinite series developed by Carson to solve the following integral equations:

$$[\underset{\sim}{R}_e]_{ii} + j\omega[\underset{\sim}{L}_e]_{ii} = \frac{j\omega\mu_o}{\pi}\int_o^\infty \frac{\mu \exp(-2\zeta H_i)}{\mu\zeta + (\zeta^2 + \beta^2)^{1/2}}\, d\zeta \tag{C-1}$$

$$[\underset{\sim}{R}_e]_{ij} + j\omega[\underset{\sim}{L}_e]_{ij} = \frac{j\omega\mu_o}{\pi}\int_o^\infty \frac{\mu \cos[\zeta\{D_{ij}^2 - (H_i-H_j)^2\}^{1/2}]\exp\{-\zeta(H_i + H_j)\}}{\mu\zeta + (\zeta^2 + \beta^2)^{1/2}}\, d\zeta \tag{C-2}$$

where μ is the relative permeability of the soil, μ_o is the free space permeability, H_i is the height of the i^{th} conductor above ground, D_{ij} is the center-to-center separation of conductors i and j and $\beta^2 = j\omega\mu\mu_o^2$ where σ is the conductivity of the soil.

Carson's method for solving Equations (C-1) and (C-2) was used. The real and imaginary correction component matricies $\underset{\sim}{P}$ and $\underset{\sim}{Q}$, respectively, are calculated in terms of the geometry-related terms r and θ, where

$$r_{ij} = \sqrt{\omega\mu\sigma}\; D_{ij} \tag{C-3}$$

and θ_{ij} is the angle subtended at the i^{th} conductor by the i^{th} image and the j^{th} image, see Figure (C-1). The relationship between $\underset{\sim}{R}_e(\omega)$ and $\underset{\sim}{L}_e(\omega)$ and the correction component matrices $\underset{\sim}{P}$ and $\underset{\sim}{Q}$ are

$$\underset{\sim}{R}_e(\omega) = \frac{\omega\mu}{\pi}\,\underset{\sim}{P} \tag{C-4}$$

$$\underset{\sim}{L}_e(\omega) = \frac{\omega}{\pi}\,\underset{\sim}{Q} \tag{C-5}$$

*Carson, op. cit., Reference 6

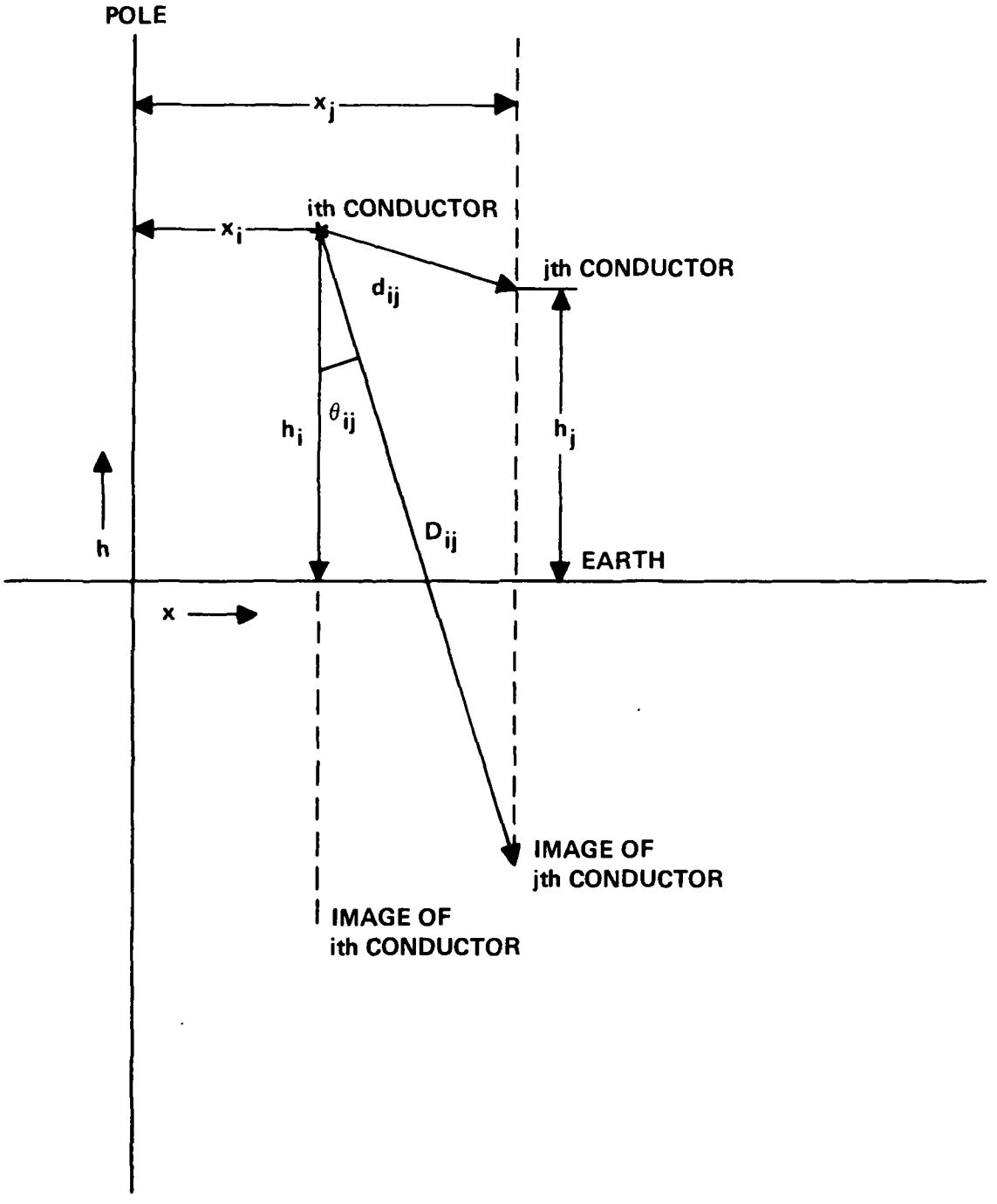

Figure C-1. Conductor-earth geometry.

Therefore, the only thing left is a method to calculate $\underset{\sim}{P}$ and $\underset{\sim}{Q}$. The determination of the correction component matrices is dependent on the parameter r. Therefore, the formulas given for $\underset{\sim}{P}$ and $\underset{\sim}{Q}$ will only be used for the ranges of r specified.

For the range where $r \leq 1/4$,

$$[\underset{\sim}{P}]_{ij} = \frac{\pi}{8} - \frac{r \cos\theta}{3\sqrt{2}} + \frac{r^2}{16}\cos 2\theta \left(0.6728 + \ell n\left(\frac{2}{r}\right)\right) + \frac{r^2}{16}\theta \sin 2\theta \quad \text{(C-6)}$$

and

$$[\underset{\sim}{Q}]_{ij} = -.0382 + \frac{1}{2}\ell n\left(\frac{2}{r}\right) + \frac{1}{3\sqrt{2}} r \cos\theta \quad \text{(C-7)}$$

For the range, $1/4 < r \leq 5$

$$[\underset{\sim}{P}]_{ij} = \frac{\pi}{8}(1 - S_4) + \frac{1}{2}\ell n\left(\frac{2}{\gamma r}\right) S_2 + \frac{\theta}{2} S_2' - \frac{\sigma_1}{\sqrt{2}} + \frac{\sigma_2}{2} + \frac{\sigma_3}{\sqrt{2}} \quad \text{(C-8)}$$

$$[\underset{\sim}{Q}]_{ij} = \frac{1}{4} + \frac{\ell n\left(\frac{2}{\gamma r}\right)(1 - S_4)}{2} - \frac{\theta S_4'}{2} + \frac{\sigma_1}{\sqrt{2}} - \frac{\pi S_2}{8} + \frac{\sigma_3}{\sqrt{2}} - \frac{\sigma_4}{2} \quad \text{(C-9)}$$

where γ is Euler's constant (1.7811) and S_2, S_2', S_4, S_4', σ_1, σ_2, σ_3, σ_4 are defined by the following infinite series:

$$S_2 = \sum_0^\infty a_n \cos(4n + 2)\theta \quad \text{(C-10)}$$

$$S_2' = \sum_0^\infty a_n \sin(4n + 2)\theta \quad \text{(C-11)}$$

$$S_4 = \sum_0^\infty c_n \cos(4n + 4)\theta \quad \text{(C-12)}$$

$$S_4' = \sum_0^\infty c_n \sin(4n + 4)\theta \quad \text{(C-13)}$$

$$\sigma_1 = \sum_0^\infty e_n \cos(4n + 1)\theta \quad \text{(C-14)}$$

$$\sigma_2 = \sum_0^\infty g_n \cos(S_2)_n \quad \text{(C-15)}$$

$$\sigma_3 = \sum_0^\infty f_n \cos(4n + 3)\theta \quad \text{(C-16)}$$

$$\sigma_4 = \sum_0^\infty h_n (S_4)_n \quad \text{(C-17)}$$

$$a_n = \frac{-a_{n-1}}{2n\ (2n+1)^2\ (2n+2)} \left(\frac{r}{2}\right)^4, \quad a_o = \frac{r^2}{8} \tag{C-18}$$

$$c_n = \frac{-c_{n-1}}{(2n+1)(2n+2)^2\ (2n+3)} \left(\frac{r}{2}\right)^4, \quad c_o = \frac{r^4}{192} \tag{C-19}$$

$$e_n = \frac{-e_{n-1}}{(4n-1)(4n+1)^2\ (4n+3)} r^4, \quad e_o = \frac{r}{3} \tag{C-20}$$

$$f_n = \frac{-f_{n-1}}{(4n+1)(4n+3)^2\ (4n+5)} r^4, \quad f_o = \frac{r^3}{45} \tag{C-21}$$

$$h_n = h_{n-1} + \frac{1}{4n+2} + \frac{1}{2n+2} + \frac{1}{2n+3} - \frac{1}{4n+6}, \quad h_o = \frac{5}{3} \tag{C-22}$$

$$g_n = g_{n-1} + \frac{1}{4n} + \frac{1}{2n+1} + \frac{1}{2n+2} - \frac{1}{4n+4}, \quad g_o = \frac{5}{4} \tag{C-23}$$

The above series converge quite rapidly; therefore, for the range $1/4 < r \leq 1$, only the first terms are important. For the range $1 < r < 2$, only the first two leading terms of each series need be retained and for the case of the range between $2 < r < 5$ the first five terms were retained in the calculation of $\underset{\sim}{P}$ and $\underset{\sim}{Q}$. However, for the range $5 < r \leq 10$, the following asymptotic expansion for $\underset{\sim}{P}$ and $\underset{\sim}{Q}$ were required:

$$[\underset{\sim}{P}]_{ij} = \frac{1}{\sqrt{2}} \frac{\cos\theta}{r} - \frac{\cos 2\theta}{r^2} + \frac{1}{\sqrt{2}} \frac{\cos 3\theta}{r^3} + \frac{3}{\sqrt{2}} \frac{\cos 5\theta}{r^5} \cdots \tag{C-24}$$

$$[\underset{\sim}{Q}]_{ij} = \frac{1}{\sqrt{2}} \frac{\cos\theta}{r} - \frac{1}{\sqrt{2}} \frac{\cos 3\theta}{r^3} + \frac{3}{\sqrt{2}} \frac{\cos 5\theta}{r^5} \cdots \tag{C-25}$$

Finally, for large values of r, i.e., $r > 10$, $\underset{\sim}{P}$ and $\underset{\sim}{Q}$ can be determined from

$$\underset{\sim}{J} = \underset{\sim}{P} + i\underset{\sim}{Q} \tag{C-26}$$

where

$$\underset{\sim}{J} = \frac{1+i}{\sqrt{2}} \frac{\cos\theta}{r} - \frac{\cos 2\theta}{r^2} \qquad \text{(C-27)}$$

These formulas will allow the determination of the line resistance and reactance, due to the earth return path, if the geometry is specified, i.e., line configuration, and the soil's constituitive parameters ($\sigma_s, \varepsilon_s, \mu_s$) are known.

The relative permeability of the soil will be assumed to be unity ($\mu_r = 1$). The relative permittivity and conductivity, on the other hand, must be determined. Because the EMP power spectrum extends over a wide range of frequencies, it was necessary to determine the relative permittivity of the soil, ε_r, and the conductivity, σ, as functions of frequency. A set of curves* have been developed which relate the conductivity and dielectric constant to frequency up to 1 MHz. (Messier** has graphically extrapolated the curves out to 100 MHz). These curves are functions of both frequency and percent by volume of water content. A curve fitting procedure was employed to obtain a second order polynomial which fits Scott's median curve (a 3% per volume water content in the soil). The resulting polynomials are:

$$K = .2139188 - .105563 * F + .0220925 * F^2 \qquad \text{(C-28)}$$

$$D = 5.607518 - 1.0794379 * F + .062138524 * F^2 \qquad \text{(C-29)}$$

where

$K = \log_{10}$ of conductivity (mho/m)

$D = \log_{10}$ of dielectric constant ($\varepsilon/\varepsilon_o$)

$F = \log_{10}$ of frequency (Hz)

*J. H. Scott, "Electrical and Magnetic Properties of Rock and Soil", United States Geological Survey, Technical Letter, Special Project 16 May 1966.

**Messier, op. cit., Reference 4

With this information, the effect of a lossy ground on the response of an overhead transmission line can be taken into account.

APPENDIX D

DETERMINATION OF THE SIMILARITY TRANSFORM T AND IT s INVERSE T^{-1}

In order to be able to perform the model decomposition suggested in Section II, it is necessary to obtain a similarity transform $\underset{\sim}{T}$ that diagonalizes the matrix product of $\underset{\sim}{Y}\ \underset{\sim}{Z}$ in

$$\underset{\sim}{\gamma}^2 = \underset{\sim\sim\sim\sim}{TYZT}^{-1} \tag{D-1}$$

where $\underset{\sim}{\gamma}^2$ is a diagonal matrix.

Equations (3) and (4) define $\underset{\sim}{Y}$ and $\underset{\sim}{Z}$ as

$$\underset{\sim}{Y}(\omega) = j\omega\underset{\sim}{C} \tag{D-2}$$

$$\underset{\sim}{Z}(\omega) = \underset{\sim}{R}_e(\omega) + j\omega\underset{\sim}{L}_e(\omega) + j\omega\underset{\sim}{L} \tag{D-3}$$

where L and C are per-unit-length transmission line inductance and capacitance matrices and $\underset{\sim}{Re}(\omega)$ and $\underset{\sim}{Le}(\omega)$ are the per-unit-length resistance and capacitance matrices of the earth return, respectively.

The matrix product $\underset{\sim}{Y}\ \underset{\sim}{Z}$ is thus:

$$\underset{\sim\sim}{YZ} = -\omega^2\underset{\sim\sim}{CL} + j\omega\underset{\sim}{C}(\underset{\sim}{R}_e(\omega) + j\omega\underset{\sim}{L}_e(\omega)) \tag{D-4}$$

Using the fact that

$$\underset{\sim\sim}{CL} = \frac{\underset{\sim}{1}_n}{c^2} \tag{D-5}$$

where 1_n is an n x n identity matrix and c is the velocity of light in free space, then Equation (D-4) reduces to

$$\underset{\sim\sim}{YZ} = \frac{-\omega^2}{c^2}\underset{\sim}{1}_n + j\omega\underset{\sim}{C}(\underset{\sim}{R}_e(\omega) + j\omega\underset{\sim}{L}_e(\omega)) \tag{D-6}$$

Thus, in order to diagonalize $\underset{\sim}{Y}\,\underset{\sim}{Z}$ a $\underset{\sim}{T}$ must be found to diagonalize the matrix product of $\underset{\sim}{C}\,\underset{\sim}{R}_e(\omega)$ and $\underset{\sim}{C}\,\underset{\sim}{L}_e(\omega)$. It is possible to diagonalize each independently but there is no guarantee the $\underset{\sim}{T}$ that diagonalizes one will diagonalize the other. Therefore, the following approximation suggested by Paul* was used

$$\underset{\sim}{R}_e(\omega) + j\omega\underset{\sim}{L}_e(\omega) \tilde{=} z_e(\omega)\underset{\sim}{U}_n \qquad \text{(D-7)}$$

where the scalar $z_e(\omega)$ is the complex equivalent impedance of the earth. The equivalent impedance was calculated by taking the average of all elements in the matrix as Paul suggests. The $\underset{\sim}{U}_n$ matrix is an n x n matrix of all ones, i.e.,

$$\underset{\sim}{U}_n = \begin{bmatrix} 1 & 1 & . & . & . & 1 \\ 1 & 1 & . & . & . & 1 \\ . & . & . & & & . \\ . & . & & & . & . \\ 1 & 1 & . & . & . & 1 \end{bmatrix} \qquad \text{(D-8)}$$

(This procedure is equivalent to representing the return path as another lossy conductor similar to one of the phase conductors, as shown in Figure 10.) Therefore, Equation (D-1) then becomes

$$\underset{\sim}{\gamma}^2 = \underset{\sim\sim\sim\sim}{TYZT}^{-1} = \frac{-\omega^2}{c^2}\,\underset{\sim}{1}_n + \underset{\sim}{\Lambda}^2 \qquad \text{(D-9)}$$

where Λ^2 is a diagonal matrix defined as follows:

$$\underset{\sim}{\Lambda}^2 = z_e(\omega)\,\underset{\sim}{T}^{-1}\underset{\sim\sim}{CU}_n\underset{\sim}{T} \qquad \text{(D-10)}$$

*Paul, op.cit., Reference 8.

The only thing left now is to find a $\underset{\sim}{T}$ which will diagonalize the matrix product $\underset{\sim}{C}\,\underset{\sim}{U}_n$. Paul in Reference 8 defines such a $\underset{\sim}{T}$.

The model decomposition matrix $\underset{\sim}{T}$ which diagonalizes $\underset{\sim}{C}\,\underset{\sim}{U}_n$ is given by

$$\left[\underset{\sim}{T}\right]_{ii} = 1 \qquad i = 1, \ldots, (n-1) \tag{D-11}$$

$$\left[\underset{\sim}{T}\right]_{in} = c_{ii} \sum_{m=1}^{n} c_{mm} \qquad i = 1, \ldots, n \tag{D-12}$$

$$\left[\underset{\sim}{T}\right]_{ni} = -1 \qquad i = 1, \ldots, (n-1) \tag{D-13}$$

with zeros elsewhere.

The inverse of the $\underset{\sim}{T}$ matrix denoted by $\underset{\sim}{T}^{-1}$, which is also needed, is given by

$$\left[\underset{\sim}{T}^{-1}\right]_{ii} = 1 - \frac{c_{ii}}{\left(\sum_{m=1}^{n} c_{mm}\right)} \tag{D-14}$$

$$\left[\underset{\sim}{T}^{-1}\right]_{ij} = \frac{-c_{ii}}{\left(\sum_{m=1}^{n} c_{mm}\right)} \tag{D-15}$$

$$\left[\underset{\sim}{T}^{-1}\right]_{nj} = \frac{1}{\left(\sum_{m=1}^{n} c_{mm}\right)^2} \qquad \begin{array}{l} i = 1, \ldots, (n-1), \\ j = 1, \ldots, n \text{ and } i = j \end{array} \tag{D-16}$$

The c's used in the calculations in Equations (D-11) through (D-16) came from the per-unit-length capacitance matrix $\underset{\sim}{C}$ for perfect conductors. The entries in $\underset{\sim}{C}$ are given by

$$\left[\underset{\sim}{C}\right]_{ii} = c_{ii} + \sum_{j=1}^{n} c_{ij} \qquad \text{F/m} \tag{D-17}$$

$$\left[\underset{\sim}{C}\right]_{ij} = -c_{ij} \qquad F/m \qquad (D\text{-}18)$$

$$i \neq j$$

It should be noted that upon careful examination of the calculation of the $\underset{\sim}{T}$ and $\underset{\sim}{T}^{-1}$ matrices, Equations (D-11) - (D-13) and (D-14) - (D-16), respectively, a numerical problem is apparent*. $\underset{\sim}{T}$ has ones in every position except the last column. For typical line parameters, c_{ii} will be on the order of picofarads/meter. Therefore, the elements in the last column will be on the order of 10^{24}; similarly each element on $\underset{\sim}{T}^{-1}$ will be on the order of unity, but the last row will again be on the order of 10^{24}. Therefore, in order to avoid this problem, the last column of $\underset{\sim}{T}_v$ can be normalized by α , where α is defined as follows

$$\alpha = \max\left[c_{ii} \sum_{m=1}^{n} c_{mm}\right] \qquad (D\text{-}19)$$

(Each column of $\underset{\sim}{T}$ is an eigenvector and hence can be arbitrarily normalized).

However, this normalization in turn requires that $\underset{\sim}{T}^{-1}$ also be fixed; this can be accomplished by multiplying all entries in the last row of $\underset{\sim}{T}^{-1}$ by α . Now all entries in $\underset{\sim}{T}$ and $\underset{\sim}{T}^{-1}$ are on the order of unity.

Thus, the diagonalization of the matrix product $\underset{\sim}{Y}\,\underset{\sim}{Z}$ can be performed using the similarity transform $\underset{\sim}{T}$ given above, model decomposition may be performed; and, finally, a solution that the multiconductor transmission line equations can be obtained.

*C. R. Paul, private communication.

APPENDIX E

DETERMINATION OF THE INDUCED VOLTAGES SOURCE $\underline{V}_s(x)$ and AND THE INDUCED CURRENT SOURCE $\underline{I}_s(x)$ FOR THE OVERHEAD TRANSMISSION LINE MODEL

In Section II, it is shown that the incident field interaction with the transmission line can be described as:

$$\hat{V}_s(x_i) = \int_{x_{i-1}}^{x_i} [\phi_{11}(x_i,\hat{x})\underline{V}_s(\hat{x}) + \phi_{12}(x_i,\hat{x})\ \underline{I}_s(\hat{x})]_i\ d\hat{x} \tag{E-1}$$

$$\hat{I}_s(x_i) = \int_{x_{i-1}}^{x_i} [\phi_{21}(x_i,x)\ \underline{I}_s(\hat{x}) + \phi_{22}(x_i,\hat{x})\ \underline{I}_s(\hat{x})]_i d\hat{x} \tag{E-2}$$

where

$$V_{sj}(\hat{x}) = j\omega\mu \int_o^{d_{jo}} H_{zj}^{inc}(y,x)dy \tag{E-3}$$

$$I_{sj}(\hat{x}) = Y \int_o^{d_{jo}} E_{yj}^{inc}(y,x)dy \tag{E-4}$$

and

$$\underset{\sim}{\Phi}_{11} = \frac{1}{2}\ \underset{\sim}{Y}^{-1}\ \underset{\sim}{T}\ (\underset{\sim}{e}^{\underset{\sim}{\gamma}\ (x_i-\hat{x})} + \underset{\sim}{e}^{-\underset{\sim}{\gamma}\ (x_i-\hat{x})})\ \underset{\sim}{T}^{-1}\ Y \tag{E-5}$$

$$\underset{\sim}{\Phi}_{12} = -\frac{1}{2}\ \underset{\sim}{Y}^{-1}\ \underset{\sim}{T}\ \ (\underset{\sim}{e}^{\underset{\sim}{\gamma}\ (x_i-\hat{x})} - \underset{\sim}{e}^{-\underset{\sim}{\gamma}(x_i-\hat{x})})\ \underset{\sim}{T}^{-1} \tag{E-6}$$

$$\underset{\sim}{\Phi}_{21} = -\frac{1}{2}\ \underset{\sim}{T}\ (\underset{\sim}{e}^{\underset{\sim}{\gamma}(x_i-\hat{x})} - \underset{\sim}{e}^{-\underset{\sim}{\gamma}(x_i-\hat{x})})\ \underset{\sim}{\gamma}^{-1}\ \underset{\sim}{T}^{-1}\ \underset{\sim}{Y} \tag{E-7}$$

$$\underset{\sim}{\Phi}_{22} = \frac{1}{2}\ \underset{\sim}{T}\ (\underset{\sim}{e}^{\underset{\sim}{\gamma}(x_i-\hat{x})} + \underset{\sim}{e}^{-\underset{\sim}{\gamma}\ (x_i-\hat{x})})\ \underset{\sim}{T}^{-1} \tag{E-8}$$

Upon substituting Equations (E-3) through Equation (E-8) into Equations (E-1) and (E-2) and expanding, they become

$$\underline{\hat{V}}_s(x_i) = \underline{\underline{C}}_1\underline{I}_1 + \underline{\underline{C}}_2\underline{I}_2 \tag{E-9}$$

$$\underline{\hat{I}}_s(x_i) = \underline{\underline{C}}_3\underline{I}_3 + \underline{\underline{C}}_4\underline{I}_4 \tag{E-10}$$

where

$$\underline{\underline{C}}_1 = j\omega\mu\, \underline{\underline{Y}}^{-1}\, \underline{\underline{T}} \tag{E-11}$$

$$\underline{\underline{C}}_2 = \underline{\underline{Y}}^{-1}\, \underline{\underline{T}}\, \underline{\underline{\gamma}} \tag{E-12}$$

$$\underline{\underline{C}}_3 = -j\omega\mu\, \underline{\underline{T}} \tag{E-13}$$

$$\underline{\underline{C}}_4 = -\underline{\underline{T}} \tag{E-14}$$

and

$$I_{1i} = \int_{x_{i-1}}^{x_i} \int_{o}^{d_{jo}} \cosh\left(\underline{\underline{\gamma}}\,(x_i - \hat{x})\right) \underline{\underline{M}}_1\, \underline{H}_z^{inc}(y,\hat{x})\, dy d\hat{x} \tag{E-15}$$

$$I_{2i} = \int_{x_{i-1}}^{x_i} \int_{o}^{d_{jo}} \sinh\left(\underline{\underline{\gamma}}(x_i - \hat{x})\right) \underline{\underline{M}}_1\, \underline{E}_y^{inc}(y,\hat{x})\, dy d\hat{x} \tag{E-16}$$

$$I_{3i} = \int_{x_{i-1}}^{x_i} \int_{o}^{d_{jo}} \sinh\left(\underline{\underline{\gamma}}(x_i - \hat{x})\right) \underline{\underline{M}}_2\, \underline{H}_z^{inc}(y,\hat{x})\, dy d\hat{x} \tag{E-17}$$

$$I_{4i} = \int_{x_{i-1}}^{x_i} \int_{o}^{d_{jo}} \cosh\left(\underline{\underline{\gamma}}\,(x_i - \hat{x})\right) \underline{\underline{M}}_1\, \underline{E}_y^{inc}(y,\hat{x})\, dy d\hat{x} \tag{E-18}$$

where

$$\underset{\sim}{M}_1 = \underset{\sim}{T}^{-1}\ \underset{\sim}{Y} \tag{E-19}$$

$$\underset{\sim}{M}_2 = \underset{\sim}{\gamma}^{-1}\ \underset{\sim}{T}^{-1}\ \underset{\sim}{Y} \tag{E-20}$$

The terms $\sinh \underset{\sim}{\gamma}$ and $\cosh \gamma$ represent diagonal matrices where

$$[\sinh \underset{\sim}{\gamma}]_i = \sinh (\gamma_i) \tag{E-21}$$

and

$$[\cosh \underset{\sim}{\gamma}]_i = \cosh (\gamma_i) \tag{E-22}$$

Making use of Faraday's Law in differential form, then

$$\underline{H}_z^{\text{inc}} = \frac{1}{j\omega\mu}\left[\frac{\partial \underline{E}_x^{\text{inc}}}{\partial y} - \frac{\partial \underline{E}_y^{\text{inc}}}{\partial \hat{x}}\right] \tag{E-23}$$

Upon substituting Equation (E-23) into $\underline{I}_1$ and $\underline{I}_3$ and integrating by parts with respect to y and expanding Equations (E-9) and (E-10), using the definition in Equations (E-11) through Equation (E-18), the following expressions for $\underline{V}_s(\hat{x})$ and $\underline{I}_s(\hat{x})$, are obtained:

$$\underline{\hat{V}}_s(\hat{x}) = \underset{\sim}{Y}^{-1}\ \underset{\sim}{T}\ [\underline{M}] - [\underline{E}_y^{\text{inc}}(x_i)] \tag{E-24}$$

$$+ \underset{\sim}{Y}^{-1}\ \underset{\sim}{T} \cosh \underset{\sim}{\gamma}\ (x_i - x_{i-1})\ \underset{\sim}{T}^{-1}\ \underset{\sim}{Y}\ [\underline{E}_y^{\text{inc}}(x_{i-1})]$$

$$\underline{\hat{I}}_s(\hat{x}) = -\underset{\sim}{T}\ [\underline{N}] - \underset{\sim}{T} \sinh \underset{\sim}{\gamma}\ (x_i - x_{i-1})\ \underset{\sim}{\gamma}^{-1}\ \underset{\sim}{T}^{-1}\ \underset{\sim}{Y}\ [\underline{E}_y^{\text{inc}}(x_{i-1})] \tag{E-25}$$

where

$$[\underline{E}_x^{inc}(\hat{x})]_j = E_{xj}^{inc}(d_{jo},\hat{x}) = E_{xj}^{inc}(0,\hat{x}) \tag{E-26}$$

$$[\underline{E}_y^{inc}(x_i)]_j = \int_o^{d_{jo}} E_{yj}^{inc}(y,x_i)dy \tag{E-27}$$

$$[\underline{E}_y^{inc}(x_{i-1})]_j = \int_o^{d_{jo}} E_{yj}^{inc}(y,x_{i-1})dy \tag{E-28}$$

$$[\underline{M}]_j = \int_{x_{i-1}}^{x_i} \cosh \gamma_j (x_i - \hat{x}) \, [\underset{\sim}{T}^{-1} \underset{\sim}{Y} \underline{E}_x^{inc}(\hat{x})]_j \, d\hat{x} \tag{E-29}$$

$$[\underline{N}]_j = \int_{x_{i-1}}^{x} \sinh \gamma_j (x_i - \hat{x}) \, [\underset{\sim}{\gamma}^{-1} \underset{\sim}{T}^{-1} \underset{\sim}{Y} E_x^{inc}(\hat{x})]_j d\hat{x} \tag{E-30}$$

Therefore, the only terms needed to complete the calculation of Equations (E-1) and (E-2) are the terms in Equations (E-26) - (E-30). However, to evaluate Equations (E-26) - (E-30), it is necessary to determine $\underline{E}_x^{inc}$ and $\underline{E}_y^{inc}$ taking into consideration the effects of reflections off an imperfect (lossy) earth. Thus, $\underline{E}_x^{inc}$ and $\underline{E}_y^{inc}$ become

$$\underline{E}_x^{inc} = \underline{E}_{xm}^{inc} \; e^{-(\underset{\sim}{\gamma}_x x + \underset{\sim}{\gamma}_z z)}[-2\sinh(\underset{\sim}{\gamma}_y y) + (1 + \Gamma)e^{\underset{\sim}{\gamma}_y y}] \tag{E-31}$$

$$\underline{E}_y^{inc} = \underline{E}_{xm}^{inc} \; e^{-(\underset{\sim}{\gamma}_x x + \underset{\sim}{\gamma}_z z)}[-2\sinh(\underset{\sim}{\gamma}_y y) + (1 + \Gamma)\, e^{\underset{\sim}{\gamma}_y y}] \tag{E-32}$$

where the incident angles are defined as shown in Figure E-1 and

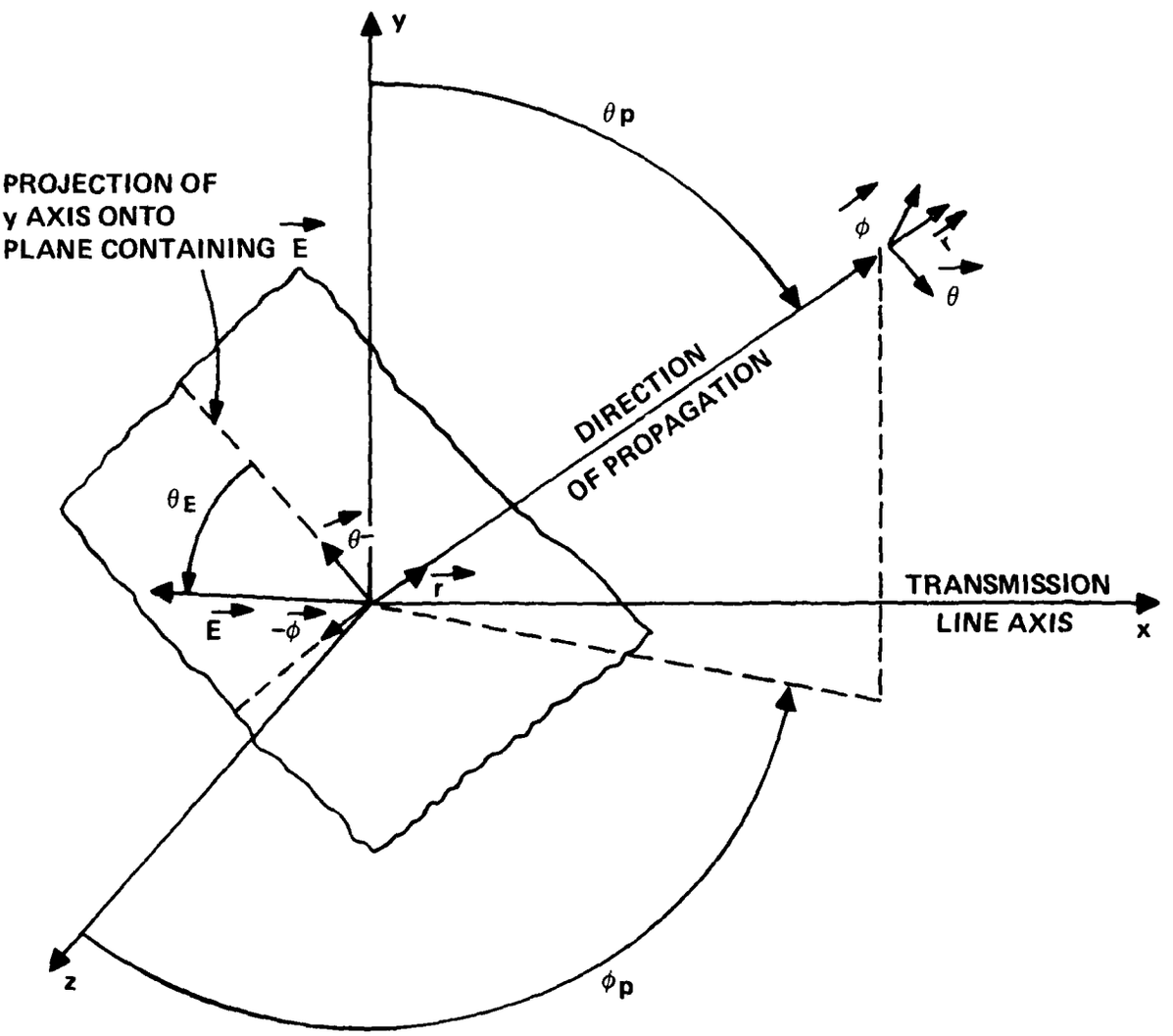

NOTE: ZERO PHASE REFERENCE TAKEN AT x = O, y = O, z = O.

Figure E-1. Definition of the uniform plane wave parameters.

$$\underset{\sim}{E}_{xm}^{inc} = -\underset{\sim}{E}_{m}^{inc} e^{j\phi}(\cos\theta_E \cos\theta_p \sin\phi_p + \sin_E \cos\phi_p) \quad \text{(E-33)}$$

$$\underset{\sim}{E}_{ym}^{inc} = \underset{\sim}{E}_{m}^{inc} e^{j\phi}(\cos\theta_E \sin\theta_p) \quad \text{(E-34)}$$

$$[\underset{\sim}{\gamma}_x] = [\underset{\sim}{\gamma}] \sin\theta_p \sin\phi_p \quad \text{(E-35)}$$

$$[\underset{\sim}{\gamma}_y] = [\underset{\sim}{\gamma}] \cos\theta_p \quad \text{(E-36)}$$

$$[\underset{\sim}{\gamma}_z] = [\underset{\sim}{\gamma}] \sin\theta_p \cos\phi_p \quad \text{(E-37)}$$

and Γ, the horizontal polarization reflection coefficient, is defined as

$$\Gamma = \frac{\eta_2\cos\theta_1 - \eta_1\cos\theta_2}{\eta_2\cos\theta_1 + \eta_1\cos\theta_2} \quad \text{(E-38)}$$

where η_i, the intrinisic impedance, is defined as

$$\eta_i = \sqrt{\frac{j\omega\mu_i}{\sigma_i + j\omega\varepsilon_i}} \quad \text{(E-39)}$$

and θ_1 is the angle of incidence and θ_2 is defined to be

$$\theta_2 = \sin^{-1}\left[\frac{j\omega\sqrt{\mu_1\ \varepsilon_1}\ \sin\theta_1}{\sqrt{-\omega^2\mu_2\varepsilon_2 + j\omega\mu_2\sigma_2}}\right] \quad \text{(E-40)}$$

Upon substitution of Equations (E-31) and (E-32) into Equations (E-26)-(E-30), they become

$$[\underline{E}_y^{inc}(x_i)]_j = [\underline{E}_{ym}^c]_j \, e^{-(\gamma_{x_i} x_i + \gamma_{z_j} z_j)} \tag{E-41}$$

$$[\underline{E}_y^{inc}(x_{i-1})]_j = [\underline{E}_{ym}^c]_j \, e^{-(\gamma_{x_i} x_{i-1} + \gamma_{z_j} z_j)} \tag{E-42}$$

$$[\underline{M}]_j = \sum_{k=1}^{N} \underline{A}_{jk}^c \tag{E-43}$$

$$[\underline{N}]_j = \sum_{k=1}^{N} \underline{B}_{jk}^c \tag{E-44}$$

where

$$[\underline{E}_{ym}^c]_j = [\underline{E}_{ym}^{inc}]_j \, e^{j\phi} \, [E2(0, y_j, -[\underline{\gamma}_y]_j) - \Gamma \, E2(0, y_j, -[\underline{\gamma}_y]_j)] \tag{E-45}$$

$$\underline{A}_{jk}^c = \int_{x_{i-1}}^{x_i} \underline{A}_{jk}(\hat{x}) = [\underline{\underline{T}}^{-1} \underline{\underline{Y}}]_{jk} \, \underline{E}_{xm}^c \, [\underline{I}_1 + \underline{I}_2] \tag{E-46}$$

$$\underline{B}_{jk}^c = \int_{x_{i-1}}^{x_i} \underline{B}_{jk}(\hat{x}) = [\underline{\underline{\gamma}}^{-1} \underline{\underline{T}}^{-1} \underline{\underline{Y}}]_{jk} \, \underline{E}_{xm}^c \, [\underline{I}_1 - \underline{I}_2] \tag{E-47}$$

and

$$\underline{E}_{xm}^c = \underline{E}_{xm}^{inc} \, e^{j\phi} [e^{-\gamma_{zk} z_k} (-2 \sinh \gamma_{yk} y_k) + (1 + \Gamma) \, e^{\gamma_{yk} y_k} - (1 + \Gamma)] \tag{E-48}$$

$$\underline{I}_1 = \frac{1}{2} \, e^{[\underline{\gamma}]_{jj} \, x_i} \, E2(x_{i-1}, x_i, -([\underline{\gamma}]_{jj} + \gamma_{xk})) \tag{E-49}$$

$$\underline{I}_2 = \frac{1}{2} e^{-[\underline{\gamma}]_{jj}} {}^{x}_{i} E2(x_{i-1}, x_i, ([\underline{\gamma}]_{jj} - \gamma_{xk})) \qquad \text{(E-50)}$$

and finally

$$E2(a,b,k) = \int_a^b e^{ks}\, ds \qquad \text{(E-51)}$$

Therefore, substituting Equations (E-41) - (E-44) into Equations (E-24) and (E-25), the distributed source along the transmission line due to the incident field interaction (i.e., evaluate Equations (E-1) and (E-2), taking into account the reflection direct to a lossy ground, can be determined.

APPENDIX F

SOIL PARAMETER IDENTIFICATION TECHNIQUES

The electrical parameters which characterize any medium are:

(1) Conductivity, σ

$$\sigma = \frac{\rho_c \, q}{m(j\omega + \nu_c)} \quad \frac{\text{m hos}}{\text{m}} \tag{F-1}$$

where

ρ_c = resistivity

q = charge

m = mass of the charge

ω = sinusoidal excitation frequency

ν_c = electron collison frequency

(2) Permittivity, ε

$$\varepsilon = \varepsilon_o(1 + \chi_e) \quad \frac{\text{farad}}{\text{m}} \tag{F-2}$$

where

ε_o = permittivity of free space

χ_e = electric susceptibility

the complex permittivity

$$\varepsilon_c = \frac{\sigma}{j\omega} + \varepsilon$$

and the relative dielectric constant

$$\varepsilon_r = \varepsilon/\varepsilon_o$$

(3) Permeability,

$$\mu = \mu_o(1 + \chi_m) \quad \frac{\text{henry}}{\text{m}} \qquad \text{(F-3)}$$

where

μ_o = permeability of free space

χ_m = proportionality constant, magnetism per applied external field

Typically, soil is non-magnetic (i.e., low iron ore content) and its permeability is that of free space, $\mu = \mu_o$. Thus, the soil parameters of interest to this study are the conductivity, σ, and the permittivity, ε. The determination of these two parameters for any given soil will be a function of (1) frequency (2) hydration, and (3) ionization.

The frequency range of interest to this study is 100 Hz to 500 MHz. Thus we must find a method of determining σ and ε over this frequency range.

The hydration is a function of the climate and current weather conditions. Thus the parameters σ and ε must be determined for the entire range of hydration expected in the region of interest.

Finally, the ionization is a function of the mineral content of the soil. There will be a natural value of σ and ε for a region due to the mineral content. If desired though, the σ and ε may be changed by altering the chemical (mineral) content of the soil.

The changes in σ and ε of soil for variations in frequency, water content, and ion content are shown in Figures F-1, F-2, and F-3. Increasing the frequency of excitation will increase the soil's σ and decrease ε, all other parameters held constant. Increasing the water content of the soil will increase σ and ε. Increasing the ion content, by adding earth salts, will increase the σ of the soil [F-3]. (This technique is used by utilities to lower tower footing resistance to earth.)

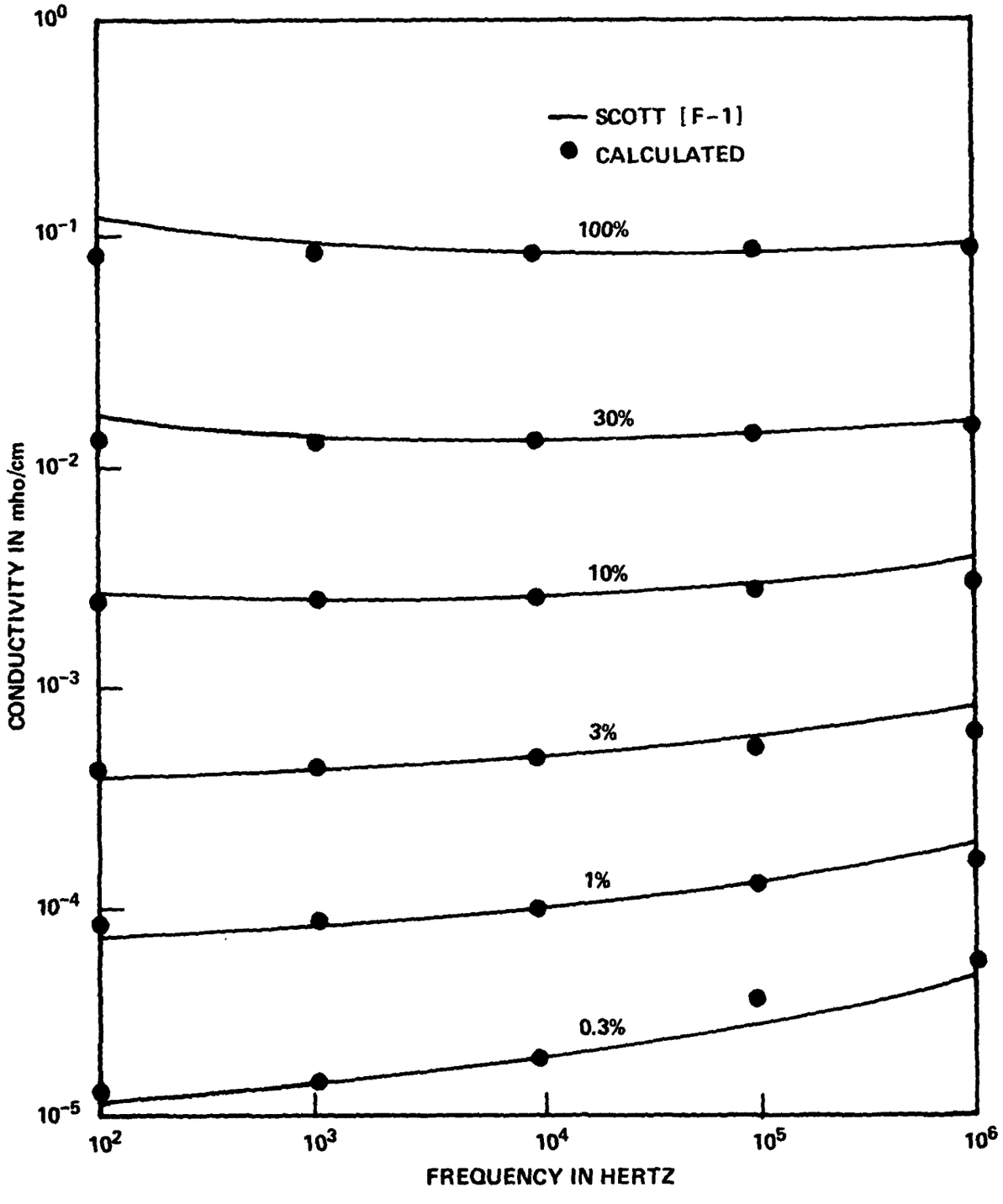

Figure F-1. Conductivity of soil versus frequency for various volume percent of water.

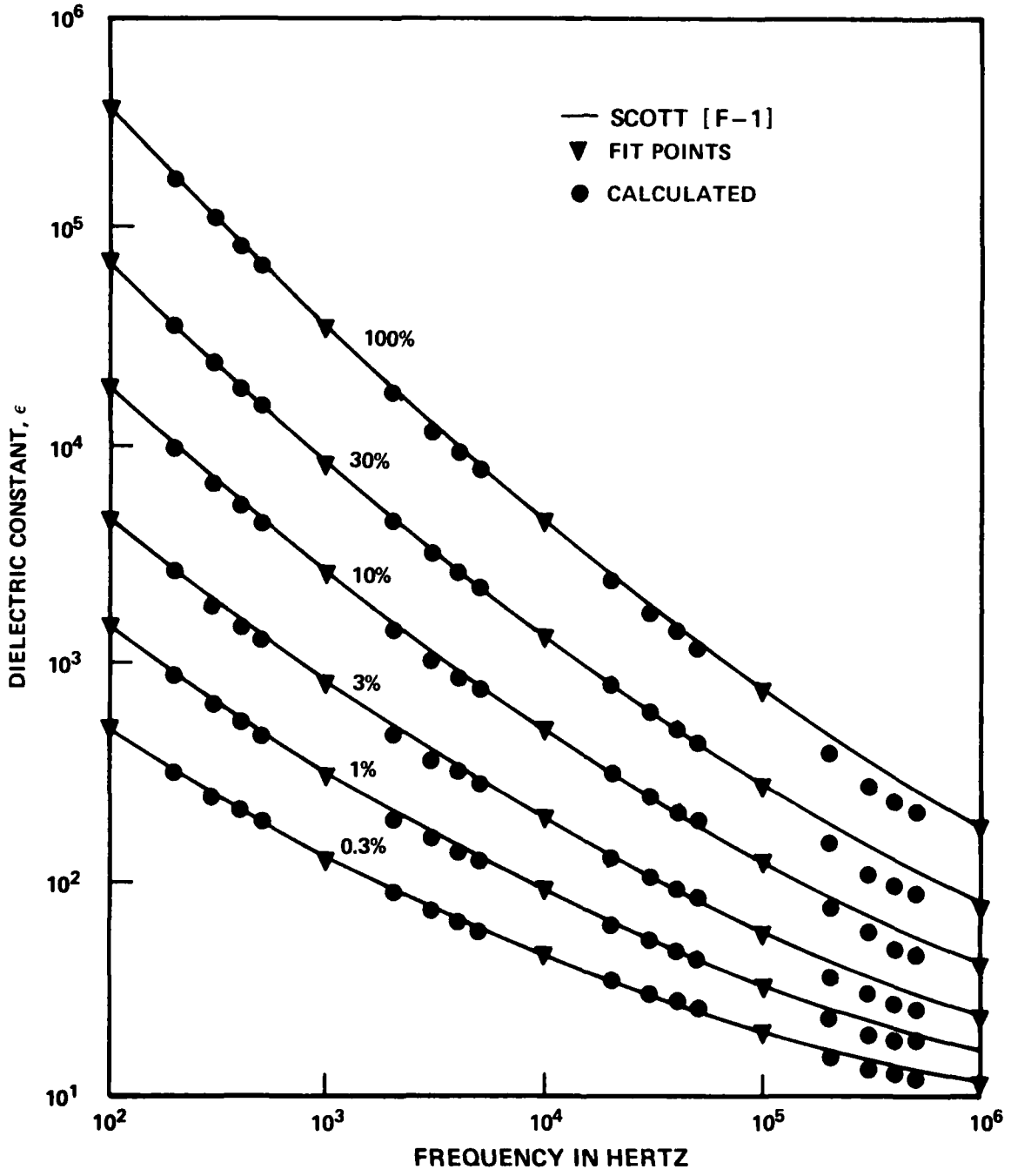

Figure F-2. Soil dielectric constant versus frequency for various volume percent of water.

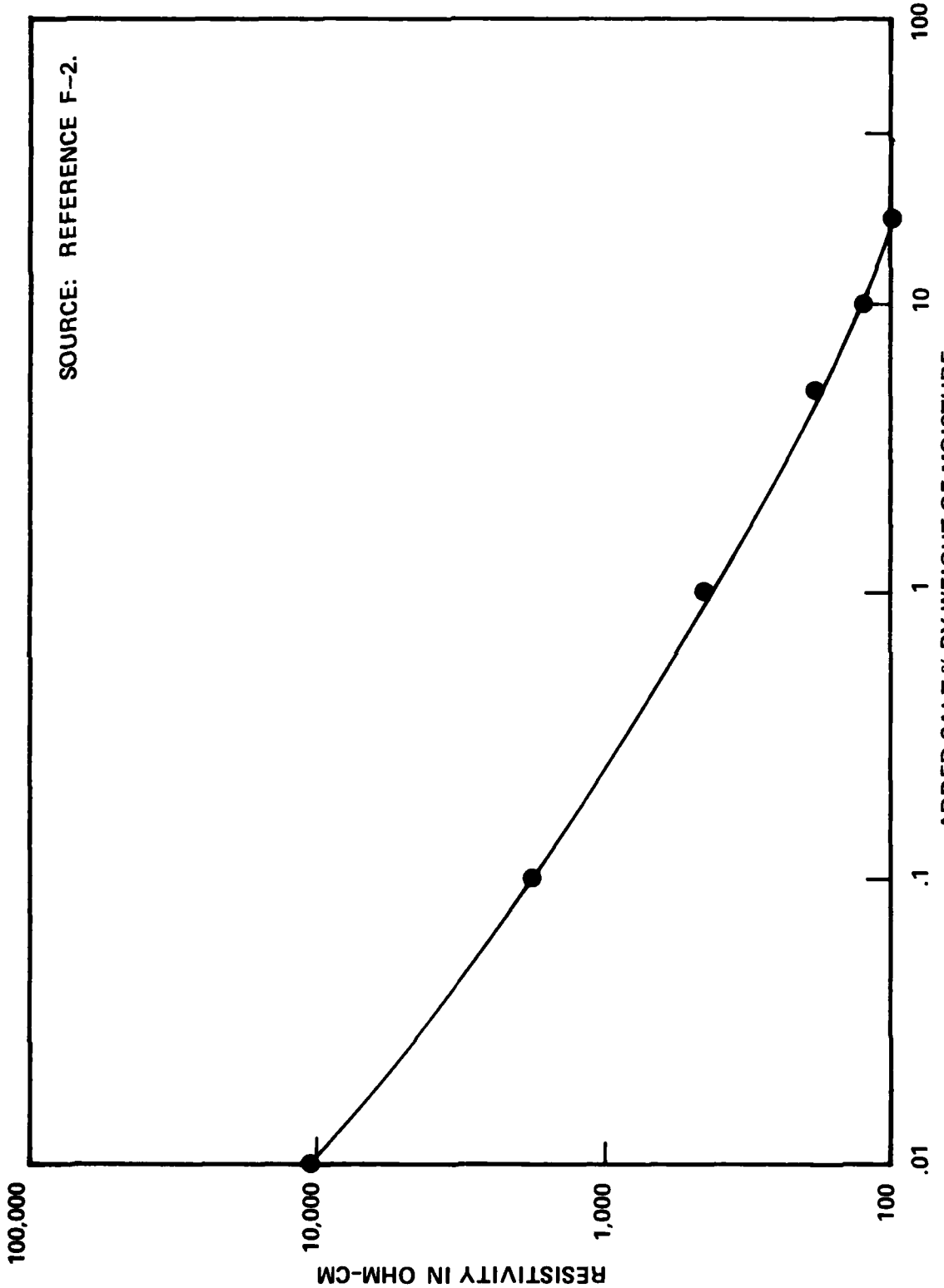

Figure F-3. Soil resistivity versus salt content.

Properties of soil have been researched for many years [F-4]. Typical soil parameters for given conditions are listed in Table F-1, F-2, and F-3. From these tables a general range of values are:

$$3 \leq \varepsilon_r \leq 24$$

$$0.5 \leq \sigma \leq 30 \text{ mmho/m}$$

Survey of Techniques

Ground parameter measurement techniques fall into two major categories, depending on the location of the tests [F-5]. These are:

(1) Laboratory
(2) In-Situ

As expected, the laboratory tests will yield the more accurate measurement of the constituents of a given soil sample, but may not reflect the environment from which the sample came.
The laboratory methods are:

(1) Parallel Plate Capacitor
(2) Coaxial Transmission Line
(3) Resonant Cavity

The In-Situ tests, which are carried out in the field, will measure the characteristics of a greater volume of soil. These tests will yield parameters which will be more representative of the site conditions especially if the soil in the area is non-homogeneous. The In-Situ measurements will not be as accurate, per sample, as the laboratory tests. The In-Situ methods are:

(1) Four Probe
(2) Two-Loop
(3) Wave Tilt
(4) Field Decay
(5) Coaxial In-Situ
(6) Resonant Antenna

Table F-1. Low frequency electrical characteristics of various types of soils [F-4].

Type of Terrain	Relative Dielectric Constant	Conductivity (mmho/m
Fresh Water	80	1
Sea water, minimum attenuation	81	4640
Pastoral, low hills, rich soil typical of Dallas, Texas, Lincoln, Nebraska, areas	20	30
Pastoral, low hills, rich soil typical of Ohio and Illinois	14	10
Flat country, marshy, densely wooded, typical of Louisiana near Mississippi River	12	7.5
Pastoral, medium hills and forestation, typical of Maryland, Pennsylvania, New York, exclusive of mountainous territory and seacoasts	13	6
Pastoral, medium hills and forestation, heavy clay soil, typical of central Virginia	13	4
Rocky soil, steep hills, typical of New England	14	2
Sandy, dry, flat, typical of coastal country	10	2
City, industrial areas, average attenuation	5	1
City, industrial areas, maximum attenuation	3	0.5

Table F-2. Dielectric and conductivity properties of various terrain at Selected wavelengths [F-4].

	> 3m		10 cm		3 cm		1 cm	
	ε_r with respect to vacuum	σ^a (mho/m)	ε_r	σ	ε_r	σ	ε_r	σ
Sea water	80	1-5	69	6.5	65	16	22	50
Fresh water	80	0.00-0.1						
Humid soil, clay	30	0.01-0.02	24	0.6				
Fertile cultivated soil	15	0.005						
Grass, meadow, race courses, sports grounds			3-6	0.05 0.11				
Rocky ground	7	0.001						
Urban areas, large towns	5	0.001						
Dry soil	4	0.01						
Very dry soil, deserts	4	0.001-0.0001	2	0.03	about 3	0.007 -0.1		

Table F-3. Dielectric properties of earth media at selected frequencies [F-4].

Material	Composition	Temp. (°C)	10^3	10^6	10^8	10^9
Soil	Sandy dry	25	2.91	2.59	2.55	2.55
Soil	Loamy dry	25	2.83	2.53	2.48	2.44
Ice	From pure distilled water	-12		4.15	3.45	3.20
Snow	Freshly fallen	-20	3.33	1.20	1.20	1.20
Snow	Hard-packed followed by rain	-6		1.55		1.5

Capacitor Method

As the name implies, this method is based on measuring the dielectric in the volume of a standard parallel plate capacitor. The capacitor with an air dielectric is connected to a capacitance bridge and the capacitance, C_o, and conductance, G_o, are noted. A right circular disc made from the soil sample is then placed between the plates and the capacitance, C, and conductance, G, are again measured. The complex permittivity of the sample can then be computed as follows:

$$\varepsilon^* = \varepsilon' - j\varepsilon'' \qquad \text{(F-4)}$$

with

$$\varepsilon' = 1 + \Delta C/C_o$$

where

$C_o = \varepsilon_o A/d$ is the capacitance of the sample volume with no sample in place.

ΔC = the change in capacitance due to sample insertion

ΔG = the change in conductance due to sample insertion

The Capacitor Method may be used over a wide range of frequencies from .01 Hz to 1 GHz. However, different measurement apparatus must be employed for different frequency ranges [F-6].

Transmission Line Method

A coaxial transmission line terminated with the soil sample and short-circuited can be used to determine the dielectric constant of the sample. A traveling probe inserted in the line is used to find the first null from the sample (see Figure F-4). From this position, d_2, and the VSWR of the probe, the impedance of the sample is determined via a Smith Chart. The propagation constant, γ , is then calculated from

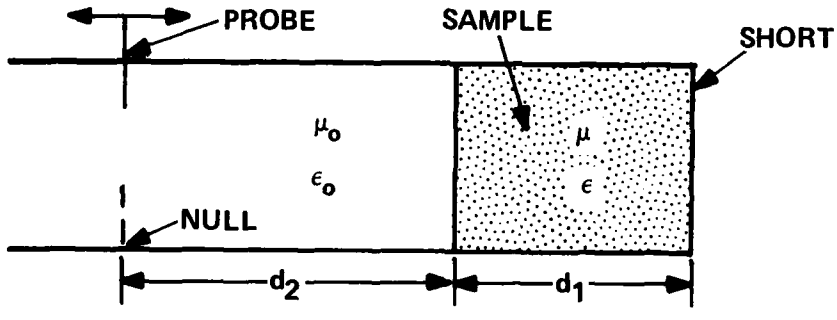

Figure F-4. Transmission line method for determining soil properties.

$$Z = (j \omega \mu_o / \gamma) \tanh(\gamma d_2) \qquad \text{(F-5)}$$

Once γ has been determined, the dielectric constant ε^* may be calculated from

$$\gamma^2 = k_c^2 - \varepsilon^* \omega^2 / c^2 \qquad \text{(F-6)}$$

where

k_c = cutoff wave number
c = speed of light.

This method is similar to the capacitor methods and has similar problems of air gap (between sample and conductors) flux fringing. The gaps can be filled with conducting epoxy for more accurate measurements.

Resonant Cavity Method

A cavity resonator in the TE_{01} mode can conveniently measure the relative dielectric constant, ε_r, of a sample in the range of 1 to 100. Either a disk or a rod type sample may be used (see Figure F-5)[F-7]. The same equations that are used for the transmission line method are applied, where d is now the length from the cavity wall to the sample.

Four Probe Method

The most common of the In-Situ methods is the four-probe method. With this method, four electrodes are placed in the earth in a specific pattern (see Figure F-6 for typical geometries) [F-7]. Two of the probes are transmitters (current injectors) and two of the probes are receivers (voltage probes). This method works well for low frequencies where induction effects and attenuation can be neglected. The resistance of the soil can be determined from V, I, and the geometry and spacing of the probes. This is the typical method used to determine the DC (low frequency) impedance of a ground circuit (see Figure F-7).

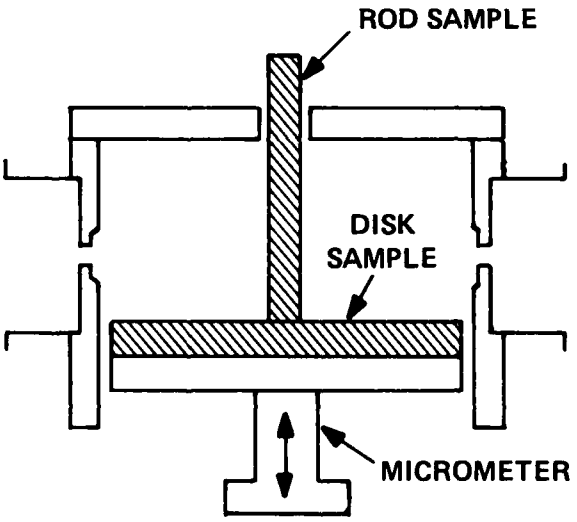

Figure F-5. Resonant cavity method for determining soil parameters.

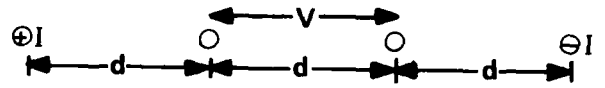

(a) WENNER ARRAY

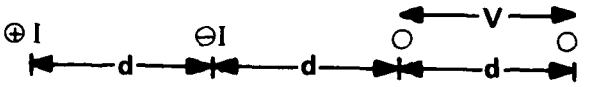

(b) ELTRAN ARRAY

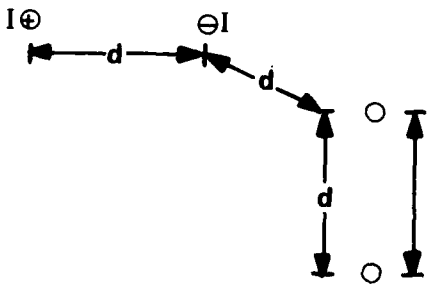

(c) RIGHT–ANGLE ARRAY

Figure F-6. Commonly used four-probe arrays.

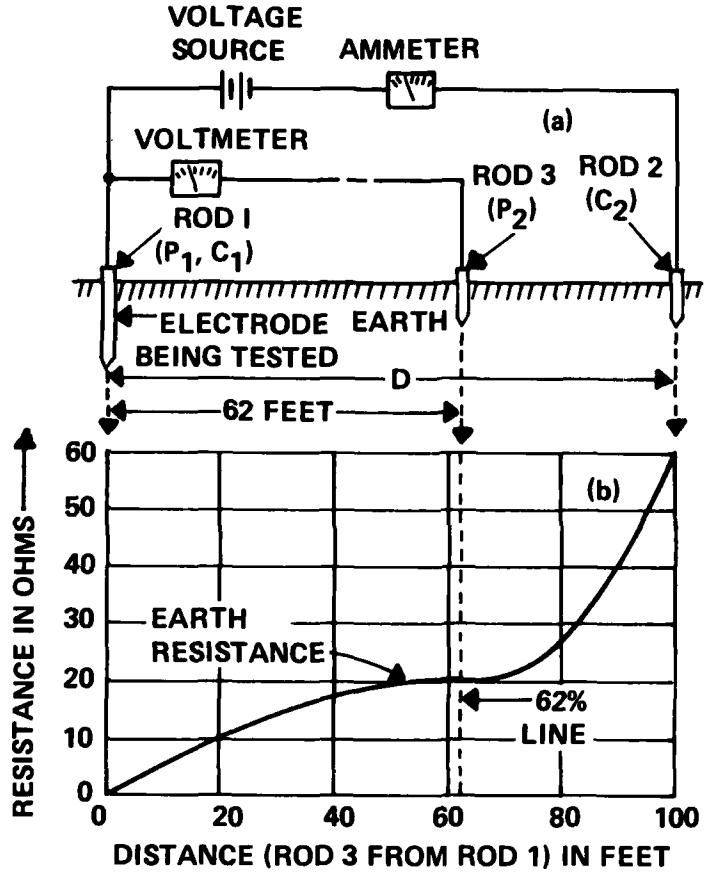

Figure F-7. Electrode resistance versus probe spacing.

Two-Loop Method

The measurement of the mutual impedance between two above ground loops allows σ and ε of the transversed earth to be estimated. This method is used extensively in ground conductivity surveys and in geophysical prospecting. The technique works in the 0.1 to 21 MHz range and is capable of measuring conductivities from 10^{-4} to 2×10^{-1} mho/m and relative dielectric constants of 5 to 25. The test setup for swept frequency measurements is shown in Figure F-8; typical loop orientations are shown in Figure F-9. Reference F-8 presents the theory of this method and gives typical curves relating loop impedance to ground conductivity.

Wave Tilt Method

The tilt of an EM wave near the ground between transmitting and receiving antennas, a moderate distance apart (see Figure F-10), is determined by soil properties and the frequency of the signal. By finding the tilt angle, θ, of a vertically polarized wave, the conductivity and dielectric constant of the ground can be calculated from the following equation [F-4]:

$$\tan^2 \theta \simeq \frac{\varepsilon_r + \sqrt{\left[\varepsilon_r^2 + \frac{(18 + \sigma)^2}{f}\right]}}{2\left[\varepsilon_r^2 + \frac{(18\,\sigma)^2}{f}\right]} \qquad \text{(F-7)}$$

For high frequencies, $(18\sigma)^2 / f$ will be small and Equation (F-7) becomes

$$\tan^2 \theta \simeq \frac{1}{\varepsilon_r} \qquad \text{(F-8)}$$

This method has proven effective at frequencies from 100 kHz to 10 MHz for ground conditions of $\sigma = 10^{-4}$ to 10^{-2} mho/m and $\varepsilon_r = 10$ to 40. The equipment required to perform the test is a transmitter and a receiver. The receiving antenna must have an angular scale and be capable of rotating about the horizontal axis. The receiving antenna can measure the tilt angle

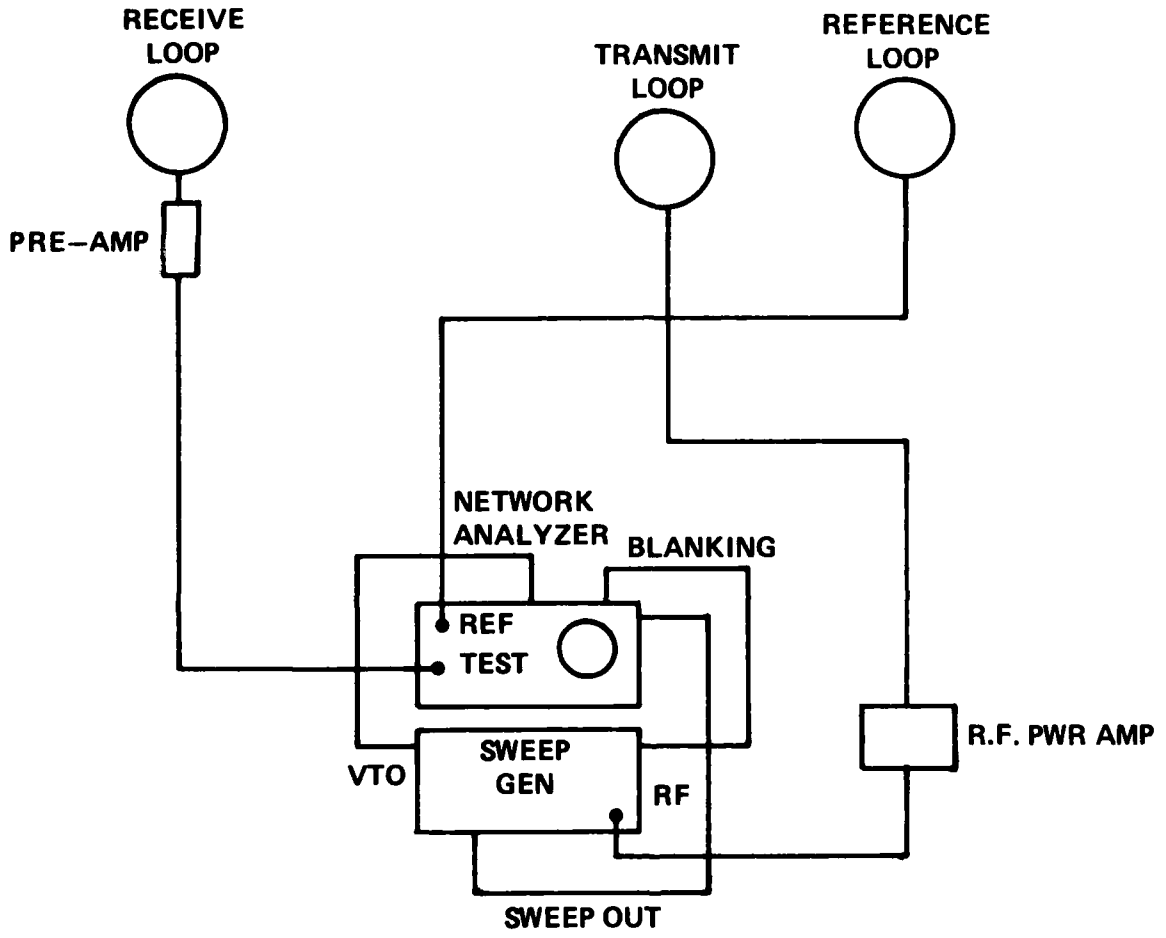

Figure F-8. Two-loop method for determining soil parameters.

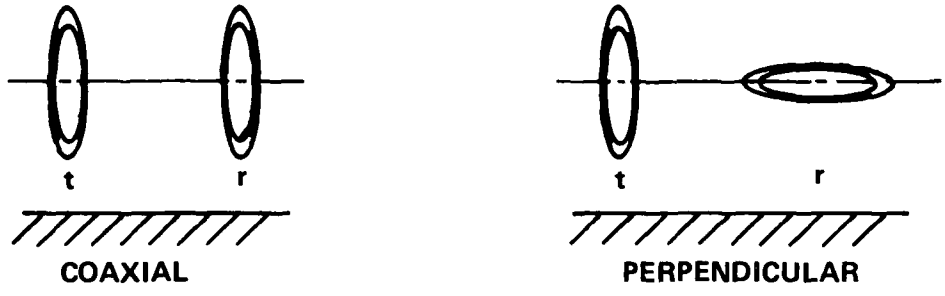

(a) HORIZONTAL MAGNETIC DIPOLE TRANSMITTER CASES

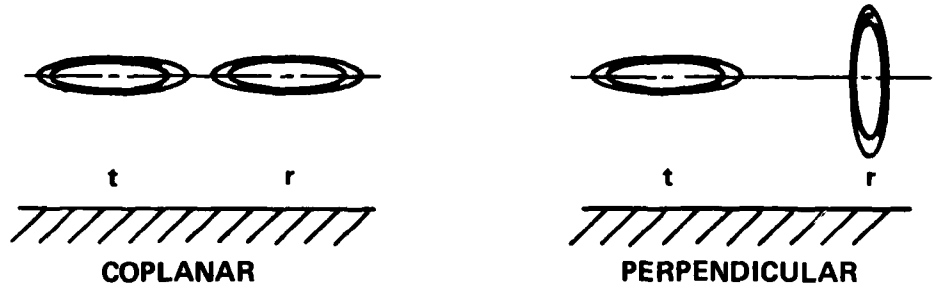

(b) VERTICAL MAGNETIC DIPOLE TRANSMITTER CASES

Figure F-9. Loop orientations for two-loop method for determining soil parameters.

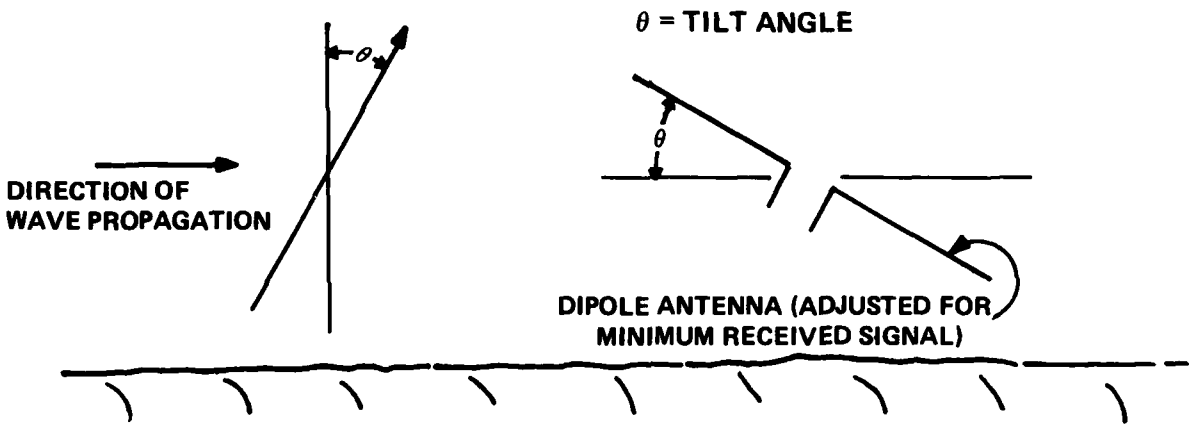

Figure F-10. Illustration of wave tilt method of determining soil parameters.

directly by rotating to find the minimum received signal, at which point the antennas will be perpendicular to the E field.

Field Intensity Method

This is a widely used method for determining ground conductivity. Field strength is measured as a function of distance from a transmitter and compared with computed field intensities for different values of ground constants. The data are then correlated, and the ground conductivity determined. This method works well in flat, homogeneous regions with a smooth field decay.

Coaxial In-Situ

This method employs a specially built [F-9] coaxial line with a hollow end which is inserted directly into the soil. The line is removed from the ground with soil sample intact. The EM properties of the soil can then be determined from the open circuited lossy coaxial transmission line [F-10]. This method is similar to the classical laboratory method of the short circuited coaxial transmission line, and the same equations are used. The reliable frequency range is 300 to 4000 MHz. However, the method could be adapted to lower frequencies by using a larger diameter coaxially line and an impedance bridge rather than a VSWR meter.

Resonant Linear Antenna Method

The resonant linear antenna is used as a probe to measure the EM properties of soil [F-11]. The properties are determined from the length of the antenna and the input impedance at resonance. The equipment for making the measurement of input impedance is a vector voltmeter with voltage and current probes delicately inserted into the coaxial line feeding the linear antenna (see Figure F-11). An experimental test setup is depicted in Figure F-12. This method of soil parameter identification has proved useful in geological surveying and can be used over the frequency range of interest.

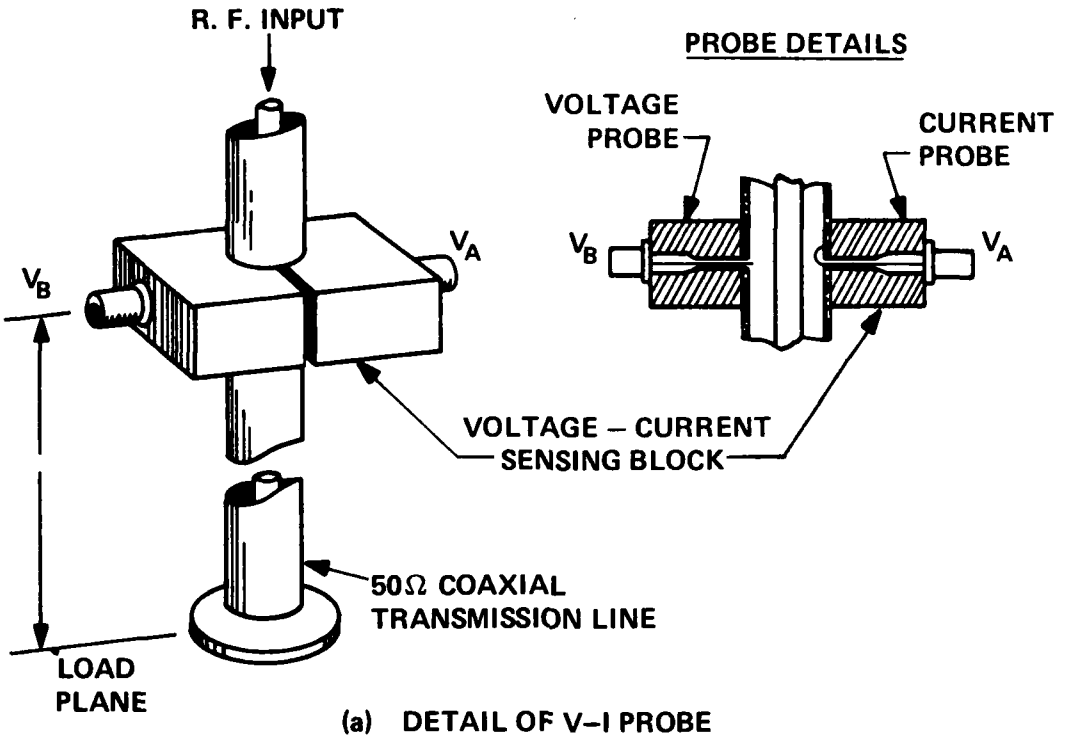

(a) DETAIL OF V–I PROBE

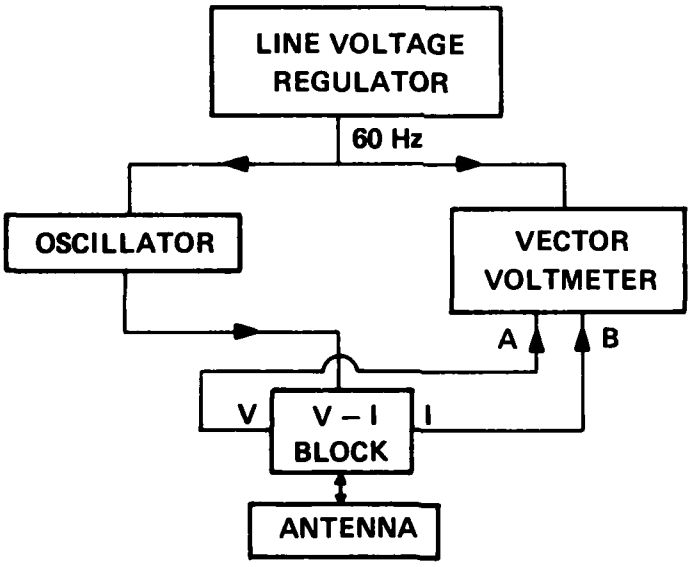

(b) ADMITTANCE MEASURING EQUIPMENT

Figure F-11. Coaxial in-situ method for measuring soil parameters.

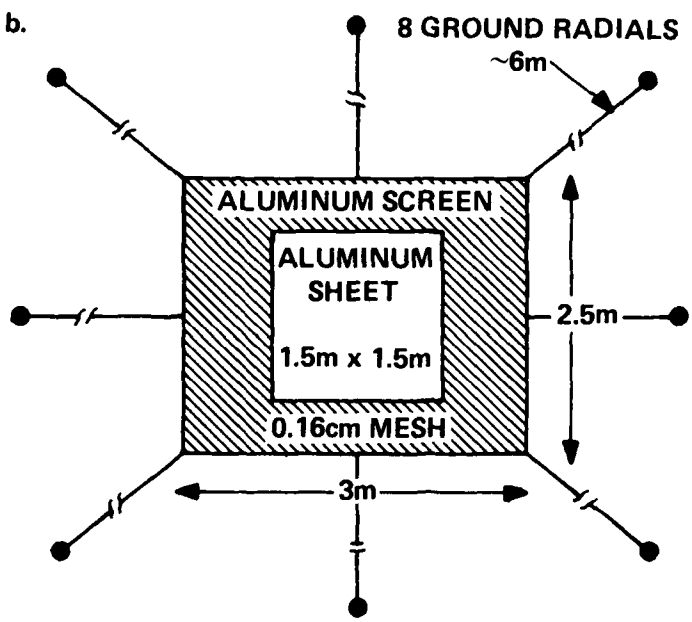

Figure F-12. Illustration of electrode layout of the linear antenna method for determining soil parameters.

APPENDIX F

REFERENCES

F-1. Longmire, L., and Smith, K. S., "A Universal Impedance for Soils," Missions Research Corporation, Santa Barbara, CA, DNA 3788T AD-A025759, Oct. 1975.

F-2. "Getting down to earth . . .", James G. Biddle Co., Plymouth Meeting, Pennsylvania 19462, October 1970.

F-3. Scott, H., Carroll, D., and Cunningham, R., "Dielectric Constant and Electrical Conductivity Measurements of Moist Rock: A New Laboratory Method, "Journal of Geophysical Research, Vol. 72, No. 20 Oct. 15, 1967 pp, 5101-5115.

F-4. Kovattana, T., "Electrical Constant of Central, Eastern, and Northeastern Thailand," STR No. 29, Contract DA 36-039AMC-00040(E), Stanford Research Institute, Palo Alto, CA, February 1967.

F-5. Bussey, H. E., "Measurement of RF Properties of Materials-A Survey", Proceedings of the IEEE, Vol. 55, No. 6, June 1967, pp. 1046-1053.

F-6. Collett, L. S., and Katsube, T. J., "Electrical Parameters of Rocks in Developing Geophysical Techniques," Geophysics, Vol. 38, No. 1, Feb. 1973, pp. 76-91.

F-7. Lytle, R. J., "Measurements of Earth Medium Electrical Characteristics: Techniques, Results, and Applications," Lawrence Livermore Laboratory, EMP Sensor and Simulation Note No. 188, Kirtland AFB, Albuquerque, NM, Nov. 12, 1973.

F-8. Lytle, R. J., Laine, E. and Lager, D., "Determination of the IN SITU Ground Conductivity and Relative Dielectric Constant Via the Two-Loop Method Using Swept Frequency Excitation," AFWL EMP Sensor and Simulation Note No. 187, Kirtland AFB, Albuquerque, NM, Aug. 8, 1972.

F-9. Hipp, J. E., "'IN SITU' EM Soil Properties Measurement: Instrumentation, Theory, and Method," Southwest Research Institute, San Antonio, TX AD-784282, June 7, 1974.

F-10. Hipp, J. E., "Soil Electromagnetic Parameters as Functions of Frequency Soil Density, and Soil Moisture," Proceedings of the IEEE, Vol. 62, No. 1, Jan. 1974, 98-103.

F-11. Smith, G. A., and King, R. W. P., "The Resonant Linear Antenna as a Probe for Measuring the In Situ Electrical Properties of Geological Media", Journal of Geophysical Research, Vol. 79, No. 17, June 10, 1974, pp. 2623-2628.

DISTRIBUTION LIST

DEPARTMENT OF DEFENSE

Commander-in-Chief, Pacific
5 cy ATTN: C3SRD

Defense Communications Agency
ATTN: WWMCCS Sys Engr

Defense Communications Agency
ATTN: Commander

Defense Communications Engineer Ctr
ATTN: Code R720, C. Stansberry

Defense Intell Agency
ATTN: DT, Sci-Tech Intell

Defense Nuclear Agency
ATTN: RAEE
ATTN RAAE
ATTN: NATA
4 cy ATTN: TITL

Defense Tech Info Ctr
12 cy ATTN: DD

Deputy under Secretary of Defense
Comm, Cmd, Cont & Intell
ATTN: Telecomm Systems
ATTN: Programs & Resources
ATTN: Assistant Director (Sys)
ATTN: Surveillance & Warning Sys

Field Command
Defense Nuclear Agency
Lawrence Livermore Lab
ATTN: FC-1

Field Command
Defense Nuclear Agency
ATTN: FCTT, G. Ganong
ATTN: FCTT, W. Summa
ATTN: FCTXE
ATTN: FCPR

Joint Chiefs of Staff
ATTN: GD10, J-5, Nuc & Chem Div
ATTN: SAGA
ATTN: C3S, Evaluation Ofc, (HD00)
ATTN: J-3, WWMCCS & Telecommunications

Joint Strategic Connectivity Staff
ATTN: JCC, A. Buckles

Joint Tactical Comm Ofc
ATTN: TT-E-SS

National Central Security Svc, Pacifia Area
ATTN: Central Sec Serv, Pac Area

National Communications system
ATTN: NCS-TS

National Security Agency
ATTN: S-15
ATTN: R-52

DEPARTMENT OF DEFENSE (Continued)

Office of the Secretary of Defense
Net Assessments
ATTN: Military Assistants

US National Military Representative, SHAPE
ATTN: Surv Sect

Under Secretary of Defense for Rsch & Engrg
ATTN: DEPUNDSEC, C31-Strategic & C2 Sys
ATTN: Strategic & Space Sys (OS)
ATTN: DEPUNDSEC Com Sys
ATTN: Strat & Theater Nuc Forces, B. Stephan

DEPARTMENT OF THE ARMY

Defense Communications Sys
ATTN: DRCPM-COM-W-D

Deputy Chief of Staff for Rsch Dev & Acq
ATTN: DAMA-CSS-N

Headquarters
Department of the Army
ATTN: DAMO-TCV-A

Harry Diamond Labs
ATTN: 00100 Commander/Tech Dir/Div Dir
ATTN: DELHD-TA-L, 81100
ATTN: Chief Div 30000
ATTN: Chief Div 20000
ATTN: Chief Div 10000
ATTN: DELHD-NW, J. Bombardt, 20000
ATTN: Chief Div 40000
ATTN: Chief Div 50000
ATTN: Chief 21500
ATTN: DRDEL-CT
2 cy ATTN: Chief 21000
2 cy ATTN: Chief 22000
3 cy ATTN: Chief 20240

Multi Service Comm Sys
ATTN: DRCPM-MSCS-APB, M. Francis

US Army Communications Cmd
ATTN: CC-OPS-WR

US Army Communications Sys Agency
ATTN: CCM-AD-LB
ATTN: CCM-RD-T
ATTN: CCM-AD-SV

US Army Materiel Dev & Readiness Cmd
ATTN: DRXAM-TL

US Army Nuclear & Chemical Agency
ATTN: Library

US Army Western Cmd
ATTN: Communications Electronics Div

DEPARTMENT OF THE NAVY

Naval Electronic Sys Cmd
ATTN: PME, 117-20
ATTN: Tech Library

Headquarters
Naval Material Cmd
ATTN: 08DE1, N. Jackson

Naval Ocean Sys Ctr
ATTN: Code 4471

Naval Postgraduate School
ATTN: Code 1424, Library

Naval Rsch Lab
ATTN: Code 2627

Naval Sea Sys Cmd
ATTN: SEA-6431

Naval Security Group Cmd
ATTN: G83

Naval Shore Electronics Engrg
ATTN: D. Koide

Naval Surface Weapons Ctr
ATTN: Code F30
ATTN: Code F32

Naval Telecommunications Cmd
ATTN: Deputy Director Systems

NAVCAMS, Eastpac
ATTN: Commander

NAVCAMS, Westpac
ATTN: Commander

Office of the Deputy Chief of Naval Ops
ATTN: NOP 98
ATTN: OP 94

Strategic Sys Project Ofc
ATTN: NSP-43

DEPARTMENT OF THE AIR FORCE

Air Force Communications Cmd
ATTN: XOT

Air Force Electronic Warfare
ATTN: XRX

Air Force Ofc of Scientific Rsch
ATTN: J. Allen

Air Force Weapons Lab
ATTN: SUL

Air University Library
ATTN: AUL-LSE

DEPARTMENT OF THE AIR FORCE (Continued)

Assistant Chief of Staff
Studies & Analyses
ATTN: AF/SA

Deputy Chief of Staff
Rsch, Dev, & Acq
ATTN: AFRDS, Space Sys & C3 Dir

Deputy Chief of Staff
Operations and Plans
ATTN: AFXOK, C2 & Telecom

Foreign Technology Div
ATTN: NIIS, Library

Pacific Air Forces
ATTN: Communications Electronics

Pacific Communications Area
ATTN: Comm Electronics Eng

Rome Air Dev Ctr
ATTN: TSLD

Strategic Air Cmd
ATTN: NRI-STINFO, Library
ATTN: XPFS

Headquarters
United States Air Force
ATTN: SAS

OTHER GOVERNMENT AGENCIES

Central Intelligence Agency
ATTN: OSR/SE/C

Federal Emergency Management Agency
ATTN: Office of Rsch, NPP, J. Hain

DEPARTMENT OF DEFENSE CONTRACTORS

American Telephone & Telegraph Co
ATTN: W. Edwards

BDM Corp
ATTN: L. Jacobs
ATTN: W. Sweeney

Boeing Co
ATTN: R. Scheppe, MS 9F-01

Booz-Allen & Hamilton, Inc
ATTN: D. Durgin

EG&G Wash Analytical Svcs Ctr, Inc
ATTN: A. Bonham

Horizons Technology, Inc
ATTN: R. Lewis

DEPARTMENT OF DEFENSE Contractors (Continued)

Georgia Institute of Technology
Attention Res & Sec Coord for:
2 cy ATTN: D. Acree
2 cy ATTN: G. Melson
2 cy ATTN: D. Millard
6 cy ATTN: H. Denny

Institute for Defense Analyses
ATTN: Classified Library

IRT Corp
ATTN: R. Stewart
ATTN: B. Williams

JAYCOR
ATTN: R. Schaeffer
ATTN R. Poll

Kaman Tempo
ATTN: DASIAC

ORI, Inc
ATTN: R. Hendrickson, Crystal Square 2

Pacific-Sierra Rsch Corp
ATTN: H. Brode, Chairman SAGE

R & D Associates
ATTN: Library

DEPARTMENT OF DEFENSE CONTRACTORS (Continued)

R & D Associates
ATTN: P. Haas
ATTN: W. Karzas
ATTN: W. Graham

Rockwell International Corp
ATTN: G. Morgan

Science & Engrg Associates, Inc
ATTN: B. Gage
ATTN: V. Jones

SRI International
ATTN: A. Grant
ATTN: E. Clark
ATTN E. Vance
ATTN: A. Whitson

Sylvania Systems Group
ATTN: R. Steinhoff

Systems Rsch & Applications Corp
ATTN: S. Greenstein

TRW Electronics & Defense Sector
ATTN: J. Brossier

TRW Electronics & Defense Sector
ATTN: Librarian

END

FILMED

9-83

DTIC